

JAERI - M
91-159

ANNUAL REPORT OF THE NAKA FUSION RESEARCH ESTABLISHMENT
FOR THE PERIOD OF APRIL 1, 1990 TO MARCH 31, 1991

October 1991

Naka Fusion Research Establishment

日本原子力研究所
Japan Atomic Energy Research Institute

JAERI-Mレポートは、日本原子力研究所が不定期に公刊している研究報告書です。
入手の問合わせは、日本原子力研究所技術情報部情報資料課（〒319-11茨城県那珂郡東海村）あて、お申しこしください。なお、このほかに財団法人原子力弘済会資料センター（〒319-11茨城県那珂郡東海村日本原子力研究所内）で複写による実費頒布をおこなっております。

JAERI-M reports are issued irregularly.

Inquiries about availability of the reports should be addressed to Information Division, Department of Technical Information, Japan Atomic Energy Research Institute, Tokai-mura, Naka-gun, Ibaraki-ken 319-11, Japan.

© Japan Atomic Energy Research Institute, 1991

編集兼発行 日本原子力研究所
印 刷 株原子力資料サービス

Annual Report of the Naka Fusion Research Establishment
for the period of April 1, 1990 to March 31, 1991

Naka Fusion Research Establishment
Japan Atomic Energy Research Institute
Naka-machi, Naka-gun, Ibaraki-ken

(Received September 9, 1991)

R&D activities of the Naka Fusion Research Establishment, JAERI, are reported for the period from April 1, 1990 to March 31, 1991.

Since the shutdown of JT-60 in November 1989, the reconstruction work of the JT-60 device was continued until the end of March 1991. In the JT-60 Upgrade, the poloidal field coils and vacuum vessel were renewed and the plasma current was planned to increase up to 6 MA with lower single null divertor. The divertor plates were designed to be toroidally continuous and to use high-heat-conduction C/C composite materials. Another objective of JT-60U is to facilitate tokamak experiments with deuterium as the working gas. Neutron shields were added to the tokamak hall.

In the JFT-2M program, a system for divertor bias experiments was brought into operation and initial experiments were started to study its effects on plasma discharges. Effects of ergodic magnetic limiter on H-modes were examined and stationary H-modes were obtained under the control of ergodic magnetic limiter currents. The DIII-D program was highlighted by the attainment of 11 % beta with a double null divertor plasma.

Concerning the theoretical and computational studies, effort was focused on the analyses of MHD equilibria and stabilities, and burning plasma problems in relation to the design study of the next generation tokamaks.

As for the fusion engineering research, development activities of the ceramic turbo-viscous pump and the surface insulation techniques for the tokamak in-vessel components are remarked in the vacuum technology area. In the high heat flux experiments with the JAERI Electron Beam Irradiation Stand (JEBIS), carbon-based materials and refractory metals were tested to evaluate surface erosion at plasma disruptions. Concerning the plasma heating technologies, much effort was devoted to the development of negative ion sources to produce high current (>10 A), high energy (500 keV-1.3 MeV) negative ion beams for long durations. The JAERI Klystron Test Facility was modified for the testing of high power gyrotrons and their related components by March 1991. A millimeter wave FEL experiments was carried out by using a 1 MeV, 3 kA induction linac.

The main results in the superconducting magnet technology development were the attainment of a ramp rate of 7 T/3 s on the US Demo Poloidal Coil and the fabrication of a 30 kA-12 T pancake coil using a Nb₃Sn hollow monolith conductor. Concerning the tritium processing technology, a fuel cleanup system, which had been developed and designed by JAERI, was installed in the TSTA at LANL to test its applicability to 100 g-level tritium experiments. Experiments at the Tritium Processing Laboratory were also advanced.

The ITER Conceptual Design Activities, which began in April 1988 under the auspices of the IAEA, were successfully completed in December 1990. A lot of contributions to the program were made by JAERI people to support the design and R&D activities and to prepare a plan for the forthcoming Engineering Design Activities. The design study of FER was continued in parallel with its related technology R&D. The concept study of the SSTR (Steady State Tokamak Reactor) and the safety analysis of a fusion reactor were also carried out to clarify the aim of fusion reactor R&D's.

Keywords: Fusion Research, JAERI, JT-60U, JFT-2M, DIII-D, Plasma Physics, Fusion Engineering, ITER, FER, Fusion Reactor Design, Annual Report

Editors: Y. Murakami (in chief), T. Kanazawa, T. Kuroda, M. Saidoh, T. Yamamoto

那珂研究所年報（平成2年度）

日本原子力研究所
那珂研究所

(1991年9月9日受理)

原研・那珂研究所における平成2年度（1990年4月～1991年3月）の研究開発活動について報告する。

JT-60は、平成元年11月に運転を停止して、3年3月末まで改造工事が行われた。改造後のJT-60Uでは、ポロイダル磁場コイルと真空容器が新しいものに取り換えられ、下側X点ダイバータ配位で6 MAのプラズマ電流が流せるように計画された。ダイバータ板は、高熱伝導性の炭素複合材料で作られ、トロイダル方向に切れ目なく設置された。JT-60Uの他の目的は重水素を用いたトカマク実験を可能にすることであり、このため、実験棟に中性子遮蔽が設けられた。

JFT-2M計画では、ダイバータバイアスの効果を調べるための実験装置を整備して、実験を開始した。エルゴディック磁気リミターによるHモード発生の実験では、リミター電流の制御により人為的に定常状態が作り出せることが示された。DIII-D計画では、ダブルX点ダイバータ配位で、ベータ値11%を達成した。

理論解析に関する研究では、次期装置の設計検討に関連して、磁気流体平衡と安定性の解析や核燃焼プラズマの解析が行われた。

核融合工学の研究に関しては、真空技術の分野で、セラミック・ターボ型粗引きポンプと炉内構造物表面への絶縁被膜形成技術の開発が進化した。JEBISを用いた高熱負荷試験では、炭素系材料や高融点金属について、プラズマ・ティスラプション時の表面損傷の評価が行われた。プラズマ加熱技術では、大電流(>10 A)、高エネルギー(0.5~1.3 MeV)、長パルスの負イオンビームを作るための負イオン源の開発に力が注がれた。また、クライストロン試験装置を大出力ジャイロトロンとその関連部品の試験に利用できるようにする改造工事が年度内に終了した。さらに、ミリ波FELの実験が1 MeV、3 kA誘導線型加速器を用いて開始された。

超電導磁石技術の開発では、米国の実証ポロイダルコイルにおける7 T/3秒の立上げ性能の確認、Nb₃Snホロ一形導体を用いた30 kA-12 Tのバンケーキコイルの製作等が主な成果としてあげられる。トリチウム取扱い技術の開発においては、100 gレベルのトリチウムが使用できる米国のTSTAに原研の燃料精製システムが組み込まれ、試験が開始された。TPLにおける各種試験も進展した。

昭和63年4月にIAEAの枠組みで開始されたITERの概念設計活動は、平成2年12月に成功裏に終了した。原研の研究者は、その設計およびR&Dの活動、さらには工学設計活動の準備において、多大の貢献をした。FERの設計検討とR&Dも継続された。また、SSTRの概念検討や核融合炉の安全性解析も炉のR&Dの目的をより明確にする立場から行われた。

那珂研究所：〒311-01 茨城県那珂郡那珂町大字向山801-1

編集者：村上義夫、金澤哲男、黒田敏公、西堂雅博、山本 巧

FOREWORD

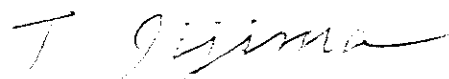
The past fiscal year has brought significant progress in many areas of the JAERI Fusion Program.

Since the shutdown of JT-60 in November 1989, the reconstruction work of the JT-60 device was continued throughout the year and the JT-60 Upgrade (JT-60U) has been completed in March 1991. The main objective of JT-60U is to investigate energy confinement near the break even condition, non-inductive current drive and burning plasma physics with deuterium plasmas. The JFT-2M and DIII-D programs have been highlighted by the attainments of a stationary H-mode with ergodic magnetic limiter and a high beta of 11 % with a double null diverted plasmas, respectively.

The ITER Conceptual Design Activities, which began in April 1988 under the auspices of the IAEA, were successfully completed in December 1990. JAERI people made many contributions to the program with a conviction that strong international integration of fusion research and development is essential and ITER can serve as a central project for the next step.

Continued efforts were laid on the research and development of fusion technologies. The technical area included superconducting magnet, plasma heating, vacuum technology, tritium handling and high heat flux technology. Some of the works were carried out as cooperative international programs.

The development of thermonuclear fusion as an energy source is a central element of a national and international energy strategy. With increasing recognition of environmental issues, the features of a fusion power source are even more attractive. We should now address vigorously the study of physics of ignited plasmas as well as the development of related fusion reactor technologies. We value the continuing support from persons and organizations concerned, and we welcome comments and suggestions on all aspects of our works.



Tsutomu Iijima
Director General
Naka Fusion Research Establishment

Contents

I. PLASMA THEORY AND COMPUTATION	1
1. Introduction	1
2. Analyses of Confinement and Heating Processes	1
2.1 Radiative thermal instability and anomalous edge transport	1
2.2 Synchrotron emission from a nonuniform plasma in a tokamak	2
2.3 Development of TPC code	3
2.4 Mode-coupling theory in multi-frequency Raman regime free electron laser	4
2.5 Space charge modelling in 3-dimensional Raman regime free electron laser	4
3. MHD Equilibrium and Stability Analyses	5
3.1 Current profile and MHD stability in tokamak plasmas	5
3.2 Profile effects on ideal MHD beta limit	5
3.3 Axisymmetric tokamak simulation by using the TSC code	5
3.4 Effect of pellet injection on sawtooth oscillation	6
4. Analyses of Burning Plasma in Tokamaks	7
4.1 D- ³ He fusion yield with higher harmonic ICRF heating of ³ He beams	7
4.2 Ripple-assisted fueling in tokamak reactors	7
4.3 Reduction of divertor heat load by magnetic field perturbation with in-vessel coils in ITER	7
5. TRITON System and Plasma Simulator	8
5.1 Vacuum magnetic energy computation for the new version ERATO code without the mirror symmetry	8
5.2 Development of an FACR solver for MHD equilibrium code SELENE	8
5.3 Development of the GAEA system	9
5.4 Development of plasma simulator	9
II. JFT-2M PROGRAM	10
1. Toroidal Confinement Experiments	10
1.1 Introduction	10
1.2 Confinement studies	10
1.2.1 Improved confinement on JFT-2M	10
1.2.2 Steady state H-mode by ergodic magnetic layer (EML)	11
1.2.3 Divertor bias experiment	13
1.3 RF experiments	14
1.3.1 Coupling studies of a phased array antenna for fast wave current drive	14
1.3.2 Preionization and plasma current initiation by using electron cyclotron heating	16
1.4 Diagnostics	17
1.4.1 Impurity behavior on JFT-2M	17
1.4.2 Development of TV Thomson scattering system with high spatial resolution and high sensitivity	18
2. Operation and Maintenance	20
2.1 Introduction	20
2.2 Operation and maintenance	20
2.3 Development of equipments and instruments	20
III. COOPERATIVE PROGRAM ON TOKAMAK EXPERIMENT	23
1. DIII-D (Doublet III) Experiment	23
1.1 Introduction	23

1.2 Highlights of FY1990 research results and device improvements	23
1.3 JAERI collaboration	25
1.4 Plans for the next year	25
2. Microwave Tokamak Experiment	25
2.1 Present status of MTX experiment	25
2.2 JAERI activity	26
2.3 LAPPS (Laser Aided Particle Probe Spectroscopy)	26
IV. JT-60 PROGRAM	28
1. Overview	28
1.1 Confinement study near the thermal break even condition	28
1.2 Non-inductive current drive	28
1.3 Energetic particle physics relating burning plasmas	29
2. Construction and Development of JT-60 Upgrade	29
2.1 Tokamak	29
2.1.1 Summary of status	29
2.1.2 Vacuum vessel	30
2.1.3 Poloidal field coil	31
2.1.4 Toroidal field coil	32
2.2 Control system	32
2.2.1 Plasma control	32
2.2.2 Man/machine interface	33
2.3 Power supply	34
2.4 Neutral beam injection system	37
2.5 Radio-frequency system	38
2.5.1 LHRF system	38
2.5.2 ICRF heating system	40
2.6 Diagnostic systems	41
2.6.1 Thomson laser scattering apparatus	41
2.6.2 Soft X-ray arrays	44
2.6.3 Bolometer array	44
2.7 System integration tests	45
3. Experimental Results and Analysis	46
3.1 Transport and MHD analysis	46
3.1.1 Transport study of pellet fuelled plasmas in JT-60	46
3.1.2 Local transport analysis of L-mode plasma	46
3.1.3 Nonlinear simulation of η_i -mode and comparison with experimental results	47
3.1.4 Density pulse propagation analysis	48
3.1.5 Bootstrap current analysis	48
3.1.6 MHD stability analysis of high- β_p plasmas	49
3.2 LHRF experiments	50
3.2.1 Analysis of lower hybrid wave propagation and absorption	50
3.2.2 Effect of the spectral gap on current drive efficiency	51
3.3 ICRF experiments	51
3.3.1 Heating properties of higher harmonic regimes	51
3.3.2 Theoretical estimation of stored energy	53
3.4 Topics	53
3.4.1 Limiter H-mode with LHCD	53

3.4.2	MARFE phenomena on neutral beam heated JT-60 plasmas	54
3.4.3	Impurity behavior	54
3.4.4	Divertor study	55
3.4.5	Heat flux onto divertor plates	55
3.4.6	Helium ash exhaust and transport	56
3.4.7	Measurement of neutral beam stopping for hydrogen in the JT-60 plasma	56
3.4.8	Confined alpha particle diagnostics in JT-60	57
3.5	Transport database	57
3.5.1	Transport database	57
3.5.2	Retrieval system for experimental database of JT-60	58
3.6	Development of fusion plasma analysis codes	58
3.6.1	Data handling system	58
3.6.2	1.5D tokamak transport code system: TOPICS	59
3.6.3	Current drive analysis code: ACCOME	59
3.7	Plasma-surface interaction	60
3.7.1	Gas-release during a plasma disruption	60
3.7.2	Performance of divertor plates under high-power and long pulse heating divertor experiments	60
4.	Related Developments and Maintenance	61
4.1	Power supply	61
4.1.1	MG overhaul and maintenance of facilities	61
4.1.2	Power transmission for superconducting coil	62
4.2	RF development	62
4.2.1	LHRF system development	62
4.2.2	ICRF system development	62
4.2.3	Electron cyclotron heating system	63
V.	TECHNOLOGY DEVELOPMENT	65
1.	Vacuum Technology	65
1.1	Introduction	65
1.2	Progress in ceramic vacuum pump development	65
1.3	Zr-bearing OFC gasket for knife-edge-type vacuum flanges	66
1.4	Improvement of QMS by using second stable zone in Mathieu's stability diagram	67
1.5	Coating techniques for ITER/FER in-vessel components	68
1.6	Development of ceramic-insulated wires	69
2.	Superconducting Magnet Technology	70
2.1	Introduction	70
2.2	Proto coil project	71
2.2.1	Verification tests	71
2.2.2	The model pancake coil	72
2.3	The Demo Poloidal Coil project	73
2.3.1	Project status	73
2.3.2	Experimental results of the US-DPC	74
2.4	High field coil development	76
2.5	Cryogenic system development	77
2.5.1	Cryogenic system for the C.S. scalable model coils	77
2.5.2	Development of a large helium turbo-expander with variable capacity	77
2.6	Development of cryogenic structural materials	77

3. Beam Technology	80
3.1 Introduction	80
3.2 Negative ion beam technology	80
3.2.1 Improvement of high current source	80
3.2.2 Long pulse operation	81
3.2.3 High energy acceleration and the beam optics	81
3.3 Design work of negative-ion-based NB system	83
3.4 Positive ion beam technology	84
3.4.1 ECR/RF plasma generator	84
3.4.2 Large scale cryo-sorption pump	84
4. RF Technology	84
4.1 Introduction	84
4.2 Construction of gyrotron test facility and development of the LHRF launcher	85
4.3 Investigation of high power gyrotron and ECH components	85
4.3.1 Developments of 120 GHz gyrotron	85
4.3.2 Component of high power millimeter wave transmission system	86
4.4 FEL research	88
4.5 Design study of RF heating and current drive system for FER and ITER	89
5. Tritium Technology	90
5.1 Introduction	90
5.2 Development of tritium processing technology in TPL	91
5.2.1 Fuel cleanup	91
5.2.2 Hydrogen isotope separation	91
5.2.3 Tritium analysis and measurement	93
5.2.4 Tritium-material interaction	94
5.3 Development of fuel processing technology under JAERI-LANL(DOE)	95
5.4 Development of tritium safe handling technology	97
5.4.1 Separation of tritium using polyimide membrane	97
5.4.2 Operation of tritium safety systems	98
5.5 Development of blanket technology	98
5.5.1 Design works	98
5.5.2 Experimental works	99
5.6 System analysis	100
5.6.1 Design works of tritium systems	100
5.6.2 Development of components for the FER	101
6. High Heat Flux Technology	101
6.1 Introduction	101
6.2 Activities on divertor plate development	101
6.2.1 Thermal cycling experiments on divertor modules without a swirl tube at PBEF	102
6.2.2 Thermal cycling experiments on divertor modules with a swirl tape in JEBIS	102
6.3 Development of a first wall	103
6.4 Disruption simulation experiments	103
VI. NEXT STEP FOR JAERI TOKAMAK PROGRAM	105
1. International Thermonuclear Experimental Reactor (ITER)	105
1.1 Introduction	105
1.2 ITER conceptual design	105
1.3 CDA R&D	107

1.3.1	Physics R&D	107
1.3.2	Technology R&D	107
1.4	Long-term R&D program	108
1.4.1	Physics R&D	108
1.4.2	Technology R&D	109
2.	Fusion Experimental Reactor (FER)	109
2.1	Introduction	109
2.2	FER design	110
2.3	Technology R&D	112
3.	Fusion Reactor Design	113
3.1	Introduction	113
3.2	Steady-State Tokamak Reactor (SSTR) design	113
3.3	Safety analyses	115
SOME PICTURES IN COLOR		117
APPENDICES		
A.1	Publication List (April 1990 - March 1991)	119
A.2	Personnel and Financial Data	127
A.2.1	Change in number of personnel and annual budget (FY1985-1990)	127
A.2.2	Organization chart (March 31, 1991)	127
A.2.3	Scientific staffs in the Naka Fusion Research Establishment (March 31, 1991)	128

目 次

I. プラズマ理論と計算	1
1. はじめに	1
2. 閉じ込め・加熱の解析	1
2.1 放射熱的不安定性と表面付近の異常輸送	1
2.2 非一様トカマク・プラズマからのシンクロトロン放射	2
2.3 TPCコードの開発	3
2.4 多周波ラマン領域自由電子レーザーのモード結合理論	4
2.5 3次元ラマン領域レーザーの空間電荷モデル	4
3. 磁気流体平衡と安定性解析	5
3.1 トカマク・プラズマの電流分布と磁気流体安定性	5
3.2 理想的磁気流体ベータ限界に対する分布の効果	5
3.3 TSCコードによるトカマクの軸対称シミュレーション	5
3.4 鋸歯振動に対するベレット入射の効果	6
4. トカマク中の核燃焼プラズマの解析	7
4.1 ^3He ビームのICRF高調波加熱によるD- ^3He 核融合収率	7
4.2 トカマク炉に於けるリップル利用燃料補給	7
4.3 ITER容器内コイルによる磁気摂動を使ったダイバータ熱負荷の低減	7
5. TRITONシステムとプラズマ・シミュレータ	8
5.1 上下非対称版ERATOコードの為の真空磁気エネルギー計算	8
5.2 磁気流体平衡コードSELENEの為のFACRソルバーの開発	8
5.3 GAEAシステムの開発	9
5.4 プラズマ・シミュレータの開発	9
II. JFT-2M計画	10
1. 閉じ込め実験	10
1.1 はじめに	10
1.2 閉じ込めの研究	10
1.2.1 JFT-2Mの改善された閉じ込め	10
1.2.2 エルゴディック磁気層(EML)による定常Hモード	11
1.2.3 ダイバータ・バイアス実験	13
1.3 高周波実験	14
1.3.1 速波電流駆動におけるアンテナの結合実験	14
1.3.2 電子サイクロトロン加熱によるプラズマ電流立上げ実験	16
1.4 計測	17
1.4.1 JFT-2Mの不純物挙動	17
1.4.2 高空間分解、高感度TVトムソン散乱システムの開発	18
2. 運転管理	20
2.1 はじめに	20
2.2 運転管理	20
2.3 ベレット入射装置の開発	20
III. トカマク実験に関する研究強力計画	23

3.2.2	電流駆動効率に対するスペクトルギャップの効果	51
3.3	ICRF実験	51
3.3.1	高次共鳴の加熱特性	51
3.3.2	プラズマ蓄積エネルギーの理論的評価	53
3.4	その他の実験	53
3.4.1	低域混成波電流駆動によるリミタHモード	53
3.4.2	JT-60のNBI加熱プラズマにおけるMARFE現象	54
3.4.3	不純物の挙動	54
3.4.4	ダイバータ研究	55
3.4.5	ダイバータ板の熱負荷	55
3.4.6	ヘリウム灰排気と輸送	56
3.4.7	JT-60プラズマにおける水素ビームストップング断面積測定	56
3.4.8	JT-60Uにおける α 粒子計測	57
3.5	輸送データベース	57
3.5.1	輸送データベース	57
3.5.2	JT-60実験データベース検索システム	58
3.6	核融合プラズマ解析コードの開発	58
3.6.1	データ・ハンドリング・システム	58
3.6.2	1.5次元輸送コードシステム: TOPICS	59
3.6.3	電流駆動解析コード: ACCOME	59
3.7	プラズマ表面相互作用	60
3.7.1	ディスラプション時のガス放出	60
3.7.2	高加熱実験におけるダイバータ板材料の挙動	60
4.	関連技術開発と大型装置の保守	61
4.1	電源	61
4.1.1	MGオーバーホールと設備の保守	61
4.1.2	超電導コイルへの送電	62
4.2	高周波加熱装置の開発	62
4.2.1	LHRFシステム	62
4.2.2	ICRFシステム	62
4.2.3	ECHシステム	63
V.	技術開発	65
1.	真空技術	65
1.1	はじめに	65
1.2	セラミック真空ポンプ開発の進展	65
1.3	ナイフエッジ式フランジ用ジルコニウム入無酸素銅ガスケット	66
1.4	マシユー線図の第II安定領域を利用した四重極質量分析計の改良	67
1.5	ITER/FER用炉内構造物における被覆技術	68
1.6	セラミック被覆電線の開発	69
2.	超電導磁石技術	70
2.1	はじめに	70
2.2	原型トロイダルコイル計画	71
2.2.1	実証試験	71

3.2.2	電流駆動効率に対するスペクトルギャップの効果	51
3.3	ICRF実験	51
3.3.1	高次共鳴の加熱特性	51
3.3.2	プラズマ蓄積エネルギーの理論的評価	53
3.4	その他の実験	53
3.4.1	低域混成波電流駆動によるリミタ Hモード	53
3.4.2	JT-60のNBI加熱プラズマにおけるMARFE現象	54
3.4.3	不純物の挙動	54
3.4.4	ダイバータ研究	55
3.4.5	ダイバータ板の熱負荷	55
3.4.6	ヘリウム灰排気と輸送	56
3.4.7	JT-60プラズマにおける水素ビームストップング断面積測定	56
3.4.8	JT-60Uにおける α 粒子計測	57
3.5	輸送データベース	57
3.5.1	輸送データベース	57
3.5.2	JT-60実験データベース検索システム	58
3.6	核融合プラズマ解析コードの開発	58
3.6.1	データ・ハンドリング・システム	58
3.6.2	1.5次元輸送コードシステム: TOPICS	59
3.6.3	電流駆動解析コード: ACCOME	59
3.7	プラズマ表面相互作用	60
3.7.1	ディスラプション時のガス放出	60
3.7.2	高加熱実験におけるダイバータ板材料の挙動	60
4.	関連技術開発と大型装置の保守	61
4.1	電源	61
4.1.1	MGオーバーホールと設備の保守	61
4.1.2	超電導コイルへの送電	62
4.2	高周波加熱装置の開発	62
4.2.1	LHRFシステム	62
4.2.2	ICRFシステム	62
4.2.3	ECHシステム	63
V.	技術開発	65
1.	真空技術	65
1.1	はじめに	65
1.2	セラミック真空ポンプ開発の進展	65
1.3	ナイフエッジ式フランジ用ジルコニウム入無酸素銅ガスカート	66
1.4	マシユー線図の第II安定領域を利用した四重極質量分析計の改良	67
1.5	ITER/FER用炉内構造物における被覆技術	68
1.6	セラミック被覆電線の開発	69
2.	超電導磁石技術	70
2.1	はじめに	70
2.2	原型トロイダルコイル計画	71
2.2.1	実証試験	71

2.2.2	モデル・バンケーキ・コイル	72
2.3	実証ポロイダル・コイル計画	73
2.3.1	計画の現状	73
2.3.2	US-DPCの実験結果	74
2.4	高磁界コイル開発	76
2.5	冷凍システム開発	77
2.5.1	C.S. スケーラブル・モデル・コイルの冷凍システム	77
2.5.2	可変容量大型ヘリウムターボ膨張機の開発	77
2.6	極低温構造材料の開発	77
3.	ビーム技術	80
3.1	はじめに	80
3.2	負イオンビーム技術	80
3.2.1	大電流負イオン源の開発	80
3.2.2	長パルス運転	81
3.2.3	高エネルギー加速とビーム光学	81
3.3	負イオンNBシステムの設計	83
3.4	正イオンビーム技術	84
3.4.1	ECR/RFプラズマ源	84
3.4.2	大容量クライオ・ソープションポンプ	84
4.	高周波加熱技術	84
4.1	はじめに	84
4.2	高周波工学試験装置の建設と低域混成波帯電流駆動用ランチャーの開発	85
4.3	大電力ジャイロトロンとミリ波帯伝送システム構成部品の開発	85
4.3.1	120 GHz帯ジャイロトロンの開発	85
4.3.2	大電力ミリ波帯伝送システム構成部品の開発	86
4.4	自由電子レーザーの研究	88
4.5	FER、ITER用高周波加熱装置、電流駆動装置の設計研究	89
5.	トリチウム技術	90
5.1	はじめに	90
5.2	トリチウムプロセス技術の開発	91
5.2.1	燃料精製	91
5.2.2	水素同位体分離	91
5.2.3	トリチウム計量管理技術	93
5.2.4	トリチウム-材料相互作用	94
5.3	原研-ロスアラモス国立研究所核融合技術協力における燃料システムの開発	95
5.4	トリチウム安全取扱い技術の開発	97
5.4.1	ポリイミド膜によるトリチウム分離	97
5.4.2	トリチウム安全システムの運転・操作	98
5.5	ブランケット技術の開発	98
5.5.1	設計研究	98
5.5.2	実験研究	99
5.6	システム解析	100
5.6.1	トリチウムシステムの設計	100
5.6.2	FER用コンポーネントの開発	101

6. 高熱負荷受熱機器の開発	101
6.1 はじめに	101
6.2 強制冷却型ダイバータの開発	101
6.2.1 PBEFにおける平滑冷却管を持ったダイバータ試験体の熱サイクル試験	102
6.2.2 JEBISにおけるスワール管を持ったダイバータ試験体の熱サイクル試験	102
6.3 第1壁の開発	103
6.4 デイスラプション模擬実験	103
VI. 原研における次期トカマク開発計画	105
1. 国際熱核融合実験炉(ITER)	105
1.1 はじめに	105
1.2 ITER 概念設計	105
1.3 概念設計活動におけるR&D	107
1.3.1 物理R&D	107
1.3.2 工学R&D	107
1.4 工学設計活動におけるR&D計画	108
1.4.1 物理R&D	108
1.4.2 工学R&D	109
2. 核融合実験炉(FER)	109
2.1 はじめに	109
2.2 FER設計	110
2.3 工学R&D	112
3. 核融合炉設計	113
3.1 はじめに	113
3.2 定常運転トカマク型動力炉(SSTR)設計	113
3.3 安全解析	115
カラー写真	117
付録	
A.1 論文リスト(1990年4月-1991年3月)	119
A.2 人員及び予算に関するデータ	127
A.2.1 職員数及び年間研究開発予算の推移(1985-1990年度)	127
A.2.2 組織図(1991年3月31日現在)	127
A.2.3 研究開発スタッフ・リスト(1991年3月31日現在)	128

I. PLASMA THEORY AND COMPUTATION

1. Introduction

During the period from April 1, 1990 to March 31, 1991 the following theoretical and computational works were carried out extensively (1) studies of various problems relating with confinement and heating of a tokamak plasma, (2) analyses of MHD equilibria and stabilities, especially, in relation to design studies of next generation tokamaks, (3) analyses of the burning plasma physics in a tokamak, and (4) development of numerical codes and a plasma simulator.

Concerning the first problems radiative thermal instability and anomalous edge transport was studied. An expression for the synchrotron emission from a nonuniform plasma in a tokamak was derived and calculations for nonuniform density and temperature profiles were carried out. The TPC (toroidal particle code) originally developed at the University of Texas was introduced into the JAERI computer system and enhanced several ways. Several problems concerning the free electron laser were also analyzed.

Major efforts of the MHD studies were focused on the analyses relating with the next generation tokamaks. In order to attain a stable high beta tokamak equilibrium the plasma profile dependence on the stability properties were studied. Analyses of the positional instabilities and the sawtooth oscillation were carried out by nonlinear simulations.

As for the burning plasma physics the fusion yield enhancement of D-³He reaction by combined ³He beam and higher harmonic ICRF heating was analyzed. In order to solve engineering problems appearing in the future reactor studies, a ripple-assisted fueling method and a method to reduce the divertor heat load by magnetic field perturbation were investigated.

Physics codes developed in this period were added to the TRITON system. Development and improvement of supporting codes were also continued. As for the plasma simulator METIS new application fields such as the analyses of a free electron laser and a tokamak equilibrium were investigated and conceptual design of a debugging software system was carried out.

As for the US-JAERI datalink operated under Annex IX the gateway computer VAX8350 was connected to the Naka front end computer FACOM M780 via ethernet with the TCP/IP protocol. This system is being effectively used for various international collaboration programs.

2. Analyses of Confinement and Heating Processes

2.1 Radiative thermal instability and anomalous edge transport

Significant fraction of input power is lost by impurity radiation from a tokamak plasma. Existence of impurity ions also affects the MHD behavior of the plasma, transport and L-H transition phenomena. Middle-m ($m \sim 10$, m : poloidal mode number) magnetic fluctuations are observed in many tokamaks and it is shown that they correlate with the confinement of tokamaks. Radiation loss due to impurity ions has strong electron temperature dependence. Within a certain temperature range, radiation loss decreases with temperature raise and due to this fact the plasma

behaves as an active medium. In this situation a radiative thermal instability becomes unstable. At an edge region, this radiative thermal instability has a large growth rate and can modify the MHD phenomena and the transport processes.

In this study, we examined the relation among the impurity radiation, the middle-m magnetic fluctuation, and the edge transport phenomena. First we study the instability for the case without the magnetic fluctuation. For a slab plasma in a cartesian coordinates (x,y,z) with sheared magnetic field $\mathbf{B} = B_0(0, \frac{x}{L_s}, 1)$ the growth rate and the localization width are given as

$$\gamma = -n_I \frac{\partial L}{\partial T_e} - k_y \chi_{\perp} - \sqrt{\chi_{\perp} \chi_{\parallel}} \frac{k_y}{L_s} \quad \text{and} \quad \delta = \left(\frac{\chi_{\perp}}{\chi_{\parallel}} \right)^{1/4} \left(\frac{L_s}{k_y} \right)^{1/2},$$

where χ_{\perp} and χ_{\parallel} are perpendicular and parallel electron thermal conductivities, respectively, and other notations are standard. This mode is stabilized by magnetic shear except for $T_e < 100\text{eV}$ for typical plasma parameters of a tokamak plasma. Next we study the case with the magnetic fluctuation. In a plasma with a magnetic island formed by the magnetic fluctuation the radiative thermal instability grows even if the instability is linearly stable in the original plasma. And once the radiative thermal instability occurs, electron temperature perturbation grows at resonant surfaces and helically perturbed current flows as

$$j_{\parallel} \sim -\frac{\tilde{\eta}}{\eta_0} j_0 \sim \frac{3}{2} \frac{\tilde{T}}{T_e} j_0.$$

With this helically perturbed current, radiative thermal instability, in turn, enhances the growth of the island. For middle-m modes, radiative thermal instability can grow up to the level that overlapping of islands occurs in the case of a large impurity level. In this situation enhanced perpendicular transport stabilizes the instability and the saturated state which results in an anomalous transport is attained. Thus obtained theoretical anomalous transport is consistent with experimental results.

2.2 Synchrotron emission from a nonuniform plasma in a tokamak

Synchrotron radiation loss becomes important for the power balance in a high-temperature and high-magnetic-field tokamak reactor. According to the Trubnikov's expression [2.2-1], the ratio of synchrotron loss power, P_{syn} , to alpha heating power, P_{α} , is estimated as about 25% for an experimental reactor with $B_t = 7\text{T}$, $T_e = 20\text{keV}$, $P_{\alpha} = 200\text{MW}$, and the wall reflection coefficient $\mathcal{R} = 0.7$. The expression by Trubnikov is given for a uniform plasma. A numerical code for a plasma with nonuniform electron density n_e and temperature T_e has been developed. Toroidal effect ($B_t \neq \text{constant}$) is also included. Two cases for the wall reflection are considered; one is the usual mirror reflection, and the other is the random reflection (cosine reflection). The

code reproduces well the results by Trubnikov for uniform plasmas. The inhomogeneity of the density and the temperature is introduced as $n_e \propto (1-\rho^2)\alpha_n$ and $T_e \propto (1-\rho^2)\alpha_T$.

Figure I.2-1 shows the ratio, $P_{\text{syn}}(\alpha_T, \alpha_n) / P_{\text{syn}}(0,0)$, for the density-weighted-average temperature, $\langle T_e \rangle = 20\text{keV}$ and the dimensionless parameter, $p \equiv 6 \times 10^3 a n_{20} / B_t = 10^3$ (a : minor radius in m, n_{20} : density in 10^{20}m^{-3} , B_t : toroidal magnetic field in T). The radiation loss increases very steeply with the peaking of the T_e profile for a flat density profile, $\alpha_n = 0$. On the contrary, the enhancement of the loss becomes small for the slightly peaked n_e profile, $\alpha_n = 0.5 - 1.0$.

Reference

- [2.2-1] B.A. Trubnikov, in *Reviews of Plasma Physics*, Vol. 7 (Consultants Bureau, New York, 1979) p.345.

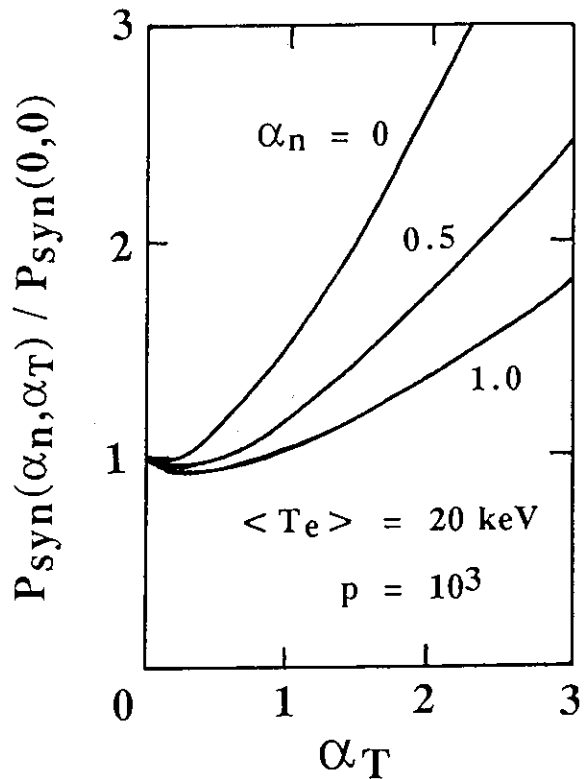


Fig. I.2-1 Dependence of radiation loss power, P_{syn} , on plasma inhomogeneity, $n_e \propto (1-\rho^2)\alpha_n$ and $T_e \propto (1-\rho^2)\alpha_T$

2.3 Development of TPC code

The toroidal particle code, TPC, developed originally at the University of Texas, was enhanced in several ways. This code self-consistently models a kinetic ion species and kinetic or quasineutral electron species in a toroidal coordinate system with static tokamak-like magnetic fields. Enhancements include improvement of ion gyrokinetic species option. Further investigation and implementation of a Lagrangian Vlasov method (also known as "delta-f" method) was pursued. This method allows a dramatic reduction in noise as compared to standard particle models, as well as convenient specification of background profile, source and loss terms. Many new diagnostics were developed for studying phase space and electric field evolution, primarily to assist testing of the delta-f method. A portable (public domain) graphics system was ported to the Unix operating system, enhanced for use with TPC, and interface library (to meet TPC's system-independent graphics specification) was developed. Collaboration with US researchers on existing projects continued, including development of time varying magnetic field

effects in TPC via the Darwin model, and time evolution of toroidal η -i modes with a quasineutral electron response.

2.4 Mode-coupling theory in multi-frequency Raman regime free-electron laser [2.4-1,-2]

Parasitic wave excitation in a Raman regime free electron laser(FEL) was investigated by using one-dimensional multi-frequency amplification code[2.4-3]. It was found that the multi-mode-coupling among sideband waves and the primary wave plays an important role in the parasitic wave excitation in addition to the so-called sideband instability. In the present study we examined the underlying physical mechanisms leading to the observed results by introducing an analytical model in which two radiation fields with (ω_1, ω_2) simultaneously exist. We found that the nonlinear coupling between two fields induces a beat field with $\Delta\omega \equiv \omega_1 - \omega_2$ and corresponding momentum and the density modulations. The lower frequency beam modulation couples with the original fields and excites new modulations with $(\omega_1 + \Delta\omega, \omega_2 - \Delta\omega)$. The transverse current produced by the beam modulations causes new radiations. The process is systematically repeated and a broad excitation spectrum is obtained. Especially, "an additive law" for the growth rates of the parasitic waves observed in the previous simulation [2.4-3] is also analytically deduced.

References

- [2.4-1] Y. Kishimoto, H. Oda, and M. Shiho, to be published in Nucl. Inst. and Meth. (1991).
- [2.4-2] Y. Kishimoto, H. Oda, and M. Shiho, JAERI-M 90-211.
- [2.4-3] Y. Kishimoto, H. Oda, and M. Shiho, Phys. Rev. Lett. **65** (1990) 851.

2.5 Space charge modelling in 3-dimensional Raman regime free electron laser

The effect of space charge field in a Raman regime FEL was investigated in an ideal 1-dimensional case and in a realistic 3-dimensional configuration. Ganguly and Freund[2.5-1] presented a 3-dimensional model for a helical wiggler case by using the method of the Gould-Trivelpiece(G-T) mode expansion. We extend this method to the linearly polarized focusing wiggler and investigate the wave amplification in the presence of an axial guiding field[2.5-2]. The stable propagation of the electron beam in the focusing wiggler is assured by the axial guiding field which rotates the beam by a force $B_0 \hat{e}_z \times \nabla(B_w) \equiv B_0 B_w r \hat{e}_\theta$. In the presence of the electrostatic field, the field cannot be represented only by the TE or the TM mode but the coupling of both the TE and the TM mode exists. It is, however, found that the coupling is weak and cancels out after taking the wiggler average. The rapid convergence of the G-T mode expansion is obtained in the simulation when the initial filling factor is appropriately chosen. In the Raman regime operation with the beam energy $E_b \sim 1\text{MeV}$ and the beam current $I_b \sim 0.5\text{-}1\text{kA}$, the growth rate of the wave is suppressed small($\sim 1/2$) and the resonance condition becomes narrower in comparison with the case without the electrostatic field.

References

- [2.5-1] A.K. Ganguly and H.P. Freund, Phys. Fluids 31 (1988) 387.
 [2.5-2] M. Shiho, K. Sakamoto, S. Maebara, et al., to be published in Nucl. Inst. and Meth. (1991) (Proc. 12th Internat. FEL Conf., Paris, Sept. 1990).

3. MHD Equilibrium and Stability Analyses**3.1 Current profile and MHD stability in tokamak plasmas[3.1-1]**

In order to attain a high beta plasma in a tokamak-type reactor (ITER) the relation between the MHD stability and the current profile was investigated by taking into account of the neoclassical Ohm's law, and the necessary amount and the profile of the non-inductive current were estimated. For a peaked temperature profile required to attain a high fusion yield the neoclassical current profile is rather peaked in the plasma with only inductively driven current. This equilibrium is unstable because of too low safety factor at the axis. Therefore, an additional non-inductive current must be forced to flow to make the current profile flatter and keep the safety factor at the axis around unity. The necessary amount of the non-inductive current is about 30% of the total current and the shape of the driven current profile is moderate, which can be realizable from the engineering viewpoint. In this case the beta limit (the Troyon factor) of 2.2 is obtained.

Reference

- [3.1-1] S. Tokuda, G. Kurita, M. Azumi, et al., in Proc. 13th Internat. Conf. on Plasma Phys. and Controlled Nucl. Fusion Research (Washington D.C., 1990), IAEA-CN-53/D-4-1.

3.2 Profile effects on ideal MHD beta limit

Effects of plasma pressure and current density profiles on the ideal MHD beta limit were studied. On the ITER-like plasma with $\kappa=2$, $\delta=0.4$, $A=2.8$ and $I_p=22\text{MA}$, the beta limits for the $n \leq 4$ and $n = \infty$ modes are studied for different pressure profiles and internal inductance, l_i . Preliminary result suggests: the maximum beta value is obtained at lower l_i ($l_i < 0.7$) for a peaked pressure profile and at high l_i ($l_i > 0.9$) for a flat pressure profile. In the former case, the beta value is limited by ballooning modes near the plasma center. A strong coupling between the $m=1$ and $m \geq 3$ poloidal components of the plasma displacement is observed and the most unstable toroidal mode number is sensitive to the choice of the safety factor at the plasma center, q_0 . A kink or ballooning mode limits the beta value in the latter case depending on a slight change in pressure profile near the plasma surface. The mode is much more localized near the plasma edge than in the former case. The work is being continued for different I_p and the aspect ratio.

3.3 Axisymmetric tokamak simulation by using the TSC code

In a highly elongated cross sectional plasma with a double null separatrix as ITER, transition from the double null to the single null configurations is always unavoidable unless some proper measure to control it is adopted. Partial conductive shells with small resistivity located near the plasma surface inside the complete conductive vessel wall may be effective to suppress

the instability. In this case the deformation of the shape of the plasma cross section associated with the movement of the plasma is very important to analyze the instability, and we cannot rely upon the rigid model even when we need only the growth rate of the axisymmetric instability. We investigated, therefore, the plasma dynamics of the highly elongated cross sectional plasma by using the TSC code (tokamak simulation code). We carried out a series of simulations to investigate the plasma dynamics in the existence of the partial shells [3.3-1], and now we are analyzing the growth rate of the axisymmetric instability of the above system.

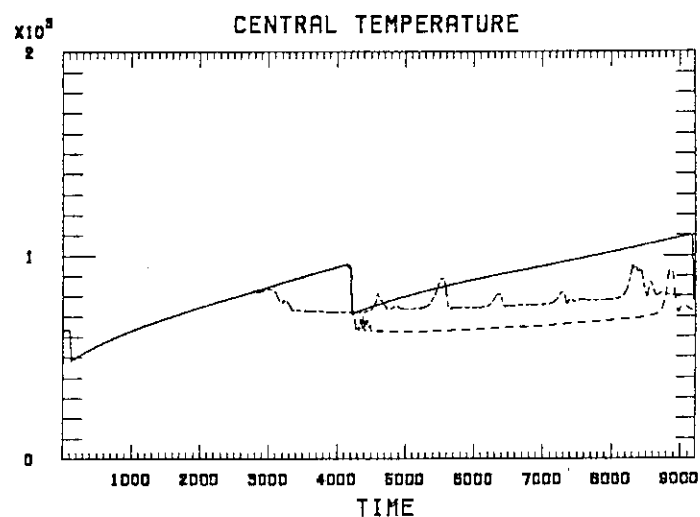
Reference

[3.3-1] Y. Nakamura, Proc. 1990 Workshop on MHD Computations (National Institute for Fusion Science, Nov. 15-17, 1990) (1991).

3.4 Effect of pellet injection on sawtooth oscillation

To investigate the effect of pellet injection on the sawtooth oscillation, we investigated the behavior of the modes with the helicity (m/n) of unity by the nonlinear simulation based on the reduced set of the resistive MHD equations with an electron temperature transport equation. We analyze a plasma in which the normal sawtooth oscillation of the central electron temperature is observed (Fig.I.3-1 solid line) in the case without the pellet injection. When we inject a pellet into the plasma from outside, a cold column is formed along the radius of the injection. Because of the large parallel heat conduction this cold column disappears instantaneously except for the vicinity of the rational magnetic surface. At the rational magnetic surface the cold region remains and a "snake" (a helical structure of a cold plasma column along the magnetic field lines) is formed. The snake is surrounded by a magnetic island where a local negative current flows. The negative current destabilize a thermal instability which is, otherwise, stabilized by the large parallel heat conduction and the snake structure survives for a long time. In reality, however, the snake moves to the magnetic axis rather quickly and the helical structure changes to a straight one. The electron temperature at the "straight snake" remains low due to the radiation cooling (Fig.I.3-1 dotted line). This phenomenon depends hardly on the time of the pellet injection as long as there exists the $q=1$ rational surface inside the plasma (Fig.I.3-1 dotted broken line).

Fig.I.3-1 Time evolution of the electron temperature at the magnetic axis. The solid line shows the normal sawtooth oscillation observed in the case without the pellet injection. The dotted line shows the case where the pellet is injected at $t=4100$. The dotted broken line shows the case where the pellet is injected just after the $q=1$ rational surface is formed ($t=2900$).



4. Analyses of Burning Plasma in Tokamaks

4.1 D-³He fusion yield with higher harmonic ICRF heating of ³He beams

D-³He fusion yield enhancement by combined ³He beam and higher harmonic ICRF heating was investigated on the basis of the local Fokker-Planck calculation. The fusion yield with the fourth harmonic heating of 100-keV ³He beams is enhanced most efficiently when the ratio of the beam power density to the RF power density is 1/5. The maximum of the fusion power multiplication factor is roughly given by $\Delta Q_{\max} \sim 0.043(T_e/10) (n_e/10^{20})^{1.5}$ where the electron temperature T_e and the density n_e are given in keV and m^{-3} , respectively. Comparison was made with the case of the fundamental minority heating of ³He beams and with the case of 500-keV D beam injection. In the high n_e case, the fourth harmonic heating can enhance the fusion power more efficiently than the fundamental heating. In the high ³He concentration, 500-keV D beam injection was found to be more effective than combined ³He beam and ICRF heating, in the fusion yield enhancement.

4.2 Ripple-assisted fueling in tokamak reactors [4.2-1]

It has been proposed to apply the "ripple injection" to refuel tokamak reactors. By using an orbit-following Monte-Carlo code, we have studied the usefulness of the ripple-assisted fueling. The penetration depth strongly depends on the beam energy. The ripple-enhanced outward flow of ripple-detraped fast ions is not a serious problem. If we choose the ratio of beam energy to the central electron temperature less than 4, the fueling efficiency becomes more than 80%. The range of the toroidal angle of beam injection effective for fueling is rather wide. By regulating the shape of the ripple-well region, the power fraction of alpha-particle ripple loss incident to the fueling can be reduced to less than 5%.

Ripple-assisted fueling in ITER has been evaluated. Due to the small aspect ratio, the field ripple steeply decays in the plasma. Consequently, central fueling presents some difficulties. Effective fueling near half of the minor radius is possible with about 6% power loss fraction of α particles. If we employ the injection of 8mm ϕ pellets, the injection speed of more than 50km/s is necessary to obtain a similar fueling profile.

In the present calculations, we employ a field ripple cyclic with respect to toroidal angle. If we employ a toroidally localized field ripple, the fueling profile and efficiency are maintained as they are with the desirable reduction of α -particle loss.

Reference

[4.2-1] K. Tani, R. Yoshino, T. Tuda, et al., submitted to Fusion Technol.

4.3 Reduction of divertor heat load by magnetic field perturbation with in-vessel coils in ITER [4.3-1,-2]

One of the most serious problems in the design of ITER is the high heat load on the divertor plates. The peak value may become more than 30 MW/m^2 for the steady state operation with low density. To reduce this high heat load, an additional method by using the in-vessel coils for plasma position control is proposed. The coil current is toroidally modulated as $I_c \propto \sin(\phi - \omega t)$, where ϕ is the toroidal angle and the frequency ω is about 1Hz. The magnetic field near the equilibrium separatrix is perturbed, and the heat flux parallel to the field line spreads radially in the scrape-off layer. Numerical calculation for the coil current of $I_c = 10\text{kA}$ shows that the radial spread of the heat load on the plate (angle between the plate and separatrix is 15°) is about 3cm. The spread is proportional to I_c . The heat diffusivity inside the separatrix is not significantly enhanced for $I_c \leq 20\text{kA}$. Effect on the profile of the divertor plate heat load is estimated. The peak heat load, for the most serious case mentioned above, is reduced by about 30% and the half-width becomes wider by a factor of 1.6 with $I_c = 20\text{kA}$.

References

- [4.3-1] M. Azumi, T. Takizuka, M. Sugihara, et al., ITER-IL-PH-13-0-J-5 (1990).
- [4.3-2] Y. Shimomura, "ITER: Operational Scenario," 13th Internat. Conf. on Plasma Physics and Controlled Nuclear Fusion Research, Washington, 1990, IAEA-CN-53/F-2-1

5. TRITON System and Plasma Simulator

5.1 Vacuum magnetic energy computation for the new version ERATO code without the mirror symmetry

For the new version ERATO code which analyzes the linear ideal MHD stability of a toroidal plasma without the mirror symmetry a new module ERATO-ASC to calculate the vacuum magnetic energy was developed on the basis of the Green function method. By employing a consistent representation of the vacuum meshes with that of the plasma meshes at the surface the deviation of the resultant vacuum energy matrix from an Hermite matrix was made extremely small, and calculation with very high accuracy becomes possible. Eigenvalues obtained by the new version ERATO code are in good agreement with those by the old version code for analytical equilibrium with the mirror symmetry.

5.2 Development of an FACR solver for MHD equilibrium code SELENE

The DCR (double cyclic reduction) algorithm used in the MHD equilibrium code SELENE suffers from over-flow for mesh numbers larger than a certain limit (for FACOM M-series the limit is 512). In order to calculate a numerical equilibrium for a large mesh number and realize a stability analysis with higher accuracy the FACR (Fourier analysis cyclic reduction) algorithm which is numerically stable against the over-flow was substituted for the DCR method in the SELENE code. The new version assumes neither uniform meshes nor the 2^n+1 mesh number in the R-direction, which makes mesh accumulation in the R-direction possible and will be useful for equilibrium calculation for high β_j plasmas.

5.3 Development of the GAEA system

As for the simulation database system GAEA[5.3-1] a new function which combines successive restart jobs into one job with a new RUN number was developed. Several graphical options (grids, polygons, centered symbols) were also added in the GAEA system.

Reference

[5.3-1] S. Tokuda, T. Tsunematsu, T. Takeda, *Comput. Phys. Commun.* **44** (1987) 21.

5.4 Development of plasma simulator

In order to satisfy the requirement to produce enormous theoretical datasets necessary for the design studies of the next generation tokamaks, conceptual design work of a plasma simulator METIS dedicated for the calculations of the alpha-particle loss analysis and the nonlinear MHD simulation was continued from the last fiscal year on. In this fiscal year a new application softwares as the beam-wave interaction in a free electron laser and the Poisson solver appearing in the MHD equilibrium analysis were developed. For both the problems it was concluded that good performance in the METIS plasma simulator is expected by the extrapolation from the test by the Proto-METIS simulator. Conceptual design of debugging system for METIS was also made.

II. JFT-2M PROGRAM

1. Toroidal Confinement Experiments

1.1 Introduction

The main progress in JFT-2M program is summarized. For 1990, a system for divertor bias experiments has been brought into operation and initial experiments have begun to study its effects on plasma discharges. Effects of ergodic magnetic limiter on H-modes have been examined and stationary H-modes have been produced under the control of ergodic magnetic limiter currents.

1.2 Confinement studies

1.2.1 Improved confinement on JFT-2M

Many kinds of improved discharges have been discovered in numerous tokamak experiments. Some of them have been realized or found in JFT-2M limiter or divertor discharges. These are H-mode[1.2-1], improved L-mode (IL-mode)[1.2-2], counter neutral beam injection (CTR-NB) and pellet injected H-mode. The differences of these improved confinement modes are characterized by the density profile.

As is well known, the so-called electron temperature 'pedestal' is quickly formed at the L/H transition. The electron density and ion temperature profiles also show a pedestal at the edge. The increase in the total stored energy in the H-mode is largely due to pedestal formation. On the other hand, IL-mode or CTR-NB does not show electron density and temperature pedestals at the edge. The improvement of CTR-NB is due to the increase of density and ion temperature and the confinement time is about 30 % higher than that in CO-NB heating. The density (Fig.II.1.2-1) and ion temperature profiles show highly peaked profiles. The toroidal rotation velocity has a high shear and the velocity of the center reaches about 100km/s. In this case, the sawtooth period increases up to 40 msec or more and then disappears. After that, the plasma sometimes undergoes a disruption due to a large impurity accumulation at the center. The IL-mode appears after the H/L transition. This means that this mode appears after a fast decay of the edge density. Then this mode shows a peaked density profile (Fig.II.1.2-2). The ion temperature and the toroidal rotation velocity also show peaked profiles, even in the case of CO-NB heating. In this mode, the sawtooth period increases and then disappears. If a large sawtooth occurs after H/L transition, then the discharge shows H/L/H/L.. transitions. The improved mode found in JFT-2M is characterized by two kinds of improvement. One is the H-mode which has a sharp density and temperature gradients at the edge, and the other mode has peaked density, temperature and toroidal rotation profiles around the center. The improvement of the pellet injected H-mode achieved at optimum conditions of the pellet injection experiments may consist in a coupling of H-mode and peaked profile improvements. The critical condition is deep penetration of the pellet injection. One condition to perform deep penetration is the injection of pellets before H-transition. In this

mode, the density profile shows a peaked profile with a pedestal (Fig.II.1.2-3) and the stored energy is about 30% higher than in a gas fueled H-mode. However, this coupled improvement does not persist for a long time. As a result of the large impurity accumulation at the center, the stored energy rolls over and decays faster than in a gas fueled H-mode.

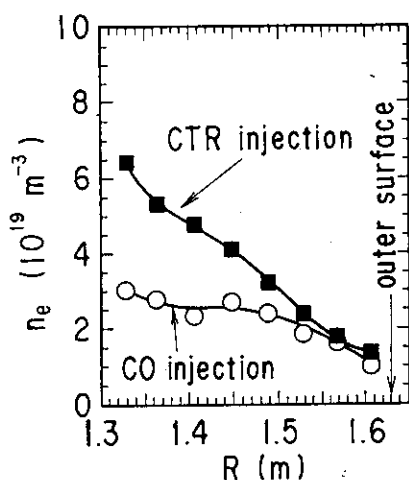


Fig.II.1.2-1
Density profiles of CRT-NB and CO-NB at limiter configuration.

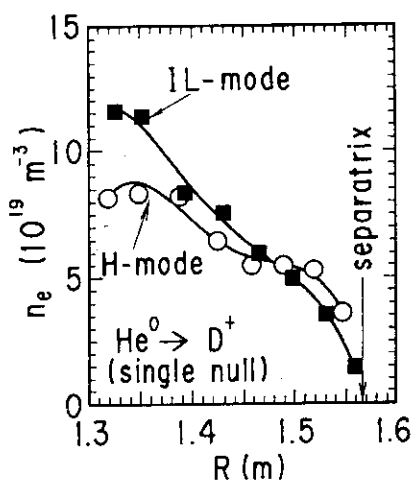


Fig.II.1.2-2
Density profiles of IL-mode and H-mode.

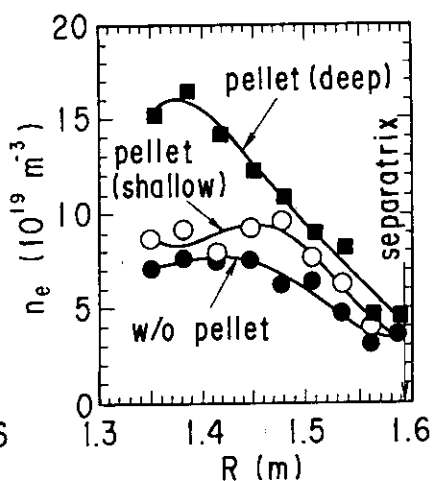


Fig.1.2-3
Density profiles of H-mode without and with pellets.

1.2.2 Steady state H-mode by ergodic magnetic layer (EML)

The burst free H-mode has little controllability from the point of a steady state operation. We try to control the H-mode by applying an ergodic magnetic field produced by two local coil sets installed outside the vacuum vessel. The magnetic field structure calculated by Fourier analysis and field line tracing shows a broad poloidal mode spectrum due to the locality of the EML coil. It has the peaks of the poloidal mode numbers $m = 5$ and $m = 11$ near the plasma surface for the low- m and high- m connections respectively[1.2-4]. By applying a high- m ergodic magnetic field, the suppression in density, radiation increase and a steady state H-mode can be realized with H_{α} burst(Fig.II.1.2-4). It is noted that the total stored energy of the steady state H-mode shows some loss compared with that of the burst free H-mode. But it is only less than 10% due to the suppression of density increase (the total stored energy of the steady state H-mode is almost the same as that of the burst free H-mode at the same density). Figure II.1.2-5 shows the difference of the H-mode enhancement to ITER89P between with and without EML (H_{α} bursts). Only the power scan data are included in this case, and the enhancement of burst free H-mode is set to one for comparison. The average enhancement at the steady state operation is reduced about 14% and the histogram shows the large deviation. The profiles of ion and electron temperature are almost the same with and without the ergodic field. It means that the created H_{α} burst by EML

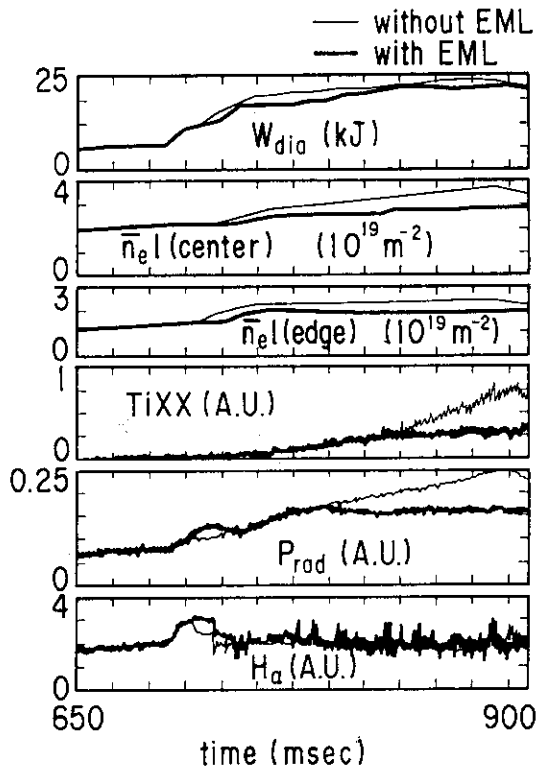


Fig.II.1.2-4
The difference of plasma parameters between with and without EML.

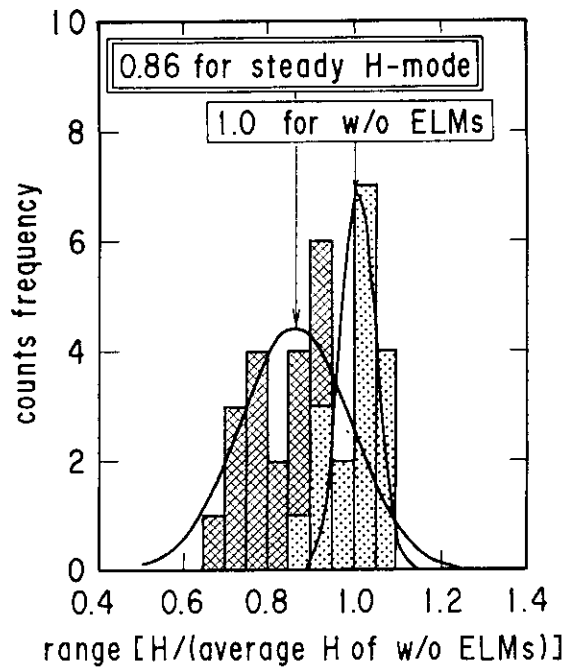


Fig. II.1.2-5
Histogram of the H-mode enhancement with and without ELM.

suppresses the increase of density and radiation with keeping temperature. Figure II.1.2-6 shows the dependence of the power threshold and the steady region on the high-m mode of EML coil current. The power threshold increases with increasing EML coil current (maximum 5.5 kA = 44 kAT), and the controlled region of the steady state H-mode can be seen as a belt above its power threshold. The controlled region increases with increasing the ergodic field. This demonstrates an active controllability of the H-mode[1.2-5].

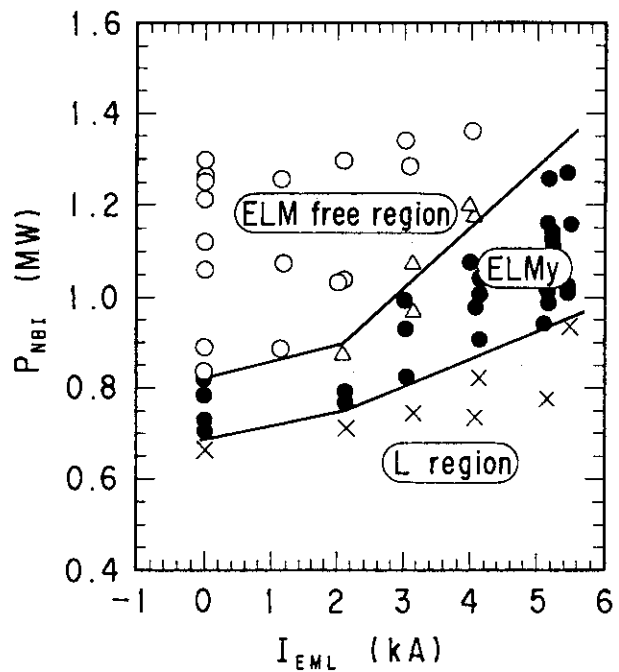


Fig.II.1.2-6 Power threshold and controlled region of the H-mode by the high-m ergodic field.

1.2.3 Divertor bias experiment

The divertor bias experiments started May in this year on the JFT-2M tokamak to study the possibility of improvements of tokamak performance such as confinement, edge stability and non-inductive current drive.

The characteristics of JFT-2M divertor biasing system are as follows(Fig.II.1.2-7);

- * Biased divertor consisting of 34 carbon plates (inside 16 and outside 18).
- * Two biasing power source; the condenser (300V,1.7F) between divertor plates and vacuum vessel for uniform biasing and the thyristor power supply (250V,10kA) between inner and outer divertor plates for differential biasing.
- * Open and semi-closed divertor operation.

The preliminary experimental results by using the condenser power source are as follows;

- * For ohmic heating phase, H_{α} emission was reduced by 15-30 % by negative uniform biasing and the mean electron density increases gradually, which means the improvement of particle confinement. The total radiation slightly decreases.
- * The biasing current is about -200A at the negative biasing of -150V, which consist of the ion (inner) side current of -250A and the electron (outer) side current of 50A.

For no biasing case the natural current of about 80A which flows from the electron side plates to ion side plates, it seems, driven by the thermal force, was observed.

- * For NBI heating case, the threshold power for L/H transition could be reduced by about 200kW (from 340kW to 140kW in deuterium plasma) due to the negative biasing of about 80V. The potential formation with negative gradient at just outer separatrix (about 2 cm) was observed (Fig.II.1.2-8).

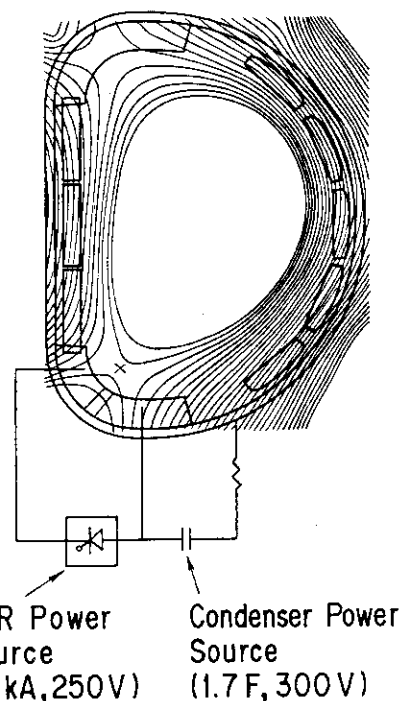


Fig.II.1.2-7 Divertor biasing system diagram of JFT-2M(two biasing power sources. 34 carbon plates are biased (inside 16, outside 18)).

References

- [1.2-1] S.SENGOKU, et al., J. Nucl. Mater. **145/147** (1987) 556.
- [1.2-2] M.MORI, et al., Nucl. Fusion **28** (1988) 1892.
- [1.2-3] Y.MIURA, et al., 'Characteristics of Pellet and Neutral-Beam Injected Single Null Divertor Discharges of the JFT-2M Tokamak' JAERI-M 86-148.
- [1.2-4] T.SHOJI, et al., in Controlled Fusion and Plasma Physics (Proc. 17th Eur. Conf. Amsterdam, 1990), Part. 3, European Physical Society (1990) 1452.

[1.2-5] Y.MIURA, et al., in Plasma Physics and Controlled Nuclear Fusion Research (Proc. 13th Int. Conf. Washington, 1988) IAEA-CN-53/A-4-6.References

[1.2-6] T.Shoji, et al., Abstract of 1990's JPS Meeting (1990, Oct. Gifu) 3aS2; to be published in paper.

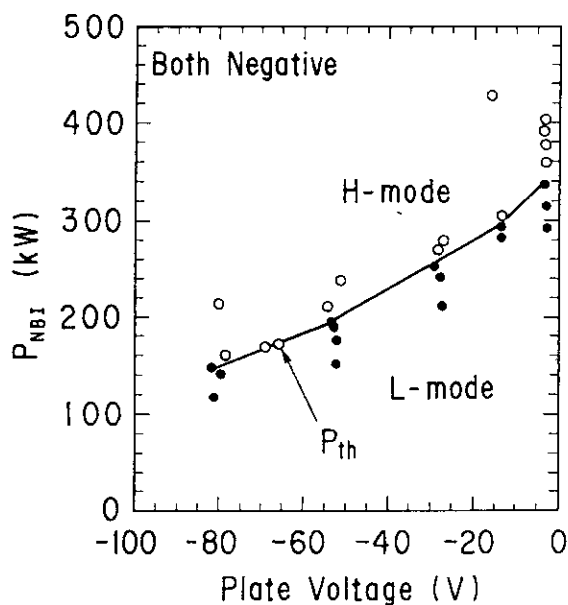


Fig.II.1.2-8 Reduction of threshold power for L/H transition by uniform (unipolar) negative biasing.

1.3 RF experiments

1.3.1 Coupling studies of a phased array antenna for fast wave current drive

Fast wave current drive (FWCD) by using a phased four-loop array antenna has been investigated experimentally in the JFT-2M tokamak. The RF output power of 0.8 MW is available and the frequency is 200 MHz, which corresponds to approximately the tenth harmonic of ion cyclotron frequency of hydrogen. In the previous experiment, an appreciable electron heating by the fast waves was performed successfully by using the antenna which has a refractive index of $N_z \sim 7$ at the phasing of $\Delta\phi=(0,\pi,0,\pi)$. However, no electron heating with the highly directional wave phasing of $\Delta\phi=(0,\pi/2,\pi,3\pi/2)$, which is preferred for the current drive, was observed because of the spectral gap. A new antenna having $N_z \sim 6$ at $\Delta\phi=(0,\pi/2,\pi,3\pi/2)$ has been employed to improve absorption of a directionally propagating wave. The new antenna has, however, indicated lower loading resistance and stronger mutual coupling between the loop antennas.

We have developed a tuning procedure for multiple transmission lines including mutually coupled antennas [1.3-1] since the new antenna has made the tuning difficult. This procedure at first identifies the antenna impedance using measured data and second searches for the optimum operating parameter conditions. The whole process is repeated so that predicted operating parameters realize good performance. The usefulness of this procedure has been confirmed experimentally. Nearly satisfactory performances for $\Delta\phi=(0,\pi/2,\pi,3\pi/2)$ and $(0,\pi,0,\pi)$, corresponding to current drive and heating modes, have been realized by repeating the whole tuning process twice.

Meanwhile, a new coupling code has been developed for an antenna array of the fast waves [1.3-2]. The self-consistent current profile on current strap can be obtained by using the variation theory. The coupling properties of four loop antenna array for the experiments was investigated with comparison of calculation and experimental results. The calculation can explain well the complicated coupling properties obtained experimentally. Fig.II.1.3-1 shows the phase dependence of the loading resistance. The calculation also indicates that a down shift of a peaked N_z of the excited fast waves is remarkable for low electron density. The down shift of N_z makes the spectrum gap large and then lessen the absorption of the fast waves. The down shift of N_z can, however, be improved by a steep electron density gradient nearby plasma edge.

An appreciable interaction of the fast waves with electrons by the new antenna has been observed with combination of the electron cyclotron heating $P_{ECH}=0.17$ MW. The launched power of the fast waves is about 0.25 MW, which is limited by withstanding voltage of the tuning circuit. At $\Delta\phi=(0,\pi/2,\pi,3\pi/2)$, the tail electron temperature measured from a soft x-ray pulse height analysis increases slightly but the loop voltage does not change. As shown in Fig.II 1.3-2, we have observed increased electron temperature at the plasma center and drop of the loop voltage at $\Delta\phi=(0,0,\pi,\pi)$, which has the same peaked N_z as that of $\Delta\phi=(0,\pi/2,\pi,3\pi/2)$ but bidirectional propagating waves. The figure also shows the bremsstrahlung radiation which infers increase in effective charge at application of the fast waves

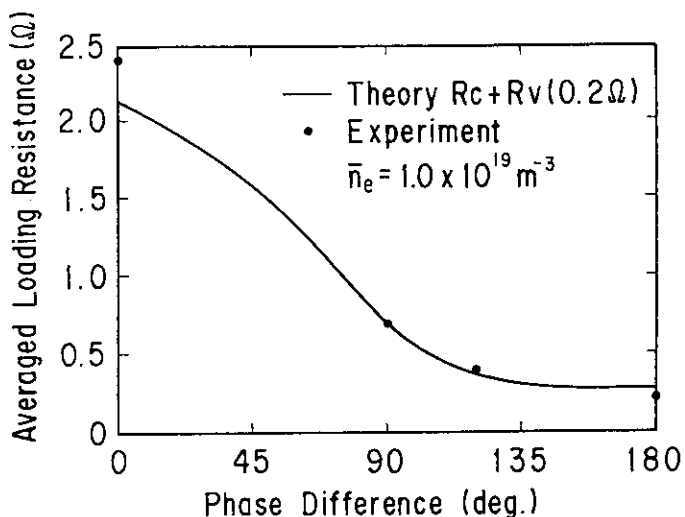


Fig.II.1.3-1 Phase dependence of the averaged loading resistance. The close circles and the solid line indicate the averaged loading resistance measured and calculated, respectively.

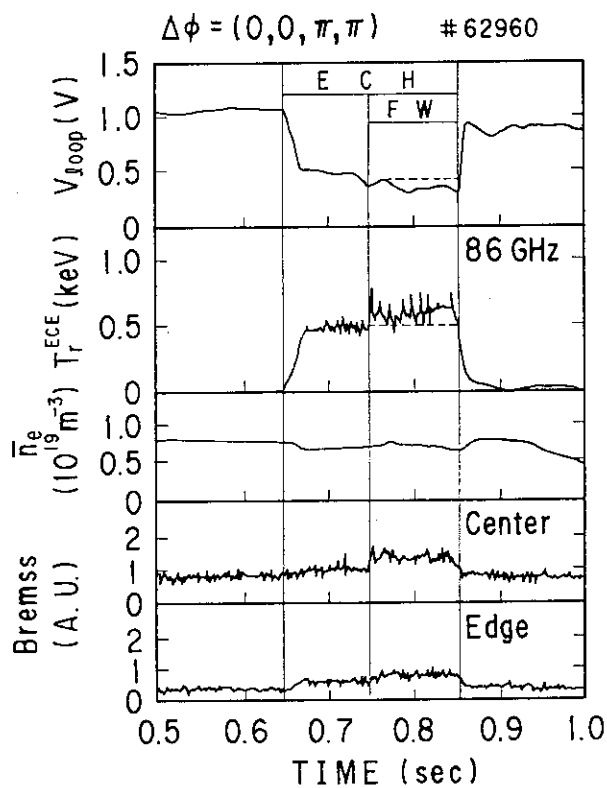


Fig.II.1.3-2 The time behavior of the loop voltage V_l , the radiation temperature of cyclotron emission T_r , line averaged electron density n_e and the bremsstrahlung radiation. $I_p=100$ kA, $B_t=1.07$ T, $P_{ECH}=170$ kW and $P_{FW}=240$ kW.

pulse. Analysis of the plasma resistivity suggests non-thermal electrons generated by the fast waves.

1.3.2 Preionization and plasma current initiation by using electron cyclotron heating

Experiments on plasma production (toroidal magnetic field and gas present) and plasma current initiation (toroidal magnetic field and gas prior to an ohmic discharge) have been performed with electron cyclotron heating (ECH) on the JFT-2M tokamak. The ECH system consists of two gyrotron, capable of producing 200 kW at frequency of 60 GHz for up to 0.5 s, and two transmission lines[1.3-3]. Second harmonic extraordinary mode was launched from the outer side of torus at the mid-plane.

Investigation on the plasma production by ECH was conducted with a range of gas filling pressure p between 3×10^{-5} and 5×10^{-4} Torr, applied vertical field $B_v=0.0-38$ Gauss and of the toroidal magnetic field of $B_t=0.8-1.28$ T. We have obtained the maximum line integrated electron density $n_{el}=0.3 \times 10^{19}/m^2$ at $p=3.4 \times 10^{-4}$ Torr, $B_v=27$ Gauss and $B_t=1.07$ T with the ECH power of 180 kW. From a spatial profile measurement of H_α radiation, plasma production is inferred to be localized at the electron cyclotron resonance layer with full-half width of ~ 20 cm in the major radial direction. This indicates the maximum line averaged electron density of $1.5 \times 10^{19}/m^3$ which is close to the cut-off density of the second harmonic extraordinary mode.

Current initiation for a start-up of the ohmic discharge with ECH has been investigated by changing the applied primary voltage which is operated to keep constant during the discharge. The ECH power is 180 kW and $B_t=1.06$ T. Fig.II.1.3-3 shows the typical time evolution of the plasma parameters and the ECH pulse. It is found that with ECH most of the loop voltage V_1 is consumed to make the ramp-up of the plasma current I_p , e.i., $V_1 \sim L_p dI_p/dt$ where L_p is the inductance of the plasma column. The electron cyclotron emission indicates appreciable energetic electrons generated by ECH which lead to lessen the plasma resistivity. We have also achieved that the plasma current is ramped-up with the loop voltage of 0.4 volts at the rate of 0.25 MA/s.

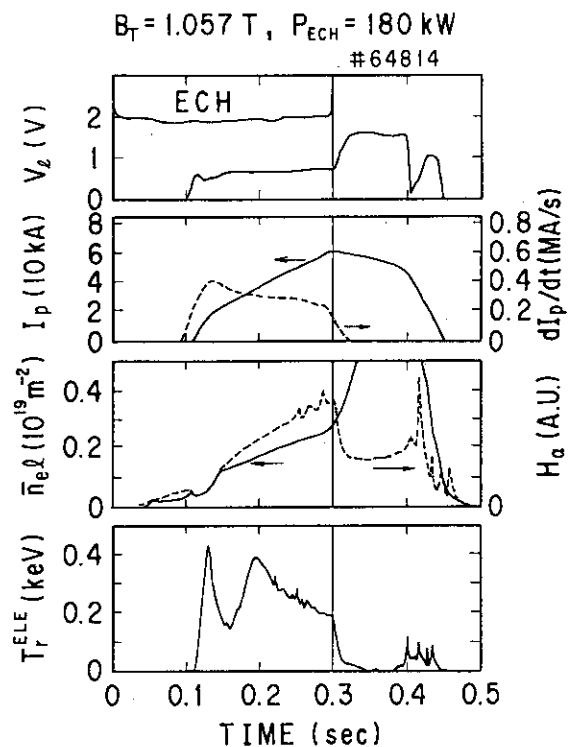


Fig.II.1.3-3 The time evolution of the plasma parameters for the initiation of the plasma current with ECH. dI_p/dt is the time derivation of the plasma current.

The minimum loop voltage to initiate the current seems to depend on controllability of a position of the plasma current channel.

References

- [1.3-1] H.Kazumi, et.al., in Proc. 18th EPS Conf. Berlin Part III (1991) 329.
- [1.3-2] M.Saigusa, et.al., private communication.
- [1.3-3] M.Kawashima, et.al., Nucl.Fusion 31 (1991) 495.

1.4 Diagnostics

1.4.1 Impurity behavior on JFT-2M

Sawtooth activities play the important role on the impurity transport. In JFT-2M impurity behaviors in discharges during the neutral beam (NB) heating concerned with sawtooth activities were studied by using the grazing-incident monochromator (3-60nm) and the 1-D impurity transport code (MIST code) [1.4-1]. The impurity transport during the ELM-free H-mode with and without clear sawtooth activities were presented. By changing the plasma current (I_p), the amplitude of sawtooth activities was controlled in these experiment. In discharges with high- I_p ($I_p=0.28\text{MA}$, $q_s=2.7$ where q_s is the safety factor at the plasma surface), clear sawtooth activities were observed, while no large sawtooth activities in the discharge with low- I_p ($I_p=0.17\text{MA}$, $q_s=4.0$). The position of $q=1$ surface, which was determined by the sawtooth inversion radius, was that $r=0.12\text{m}$ in the high- I_p discharge and $r=0.06\text{m}$ in low- I_p discharges. The H-mode transition occurred about 5ms earlier in high- I_p discharges but the electron density and radiation losses in low- I_p discharges increased with time more rapidly. From detailed measurement of time evolutions of the emissions from impurity ion lines in both discharge conditions, emissions from highly ionized ion lines such as TiXX, FeXVIII and FeXIX increased faster in low- I_p discharge although emissions of less ionized ion lines such as TiXI, CIV, and FeX were almost the same. The measured radial profile of Ti^{19+} ion density in low- I_p discharges became more centrally peaked. In the previous work on JFT-2M, impurity ions were accumulated into the plasma center during the ELM-free H-mode [1.4-2]. These experimental results suggest that the impurity accumulation was more enhanced in low- I_p discharges although the influx in both discharges were almost the same. These impurity behaviors were analyzed by using MIST code. Measured electron temperature and density were used and the corona equilibrium was assumed to calculate line emissions. Transport coefficients (diffusion coefficient (D) and convective velocity (v_{in})) were determined to fit the intensity ratio of TiXX and TiXV line emissions, and the measured and calculated Ti^{19+} ion density profile shown in Fig.II. 1.4-1. The obtained transport coefficients in both discharges were that $D/D_{NC}>10$ at the inside of the $q=1$ surface and $D/D_{NC}<2$ at the outside of the $q=1$ surface, and $v_{in}/v_{NC}=1$, where D_{NC} and v_{NC} were the transport coefficients calculated from the neoclassical theory [1.4-3]. These results indicate that the impurity ions exhausted from the inside of the $q=1$ surface by the sawtooth activities. By using these transport coefficients, the radiation power loss of the titanium ion (P_{RadTi}) near plasma center were estimated. Obtained

results were that $P_{\text{RadTi}}=8.6 \times 10^{-3} \text{ W/cm}^3$ in low- I_p discharges and $P_{\text{RadTi}}=3 \times 10^{-3} \text{ W/cm}^3$ in high- I_p discharges which were qualitatively agreed with that the radiation loss profiles measured by the bolometer array.

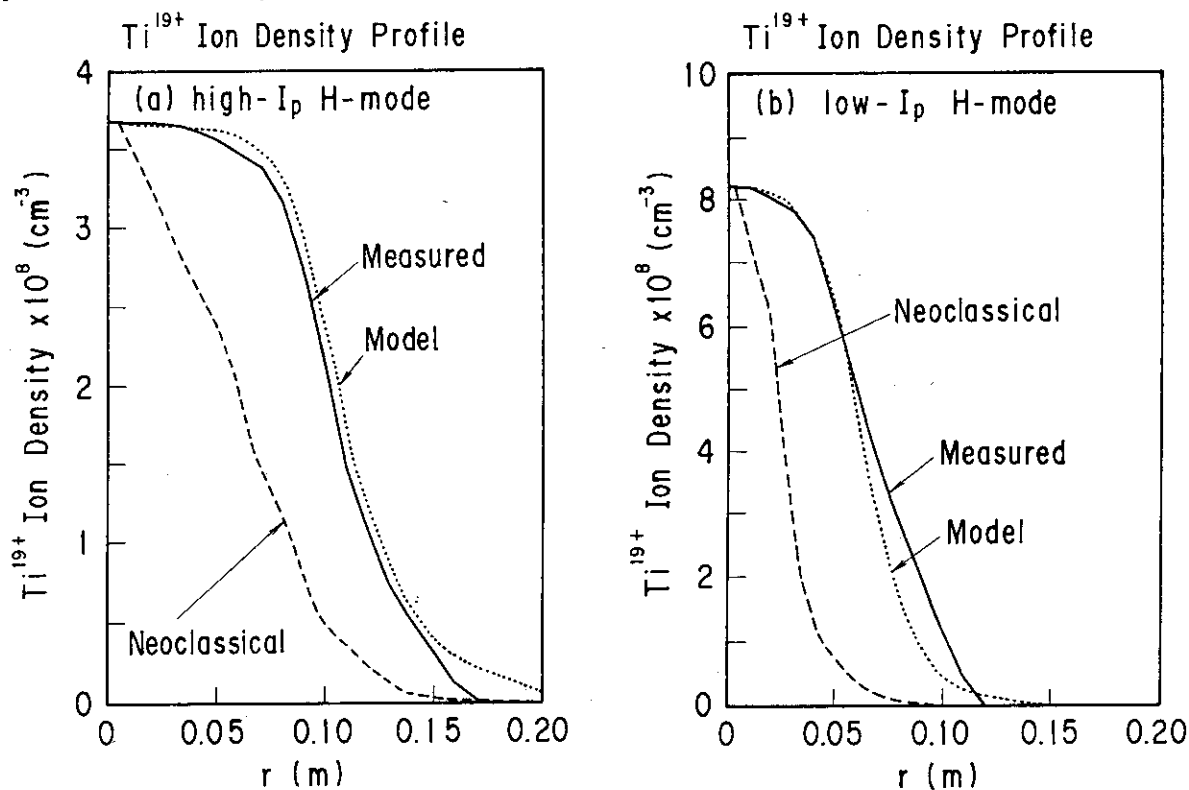


Fig.II.1.4-1 Measured (solid line) and calculated (dashed line) Ti19+ ion density profiles in high- I_p (a) and low- I_p (b) discharges.

References

- [1.4-1] R.A.Hulse; Nucl. Technology/ Fusion 3 (1983) 259.
- [1.4-2] H.Ogawa, et al. ; J. Phy. Soc. Jpn. 59 (1990) 3962.
- [1.4-3] P.H.Rutherford, et al.; Princeton Plasma Physics Laboratory Report PPPL-1297 (1976).

1.4.2 Development of TV Thomson scattering system with high spatial resolution and high sensitivity

A high spatial resolution Thomson scattering system is being installed on the JFT-2M tokamak in a collaboration between JAERI and PPPL. A total of 81 spatial channels are distributed along a major radius chord on the horizontal midplane of the tokamak, allowing for a spatial resolution better than 1 cm (plasma width of 70 cm). The system is based on a single detector constituted of two imaging tubes in series and a CCD detector (385x288 pixels). The background plasma light can be measured either by 10 background spatial channels located along the 81 channels mentioned above (with a toroidal offset of about 1 cm) or by taking a second exposure at a few ms after the laser pulse. The system will generate T_e and n_e profiles with an expected operational range of 50 eV to 8 keV and $(0.1-0.3) \times 10^{13}$ to $4 \times 10^{14} \text{ cm}^{-3}$.

A few topics of this development are described below as follows;

1) Laser subsystem

A TEM₀₀ mode was obtained with the fix of aperture within the laser cavity. The measured beam divergence 0.3 mr was almost equal to the diffraction limit. The laser system oscillated with a few longitudinal modes, and it was a problem since they produced high peak power and low laser energy. The installation of an intracavity mirror (glass plate with an AR coating) has removed the above problems and produced a Gaussian shape waveform. The results is shown in Fig.II.1.4-2, where the waveform of Gaussian type is produced by overlapping the additional longitudinal modes on the fundamental longitudinal modes.

2) High spatial resolution optics subsystem

An important feature of the system is the low number of the collecting optics, see Fig.II.1.4-3. It is a Bouwers concentric (mirror) optics of the type which has been developed at PPPL for the Thomson scattering diagnostics. With such a construction, the collecting optics aperture of each spatial channel spans the whole vacuum window. The folded optics of the system is also compact and well suited for imaging onto fiber optic bundles. The laser beam path is imaged (by the concentric optics) on a non flat surface on which the fiber bundles are located. The use of coherent fiber bundles allows for high spatial resolution.

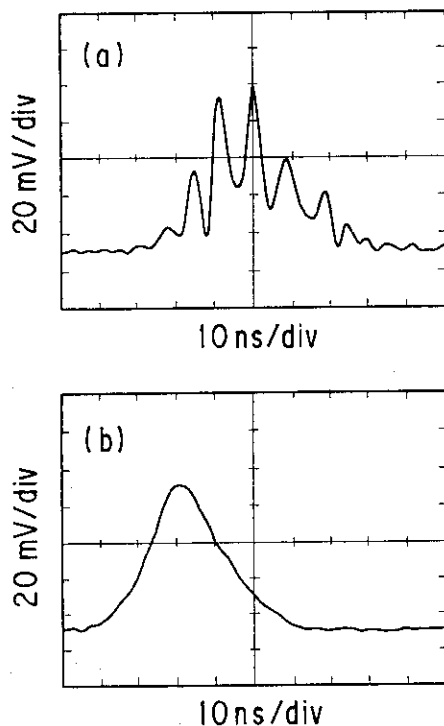


Fig.II.1.4-2 Pulse waveform of ruby laser beam; (a) without additional mirror, (b) with additional mirror.

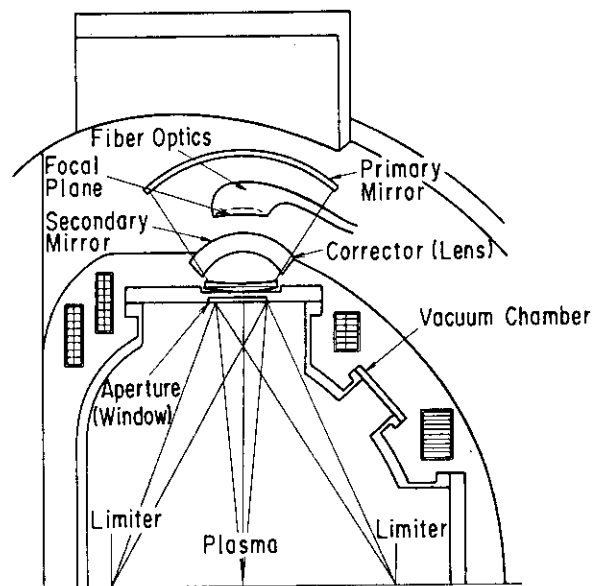


Fig.II.1.4-3 Cross-section of JFT-2M showing the Thomson scattering collecting optics with Bouwers concentric double mirror

3) High sensitivity detector subsystem

The detector is composed of two image intensifiers and CCD camera. The intensifier has a gain of 70 and decrease the image size to one fifth. The second intensifier has a magnification of 0.6 and a gain of 300. Fast phosphors are used to allow successive measurements within a few millisecond. The CCD camera works in frame transfer mode and has a high quantum efficiency. The sensitivity of the detector is expected to be comparable to that used on the TFTR Thomson scattering system.

2. Operation and Maintenance

2.1 Introduction

Facility operation and Engineering Division has been engaged in operation and maintenance of flywheel motor-generator (MG), JFT-2M machine, neutral beam injection system (NBI), electron cyclotron heating system (ECH) and fast wave current drive system (FW). In this fiscal year, each apparatus has been operated smoothly on schedule, and careful examination of machine status has been performed daily and periodically. In another field on development of auxiliary equipments and instruments, pellet injection system has made good progress and installation of new control coils placed inside of vacuum chamber has started for the plasma disruption study.

2.2 Operation and maintenance

Summary of operation records in each apparatus is listed in Table II.2.2-1. Each apparatus has been operated smoothly according to the experimental schedule and has paved the way for good experimental results. Maintenance works and overhauls have been carried out during machine vent period. In this fiscal year, regular examination of the motor-generator and its cooling system and periodical cleaning of carbon dust were performed, and old filter chambers in the MG building were replaced by a new one. As for JFT-2M machine, overhaul of cryo-pump, replacement of vacuum gate valve, repair of feedthrough parts in the divertor-bias system and renewing of secondary cooling towers were performed. As for heating apparatus, minor overhaul of NBI power supply, adjustment of ion-source alignment, test of new ECH power supply and a new gyrotron, overhaul of FW stab-tuners and repair of FW antenna were carried out.

2.3 Development of equipments and instruments

A gun assembly of a multi-pellet injector, extruder type, was modified to get large pellets and a high velocity in 1989 as shown in Fig. II.2.3-1. An extrusion nozzle was changed from rectangular cross-section to circular one. A diameter of an extruding solid-hydrogen filament is 4 mm. A cutting tube with a knife edge, which is mounted on a punch-type chambering mechanism, and a gun barrel are 3 mm in diameter. A delivering pellets size is 3 mm in diameter and 4 mm in

Table II.2.2-1 Operation records of MG, JFT-2M, NBI, ECH and FW.

Fiscal Year Apparatus		FY 1989	FY 1990				Total	
			APR-JUN	JUL-SEP	OCT-DEC	JAN-MAR		
MG	MG(#1) Operation (hours)	868	274	341	253	136	1,004	
	MG(#2) Operation (hours)	866	273	340	254	136	1,003	
JFT-2M	Total Operation (days)	112	36	46	35	18	135	
	Discharges Numbers (shots)	5,902	1,359	2,287	1,738	689	6,118	
	Discharge Cleaning (hours)	175	73	65	51	29	218	
	Baking (times)	2	1	0	1	0	2	
	Pellet Injection (days)	22	3	4	3	3	13	
NBI	Total Operation (days)	85	24	28	14	14	80	
	Total Shots of Injection (times)	A-line	43,770	11,082	12,456	6,943	6,884	37,365
		B-line	41,527	11,565	14,828	7,378	4,884	38,655
ECH	Total Operation (days)	25	10	19	16	6	51	
	Total Injection (times)	94,775	7,201	127,414	16,967	5,548	157,130	
FW	Total Operation (days)	57	16	6	20	0	42	
	Total Injection (hours)	460	110	42	168	0	320	

length. Two fast-opening magnetic valves were used to get a higher repeating rate, which were able to alternately open at time-intervals of 100 ms. The rise time for full-open of the valves is less than 0.5 ms. A propellant gas, helium, which is pressurized to 100 kgf/cm², can be heated at 100 C. In this configuration, the performance tests have been done. Velocities of up to 1.7 km/s were measured with hydrogen pellets at the pressure of 100 kgf/cm². The unique feature of this injector is its repetitive capability. Delivering rates of 2-2.5 Hz were easily obtained with large size pellets. The operating limitation has been attributed to a heating of the gun block above the freezing point for the hydrogen by the propellant (298 K) and consequent melting of the filament before it enters the pellet chambering section. However, the injector could operate at higher firing rates on several tests. The shadowgraphs in Fig.II.2.3-2 show 8 consecutive hydrogen pellets that have been delivered at time-intervals of 300 ms (pellet velocity=0.9-1 km/s). To accomplish this operation, the open time of the propellant valves was minimized to decrease the thermal gas loading.

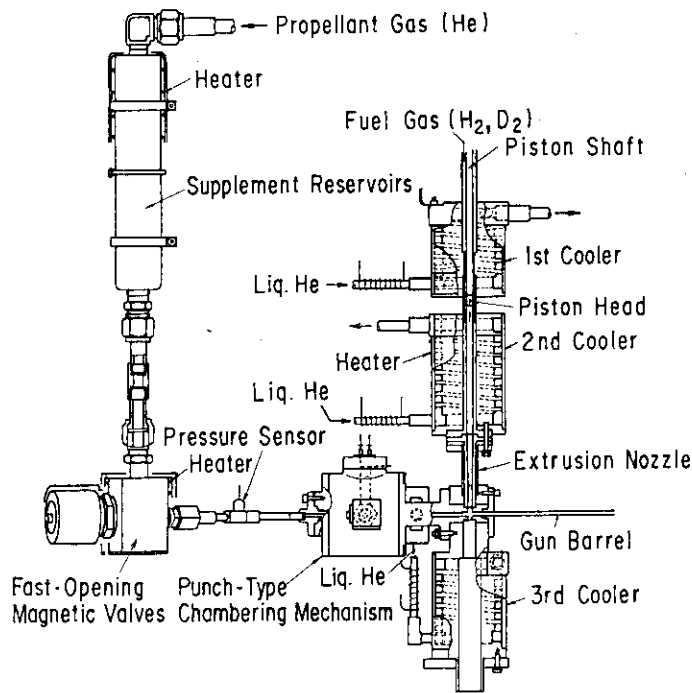


Fig.II.2.3-1 Gun assembly of the multi-pellet injector.

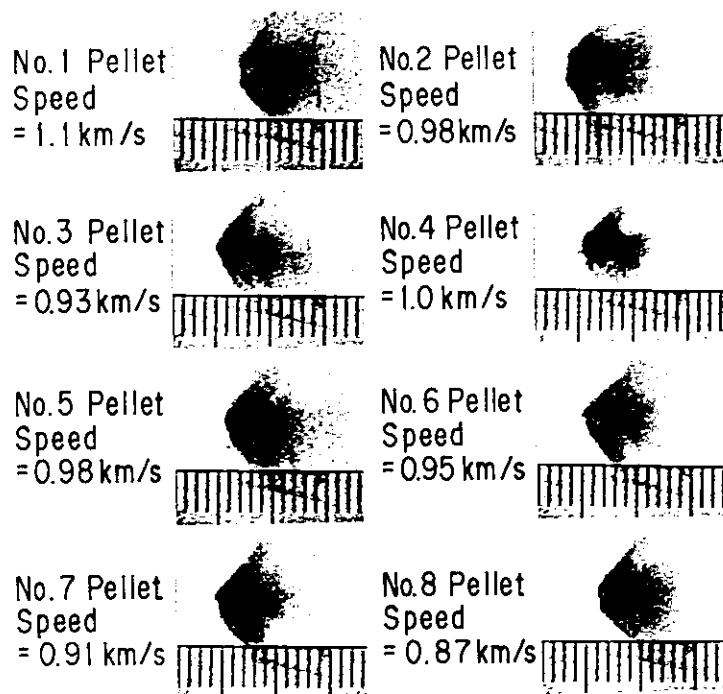


Fig.II.2.3-2 Shadowgraphs of hydrogen pellets. Delivering interval is 300 ms. Propellant gas pressure is 33 kgf/cm². Barrel length=0.8 m.

III. COOPERATIVE PROGRAM ON TOKAMAK EXPERIMENT

1. DIII-D (Doublet III) Experiment

1.1 Introduction

The long-term research objective on DIII-D continues to be the development of understanding and predictive capability leading to a demonstration of a high beta plasma with non-inductively driven toroidal current and good confinement. This year, 11 papers based on many significant DIII-D experimental results were presented at the 13th IAEA meeting in Washington. In addition, DIII-D made highly regarded contributions to 17 of 23 physics R&D tasks associated with the ITER conceptual design activity.

1.2 Highlights of FY1990 research results and device improvements

DIII-D operations in the past year were highlighted by the attainment of 11 % beta, a value nearly twice that needed for ITER, with a highly elongated, double null diverted plasma. Sufficient understanding of the physics and phenomenology of ELMs (Edge Localized Modes) enables the utilization of ELMs for impurity control, which has resulted in 10.3 second long H-mode discharges with continuously declining impurity levels (Fig.III.1-1).

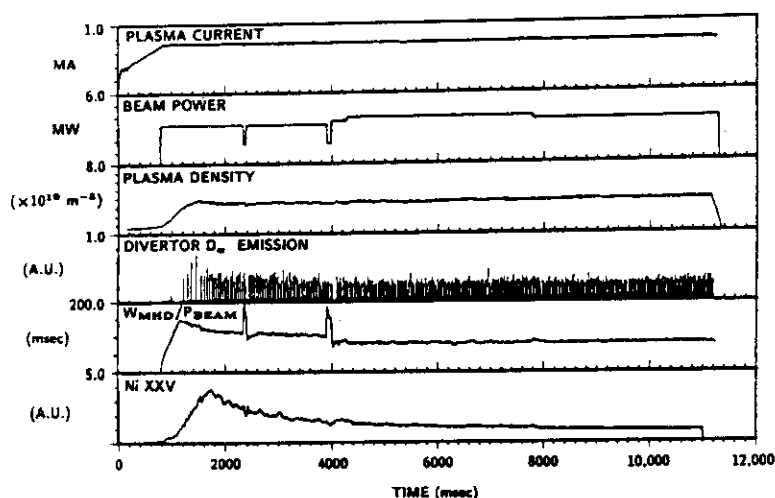


Fig.III.1-1 Ten second H-mode impurity control via ELMs [1-1].

Installation of an advanced divertor ring and baffle were completed during the last year (Fig.III.1-2). The advanced divertor system allowed DIII-D to demonstrate a reduced H-mode power threshold and increased particle flow to the divertor baffle chamber when electrical bias was applied.

In addition, important tokamak physics findings relevant to future devices have also been steadily resulting from the DIII-D, such as poloidal current flow to the

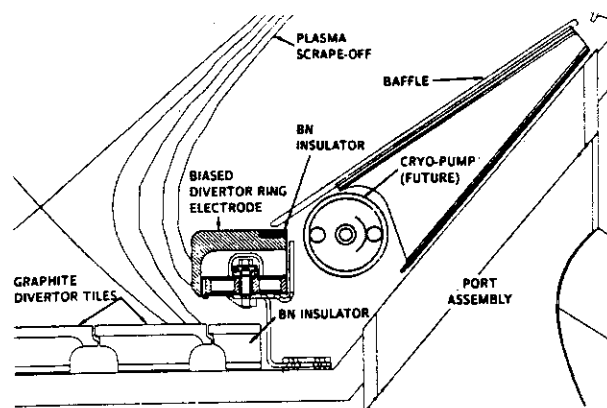


Fig.III.1-2 A view of the DIII-D advanced divertor showing the bias ring and the plate. Also shown is a cross section view of a cryopump, planned for future installation [1-2].

vessel wall during a vertical instability.

When the parallel fast ion beam velocity approached the Alfvén velocity and the volume-averaged beam beta exceeded 2 %, localized, propagating high frequency MHD oscillations with $n=2-10$ have been observed. This may represent a first experimental observation of Toroidicity-induced Alfvén Eigenmodes, although the threshold value is an order of magnitude larger than predicted [1-3].

A sudden increase in the edge electric field has been observed to be correlated with the L to H-mode transition and a decrease in plasma fluctuation is measured (Fig.III.1-3). These new observations are also being compared to H-mode theories. As for the diagnostic capabilities, following new diagnostic systems have been commissioned this last year: (1) multi-pulse Thomson scattering system, (2) single channel motional Stark effect current profile diagnostics produced by LLNL, (3) 280 GHz carinatron-scattering system for turbulence studies by UCLA, (4) correlation reflectometer by UCLA, and (5) divertor materials exposure system-DIMES.

Construction of a 2 MW, 110 GHz ECH system is proceeding and the first gyrotron is prepared for installation. The 2 MW 60 GHz ECH system was used for heating and current drive experiments. The heating experiments included ECH H-mode studies and the electron thermal transport studies. Approximately 100 kA was driven by inside launch extraordinary mode ECH in 300 kA tokamak discharges. Fokker-Planck calculations estimating tail enhancement by the remaining electric field show this effect may account for the increased ECCD efficiency (Fig.III.1-4). A new fast wave ICH antenna was operated with 1MW power levels and ion heating was demonstrated in the initial experiments.

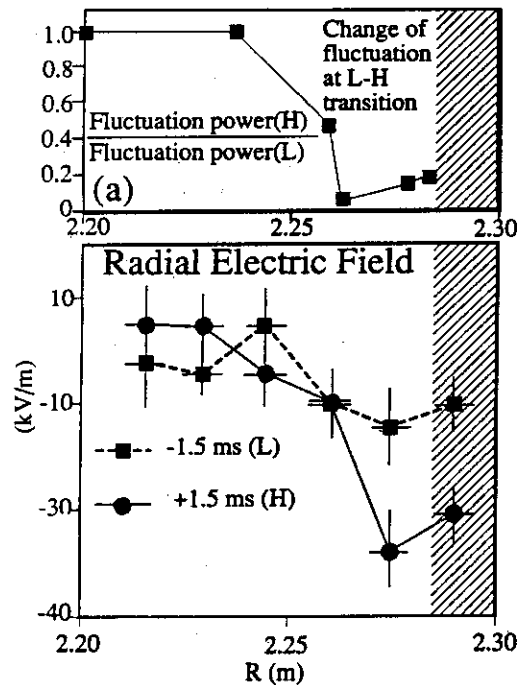


Fig.III.1-3 Comparison of sheared radial electric field (b) and suppression of the edge fluctuation (a) at L-H transition [1-4].

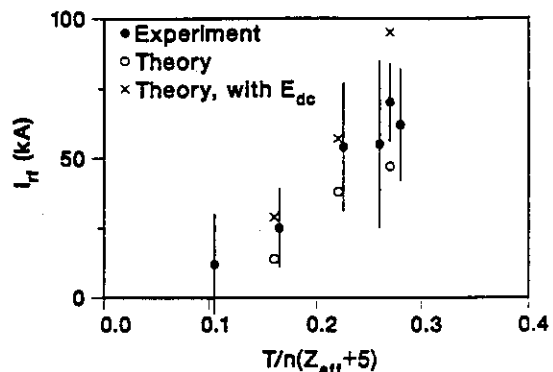


Fig.III.1-4 Current driven by ECH, measured and Fokker-Planck predictions with (x) and without (o) electric field effects on the electron distribution function [1-1].

1.3 JAERI collaboration

During JFY 1990, a total of five JAERI scientists made substantial contributions to the productivity and progress of the DIII-D experimental program. Their research has supported both the DIII-D and JAERI program efforts in the areas of H-mode physics, ECH, and tokamak diagnostics. The DIII-D fluctuation studies have been coordinated by a JAERI scientist while General Atomics and the US university participants pursued L-H transition and transport studies. JAERI personnel also participated in the development of the Motional Stark Effect polarimeter and in the broad band x-mode microwave reflectometer measurement. A database for the sawtooth period, constructed from DIII-D data, indicates the period scales as plasma resistivity[1-5]. These activities were of direct benefit to both the DIII-D and JT-60U near and long term experimental programs including physics R&D activities identified by ITER.

The continuation of the DIII-D collaboration is under consideration (The current Agreement will expire on August 28, 1992.). The two working groups have completed their assessment of the proposed joint program on high power ECH heating and current drive on DIII-D and JT-60U. The preliminary design for JT-60U EC heating device has also been completed. Initiation of this new program depends on availability of JAERI funding.

1.4 Plans for the next year

During the next year the DIII-D program will emphasize advanced divertor, transport, fast wave current drive, and initial 110 GHz ECH experiments. These experiments will be carried out with boronization techniques learned through the TEXTOR collaboration and new diagnostics added to DIII-D. Heating and current drive will be explored with ECH, ICRF and neutral beams.

References

- [1-1] DIII-D Research Operations Annual Report, GA-A20361(1991) and DIII-D Team, IAEA-CN-53/A-1-4(1990).
- [1-2] M.A. Mahdavi et al., GA-A20317(1990).
- [1-3] W.W. Heidbrink et al., GA-A20254(1991).
- [1-4] H. Matsumoto et al., GA-A20383(1991).
- [1-5] Y. Kamada et al., to be submitted.

2. Microwave Tokamak Experiment

2.1 Present status of MTX experiment

During the period April, 1990 to March 1991, the major FEL experimental activity was experiments by the LLNL accelerator group to test improvements to the ETA-II induction linear accelerator.

In parallel with the FEL effort, a Varian gyrotron (140 GHz, 400 kW CW) was installed. The gyrotron will provide the oscillator power for the FEL. In addition, tokamak plasma heating experiments will be compared with the pulsed, high peak power heating due to the FEL in order to compare the two different microwave interaction regimes.

2.2 JAERI activity

JAERI provided diagnostics on schedule. During gyrotron operation, they made significant contribution. A calorimeter, which will be used with the FEL, was used to determine the efficiency of transport of microwave power from the gyrotron to the MTX using the quasi-optical system. The measurement yielded an efficiency of 80 %, in good agreement with theory which predicted 20 % losses at the Vlasov convertor. The convertor changes high order gyrotron modes into Gaussian mode for coupling into the transmission line. JAERI also provided more efficient Vlasov convertor this year, which was tested using low power test stand at Stuttgart University in Germany.

Measurements were made by the fast soft X-ray camera[2.2-1] and neutron diagnostics[2.2-2] during brief tokamak experimental run using the gyrotron. The ECE heterodyne diagnostics was successfully tested in an experimental run during June. The final system was installed in September. A prototype of reflectometer was delivered to LLNL this fiscal year.

References

- [2.2-1] K.Ohasa, T.Ogawa, K.Hoshino, et al., IAEA TCM Report on Time Resolved Two and Three Dimensional Plasma Diagnostics (Nov. 1990, Nagoya Japan).
 [2.2-2] T.Ogawa, K.Ohasa, K.Hoshino, et al., Rev. Sci. Instrum. **61** (1990) 3181.

2.3 LAPPS (Laser Aided Particle Probe Spectroscopy) [2.3-1]

A diagnostic system for measuring the microwave electric field of a free electron laser (FEL) has been prepared at JAERI, whose design was a collaboration with Hiroshima University, LLNL and U.C.Davis. This diagnostic uses the Stark effect, and it consists of a 50 kV/400 mA neutral helium beam, a tunable dye laser, and spectroscopic equipment. The whole system is shown in Fig.III.2.3-1. Xenon is used as the helium beam neutralizer gas to produce metastable atoms with high density. Because of the restricted viewing-port size in MTX tokamak, we collect emitted light through two of the narrow slots. The LAPPS equipment is close to the MTX tokamak, so the ion source, neutralizer cell, and photomultiplier tube are shielded against magnetic fields of 250, 750 and 1000 G, respectively. The various components were first combined at JAERI for alignment, conditioning, calibration and test measurement with a DC electric field at first. Then, the entire system is going to be shipped to LLNL for installation on MTX.

References

- [2.3-1] T.Oda, K.Odajima, K.Mizuno, et al., Rev. Sci. Instrum. **61** (1990) 1.

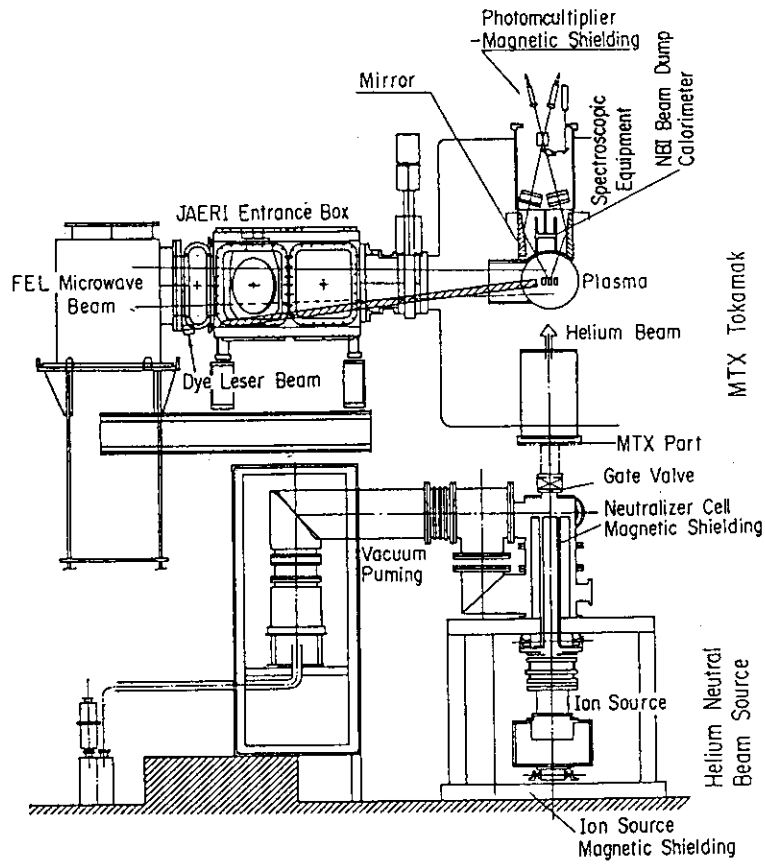


Fig.III.2.3-1 A diagnostic system for measuring the microwave electric field of a free electron laser.

IV. JT-60 PROGRAM

1. Overview

Since November 1989, JT-60 had been shut-down for the modification to the JT-60 Upgrade. In JT-60 Upgrade, the plasma current will be increased up to 6MA with lower single null divertor. The poloidal field coils and the vacuum vessel are being replaced for this modification. NB heating power of up to 40 MW and total ~20MW of LH and ICRF will be available with using deuterium as the working gas. The major radius and the toroidal field will be 3.4m and 4.2T, respectively. Plasma parameters are expected to further approach the reactor range. The divertor plates is designed to be toroidally continuous, and to use high-heat-conduction c/c composite graphite with the height misalignment of adjoining tiles in less than 0.5mm. About 3sec of period without carbon burst is estimated under ~40MW of injection power. In March 1991, the modification was completed and the discharge cleaning has been started.

The primary objective of JT-60 Upgrade in early phase of its experiment is the impurity control under favorable energy confinement conditions. The development of divertor in particle and heat control will be carried out under the collaboration with JFT-2M and DIII-D. Furthermore the addition of 500keV, 10MW negative NB in 1994, which will be primarily used for NBCD, will be allowed us to investigate physics relating burning plasmas, where the global plasma behavior will be greatly affected by energetic particles.

The future prospects of JT-60 Upgrade research are described in the following.

1.1 Confinement study near the thermal break even condition

Device capability of high power heated deuterium divertor discharge with high I_p of 6MA, B_T of 4.2T and aspect-ratio of 4.0 is expected to extend the present world confinement data base substantially more relevant to the reactor grade plasma. The ITER-89 power-law confinement scaling predicts the fusion gain proportional to $(R/a)^{1.4}$. Relatively high aspect regime of JT-60U ($R/a=4.0$ compared with 2.5 in JET with the same plasma current of 6MA) will substantially contribute to the confinement data base for the next-step device.

1.2 Non-inductive current drive

The regime of negative NB current drive will be $\bar{n}_e I_p \sim 5 \times 10^{19} \text{m}^{-3} \text{MA}$ at $T_e(0) \sim 10 \text{keV}$. With the addition of bootstrap current, full to ~70% non-inductive current drive at $I_p=2-3 \text{MA}$, $\bar{n}_e \sim 5 \times 10^{19} \text{m}^{-3}$ and $\beta_p=1 \sim 1.6$ will be the primary experimental objective. Major research issue in these operation regime is to realize long stable discharges with the bootstrap current fraction of more than 50%. The primary research objective of LHCD will be the enhancement of η_{CD} in high- T_e regime. In the case of LHCD+NBCD, absorption of LH wave by energetic ions might be

a problem. Fully non-inductive current drive of 4MA at $\bar{n}_e \sim 5 \times 10^{19} \text{m}^{-3}$ can be evaluated if the degradation of LHCD is within the range of $\sim 40\%$.

1.3 Energetic particle physics relating burning plasmas

The ability to generate α -particles due to $\text{D} + {}^3\text{He} \rightarrow {}^4\text{He}(3.6\text{MeV}) + \text{p}(14.7\text{MeV})$ reaction with 500keV D-beam at which the fusion cross section peaks will provide a good opportunity to study α -particle behavior prior to D-T operation. A real fusion reaction of 1-1.5MW range is expected. This will provide more confident confinement properties of α -particles compared with the present day's experiment producing fusion reaction of $\sim 100\text{kW}$ using ICRF. The energetic single-particle confinement concerns the effect of non-axisymmetry of the magnetic field of the reactor grade plasmas. The stochastic ripple diffusion effect may cause rapid energetic ion loss. The edge of the JT-60U plasma will have $\sim 2\%$ ripple. Detailed orbit-following Monte-Carlo calculations of this process shows $\sim 30\%$ of 120keV fast ions lost for perpendicular injection in high density discharge, compared with less than 10% loss for tangential injection. The experiment will provide an important data base to evaluate the stochastic ripple diffusion process. The other important issue of burning-plasma physics concerns the collective stability of the α -particle population and its effect on confinement. The negative NB injection experiment may be able to simulate the relevant physics before attempting a burning-plasma experiment. The expected parameter range will be $V \sim 1.4 V_{\text{Alfven}}$ and $\beta_{\text{H}} \sim 1\%$ at $B_{\text{T}} = 3\text{T}$ for 500keV, 10MW H-beam, which seems to be well in the TAE unstable regime.

2. Construction and Developments of JT-60 Upgrade

2.1 Tokamak

2.1.1 Summary of status

In light of recent results that energy confinement and beta value improve with increasing plasma current, the upgrade of JT-60 device (JT-60U) has been decided [2.1-1,2]. Objectives of the upgrade are maximization of plasma performance with minimum modification and collection of physical and engineering database for a design of next tokamak. In the modification the original poloidal field (PF) coil system and vacuum vessel are exchanged for those of large D-shaped cross sections, which allow plasma of up to 6 MA current, 100m^3 volume and 1.4 to 1.8 elongation with lower single null divertor configuration as shown in Fig. IV.2.1-1. The existing toroidal field (TF) coils and their support fixtures are used with reinforcement. The existing high power heating system and the power supply system are also used after minor modification. Neutron shields are added for deuterium operation. Table IV.2.1-1 gives main parameters of JT-60U.

The design work of the upgrade was initiated in 1987 and the fabrications of new PF coil system and vacuum vessel started at the end of 1988. These fabrications were completed from December 1989 to March 1990. Each equipment was transported to the Naka Site according to

its completion. First walls and divertor armors were delivered from July to December in 1990 according to the progress of construction. All construction process completed on mid of February 1991 and the final tests were completed by the mid of March including tests for vacuum leak, baking and overall coil excitement. The TDC started at the end of March.

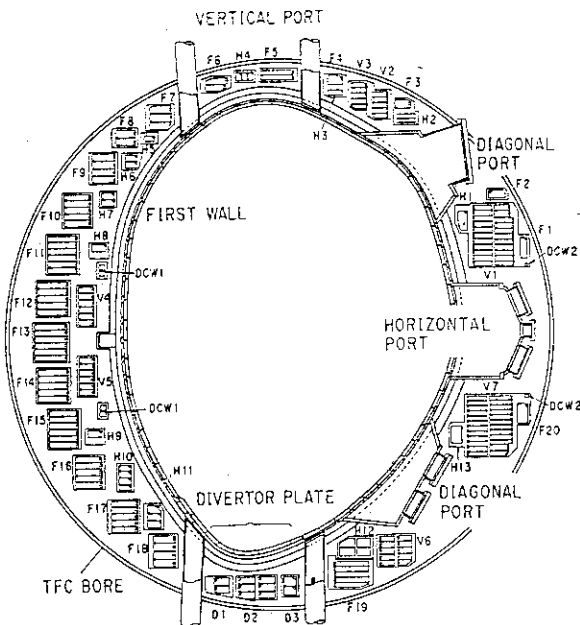


Fig.IV.2.1-1 Arrangement of the poloidal field coils and the vacuum vessel.

TableIV.2.1-1 Main parameters of JT-60U.

Parameters	Divertor	Limiter
Plasma current	6 MA	6.5 MA
Major radius	3.2 - 3.4 m	3.2 - 3.4 m
Minor radius (horizontal)	0.8 - 1.1 m	0.8 - 1.1 m
Minor radius (vertical)	1.5 m	1.5 m
Elongation	1.4 - 1.8	1.4 - 1.8
Plasma volume	< 100 m ³	< 110 m ³
Toroidal field	4.2 T (14.4 T·m)	
Discharge duration	15 s	
Discharge interval	10 ~ 15 min.	
Flux swing	61 V·s	
Neutral beam		
Torus input power	40 MW	
Beam energy	120 kV	
ICRF		
Torus input power	< 5 MW	
Frequency	110 - 130 MHz	
LHCD		
Torus input power	< 10 MW	
Frequency	1.7 - 2.3 GHz	
Pellet injection	< 2.8 km/s, 4 mm ^φ	

2.1.2 Vacuum vessel

Thickness of the vessel as well as that of the armor, were minimized in order to allow largest plasma under the given bore of the TF coil. On the other hand, the vessel suffers from integrated forces of 10 MN and 20 MN in the vertical and horizontal directions due to disruption, respectively. The new vessel must be sufficiently strong against these forces. Therefore a continuous chamber with so called double-skin structure is adopted to obtain a large and thin vessel with sufficient strength. A schematic picture of the vessel structure is shown in Fig.IV.2.1-2.

This structure was determined after stress analyses[4.1-3]. The double-skin structure consists of Inconel 625 inner and outer skins of 6.1 mm thick and poloidally-oriented square pipes of 3 mm thick. The vacuum vessel is supported by 36 support rods at the inner and outer midplane from the PF coil support structure as shown in Fig.IV.2.1-2. This support structure was designed comparing the stress analysis results of vessels supported at the midplane and at the bottom. The vessel is cooled and baked with nitrogen gas circulating through channels between the skins and pipes. It can be baked out up to 300 °C.

It is one of the most important issues to maintain a plasma in an enhanced confinement regime under intense heating. Suppression of impurity influx from divertor plates is important for this purpose. NB input power of JT-60U will be 40 MW, which is the largest in the present tokamaks. Thus, a carbon-fiber composite (C/C) with thermal conductivity of up to $300 \text{ W/m}^{\circ}\text{C}$ is used for the divertor plates. Water cooling pipes are introduced into the vacuum vessel for the heat removal of the divertor plates so as to suppress thermal stress due to low thermal conduction between the inner and outer skins. The surface of the vacuum vessel except divertor plates are covered with graphite tiles. The inboard tiles are designed to withstand the heat flux of up to 3 MW/m^2 while the heat flux onto the outboard tiles is much smaller. These graphite tiles are inertially cooled and the heat is removed through the cooling channel after shots.

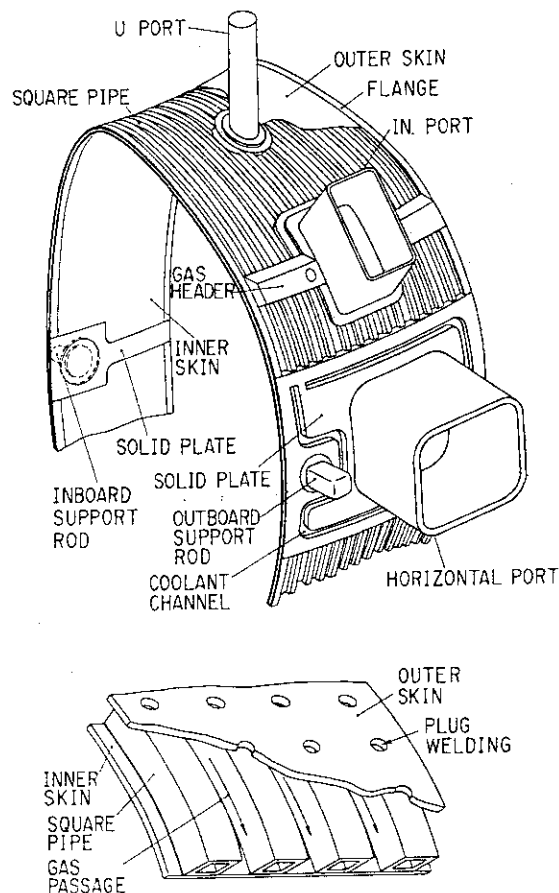


Fig.IV.2.1-2 Schematic diagram of the vacuum vessel.

2.1.3 Poloidal field coil

The PF coil system consists of an ohmic heating coil (F), a vertical field coil (V), a horizontal field coil (H), a divertor coil (D) and a sector coil (DCW) as shown in Fig.IV.2.1-1. Current ratings of each coils are similar to those of JT-60 so as to minimize modifications in the original power supply. The V-coil is divided into 4 blocks so that 3 types of divertor configurations can be selected by the tap change. This enables us to study the dependence of confinement on the aspect ratio, major radius, minor radius and elongation.

To increase the passive index n_s and to obtain stable discharges with high elongation, conductors of the H-coil were distributed around the vacuum vessel and conductors of V_2 , V_3 and V_6 were designed to serve as passive stabilizers in an elongated mode.

The capacity of the F-coil was increased up to 42 V·s by increasing its current rating from 92 kA to 120 kA. In addition the V-coil was designed to have a flux swing capacity of 19 V·s with

eliminating the return conductor. The total capacity of 61 V·s is 2.4 times as large as that of the original JT-60 while the total ampere turn increases by 25%.

Conductors of the F-coil were arranged to minimize an axisymmetric stray field inside the vacuum vessel. The design criterion of this axisymmetric stray field in the tokamak at breakdown phase is that the region with $|B_p| < 5 \times 10^{-3}$ T should be wider than 1 m². To satisfy this condition, slight excitation of the D-coil is necessary because of lack of the F-coil blocks in the bottom region.

2.1.4 Toroidal field coil

The poloidal field produced by the PF coils and the plasma cause a significant overturning moment on the TF coils. The TF coils are originally designed to withstand the overturning force of 450 tons for 50,000 shots. With the new plasma configuration, an overturning force of up to 600 tons is anticipated. Reinforcement was necessary for the TF coils and their support fixtures, since the primary stress of up to 833 MPa would be generated at the coil case in the new operation conditions. Two coils adjacent to each other were welded together at the inboard side of the coil case. The upper support structure was also reinforced to increase the stiffness and to decrease the displacement of the coils. The reinforcement reduces the stress down to 470 MPa.

References

- [4.1-1] H.Ninomiya et al., Plasma Devices and Operations, Vol 1 1990 p43-65
- [4.1-2] H. Horiike et al., Proc. 13th Symp. on Fusion Engrg., Knoxville, 1989.
- [4.1-3] Y.Neyatani et al., Plasma Devices and Operations(to be published)

2.2 Control system

2.2.1 Plasma control

(1) VME multiprocessor system

We developed a VME multiprocessor system [2.2-1] for plasma position and current control at the JT-60 upgrade (JT-60U). Parallel processing with three 32-bit RISC microprocessors MC88000 (Motorola Co., USA) in the system makes it possible to calculate plasma state variables precisely and to execute the sophisticated plasma control fast. The VME system is connected to its supervisory minicomputer HIDIC-80E (Hitachi Ltd.) in the JT-60 central control system "ZENKEI" [2.2-2] through a CAMAC serial highway. It is also connected to the direct digital controllers (DDC's) in the poloidal field coil power supply through CAMAC branch highways.

Development of the hardware including tests on the data transfer capability had been completed in the FY1989 [2.2-3]. Noise tests of the VME components had been also performed.

The software was developed and installed in the processors in this fiscal year. In the new program we prepared over ten plasma control schemes such as preprogrammed voltage/current control, PD (proportional and differential) feedback control with matrix gain, and current control proportional to plasma current. They can be dynamically switched at any time by control

algorithm preprograms and/or events. An upper byte of the CAMAC control command to the DDC's can represent whether it is voltage control command or current one.

The plasma control programs in the three RISC processors are written in C Language. The parallel processing with them is synchronized by an interruption of a 250 μ sec clock signal and flags on the shared memory. The VME multiprocessor system, then, can execute the feedback control with a cycle time of 250 μ sec for the plasma vertical position and with that of 500 μ sec for the control of the other parameters.

The system integration test was performed from July through September, 1990. The linkage test of the VME system and the DDC's was also performed from October through December, 1990.

(2) Development of a plasma shape identification method

For the JT-60U plasma position and current control, we made a MHD equilibrium database for over 900 cases of the standard divertor configuration. We decided formula to derive plasma position parameters with regression analysis on the basis of this database. We have prepared two sets of formula. In one set the tangential and normal magnetic probes and a Rogowski coil are used. In the other set tangential probes, flux loops and a Rogowski coil are used.

For identifying the shape of the JT-60U plasmas at shot-interval, the TOLFEX method [2.2-4], which is used a Legendre-Fourier expansion of the vacuum poloidal flux function in the toroidal coordinates, was installed on the workstations in the JT-60 central control system "ZENKEI". The method is based on the analytical solution of the Grad-Shafranov equation in a vacuum region. The center of the toroidal coordinates (R_0, Z_0) and the coefficients of the flux eigenfunctions are determined by "the 2-step least square method" with the observed flux and plasma current values. The shape of the plasma is given by the contour of the constant flux value, which is the minimum value among the flux values at the fixed limiters and an X-point. Figure IV.2.2-1 shows an example of the shape identified by the TOLFEX method for a divertor plasma with a current of 2 MA.

We are now developing a system for real-time visualization of the plasma shape with this method.

2.2.2 Man/machine interface

A new man/machine interface in ZENKEI was developed on the basis of the five-year operational experience. The development is focused on the following improvements: (1) the function for setting discharge condition parameters, (2) the functions for monitoring the plant status and discharge results and (3) work environments in the JT-60 central control room.

The man/machine interface is installed on a network system with 9 workstations (one Sun-3/470 for a file server of discharge condition parameters and eight Sun-3/80 for operation).

A minicomputer of HIDIC-V90/45 (Hitachi, Ltd.) is also provided as a supervisor of the workstations. This minicomputer is also connected with the present central control computer system through a shared memory and a dedicated computer linkage.

The hardware of the system had been prepared in FY1989. The software was developed in this fiscal year. Figure IV.2.2-2 shows an example of multi-window displays on the workstation. System integration test was performed from November, 1990 through January, 1991. We started a test run of the new man/machine interface system in February, 1991. The coil excitation test in the JT-60U commissioning was successfully executed with this system.

References

- [2.2-1] T. Kimura, et al., IEEE Trans. on Nuclear Science 35 (1989) 1554.
- [2.2-2] I. Kondo, et al., Fusion Engineering and Design 5 (1987) 69.
- [2.2-3] Y. Kawamata, et al., JAERI-M 90-005 (1990) (in Japanese).
- [2.2-4] K. Kurihara, et al., JAERI-M 90-001 (1990) (in Japanese).

2.3 Power supply

The poloidal field power supply (PFPS), which consists of a motor-generator and five converters' power supplies[2.3-1], has been modified to achieve the higher plasma current of

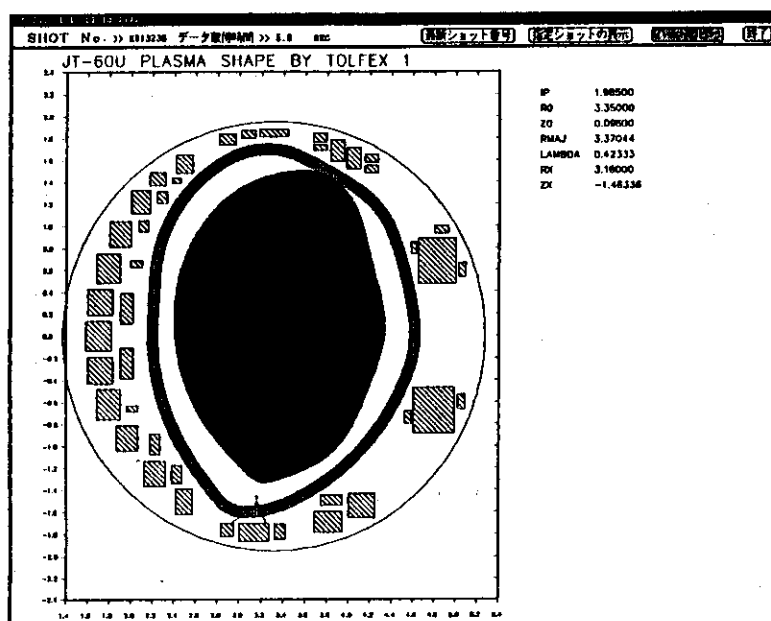


Figure IV.2.2-1 An example of the shape identified by the TOLFEX method for a divertor plasma with a current of 2 MA.

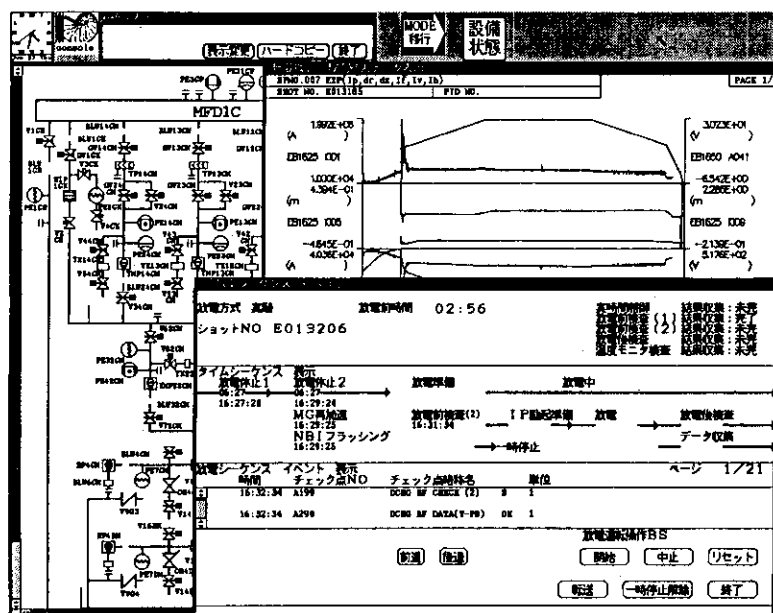


Figure IV.2.2-2 An example of multi-window displays on the workstation.

6MA, the longer current duration of 15 seconds and so on in JT-60 upgrade[2.3-2]. The currents and the waveforms of five power supplies corresponding five poloidal field coils are shown in Fig.IV.2.3-1. A part of modifications was done in FY 1989, and the rests which are mainly remodeling of control systems and tests of whole PFPS system have been performed in FY 1990 [2.3-3]. The schematic diagram of the PFPS in JT-60U is shown in Fig. IV.2.3-2.

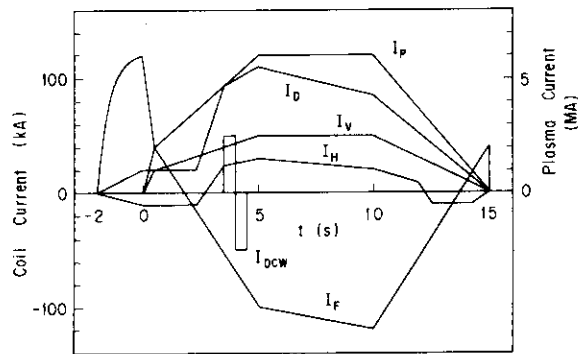


Fig. IV.2.3-1 Currents and waveforms of PFPS in JT-60U

(1) Modification of five converters' power supplies of PFPS

a) F-coil power supply (PSF)

PSF has to deliver the current of ± 120 kA to the F-coils for swinging the flux of 42 Volt-sec. For achieving it, PSF has been remodelled as follows; connecting the PSEX power supply whose rated current of 10 kA, controlling the start/stop the circulating-current between PSF1 and PSF2 and removing the DC

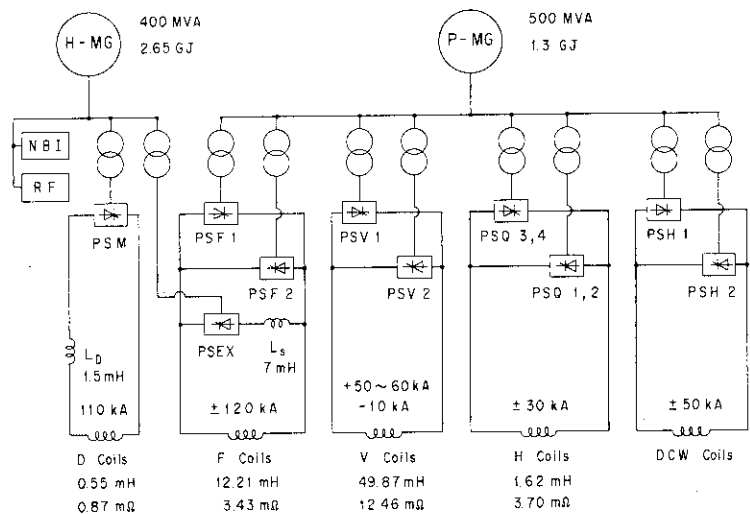


Fig. IV.2.3-2 Schematic Diagram of PFPS in JT-60U

circuit breaker because of its rated current of 92 kA. For longer current duration of 15s, all resistors of the snubber circuit of thyristors have been exchanged for new ones made by ceramics.

b) V-coil power supply (PSV)

PSV supplies the current of 60 kA to the V-coils for swinging the flux of 19 Volt-sec and the vertical field of 0.5T. In PSV, all snubber resistors were also exchanged such as PSF and the diode convertor (PSV13) was removed.

c) H-coil power supply (PSQ)

PSQ produces the horizontal field in JT-60U. In order to suppress the fast vertical movement and protect disruptions, control of the thyristor converters has been made very fast, and the power supplies have been reinforced on the rated current of ± 30 kA and also withstands the plus current of 90 kA, 10 ms and the minus current of 70 kA, 30 ms.

d) D-coil power supply (PSM)

PSM supplies the current of 110 kA to the divertor-coils, and it has been connected the external reactor whose inductance is 1.5 mH to suppress the over current at the disruptions.

e) DCW-coil power supply (PSH)

PSH delivers the current to the DCW-coils, and no modifications were done.

(2) Modifications of control system of PFPS in JT-60U

The PFPS control system consists of hardwired controllers and three CAMAC systems such as the plant support CAMAC which controls and monitors the PFPS machines, the discharge control CAMAC which performs pre-conditioning such as setting the MG and the timing system and making the circuits of PFPS by changing circuit breakers etc. and after-conditioning, and the direct digital control (DDC) CAMAC system which is engaged in real-time control of the PFPS thyristors. In FY 1990, the whole control system of PFPS, especially the discharge control and the plant support CAMAC have been largely modified according to remodeling of the converters' power supply.

A new DDC system developed in FY 1989 have been adopted to all DDC [2.3-3]. Objectives of the system are as follows; processing the DDC very fast under 0.5 ms and hopefully under 0.25 ms, switching operation modes from circulating current mode to no-circulating current mode and changing the control method from coils' current feedback control to coils' voltage control, etc. Hardwares of new DDC system showed in Fig.IV.2.3-3 consists of a host computer AS3260, five microcomputers MVME 147 with a 32-bit, 20 MHz microprocessor MC 68030 and five CAMAC crates. The host computer performs on-line processing which is setting the DDC system under conditions of the discharge and collecting and transferring data of coils' currents and voltages to the ZENKEI after the discharge, etc., and micro-computers carry out real-time processing of thyristor control every 0.5 ms or 1 ms. In FY 1990, the system design, programming and tests of whole DDC system, namely on-line and real-time processing, have been made and the results achieved the whole objectives.

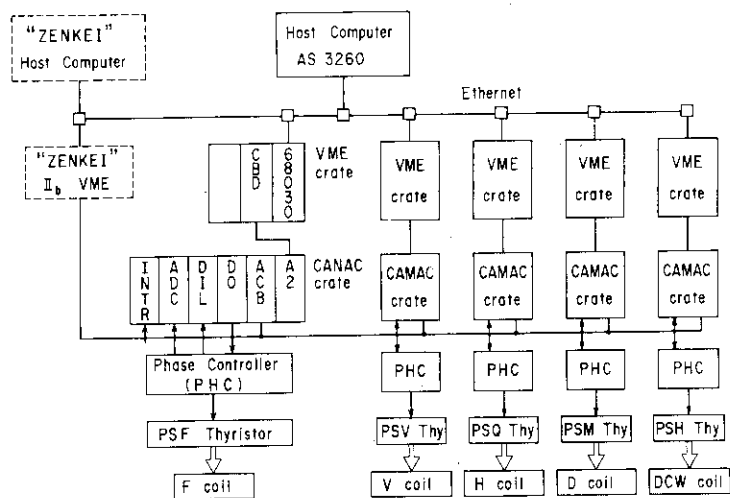


Fig. IV.2.3-3 Block diagram of new DDC system

(3) Tests of PFPS system

Tests of new PFPS system have performed as follows. Protective interlock and sequence

tests of each CAMAC system were done by the end of June, and on July, combination tests of plant support CAMAC, discharge control CAMAC and new DDC CAMAC systems were performed successfully. In August and September, new PFPS performances such as currents and controls of each converter's power supply were tested by using dummy coils, and results were very satisfactory. The linkage test with ZENKEI was done in October, December, 1990, and January, 1991, and successively system integration tests of JT-60U were performed as shown in sections 2.7.

References

- [2.3-1] R. Shimada et al., *Fusion Engineering and Design*, 5(1987) 47
- [2.3-2] Y. Matsukawa et al., *Proc. of 15th Symp. on Fusion Technol.*, Utrecht, 1988, p.293
- [2.3-3] Y. Matsuzaki et al., *Proc. of 16th Symp. on Fusion Technol.*, London, 1990

2.4 Neutral beam injection system

Concerning with the upgrade of JT-60, upper five units of quasi-perpendicular beamlines were reinstalled this year as well as all NBI ports were renewed. The acceleration power supplies were tested following to the last year modification to increase the maximum voltage from 100 kV to 120 kV [2.4-1]. To cope with the increased stray field from the JT-60U, an additional coil was installed around the neutralizers. This will reduce the leakage field at the joint of the magnetic shields for the ion sources and the neutralizers.

Four out of fourteen beamlines are being reoriented to inject beams tangentially [2.4-2]. This modification aims at the study of the loss of fast ions due to toroidal field ripple, where substantial part of the fast ions injected with the quasi-perpendicular beamlines are anticipated to be lost in the JT-60U configuration. New ports, base plates, and piping towers for the tangential beamlines were fabricated and part of them were installed this year. The remaining system such as the modified beamlines, pipes, and cables will be installed next year.

For both quasi-perpendicular and tangential beamlines, electrode gaps of the ion sources were rearranged to match 120 keV, deuterium operation. Beam characteristics, heat load in the beamline, and injection power were measured in the prototype injector unit with one of the rearranged ion sources but with hydrogen gas. The injection power per unit estimated from the measurement is plotted in Fig. IV.2.4-1. The injection power of deuterium beams will be determined by combining the value deduced from this data and the planned calorimetric measurement using both a calorimeter, and a beam profile monitor (an array of molybdenum blocks with thermocouple) newly installed in one of the NBI ports.

After the series of helium beam injection to simulate fusion-produced alpha particles, it was observed that electron emission from cathodes in the ion sources was deteriorated. A lot of hydrogen arc discharges for two weeks were required to recover the original emission characteristics. This phenomenon was studied in more detail in ion source test stands. As a

result, it was found that this seems due to a thin layer of hydrocarbon produced on the surface of the cathodes and sputtering by xenon or argon arc discharges is effective to remove the layer. The processing time to recover the original emission characteristics could be reduced to two to three hours by adopting this xenon or argon sputtering method.

A fundamental experiment on titan gettering pump was carried out to examine whether titan gettering pump is applicable to future neutral beam systems. We found the pumping speed is about 1 liter/(cm² sec) at room temperature. This value is lower than that of cryopumps by about one order of magnitude. The maintainability of the filaments would be a problem in addition to the low pumping speed.

A negative-ion-based neutral beam system proposed for JT-60U will

inject neutral beams of 0.5 MeV, 10 MW for 10 seconds [2.4-3]. This program aims at clarifying both physical and technological issues relating to high energy neutral beam systems. The system design done so far was reviewed and optimized by taking into account of the recent progress in the development of negative ion sources.

References

- [2.4-1] M. Kuriyama, et al. Proc of 13th Symp. on Fusion Engineering, Knoxville, (1989) p. 996.
- [2.4-2] M. Matsuoka, et al., JAERI-M 90-086 (in Japanese).
- [2.4-3] M. Matsuoka, et al., presented at 13th Int. Conf. Plasma Physics and Controlled Nucl. Fusion Research (Washington, DC, 1990) IAEA-CN-53/G-1-4.

2.5 Radio-frequency system

2.5.1 LHRF system

The main objective of LHRF heating system on JT-60U is to inject ~10MW by two new launchers. One is the same type as the multijunction launcher on JT-60 which was composed of 96 waveguides. Another is a new type of multijunction launcher which is composed of 192

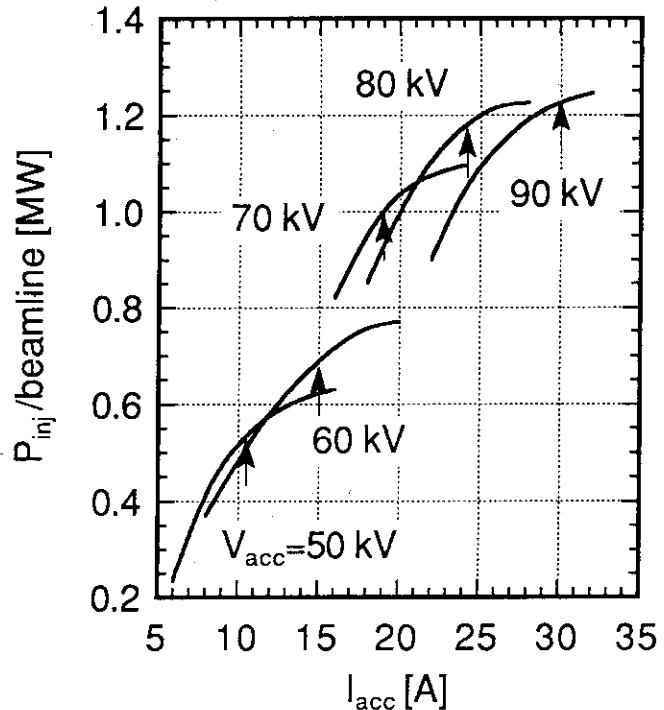


Fig. IV.2.4-1 Injection power per beamline when hydrogen beams are extracted with fixed intermediate voltage (80% of the acceleration voltage). Each arrow indicates the acceleration current I_{acc} where the beam divergence becomes minimum at the respective acceleration voltage V_{acc} .

waveguides. By using them, efficient plasma current drive and profile control are expected on JT-60U experiments.

In the former launcher 8x4 multijunction modules, each of which is divided into three sub-waveguides, is employed. (See Fig.IV.2.5-1.) This launcher was manufactured with diffusion bonding method. This bonding method was developed to easily fabricate the multijunction grill with a large number of waveguides. This launcher was designed to be operated at the wide frequency range of 1.74 to 2.23 GHz. Therefore, the $N_{||}$ spectra can be widely controlled with high directivity

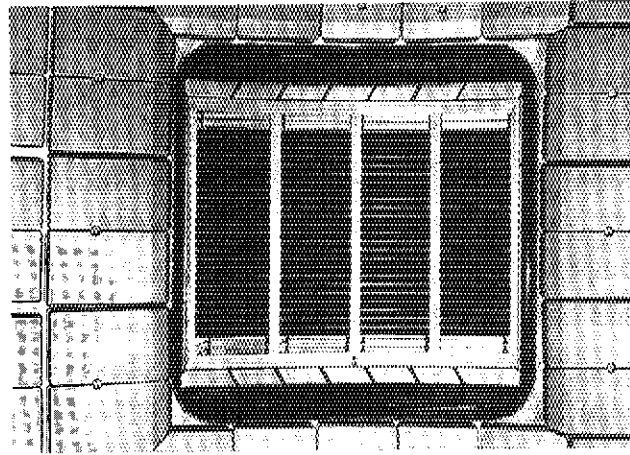


Fig.IV.2.5-1 LHRF launcher installed on JT-60U.

waves. We measured RF characteristic in this frequency range and confirmed that the dividing ratio and the phase shift of the all multijunction module were within $1/3 \pm 14/100$, $87^\circ \sim 117^\circ$, respectively, at 1.74GHz, $1/3 \pm 7/100$, $55^\circ \sim 73^\circ$ at 2 GHz and $1/3 \pm 11/100$, $47^\circ \sim 56^\circ$ at 2.23GHz. We also carried out a high power test on this launcher in a test-stand just before we installed it on JT-60U. A power level of 300~500kW/module, which is about 2~3 times higher than the required value on JT-60U experiment, was successfully injected into the test-stand vacuum tank [2.5-1]. This launcher was installed on a oblique port in 11th section of JT-60U vacuum vessel, and will be operated from July 1991.

The later is designed and optimized to drive plasma current more efficiently. 4x4 multijunction modules is used in this launcher. Each module is composed of 12 sub-waveguides in the toroidal direction. Therefore, the launcher is of 48x4 grill structure. The current drive efficiency is expected to be improved 10~20% higher than that of the previous one. The RF power of this launcher is driven by 16 high-power klystrons, and the injection power into plasmas is expected to be over ~7MW. A key of this launcher is to simplify the multijunction structure with a large number of waveguides. We are developing a new multijunction technique, in which multijunction module consists of one over-sized taper waveguide and one multi-slitted waveguide. A prototype module was well fabricated. We have started to measure RF characteristics with dummy load. This launcher will be installed on the mid-plane port and be operated at the beginning of 1993.

2.5.2 ICRF heating system

The JT-60 ICRF heating system has been upgraded in accordance with the modification of the JT-60 tokamak which allows plasma currents up to 6 MA. Its major specifications are listed in Table IV.2.5-1. Eight impedance matching circuits, 9 inch and 6 inch coaxial components forming eight transmission lines and two ICRF antennas have been already fabricated [2.5-1].

Each antenna is composed of a phased 2 x 2 loop array, an open type Faraday shield and a metal casing with a poloidal septum. They are essentially similar to the previous JT-60 ICRF antenna although their front area (0.85 m x 0.74 m) is enlarged by a factor of three.

First, we measured coupling between loops and antenna and resonance frequency. Weak toroidal loop coupling of -30.5 dB was obtained with the septum as expected. The resonance frequency of 98.5 MHz was measured for vacuum loading and was calculated as 86 MHz by a antenna-plasma coupling code including the effect of the metal casing and the septum. Therefore, the prediction of coupling resistance > 2 W by the coupling code is probable because of good agreement on the resonance frequency. Next, we preconditioned the antenna with the matching circuit for JT-60U in ICRF test stand. Each loop of the antennas was conditioned up to 30 kV for 1 s although its stand-off voltage was designed to be 50 kV for 5 s. The installation of the antennas into the JT-60U vacuum vessel is intensively conducted in this year. It is estimated that torque of 35 ton-m around the major radial direction acts on each antenna as the electromagnetic force when a plasma disruption occurs at a plasma current of 6 MA with the decay time of 5 ms.

Moreover, the antenna is restricted by a horizontal port (0.9 m x 0.8 m) and is movable by 40 mm in the major radial direction. Consequently, the antennas are held firmly by sliding double structure boxes which are supported by strong beams bridged between vacuum vessel supports. The antenna front section is flashed with the curvature of the graphite tiles arranged precisely around ICRF ports on the vacuum vessel, as shown in Fig.IV.2.5-2.

References

- [2.5-1] M.Seki et al., 16th Symp. on Fusion Tech. London, (1990).

Table IV.2.5-1 Major Specifications of JT-60U ICRF Heating System

Frequency	108 - 132 MHz
Output Power	6 MW
Pulse Length	5 s
Antenna	Phased 2 x 2 Loops
No. of Antennas	2

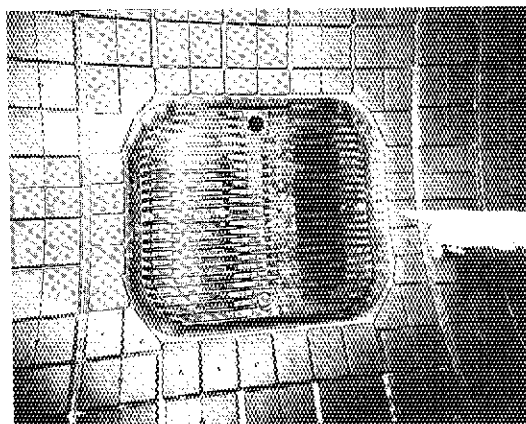


Fig.IV.2.5-2 ICRF antenna installed into the JT-60U tokamak.

[2.5-2] T. Fujii, et al., 16th Symp. on Fusion Tech., London, 1990.

2.6 Diagnostic systems

In the phase of JT-60 shut down (Nov. 1989 ~ Mar. 1991), all diagnostic systems were removed from JT-60 experimental room and most of them have been newly arranged to install corresponding with new ports of JT-60U. In this phase, we designed and fabricated new diagnostic systems and reconstructed to shield the detectors from neutrons and γ -rays generated by the JT-60U plasmas. In the Thomson laser scattering apparatus, the CXRS (Charge Exchange Recombination Spectroscopy), the $H\alpha/D\alpha$ arrays, the Visible spectrometer for divertor and Z_{eff} profile arrays, fiber optics were used to lead visible light preventing detectors from neutron noise. In the Soft X-ray arrays and the Bolometer arrays, the pre-amplifier signals of the detectors are converted to digital signals of light and they are transferred to the room where the data acquisition systems are installed. In the detector of counting type, for example, MCP (Microchannel Plate) counting mode in the Charge Exchange Neutral Particle Energy Analyzer array and the proportional counters in the X-ray crystal spectrometer, we installed neutron shields and γ -ray shields to prevent the detectors from the neutron noise. The Thomson laser scattering apparatus, the Soft X-ray arrays and the Bolometer arrays are described in the section IV.2.6.1~2.6.3. The JT-60U diagnostic system and status at the end of March 1991 are summarized in Table IV.2.6-1.

2.6.1 Thomson laser scattering apparatus

For improving time and spatial resolution, and understanding transient and precise transport phenomena concerning electron density and temperature profiles in the JT-60 Upgrade tokamak, the major part of the JT-60 Thomson scattering diagnostic system had been developed and modified as shown in Fig.IV.2.6-1. Introducing the beam combiner with 2 ruby lasers and Faraday rotator, the time resolution of 2 msec in burst mode to 2 sec in a constant repetition mode was realized. To increase in the spatial measurement capability of up to 70 points, a reflecting mirror of Cassegrain type was newly installed in collection optics, and two dimensional photodiode array detector (20 spatial channels x 12 spectral channels) with proximity focussed type image intensifier was developed. These additional devices were utilized for the measurement of the center plasma region with the spatial channels of 20 to 40 and their resolution of 22 mm. On the other hand, for the edge plasma measurement with the spatial channels of 30 and their resolution of 8 mm and 16 mm, the fiber bundles of 130 channels which connect a spectrometer to photomultipliers was set, and the number of photomultipliers will be increased up to 138 including high voltage supplier and data acquisition system in 1991.

In order to progress the system reliability, the long distance transmission of collected Thomson scattering light through fiber bundles (about 100 m) was introduced for easy adjustment of spectrometers and detectors in a separated room from JT-60U Torus hall. Also a remote

Table IV.2.6-1 Status of JT-60U diagnostic systems

Diagnostic System	Subsystem	Specification etc.	Status Mar. 1991
Electron Density Measuring System	Sub-mm Wave (FIR) Interferometer	CO ₂ Pumped CH ₃ OH Laser Vertical 2 chords	Installed
	CO ₂ Laser Interferometer	Tangential 1 chords	Designed
	Millimeter-Wave Reflectometer	4 points, $\Delta r=5\text{cm}$, $\Delta t=1\text{msec}$ (sweep time)	Designed
	Electromagnetic-Wave Scattering Array	3 points, 50kHz~1.8MHz	Designed
Electron Temperature Measuring System	Thomson Laser Scattering Apparatus	2 Ruby Lasers, 50 points Repetition Period = 4 s	Installed
	ECE Michelson Interferometer	30 points, $\Delta t \sim 20\text{ms}$	Installed
	ECE Grating Polychromator	20 points, $\Delta t=20\text{ms}$	Installed
Ion Temperature Measuring System	Charge Exchange Recombination Spectroscopy	20 points (tangential) 8 points (perpendicular)	Installed
	Active Beam Scattering Apparatus	1 point (center) He Beam 200keV, 3.5A	Installed
	Charge Exchange Neutral Particle Energy Analyzer Array	2 chords(tangential) 2 chords(perpendicular)	Installed (tangential)
Impurity Measuring System	X-ray Crystal Spectrometer (Doppler and Monochromator)	Vertical 1 chord, Ti, Ni, Kr, K α Rotating Crystal, 0.1-0.8 nm	Installed (Doppler)
	VUV Spectrometer	1 chord, 0.5-130 nm (Main) 1 chord, 0.5-130 nm (Divertor)	Installed (Main)
	Light Impurity Spectrometer (Doppler)	1 chord, 100-200 nm (Divertor)	Installing
	Grazing Incidence Monochromator	1 chord, 10-130 nm Absolutely Calibrated VUV	Installing
	Visible Monochromator	1 chord, 200-700 nm Absolutely Calibrated Visible	Installed
	Visible Spectrometer for periphery	Mirror Scan, 200-700 nm	Installing
	Visible Spectrometer for Divertor	38 points, H α , H β , CII, OII Fiber optics and Filters	Installed
	Visible Bremsstrahlung (Zeit)	10 points, 523.2nm Fiber optics and Filters	Installed
Radiation Flux Measuring System	Soft X-ray PHA	1 chord, 3-110 keV	Installed
	H α /D α Arrays	Poloidal 30 chords Toroidal 6 chords Divertor 1 chord Outer Region 1 chord	Installed
	Soft X-ray Arrays	Poloidal 64 chords Outer Region 4 chords	Installed
	Bolometer Arrays	Poloidal 32 chords Divertor 1 chord	Installed
	Hard X-ray PHA	Poloidal 7 chords Co 1 chord, Ctr 1 chord	Installed
Neutron Measuring System	Fission Chamber	3 points, $\Delta t \sim 10\text{ms}$	Installed
	Neutron Spectrometer (2.45MeV/14MeV)	1 chord, $\Delta E \sim 2\%$	Installed
Peripheral Plasma & Wall Surface Measuring System	Infrared TV	Divertor 1 chord, 400-500°C	Designed
	Visible TV	Tangential 2 chords	Installed
	High Speed TV	Tangential 1 chord, 1 field/1ms	Installed
	Electromagnetic Probes (Mirnov Coils)	40 points (poloidal and toroidal arrays)	Installed
	Electrostatic Probes	Divertor 15 points	Installed

handling system of a viewfield alignment was set in collection optics as well as that of a beam axis alignment in input optics.

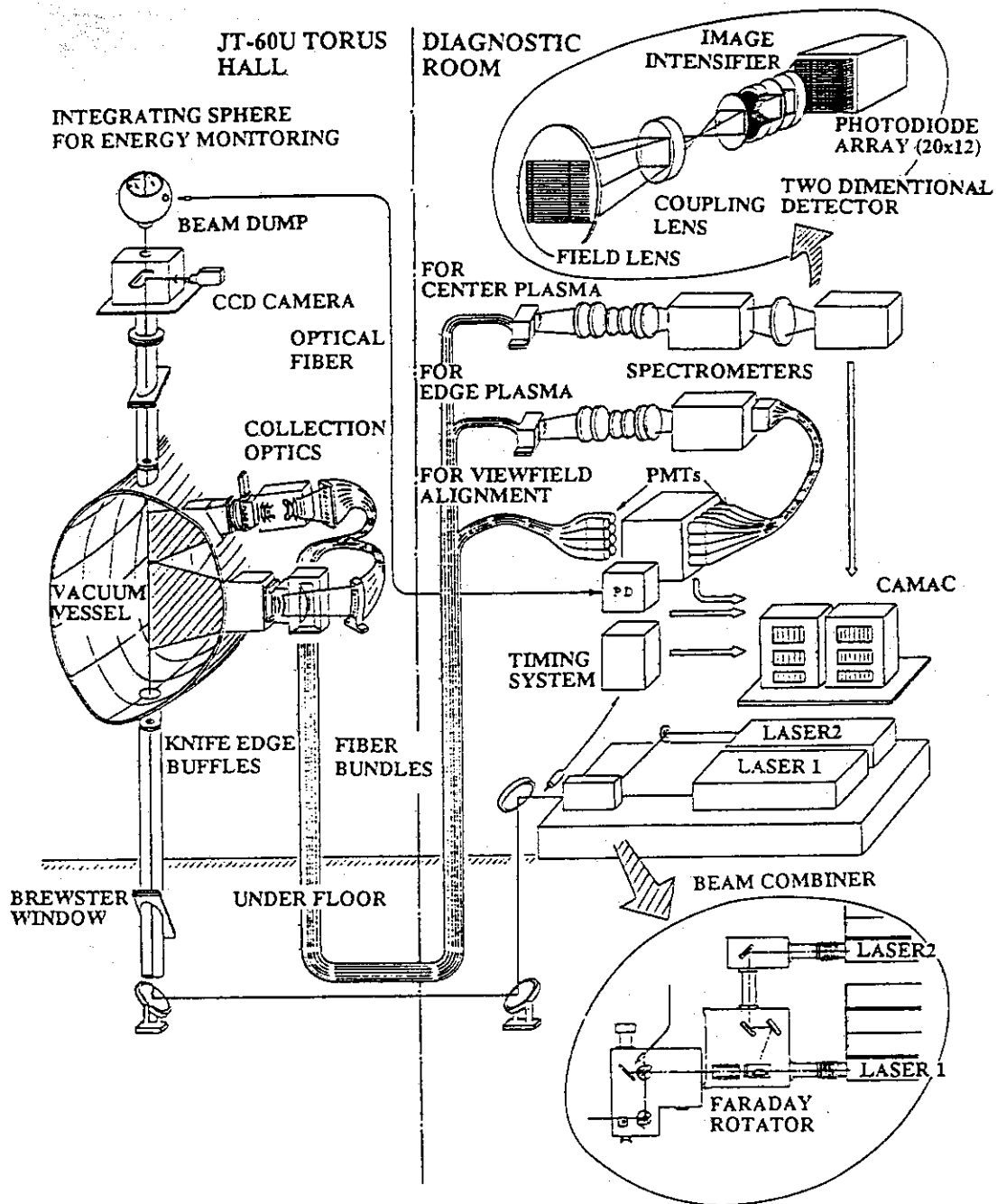


Fig.IV.2.6-1 Schematic layout of new Thomson scattering diagnostic system for JT-60 Upgrade tokamak.

2.6.2 Soft X-ray arrays

Spatial profile of soft X-ray intensity is measured by two arrays with 32-channel PIN diodes from the horizontal port. (See Fig.IV.2.6-2.) This measurement has a high temporal and spatial resolutions and provide various information about plasma MHD behaviors.

PIN diode has an active area of $2 \times 20 \text{ mm}^2$ and a thickness of depletion layer is about $200 \text{ }\mu\text{m}$. A beryllium filter of $200 \text{ }\mu\text{m}$ is used as a low energy X-ray absorber and its cut-off energy is 2.6 keV. A current is generated in PIN diode by the absorbed X-ray energy and it is amplified by the I/V convertor and digitized with a sampling frequency of 25 kHz.

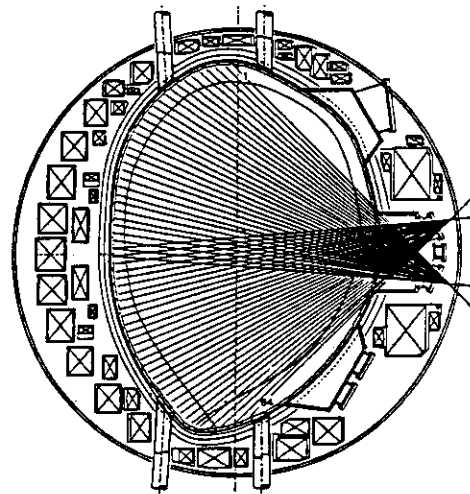


Fig.IV.2.6-2
Poloidal views of soft x-ray arrays on JT-60U

2.6.3 Bolometer array

Spatial profile of radiation loss is measured by 32 channel bolometer arrays from the horizontal port (Fig. IV.2.6-3). Diagnostic port and vacuum chamber of bolometer arrays (Fig. IV.2.6-4) have been carefully arranged in order to cover the whole plasma cross section.

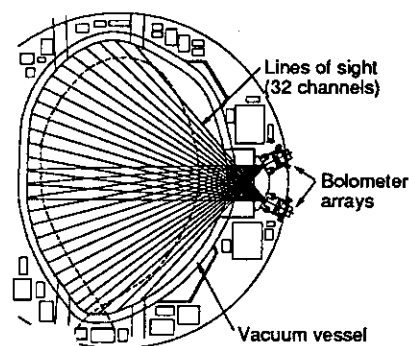


Fig. IV.2.6-3
Arrangement of the bolometers in JT-60U.
Spatial resolution is 10 cm at the plasma center.

Compact bolometric detector has been developed for the purpose of preventing neutron or gamma-ray radiation damage due to deuterium discharges [2.6-1]. Gold resistor bolometer is radiative-resistant detector developed for this measurement consisting of three layers ($5 \text{ }\mu\text{m}$ -thick gold absorber, $7 \text{ }\mu\text{m}$ -thick polyimide insulator, and gold-foil grid as a temperature-sensitive resistance). Rise time and cooling time of the detector are 0.4 ms and 6 sec, respectively.

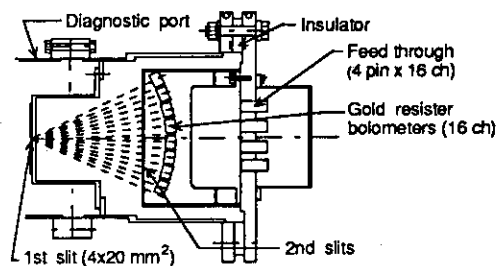


Fig. IV.2.6-4
Schematic of bolometer array. Effective area of the gold resistor bolometer is $4 \times 11 \text{ mm}^2$.

2.7 System integration tests

(1) Test schedule and procedure

Linkage performance tests between the JT-60 central control system "ZENKEI" and each subsystem were carried out for a net period of two months from October through February 1991. The control system integration test and the coil excitation tests, then, followed the above linkage tests through the first half of March 1991.

(2) Linkage performance and system integration tests of the control systems

We stressed on the following two patterns at the tests for the JT-60 upgrade: (a) protective interlock tests with hardwired relay logic and (b) sequence tests including check of communication data. As VME bus and CAMAC system complex was newly adopted in the feedback control computer system (IIB) in "ZENKEI" and in the DDC's in the PFPS, the following items were confirmed in the VME bus and CAMAC interface tests between "ZENKEI" and the PFPS: (a) grounding between the cubicles in the two systems, (b) voltage level of analog signals, (c) synchronization with a timing system, (d) communication protocol and data format and (e) application message communication. At the final stage of the linkage tests between them, operational characteristics of the IIB system and the DDC's was evaluated by exciting a dummy load coil. Check items at the control system integration tests were mainly total performance on protective interlock and discharge sequence functions.

We decided the test methods and procedure on the basis of the experience in the tests for JT-60. Then, we were able to perform these tests for a net period of two months and a half, and to reduce the number of the problems pointed out at these tests and the succeeding coil excitation tests extremely.

(3) Coil excitation tests

Check items on the tokamak system at the coil excitation tests are as follows: (a) formation of abnormal loops, (b) metal pieces left behind, (c) cooling water temperature, (d) coil temperature, (e) stress on the coils and (f) displacement of coil feeder and support structures. The electromagnetic measurement system was also evaluated at these tests. Figure IV.2.7-1 shows an example of the coil current waveforms at the tests. No big problems were found at these tests, which was followed by discharge cleaning operation.

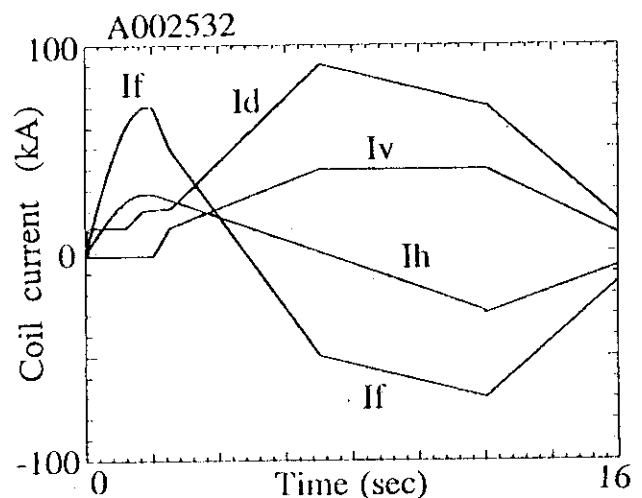


Fig. IV.2.7-1 An example of the waveforms of Ohmic heating coil current I_f , vertical field coil current I_v , horizontal field coil current I_h and diverter coil current I_d at the coil excitation tests.

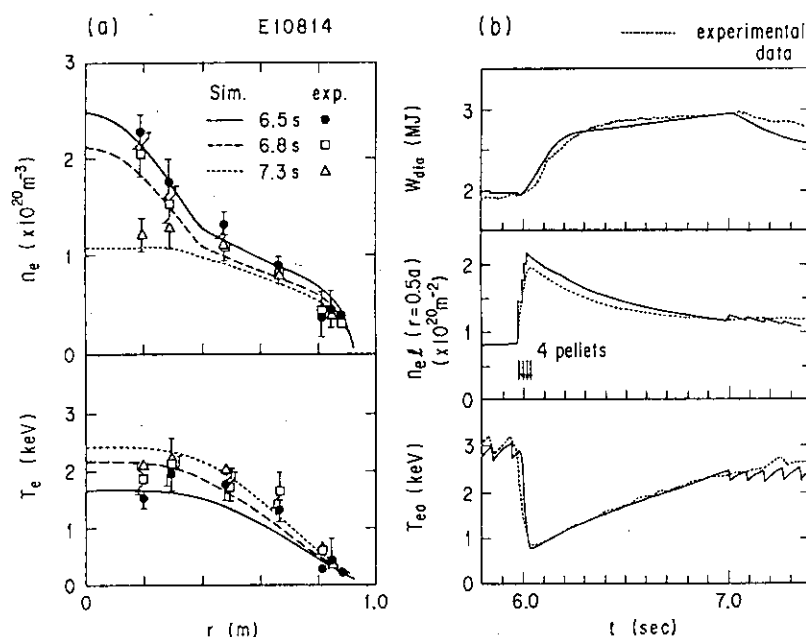
3. Experimental Results and Analysis

3.1 Transport and MHD analysis

3.1.1 Transport study of pellet fuelled plasmas in JT-60

The transport of pellet fuelled plasmas in JT-60 has been investigated with a predictive tokamak transport code. The peaked density profiles were observed in pellet fuelled plasmas during the sawtooth free phase. Simulation analysis shows that the inward pinch of ~ 0.2 m/sec at the half plasma radius and the reduced particle diffusion coefficient in the central region of 0.1 m²/s are necessary to explain the peaked density profile. Figure IV.3.1-1 shows the simulation results for the shot E10814. The recovery of the central electron temperature after pellet injection can be well reproduced with the diffusion coefficients of L-mode plasmas. This simulation results indicates that the thermal diffusivity is not improved in the pellet fuelled plasma. The plasma current dependence of the improved stored energy can be explained by the reduced particle diffusion model within the $q = 1$ surface.

Fig. IV.3.1-1 Comparison of transport simulation results with experimental ones in the pellet injection experiment.



3.1.2 Local transport analysis of L-mode plasma

Local heat transport analysis has been carried out for auxiliary heated JT-60 plasmas with emphasis on understanding the deteriorated confinement observed in L-mode plasma [3.1-1]. The dependencies of the local thermal transport on plasma current, density and heating power have been studied under both configurations of divertor (single null, lower X-point), and limiter discharges with hydrogen beam injection into hydrogen plasmas. The deterioration in the energy confinement time with increasing auxiliary heating power, the so-called power scaling, is mainly due to the enhanced role of ion heat transport. It is found that the ion thermal diffusivity has a favorable density dependence.

Ion temperature profiles have been analyzed by using χ_i model based on the η_i mode turbulence and the drift wave turbulence (trapped electron mode and circulating electron mode) [3.1-2,3]. In L-mode plasmas, the theory has been found to be in good agreement with measurements in the wide range of plasma parameter except for the 1.0 MA limiter plasmas. In

high T_i plasmas the calculated T_i profiles become broader ones comparing with the experimental data which have pedestal and highly center peaked profile.

3.1.3 Nonlinear simulation of η_i -mode and comparison with experimental results

In order to study the linear stability and the nonlinear evolution of ion temperature gradient modes (η_i -modes) and to make detail comparisons of resultant anomalous transport with experimental results, the nonlinear simulation codes based on the reduced set of fluid equations [3.1-4] has been developed. Both slab and toroidal η_i -modes have been studied in the 2-D or 3-D geometry. The inverse cascade process of turbulence energy in the poloidal wave number space has been confirmed during the nonlinear evolution stage. And, more interestingly, increasing the poloidal system size, the two different stages of turbulent energy growth was observed before the saturation, although the total energy and the energy spectrum are almost the same as those in the smaller system size in the poloidal direction. The toroidal effect is taken in to account only through the finite G term, which represents the unfavorable curvature[3.1-5]. We have systematically performed the series of numerical simulations by using experimental data in JT-60 and evaluated the anomalous thermal diffusivity derived from the convective thermal flux. Figure IV.3.1-2 shows the comparison of these theoretical diffusivities (closed circles : toroidal η_i -modes and closed squares : slab η_i -modes) with the ones evaluated by the time-slice analysis (the shadow region). For comparison, the analytic value of Romaneli's mixing model is shown by the solid line, where the absolute value is chosen the same as the one used in the analysis in the the previous subsection. This figure shows that the toroidal η_i -modes are the good candidate of anomalous ion transport in the bulk plasma region, while we have to take into account other possibilities to enhance the thermal diffusivities in the periferal plasma region, the study of which remains in future work.

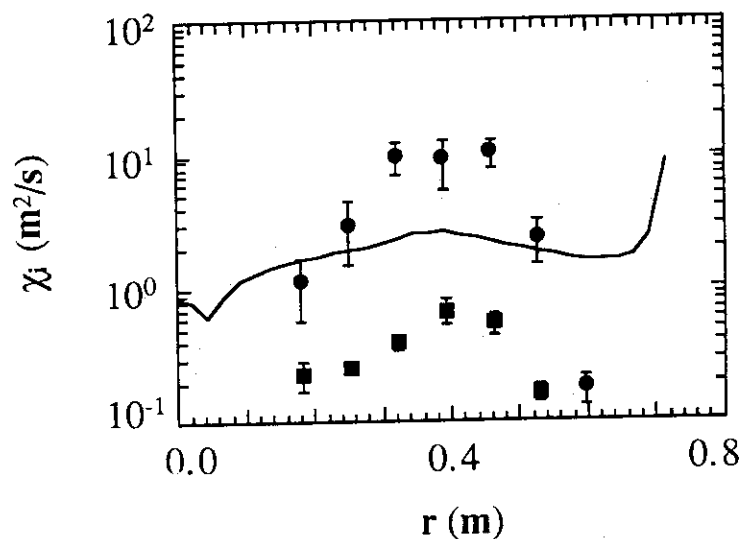


Fig.IV.3.1-2 Comparison of thermal diffusivities calculated from 2D simulation of toroidal and slab η_i -modes (closed circles and squares, respectively) with experimental analysis results (shaded region) and mixing theory values (solid line).

3.1.4 Density pulse propagation analysis [3.1-6]

Particle transport in JT-60 was investigated with a simple perturbation method from an analysis of the density pulse propagations. The particle diffusion coefficients were estimated in two experimental situations: the sawtooth induced density pulse propagation (see Fig.IV.3.1-3) and the pellet induced density perturbation. The values obtained corresponded to each other, even though the perturbed quantities were significantly different in the two cases. It was found that the particle diffusivity has an inverse dependence on the electron density. The ratio of χ_e/D was estimated from the analysis of the density and heat pulse propagation, and an approximate value of $\chi_e/D \approx 4$ was obtained.

Furthermore, to examine whether these transport coefficients are consistent with the electrostatic drift wave transport model, the experimentally estimated particle diffusivities were compared with theoretical values. It was found that the dependence of the estimated diffusivity on the collisionality is similar to that of the dissipative trapped electron mode, but the dependence on the density scale length found for this mode is not consistent with the result for pellet induced perturbations.

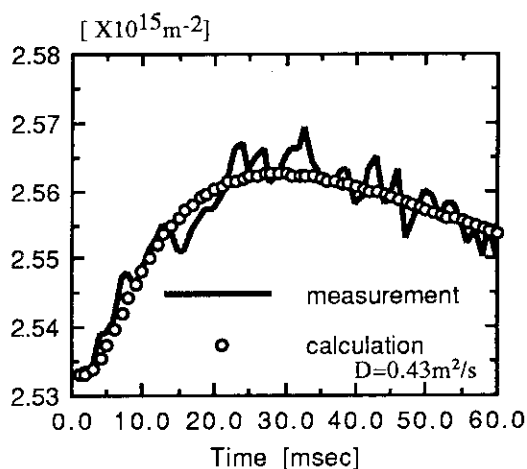


Fig.IV.3.1-3 Time evolution of the line integrated electron density just after the sawtooth disruption.

3.1.5 Bootstrap current analysis

The time-slice analysis of high poloidal beta experiments in JT-60 has systematically shown that the reduction of onturn voltage is consistent with the neoclassical bootstrap current, which flows by up to 80% of the total plasma current[3.1-7]. This result has been confirmed by the time dependent transport code analysis with using the experimental data of plasma parameters and poloidal coil currents. In the code, time evolutions of MHD equilibrium and the safety factor profile was reciprocally solved, and the neoclassical equations of particle and heat flow balance parallel to the magnetic field are directly solved to obtain the bootstrap current coefficients, taking into account of the finite aspect ratio, multi-ion species and multi-collisionality regimes. Contribution of fast ions on the bootstrap current is calculated under the assumption of isotropic velocity distribution and in the pitch-angle-scattering dominant collisionality regime[3.1-8]. Fraction of trapped particles is numerically evaluated in each magnetic surface. Figure IV.3.1-4 shows the simulation result of the typical high β_p shot E10196. After the full power NBI heating of 20 MW at 4.0 sec, the fraction of bootstrap current increases with β_p and it reaches the

maximum value of $\sim 80\%$ of the total current at 5.5 sec. At this time, the toroidal electric field is fairly flat in radius and the steady state assumption in previous analysis is shown to be the good one from the view point of the evaluation of the bootstrap current fraction.

3.1.6 MHD stability analysis of high- β_p plasmas

Effects of current profiles on the $n=1$ kink-ballooning stability in a tokamak are numerically analyzed in details by the linear ideal MHD stability code ERATO-J. For the theoretical analysis, the stability in a tokamak with circular cross-section and peaked pressure profile was investigated for three types of current profile, i.e. parabolic, flat and hollow profiles. In a

low beta state ($\epsilon\beta_p < 0.5$), the influence of the current profile on the kink-ballooning stability is small and the unstable region in the q_0 space is almost the same, while, in a high beta state ($\epsilon\beta_p > 0.5$), the stability is strongly depends on the current profile. Especially, the hollow current profile was found to extend the unstable region to the higher q_0 value ($q_0 > 2$) and the second stability region could not be obtained up to $\epsilon\beta_p < 1.2$, where the plasma is in the second stability region both for the parabolic and flat current profiles

In JT-60 high β_p experiments, the β_p collapses with fast growth rate ($\sim 200 \mu\text{sec}$) were observed and restricted the maximum β_p below some value. In these high β_p discharges, the large fraction of the neoclassical bootstrap current is estimated and the current profile is expected to be hollow. The stability analysis by using equilibria numerically evaluated for these high β_p discharges showed that the critical β_p against the $n=1$ kink-ballooning mode for the hollow current profile is consistent with the values of β_p observed at the high β_p collapse. The analysis further showed that the plasma can be stable for kink-ballooning modes with $n < 6$ even in high β_p discharges when the central current drive by NBI is employed to compensate the hollow current profile produced by the bootstrap current and q_0 is kept above 2.0, as in the planned experiments in JT-60U and in the steady state tokamak reactor SSTR.

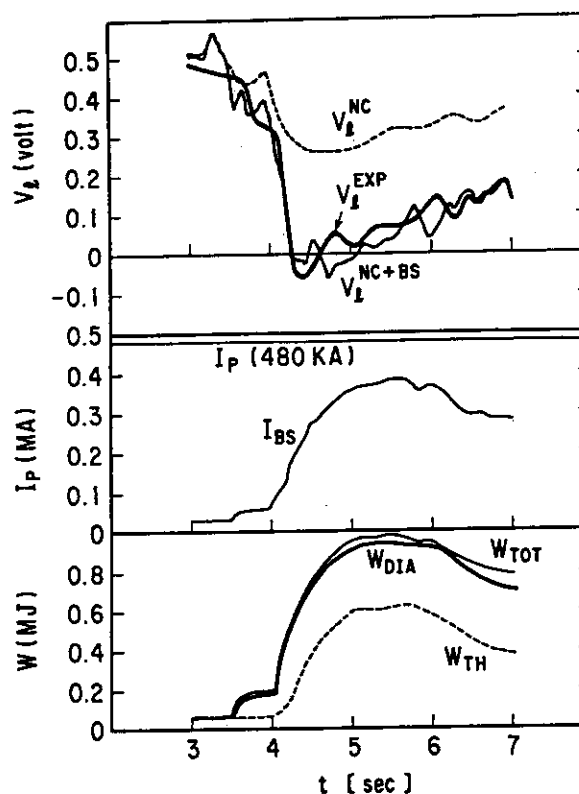


Fig.IV.3.1-4 Comparison of simulation results with experimental data on the onturn voltages, the bootstrap current and stored energies.

References

- [3.1-1] T. Hirayama, M. Kikuchi, H. Shirai, et al., JAERI-M 91-026 (1991)
- [3.1-2] R. R. Dominguez, R. E. Waltz, Nucl.Fusion, **27** (1987) 65.
- [3.1-3] H. Shirai, T. Hirayama, M. Azumi, JAERI-M 91-018 (1991)
- [3.1-4] B.G. Hong, and W.Horton, Phys.Fluids B **2** (1990) 978.
- [3.1-5] B.G. Hong, D.-I. Choi and W. Horton, Phys.Fluids **29** (1986) 1872.
- [3.1-6] K. Nagashima, T. Fukuda, M. Kikuchi, et al., Nucl. Fusion **30** (1990) 2367
- [3.1-7] Kikuchi M., Azumi M., Tsuji S., et al., Nucl. Fusion **30** (1990) 343
- [3.1-8] JT-60 Team, JAERI-M 90-066, pp 178-181

3.2 LHRF Experiments

3.2.1 Analysis of lower hybrid wave propagation and absorption

Recent progress of LHCD studies on JT-60 gives a light to steady state operation of a tokamak reactor[3.2-1~3.2-3]. It is important to explain the experimental LHCD results with theories, which ensures the extrapolation to future devices. For this purpose, we studied wave propagation and absorption.

The LHW together with low NBI power of ~1 MW as a probe of the wave measurement were injected into plasma where density ramped up linearly during the injection period, and we measured the time evolutions of the intensities of 150keV fast ion accelerated by the LHW and the intensities of the electron cyclotron emission (ECE) generated by the fast electrons ($=1.5\omega_{ce}$). The fast ion became appreciable when the ECE signal began to decrease. This critical density n_e^c gives the dispersion relation of the LHW and the ratio of the wave numbers k_{\perp}/k_{\parallel} is experimentally estimated from the E_B and T_e [3.2-4,5]. The data point of k_{\perp}/k_{\parallel} corresponding to each frequency are plotted in the Fig. IV.3.2-1. The cold electrostatic dispersion relation of the LHW

$$\omega^2 = \omega_{LH}^2 (1 + (k_{\parallel}/k_{\perp})^2 (m_p/m_e) / \gamma)$$

where $\gamma = \Sigma(n_j/n_e)(Z_j^2/A_j)$ is drawn in Fig.IV.3.2-1, too, using the n_e^c . The experimental points fits very well to the calculated dispersion curves. The point with the $E_B=40$ keV is also exactly on the curve of the corresponding density. Thus, it is found that the LHW in a tokamak plasma follows the simple linear dispersion relation[3.2-6].

Another interesting result in the LHwave-particle interaction is that the presence of the spectral gap does not degrade the wave absorption and the critical density[3.2-5]. The results suggest that the gap between wave spectrum and maxwellian electrons or beam ions was filled

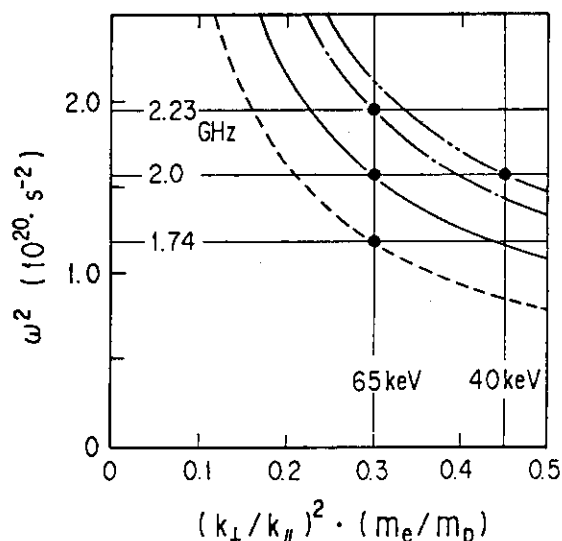


Fig. IV.3.2-1 Plots of the dispersion relation of the LHW. The closed circles indicate experimental points and four curves correspond to the dispersion relation from the critical density of each point.

with N_{\parallel} -upshifted wave. To confirm the N_{\parallel} -upshift further, two different LHW of (1.74GHz, $N_{\parallel}=1.6-2.6$) and (2.23GHz, $N_{\parallel}=2.2-3.6$) were injected simultaneously. When the density was slightly higher than the critical density of 1.74 GHz and less than that of 2.23 GHz, LH power was almost completely absorbed by beam ions in the case of 1.74 GHz only. However, when the 2.23 GHz was added in the spectral gap region of electrons and forms the bridge on the gap, fast ion flux decreases and ECE signal increases, since some part of the 1.74 GHz power could couple to the electrons before coupling to ions. It is found that the N_{\parallel} -upshift is necessary to fill the spectral gap [3.2-6].

3.2.2 Effect of the spectral gap on current drive efficiency

LHCD gives the highest CD efficiency ($\eta_{CD} = 3.4 \times 10^{19} \text{m}^{-2} \text{A/W}$), and the CD efficiency seems to depend rather strongly on the electron temperature T_e [3.2-1, 3.2-6]. Following a simple theory, the CD efficiency does not depend directly on the T_e but on wave N_{\parallel} spectrum [3.2-7]. As described in the section 3.2.1, the actual N_{\parallel} spectrum absorbed by the electrons is different from the launched spectrum since the upshifted N_{\parallel} wave fills the spectral gap. It is, therefore, quite natural that the experimental CD efficiency differs from the simple theoretical value. The modification which include the effect of the spectral gap has to be considered. Actually, this modification explains the T_e dependence of the CD efficiency [3.2-6]. More sophisticated self consistent numerical simulation with ray tracing code including the N_{\parallel} upshift due to the toroidal effect and Fokker Planck calculation code agrees well to the experimental results [3.2-8]. The theoretical efficiency η_{CD} is proportional to $1/(N_{\parallel \text{max}} N_{\parallel \text{min}})$. In the presence of the spectral gap, $N_{\parallel \text{max}}$ makes upshift until the lowest phase velocity touches to the $\sim 3v_{Te}$. It means that $N_{\parallel \text{max}} \sim c/(3v_{Te})$, which yield $\eta_{CD} \propto T_e^{1/2}$. This is the physical picture of the T_e dependence obtained in the experiments [3.2-9].

References

- [3.2-1] JT-60 Team (presented by K. Ushigusa), Plasma Phys. and Cont. Fusion 32(1990)853.
- [3.2-2] T. Imai et al., Kakuyugo-Kenkyu Supplement 65(1991)99.
- [3.2-3] O. Naito et al., Nuclear Fusion 30(1990)1137.
- [3.2-4] J. G. Wegrowe, et al., Proc. of IAEA Tech. Meeting, CLM-CD, Vol.2 (1983)343.
- [3.2-5] M. Nemoto, et al., Phys. Rev. Lett. 67(1991)70.
- [3.2-6] T. Imai, et al., in Plasma Phys. and Cont. Nucl. Fusion Res. 1990 (Proc. of 13th Int Conf., Washington) IAEA-CN-53/E-1-3.
- [3.2-7] J. Stevens, et al., Nuclear Fusion 28(1988)217.
- [3.2-8] R. S. Devoto, et al., to be published.
- [3.2-9] K. Ushigusa, et al., to be published.

3.3 ICRF experiments

3.3.1 Heating properties of higher harmonic regimes

Second and third harmonic ICRF heating experiments were carried out with a frequency of 131 MHz in JT-60 [3.3-1]. High incremental energy confinement time of ~ 110 ms is obtained for second harmonic hydrogen minority heating with helium ohmic target plasmas in a wide

density range ($2.5 \times 10^{19} \text{m}^{-3} \leq \bar{n}_e \leq 7 \times 10^{19} \text{m}^{-3}$). The energy confinement time is larger by ~25 % than values of the Goldston L-mode scaling. Giant sawteeth with extended periods appear even in high densities and low q regimes. Threshold ICRF power for producing the giant sawteeth is about 2 MW. As shown in Fig.IV.3.3-1, these results are in contrast with the JET and TFTR results which are obtained at $\bar{n}_e < 3.5 \times 10^{19} \text{m}^{-3}$ for fundamental minority heating. However, a small amount of additional NBI power (~ 1 MW) reduces the sawtooth period dramatically. Fokker-Planck calculation indicates that energetic ions of 0.5 MeV decreases with increasing NBI power since NBI of 70 keV is a lower energy hydrogen source. Thus energetic ions may play an important role in sawtooth stabilization.

Third harmonic ICRF heating experiments were performed in a density range of $\bar{n}_e = 1.7 - 4 \times 10^{19} \text{m}^{-3}$ in combination with NBI. The energy confinement time is larger by ~ 20 % than values of the Goldston L-mode scaling. A remarkably extended sawtooth period of 410 ms was obtained in combined heating of 2.3 MW ICRF and 10.3 MW NBI (shot E11446), which is about 6 times as long as the energy confinement time (73 ms). High energy ion tails (beam acceleration) were observed during combined heating. Absorbed ICRF power density p_{IC} and tail ion stored energy density w_{tail} can be estimated by fitting the ion tail calculated from one-dimensional Fokker-Planck code using measured plasma parameters to the ion tail of the measured hydrogen energy spectra at the plasma core. Then incremental fast ion stored energy by ICRF ΔW_{tail} can be calculated from

$$\Delta W_{tail} \approx (w_{tail}(IC+NB) - w_{tail}(NB)) P_{IC} / p_{IC}$$

Figure IV.3.3-2 shows a comparison between experimental (diamagnetically measured) and calculated values of the incremental stored energy by ICRF as a function of the electron density. Considering possible errors of the calculated values ($\pm 30\%$), the calculated values well agree

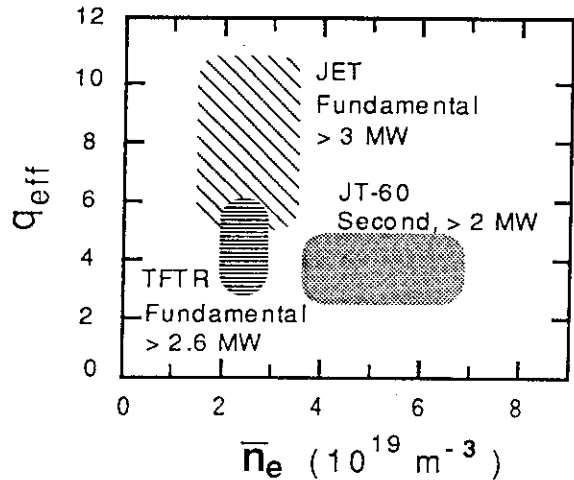


Fig. IV.3.3-1 Regions for generation of extended period sawteeth by ICRF heating.

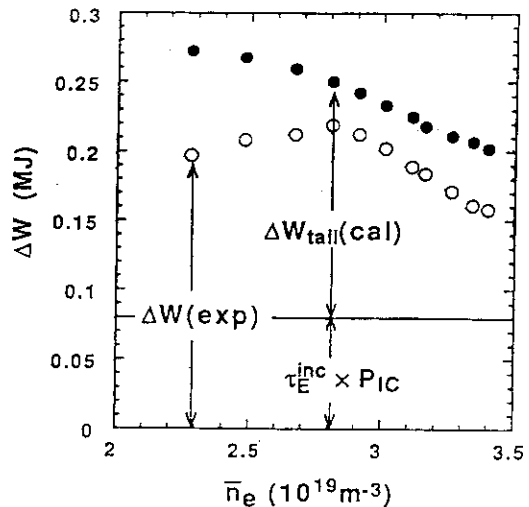


Fig. IV.3.3-2 Comparison between experimental and calculated values of the incremental stored energy as a function of \bar{n}_e .

with the experimental ones. Therefore, the enhancement of the energy confinement time during combination heating is mainly due to fast ions accelerated by third harmonic ICRF waves.

3.3.2 Theoretical estimation of stored energy

With third resonance ICRF heating, the measured stored energy, W_{exp} , is compared with the theoretical value, W_{theory} , in Table IV.3.3-1. The theoretical stored energy is obtained by a numerical code, which is a self-consistent solver of the ICRF wave propagation equation and the Fokker-Planck equation with the effects of particle acceleration due to the RF-electric field [3.3-2]. The upper side parameters in Table II.3.3-1 (from $n_e(0)$ to P_{IC}) and the density and temperature profiles are applied from measured data. The density of minority hydrogen, n_{H} , is estimated from the measured value of Z_{eff} , and $T_i(r) = T_e(r)$ is assumed. The good agreement of incremental stored energy, $\Delta W = W(t = 5.3 \text{ sec}) - W(t = 4.9 \text{ sec})$, between ΔW_{exp} and ΔW_{theory} is obtained.

Table IV.3.3-1 Comparison between experimental and numerical values of the stored energy

E11446

t [sec]	4.9	5.3
$n_e(0)$ [10^{19} m^{-3}]	2.5	2.9
$T_e(0)$ [keV]	3.5	4.3
P_{NB} [MW]	5.4	10.3
P_{IC} [MW]	1.9	2.3
$n_{\text{H}}(0)$ [10^{19} m^{-3}]	0.73	1.0
W_{exp} [kJ]	640	900
W_{theory} [kJ]	766	1054

References

- [3.3-1] T. Imai, et al., 13th Int. Conf. on Plasma Physics and Controlled Nuclear Fusion, Washington, 1990, IAEA-CN-53/E-1-3.
 [3.3-2] K. Hamamatsu, et al., Nucl. Fusion 29 (1989) 147

3.4 Topics

3.4.1 Limiter H-mode with LHCD

The H-mode has been observed in limiter discharges with lower hybrid current drive (LHCD) on JT-60 [3.4-1,2]. The threshold LH power for the H-mode transition was as low as about 1.2 MW in contrast to the threshold NB power at about 16 MW in the outer or lower divertor configurations. Suppression of electron density fluctuations was observed near the edge where sharp density gradient was formed. The hard X-ray emission measurements indicate that the H mode was triggered when hard X-ray photons emitted outer than a half tangent minor radius exceeded a threshold [3.4-3]. The fast electrons generated near the edge by LHCD appear to be connected with the low power threshold. The hard X-ray spectra were found to be different depending on the frequency combination. Around the threshold line averaged density for the H mode of $2 \times 10^{19} \text{ m}^{-3}$, the 1.74 + 2.23 GHz combination produced the photon temperatures of 110 ~ 140 keV whereas the 2.0 + 2.0 GHz combination produced those of less than about 110 keV. The threshold intensity (I_0) for H transitions drops with increasing photon temperature

(T_{ph}) on the assumption of the hard X-ray spectra as $I_{H.X.} = I_0 \exp(-hv/kT_{ph})$. Hence the favorable effect of the application of LH power at two different frequencies could be explained by the effective generation of fast electrons. The reason why the H mode with LHCD has never been obtained in divertor configurations may be explained by much more peaked hard X-ray profiles than those in limiter discharges.

3.4.2 MARFE phenomena on neutral beam heated JT-60 plasmas [3.4-4]

In JT-60, the MARFE has been observed frequently in high- I_p and high density limited discharges with NB heating after replacement of the first wall from TiC coated molybdenum tiles to graphite ones. The MARFE occurs around the midplane on the inside wall. The poloidal drift motion of the MARFE has been observed frequently in the discharges during I_p rump down and/or reducing P_{NB} . The MARFEs occur near the density limit of the JT-60 plasmas. The empirical scaling of the threshold density for MARFE onset is obtained as $\bar{n}_e = (\rho_{OH} I_p + \rho_{NB} P_{NB})/\pi a^2$ where $\rho_{OH} = 0.55 \pm 0.05 (10^{20}/MAm)$ and $\rho_{NB} = 0.07 \pm 0.01 (10^{20}/MWm)$.

The radiation power density in the MARFE is estimated to be 20-30 MW/m³ typically. The major contributors to the large emissivity in the MARFE are estimated to be carbon and oxygen in low charge states. The radiated power from the plasma with MARFE is about 90% of the absorbed power. Both stored energy and central electron temperatures do not change by the MARFE onset in spite of the such intense radiation loss. A simple model based on the thermal equilibrium and the thermal instability in a peripheral plasma calculates the onset condition of the MARFE. Figure IV.3.4-1 shows the MARFE onset conditions in the Hugill diagram calculated by the criterion for the NB heated plasma in the range of the carbon concentration 0.3-1%.

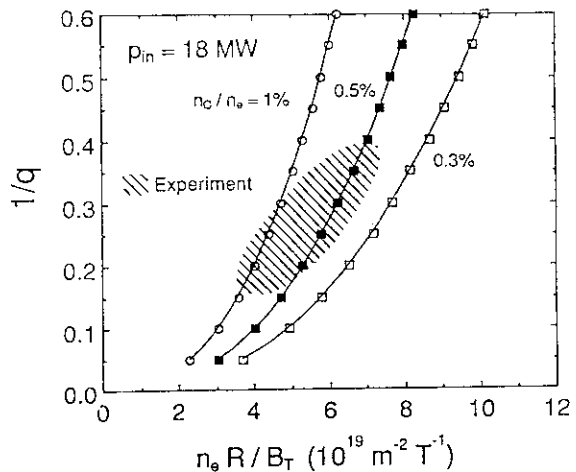


Fig.IV.3.4-1 MARFE onset condition on the Hugill diagram calculated by simple model on the radiative thermal instability for the NB heated plasma in the range of carbon concentration 0.3-1%.

3.4.3 Impurity behavior

In order to realize a fusion reactor, the impurity control in high temperature plasmas is important issue, because of the radiation loss and fuel dilution. These problems are closely related with the selection of first wall materials, with the characteristics of boundary plasmas, and also with the impurity transport in the main plasma. JT-60 experiments have been carried out with

TiC-coated molybdenum (metallic) first-walls and graphite first-walls in the outer X-point (closed divertor: with divertor chamber) configuration, and with graphite first-walls in the lower X-point (open divertor: without divertor chamber) configuration [3.4-5]. In these cases, impurity behavior has been investigated on high-power (~ 20 MW) NB-heated discharges [3.4-6]. The light impurity concentrations and Z_{eff} had the lowest values in the outer X-point discharges with TiC-coated molybdenum first walls. In high density discharges, the heat load on the divertor plate was suppressed by radiative cooling due to carbon and hydrogen in the divertor region [3.4-7-11]. Concerning the impurity transport, no impurity accumulation was observed in L-mode discharges [3.4-12]. However, when sawtooth-free plasmas with a peaked density profile were obtained by hydrogen pellet injection, impurity (titanium) accumulation was observed [3.4-13]. This accumulation was well simulated with a neoclassical transport and a very small anomalous diffusion coefficient in the inner region of $q=1$ surface [3.4-14].

3.4.4 Divertor study [3.4-11]

Remote radiative cooling can significantly reduce divertor plate heat flux, which may provide a solution to one of the major problems of present and next-step machines. In JT-60 high density divertor operation, remote radiative cooling becomes significant [3.4-9,10]. Remote radiative cooling power of up to 50 % of the total absorbed power (20MW) was observed with a short divertor channel (i.e. 4-7cm). Measurements of line intensities from lowly-ionized impurities and neutral hydrogen in the divertor suggest that remote radiative cooling is a mixture of carbon radiation, hydrogen radiation and charge exchange loss.

Dense and cold divertor plasmas can reduce erosion of divertor plates, enhance impurity shielding and remote radiative cooling. Analysis of heat flux density and H_{α} intensity suggests that JT-60 divertor plasmas are dense and cold ($n_{\text{ediv}} \approx 2.4 \times 10^{20} \text{ m}^{-3}$, $T_{\text{ediv}} \approx 26 \text{ eV}$). A simple divertor model was developed to analyze these experimental observations. This model solves three fluid equations consistently with neutral particles and radiative loss. Calculations with JT-60 parameters show that the observed values of density, temperature, radiative power and impurity concentration are consistent with the model.

3.4.5 Heat flux onto divertor plates [3.4-8]

The behaviour of heat flux onto divertor plates is investigated in Lower Hybrid Range of Frequency (LHRF) heated and neutral beam heated discharges by using a IRTV camera system. In LHRF heated discharges, power balance is dominated by interactions between the plasma and the LHRF launcher. The heat flux to the launcher is $\sim 60\%$ of the input power, while heat deposition to the divertor is $\sim 40\%$ of the input power with the gap $\delta_{30} > 2 \text{ cm}$. δ_{30} is the

aperture between the separatrix surface and the outer wall at 30 degree above the midplane. Ti gettering significantly reduces radiation loss from the main plasma due to reduction of oxygen, resulting in divertor heat load increase up to 70% even with the gap $\delta_{30} = 1$ cm.

The peakedness of heat flux (peak heat flux density divided by total heat flux) is a function of plasma density, beam power and safety factor. A one-dimensional model reproduces the parameter dependence of the peakedness of heat flux in the discharges with plasma density $\bar{n}_e < 2.5 \times 10^{19} \text{ m}^{-3}$, $P_{\text{MAX}} < 2 \text{ MW/m}^2$, beam injection power $P_{\text{beam}} < 12 \text{ MW}$ when perpendicular heat conductivity is assumed to be $6 \sim 8 \text{ m}^2/\text{s}$.

3.4.6 Helium ash exhaust and transport

In a burning plasma with deuterium and tritium fuels, concentration of helium(He) ash must be controlled at a low level, e.g. 5-10%. The first simulation experiment of He ash exhaust and transport is performed with neutral helium beam injection of 30 keV into neutral beam heated L-mode plasmas [3.4-15]. The deposition profile of He beam is calculated and supported by measured shine-through. The profile is well peaked and similar to that of a He ash production profile. Metastable fraction in the He beam is less than 1%. Experiments with He gas has been published in elsewhere [3.4-16]. He^{2+} ion density profile in the main plasma is measured by charge exchange recombination spectroscopy. Neutral particle pressures of hydrogen and He in the divertor region are $P_{\text{H}_2} = 0.43 \text{ Pa}$ and $P_{\text{He}} = 0.036 \text{ Pa}$ at $n_e = 5.8 \times 10^{19} \text{ m}^{-3}$, respectively, and increase in proportion to n_e^3 . Enrichment factor defined as $(P_{\text{He}}/2P_{\text{H}_2})^{\text{DIV}} / (n_{\text{He}}/n_e)^{\text{MAIN}}$ is 0.25 to 0.5 for $n_e = (2.9-5.8) \times 10^{19} \text{ m}^{-3}$, and increases in proportion to n_e . These characteristics are promising for efficient He ash exhaust in high density operation. Based on these results, the required pumping speed of the He ash exhaust in a reactor should be around several tens m^3/s in the L-mode discharges. Transport analysis of a peaking factor C_v and a diffusion coefficient D_a have been done by a one-dimensional time dependent transport code. C_v is defined by the inward flow velocity $v_{\text{in}} = -C_v D_a 2r/a^2$ and is in the range of 1 to 1.5. D_a is a anomalous diffusion coefficient and estimated to be $0.4 \text{ m}^2/\text{s}$ by assuming spatial uniformity. On the other hand, C_v of the bulk plasma is in the range of 0 to 1. He has a slightly more peaked density profile than the bulk plasma [3.4-7]. These results show that, in the case of L-mode discharges, thermalized α particles (He ash) generated in the core plasma can be easily exhausted in a fusion reactor.

3.4.7 Measurement of neutral beam stopping for hydrogen in the JT-60 plasma [3.4-17]

Shine-through for hydrogen and helium beams in a plasma was measured. Shine-through for an atomic hydrogen beam with $f_1 : f_2 : f_3 = 7\% : 32\% : 61\%$ (where f_1 , f_2 and f_3 represent fractions of the full, half and third energy, respectively) and a full energy of 140 keV, was smaller than a value predicted by usual cross sections without inclusion of excitation processes at an electron density (\bar{n}_e) above $3 \times 10^{13} \text{ cm}^{-3}$. A fractional beam stopping increment (δ), which

was defined by $\delta = (\sigma_S - \sigma_S^{(0)})/\sigma_S^{(0)}$ (here σ_S was an experimental stopping cross section and $\sigma_S^{(0)}$ was the cross section without including multistep processes via excited states), was about 0.2 at $\bar{n}_e = (3.1-5.0) \times 10^{13} \text{ cm}^{-3}$ and $Z_{\text{eff}} = 1.6-2.5$. The value of δ was consistent with the calculation by JANEV *et al* (1989, *Nucl. Fusion* **29**, 2125).

3.4.8 Confined alpha particle diagnostics in JT-60U

In reactor-grade tokamaks, it is important to investigate confinement properties of alpha particles. A double charge-exchange method using a high energy probing beam is considered to be the most reliable one in diagnostic methods proposed for the measurement. In JT-60U, alpha particle production experiment by D-³He ICRF heating will be performed to study behaviors of fusion product alphas. The alpha particle measurement is planned by using a helium diagnostic beam(200 keV) and a mass-resolved neutral particle energy analyzer. The expected flux and spectral shape were evaluated by taking into account the multistep ionization of helium beam atoms and neutralized alphas. The beam energy is lower than the desirable energy for measuring fast confined alphas near the birth energy. However, by using the beam system, it has been found from the evaluation that we can investigate the confinement property of fusion product alphas from the spectral shape. And also such system using a present-day He beam is useful to diagnose behaviors of confined alphas in reactor-grade tokamak like ITER[3.4-18].

References

- [3.4-1] S. Tsuji *et al.*, Phys. Rev. Lett. **64** (1990) 1023.
- [3.4-2] JT-60 TEAM, Plasma Phys. Contr. Fusion **32** (1990) 853.
- [3.4-3] S. Tsuji *et al.*, in Proc. 13th Intern. Conf. on Plasma Phys. and Contr. Nucl. Fusion Research, Washington, 1990, E-1-4.
- [3.4-4] T.Nishitani, S.Ishida, N.Hosogane, et al., Journal of Nuclear Materials 176 & 177 (1990) 763
- [3.4-5] JT-60 TEAM, in Plasma Physics and Controlled Nuclear Fusion Research 1988 (Proc. 12th Int. Conf. Nice, 1988), Vol. 1. IAEA, Vienna (1989) 67.
- [3.4-6] Kubo, H., Sugie, T., Sakasai, A., et al., Nucl. Fusion **29** (1989) 571.
- [3.4-7] Sugie, T., Itami, K., Nakamura, H., et al., in Plasma Physics and Controlled Nuclear Fusion Research 1990 (Proc. 13th Int. Conf. Washington, 1990), Vol. 1. IAEA, Vienna (1991) paper IAEA-CN-53/A-5-4.
- [3.4-8] Itami, K., Fukuda, T., Ikeda, Y., et al., J. Nucl. Mater 176 & 177 (1990) 504.
- [3.4-9] Tsuji, S., et al., in Plasma Physics and Controlled Nuclear Fusion Research 1988 (Proc. 12th Int. Conf. Nice, 1988), Vol. 1. IAEA, Vienna (1989) 265.
- [3.4-10] Kubo, H., Itami, K., Shimada, M., et al., Japan Atomic Energy Research Institute Report JAERI-M 90-066 (1990) 138.
- [3.4-11] Shimada, M., Kubo, H., Itami, K., et al., J. Nucl. Mater 176 & 177 (1990) 122.
- [3.4-12] Koide, Y., Hirayama, T., Sugie, T., et al., Nucl. Fusion **28** (1988) 1835.
- [3.4-13] Sugie, T., Kubo, H., Sakasai, A., et al., in Controlled Fusion and Plasma Heating (Proc. 17th Eur. Conf. Amsterdam, 1990), Vol. 14B Part I, European Physical Society (1990) 223.
- [3.4-14] Sugie, T., Kubo, H., Sakasai, A., et al., Kakuyugo Kenkyu **65** Supplement (1991) 287.
- [3.4-15] H.Nakamura, T.Hirayama et al., submitted to Phys.Rev.Lett..
- [3.4-16] H.Nakamura et al., Fusion Technology **18**,578(1990).
- [3.4-17] K.Tobita, T.Itoh, A.Sakasai, et al., Plasma Physics and Controlled Fusion, Vol. 32, No.6, (1990) 429.
- [3.4-18] Y.Kusama, K.Tobita, T.Itoh, et al., Rev. Sci. Instrum. **61**(10), Oct., 1990, p3220.

3.5 Transport database

3.5.1 Transport database

Since the production of the JT-60 first plasma in April 1985, many plasma discharges are produced to study the plasma confinement characteristics. One of the important subjects of the experiment is to establish well documented database so that we can derive many important physics and scalings by comparing with other tokamak database. We have conducted the database assessment in which we collect good profile measurements and analyze them with the 1D empirical transport analysis code.

The database is restricted to the JT-60 discharges produced in 1985-1987 due to limited time available for the analysis and the checking procedure of the internal consistency. Well documented 335 time slice profile data are analyzed using the empirical transport analysis codes (LOOK/OFC/SCOOP system). The results are summarized in JAERI-M 91-057[3.5-1] in which description of the JT-60 tokamak, diagnostic system, database shot lists, all Te, ne profiles and Ti(0) data and transport analysis results are shown. This database is compiled into the database utility "DARTS" described in the following section. This database is basically open to all physicists in this field.

3.5.2 Retrieval system for experimental database of JT-60 [3.5-2]

DARTS (Database Retrieval System) is a system to support users of experimental database. By using DARTS, one can easily access to his objective data among enormous experimental database. DARTS contains an index database which can also be used as a physics database. The index database consists of two data files, bit and bulk data files (about 500 data points in total per shot). The bit data is a set of data with bit form, which as refereed first in the retrieval procedures. The bulk data are composed of some plant data, some diagnostic data and some results from magnetic analysis and transport analysis. Subsequent to the retrieval step using bit file, the bulk data are refered in the next step. DARTS provides utilities to demonstrate retrieval results on a graphic terminal.

References

- [3.5-1] M.Kikuchi, K.Kikuchi, T.Aoyagi, et al., JAERI-M 91-057.
 [3.5-2] T.Aoyagi, K.Tani, H.Haginoya et al., JAERI-M 89-015 (in Japanese)

3.6 Development of fusion plasma analysis codes

3.6.1 Data handling system

We have developed a time slice monitor system for the experimental data (SLICE), in order to obtain the confinement properties such as the kinetic stored energy and the energy confinement time and to make the plasma parameter profiles for the transport analysis in JT-60 Upgrade. SLICE has the two major functions. Diagnostics data measured in the real space of (R,Z) are mapped to the flux surfaces calculated by the MHD equilibrium code (SELENE) and are reduced to the profile data as a function of effective minor radius ρ , which is defined by

$\rho = \sqrt{V / 2\pi^2 R_0}$ (V: Volume, R_0 : major radius). These profile data in the ρ space are least-square-fitted by using a proper functional form. These mapping data and fitting data are stored with the physical identification name in a data base named by MAP-DB. The user can process the profile data in MAP-DB and get a run data for the transport analysis code in the conversational form.

3.6.2 1.5D tokamak transport code system : TOPICS

In order to evaluate the plasma performance, to test the validity of theoretical models and to analyze experimental data, the tokamak transport code system TOPICS (Tokamak Performance Prediction and Interpretation Code System) has been developed. In this system, the MHD equilibrium equations, the transport equations and other related equations in physical processes like heating, current drive and MHD activities are solved under some specific constraints, which depend on the subject to be solved. The code is essentially the FORTRAN based one but the load module for the specific analysis is constructed from the subroutine library in the system by using the code-generation system NEWORG, which select only subroutines necessary for the analysis and makes the final code be compact and easy to handle. This code system can be used both for the steady state analysis and the time dependent analysis in cooperation with the time evolution of MHD equilibria, and both for predictive analysis and experimental data analysis, where profile data of plasma parameters is prepared by the profile data acquisition code SLICE. Under this system, users can link their own subroutines to the system source code and can easily test their idea both for prediction and experimental data analysis.

3.6.3 Current drive analysis code : ACCOME

ACCOMME is a numerical code to investigate steady state properties of inductive and noninductive current drives in a tokamak, consistent with MHD equilibrium[3.6-1]. This code has been developed and is continued to be updated for including new aspects of physics model and functions, under the Japan-US collaboration program. The code includes the ohmic current, bootstrap current, neutral beam driven current and lower hybrid current drive: NBI current is calculated, taking into account of the effects of mirror trapping, energy diffusion and bounce motion of fast ions, and the neoclassical bootstrap current is evaluated for multi-species ions including impurity and unthermalized fast ions. As the LH current drive module, the Bonoli code [3.6-2] is introduced in the code. With these models, the self-consistent solution of MHD equilibrium and current drives, including their combined current drive effects, is obtained by the iterative algorithm. MHD stabilities for the converged solution can also be investigated with the code. The effort of the improvement of ACCOME in 1990 has been concentrated on the update of the LH current drive module in the up-down asymmetric equilibrium with separatrix and the

bootstrap current module. The new version of ACCOME is successfully applied in the analysis of LH current drive experiments and bootstrap current experiments in JT-60.

References

- [3.6-1] K.Tani, M.Azumi and R.S.Devoto, J. Comput. Phys. (1991) (to be published)
 [3.6-2] P.T.Bonoli, and R.C.Englade, Phys. Fluids 29 (1986) 2937

3.7 Plasma-surface interaction

3.7.1 Gas-release during a plasma disruption [3.7-1]

A modified Penning-type vacuum gauge with a fast response time(<10ms) [3.7-2] was applied to measure pressures during a plasma disruption. Change in the pressure clearly reveals the gas evolution in two stages. The first gas evolution occurs at the same time as the soft-Xray crash and the second one during the plasma current decay phase. The outgassing rate could be obtained from the measured pressure change by considering that the released gas mainly originate from the wall. It was found that there are two peaks in time evolution of the outgassing rate which correspond to those of the Ha emission in the divertor region within an error of several milliseconds. This is the first confirmation of the hydrogen gas release from the first wall.

3.7.2 Performance of divertor plates under high-power and long pulse heating divertor experiments [3.7-3,4]

Damage examinations were made on the graphite and c/c composite divertor tiles which were experienced lower X-point divertor discharges from June 1988 to October 1989. Results are summarized in Table IV.3.7-1 in which those obtained under outside X-point divertor discharges as well as operational parameters are also shown. The damage of the graphite tiles in lower X-point operations were modest and breaking of tiles were avoided by introducing c/c composite. A typical erosion profile for two adjacent tiles is shown in

Table IV.3.7-1 Results and main parameters under various divertor discharges

Parameters	Configurations		
	Outside X-point (Closed)	Outside X-point (Closed)	Lower X-point (Open)
Period	June '86-March '87	June '87-Oct. '87	June '88-Oct '89
Material	TIC/No	Graphite	Graphite-C/C
Plasma Current (MA)	2.0	2.7	2.0
Heating Power (MW)	20(NBI)	30(NBI+RF)	30(NBI+RF)
Heating Duration (s)	1-2	3-5	2-4
Stored Energy (MJ)	2.0	2.4	2.0
Absorbed Energy /shot (MJ)	20	90	100
Heating Shots(>10 MW)	193	186	802
Number of Total Shots	1654	639	2521
P_{red}^{main} / P_{abs} (%)	10-15	10-25	15-30
Z_{eff}	1.5-2	2-4	2-7
P_{div} / P_{abs} (%)	50-70	30-50	20-40
Peak Heat Flux (MW/m ²)	20	20	5
Heat Width (cm)	<2	<2	3-5(FWHM)
Deposited Heat (MJ)	14	36	40
Damage	Melting of Edges	Serious	Modest

P_{div} :Power Flow to Divertor Plate

Fig.IV.3.7-1 which is measured using optical microscope. The region near the edge of the protruding tile was eroded with a gradient of about 1/20. The gradient of field line was 1/20-1/30 in the lower X-point operations, so that heat flux on this region was 2-2.5 times higher than the top surface. This clearly indicates that it is important to avoid large gaps and differences in elevation between tiles in the toroidal direction to eliminate the high heat concentration at the edge of the divertor plate.

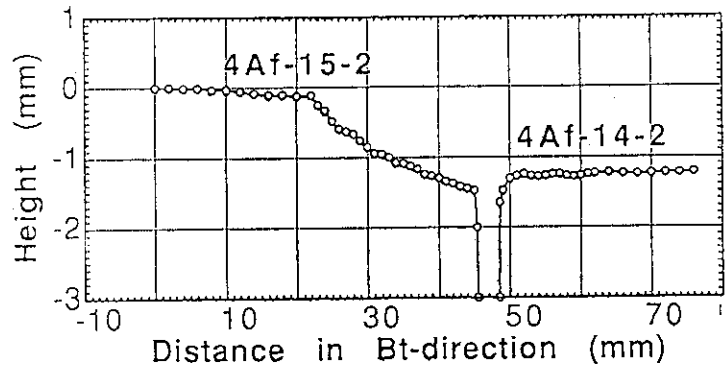


Fig. IV. 3.7-1 Typical erosion profile of graphite tiles

References

- [3.7-1] N. Ogiwara and M. Maeno, J. Nucl. Mater. 176&177 (1990) 792
- [3.7-2] Annual Report of the Naka Fusion Research Establishment JAERI-M 90-160 (1990)
- [3.7-3] T. Ando et al., J. Nucl. Mater. 179-181 (1991) 339
- [3.7-4] T. Ando et al., Kakuyugo Kenkyu 65 (1991) 27

4. Related Developments and Maintenance

4.1 Power supply

4.1.1 MG overhaul and maintenance of facilities

JT-60 power supplies have three motor-generators (MG) which are the PFPS's MG(P-MG), H-MG and TFPS's MG(T-MG) for energy storage. The MGs operate severely, namely, they start and stop every day and accelerate from 420 rpm to 600 rpm and decelerate reversely every discharge shot, and they have been operated for about six years and about 6,000-9,000 hours since their completion. In order to check flywheels and thrust bearings, they were overhauled in period of the JT-60U modification. P-MG, H-MG and T-MG were overhauled from October to December, 1989, from November, 1989 to February, 1990 and from August to December, 1990, respectively.

Overhauls were mainly the decompositions, checks and assembling of motors, generators, flywheels and thrust bearings and so on. In addition standard checks, the non-destructive inspection such as the penetrant test (PT), the ultrasonic test (UT) and the magnetic particle test (MT) were done on thrust bearings, guide bearings, flywheels, bolts of flywheels and so on. Moreover, on the rotor and the stator of the motor and the generator, respectively, diagnosis the deterioration of insulators such as measuring the $\tan\delta$, measuring corona discharges inside the insulators and so on. In FY 1990, the overhaul of T-MG, which was the last one, were performed, and whole results were very good and there is no problems on the operation for next five or six years.

The other facilities, that is, the toroidal field power supply, the poloidal field power supply, the power supply for heating facilities, the general power distribution facility and the second cooling system were maintained and checked simply once a day and in detail once a year.

4.1.2 Power transmission for superconducting coil

In order to perform tests of the United States-Demonstration Poloidal Coil (US-DPC) under the US-Japan Collaborative Program, pulsed electric power was delivered to the superconducting coils by the vertical field power supply (PSV) in December, 1990. Experimental results were very good.

4.2 RF development

4.2.1 LHRF system development

We investigated the heat load of the LHRF launcher in high-power heated divertor plasmas, where the input heating energy was 10-75 MJ and 1-6 MJ for NBI and LHRF, respectively. It was found that a good coupling of the reflection coefficient, $\rho = 15 - 20 \%$, was obtained by pushing the launcher head a few mm from the first wall even though the distance δ between the separatrix and the launcher head was more than 10 cm. In this condition, the heat load on the launcher head rapidly decreased at $\delta > 5$ cm and was estimated to be about 0.4 - 0.6 kW/cm² at $\delta = 10$ cm, $\bar{n}_e < 2 \times 10^{13}$ cm⁻³

during only LHRF injection. A higher heat load was observed on the ion side of the launcher guard limiter during combined NBI + LHRF heating at $\bar{n}_e > 3 \times 10^{13}$ cm⁻³ when fast ions were observed at the plasma edge due to parametric decay instability. Figure IV.4.2-1 shows the intensity of the decay wave, the formation of the fast ion tail and the normalized temperature rise of the LHRF effect during combined heating versus average density, where the distance δ is fixed at 6 - 8 cm. The parametric decay instability occurred with a fast ion tail at $\bar{n}_e > 3 \times 10^{13}$ cm⁻³, which corresponded to the critical density of the heat load [4.2-1].

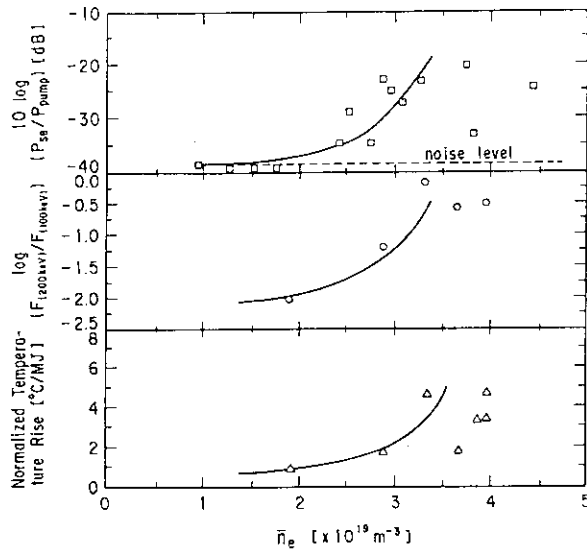


Fig. IV.4.2-1 Density dependence of various parameters at $\delta = 6-8$ cm in the NBI + LHRF heating scheme.

4.2.2 ICRF system development

An ICRF launching system, composed of antennas, feedthroughs and impedance

matching circuits, is the most important part in an ICRF heating system because available injected power into plasmas is limited by their capabilities. The feedthrough, which transmits high power and keeps vacuum, has been developed for the JT-60U ICRF system. Its structure is about 8 inch coaxial lines with bell-shaped ceramic for vacuum seal. The required performances for the feedthrough are: high stand-off voltage (designed value 60 kV) and suppression of multipactoring discharge at low power transmission.

Low power injection is necessary to adjust the impedance matching circuits and to condition the antennas in the initial phase. The multipactoring discharge limits low power injection. Hence, suppression of multipactoring discharge at the feedthrough is very significant from the viewpoint of operation. We examined multipactoring of carbon coating, having secondary electron emissivity < 1 , in the test stand. The multipactoring is caused by multiplication of secondary emitted electron. A ceramic region of the feedthrough is placed at a maximum voltage in the

coaxial line whose end is shorted. Figure IV.4.2-2 shows voltage distributions for transmittable minimum power as a function of the distance from the short plate, d , with and without carbon coating. A hatched section indicates the ceramic region and thin ($\sim 0.1 \mu\text{m}$) carbon coating is made around the ceramic from $d = 0.5 \text{ m}$ to $d = 0.7 \text{ m}$ (a dotted region). Therefore, the carbon coating is quite effective to suppress the multipactoring. The injected power, however, is still limited by the multipactoring in the coaxial line except the feedthrough while the multipactoring region is made narrow.

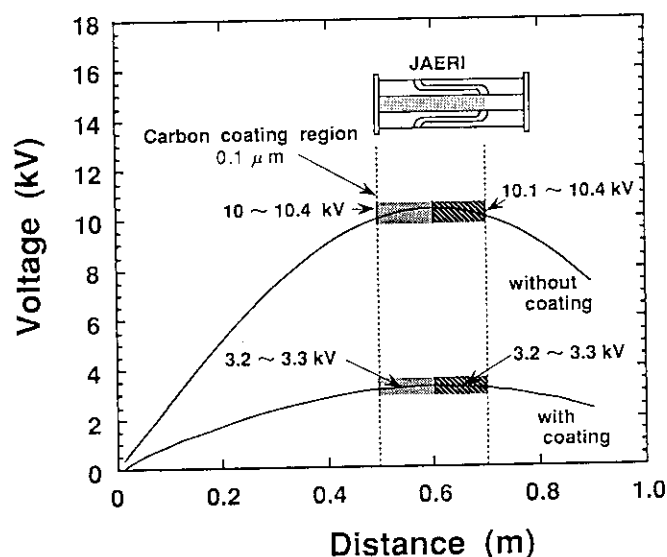


Fig. IV.4.2-2 Voltage distributions for transmittable minimum power as a function of the distance from the short plate with and without carbon coating.

4.2.3 Electron cyclotron heating system

Construction of a high density current device for the JT-60U has been planned for verification of steady-state operations from the viewpoint of improvement of tokamak-type fusion reactors. The electron cyclotron (hereafter called EC) heating device is considered for improving current drive efficiency as a part of the high density current drive device. The preliminary design for JT-60U EC heating system was made last fiscal year. The EC heating system is to be located the RF Amplifier Room of the JT-60 Experimental Building (shown in Fig.IV.4.2-3) and having the basic design characteristics shown in Table IV.4.2-1.

Reference

[4.2-1] Y. Ikeda, T. Imai, K. Ushigusa, et al., J. Nucl. Mater. 176 & 177 (1990) 306.

Table IV.4.2.-1 JT-60U Electron Cyclotron Heating System Characteristics

Output frequency	110 GHz
System output power	5 MW (target)
RF unit output power	More than 0.8 MW 1 MW (target)
Pulse length	10 sec
Transmission method	Waveguide (Use of mirrors for launcher)
Power Transmission efficiency	More than 80% (target)
Injection method	Ordinary mode

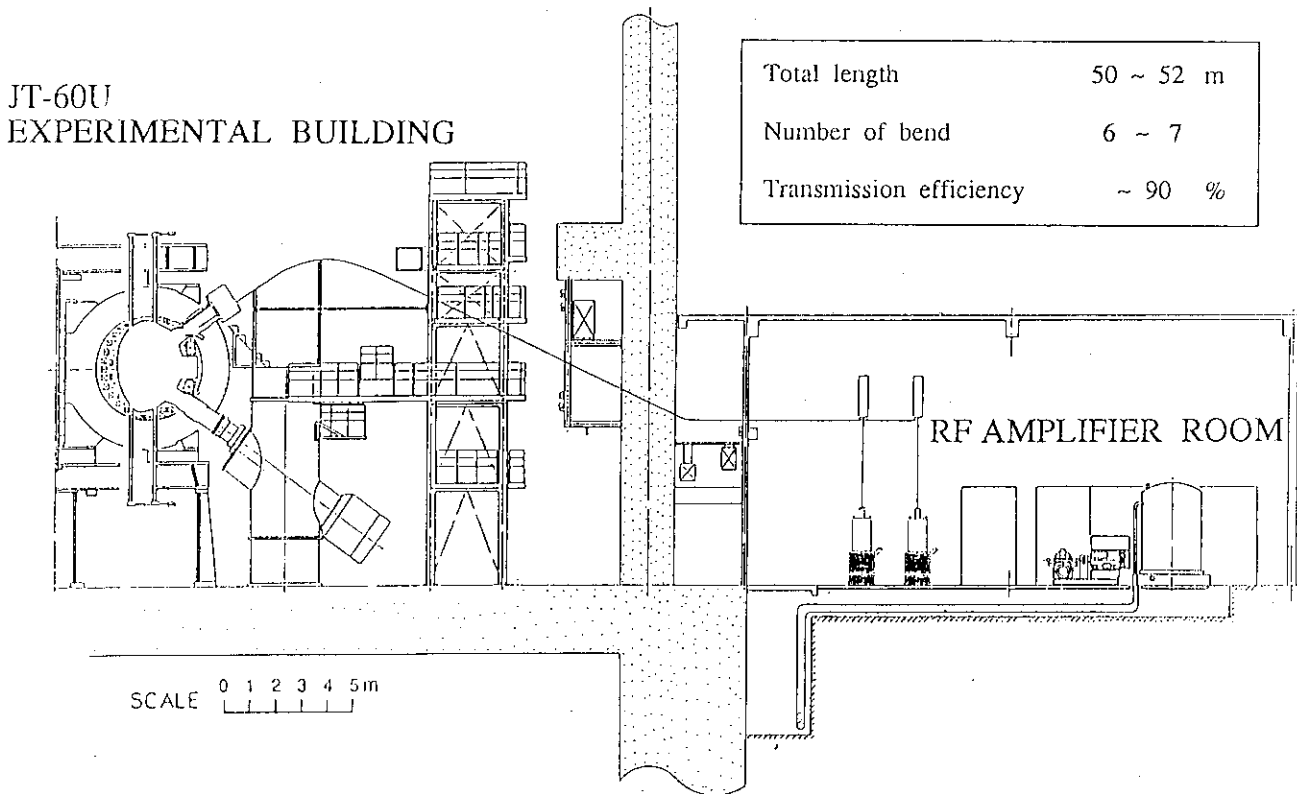


Fig.IV.4.2-3 Cross-section view of the JT-60U electron cyclotron heating system.

V. TECHNOLOGY DEVELOPMENT

1. Vacuum Technology

1.1 Introduction

Vacuum technology is one of the most important tools for the operation and maintenance of the current fusion devices. On the other hand, it has been recognized that development of innovative vacuum techniques is essential for realization of the fusion experimental reactors such as ITER and FER. The technology area includes wall preparation, pumping system, gauging, vacuum components, sealing and leak hunting.

For this fiscal year, development activities of the ceramic turbo-viscous pump and the surface insulation techniques for the ITER in-vessel components should be remarked. The Zr-bearing-copper gasket for knife-edge-type vacuum flanges and the ceramic-insulated wires, which have been developed in the Plasma Engineering Laboratory, will be commercially available in 1991. The improvement of the QMS by using the second stable zone in Mathieu's stability diagram is considered to be of great promise.

1.2 Progress in ceramic vacuum pump development

The conditions needed for the torus pumping system of the International Thermonuclear Experimental Reactor (ITER) are a large pumping speed of 350-700 m³/sec for ash (helium) and fuel gases (deuterium and tritium), and the robustness against radiation, tritium, and high magnetic fields. To establish such a system by using dynamic oil-free pumps, we have been developing two types of ceramic vacuum pumps, the ceramic turbomolecular pump and the ceramic roughing pump, for six years in cooperation with Mitsubishi Heavy Industries, Ltd. In this fiscal year, our effort was laid on the performance test and the improvement of the new ceramic roughing pump named turbo-viscous pump.

The construction of the pump features the multistage ceramic (Si₃N₄) rotor assembly and the oil-free driving unit which consists of gas bearings and gas turbines (see Fig.V.1.2-1). Although the rotor spins at a very high speed of 25,000 rpm, the pump can be operated in high magnetic fields since it does not use either a conductive (metal) rotor or an electric motor. The test has shown that the pump works in a wide pressure range from atmospheric pressure to a pressure lower than 10⁻³ Pa and has a maximum pumping speed of 0.28 m³/min for nitrogen or 0.25 m³/min for helium as shown in Fig.V.1.2-2[1.2-1]. Based on the development of the medium size pump, we have designed a larger size pump to increase the pumping speed up to 10-20 times its present level. The scaling up of the roughing pump will fulfill the ITER pumping system requirement.

References

[1.2-1] Y. Murakami, T. Abe, H. Ohsawa, et al., J. Vac. Sci. Technol. A9 (1991) 2053.

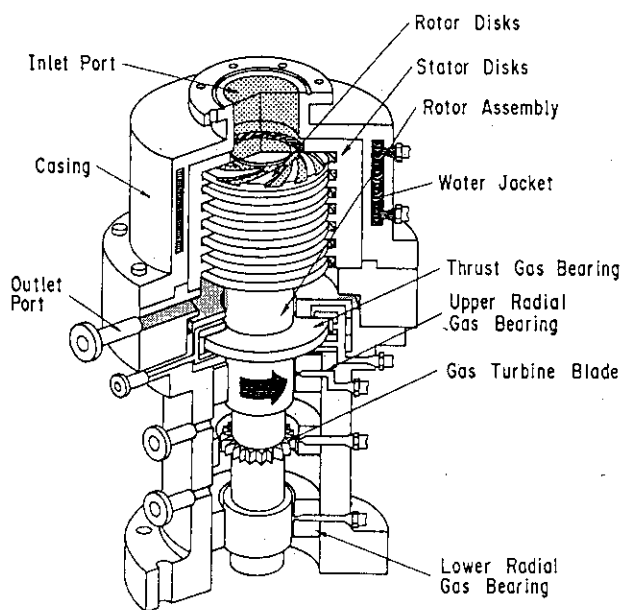


Fig.V.1.2-1 Construction of the ceramic turbo-viscous pump.

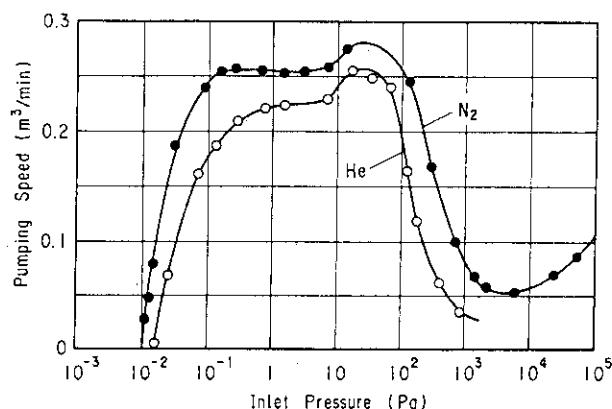


Fig. V.1.2-2 Pumping speeds for N₂ and He as a function of the inlet pressure.

1.3 Zr-bearing OFC gasket for knife-edge-type vacuum flanges

The metal gasket made of OFC (oxygen-free copper) is widely used for the knife-edge-type bakable vacuum flanges. The leaks through the gasket seals, which often occur during high temperature baking, is considered being largely due to the creep displacement and the consequent stress release of the gasket. When a compression force is applied to the gasket at elevated temperatures, the displacement of the gasket in the vicinity of the knife edge increases rapidly with time. In this case, the displacement is the sum of the three different components, namely, δ_e , δ_p and δ_c , where δ_e , δ_p and δ_c are the elastic, plastic and creep displacements, respectively. Table V.1.3-1 shows the three components of displacement analyzed for a typical OFC gasket at 300 °C as a function of baking duration. It is clear that the change in the displacement occurred during high temperature baking originates mainly from δ_c .

Based on the aforementioned analysis, we have proposed an improved metal gasket which features low creep displacement at elevated temperatures[1.3-1]. The material of the new gasket is a Zr-bearing OFC optimizing by 20% cold worked, 0.02% Zr-bearing OFC. Figure V.1.3-1 shows the crosssections of the used gaskets. In case of OFC the depth of the groove increases at a considerable rate with temperature, while in case of the Zr-bearing OFC it almost unchanged even at 400 °C.

References

[1.3-1] K. Obara, Y. Murakami, J. Vac. Soc. Jpn. 33 (1990) 804.

Table V.1.3-1 The elastic, plastic and creep displacements analyzed for a typical OFC gasket/knife-edge-type flange system at 300 °C.

Time duration (min)	0	5	10	20	40	90
Compression force (kgf mm ⁻¹)	10.6	9.49	9.11	8.50	7.90	7.90
Total displacement (mm)	0.300	0.321	0.330	0.340	0.347	0.350
Elastic displacement (mm)	0.009	0.008	0.008	0.007	0.007	0.007
Plastic displacement (mm)	0.291	0.291	0.291	0.291	0.291	0.291
Creep displacement (mm)	0	0.022	0.031	0.042	0.049	0.052

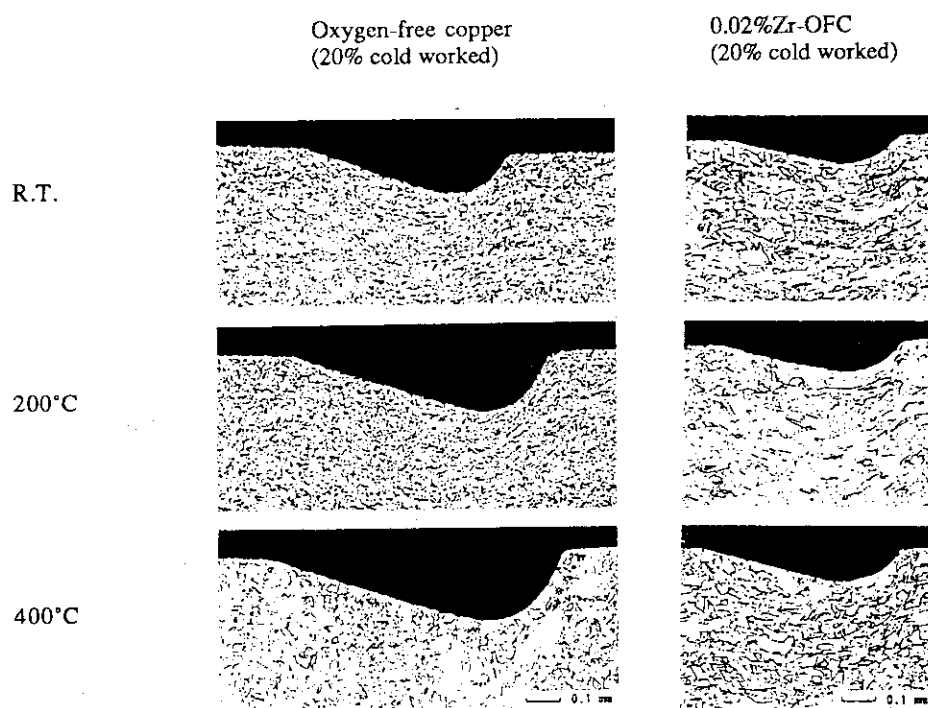


Fig.V.1.3-1 Sectional view of the used gaskets.

1.4 Improvement of QMS by using second stable zone in Mathieu's stability diagram

The quadrupole mass spectrometer (QMS) is widely used in fusion devices for measuring residual gas components, leak rates and partial pressures of working gases. The conventional QMS utilizes only the first stable zone (zone I) in Mathieu's stability diagram where specific ions can pass through the quadrupole field on conditions as shown in Fig.V.1.4-1. Although there are some other stable zones in Mathieu's diagram, the characteristics of the zones other than the first one are little known so far. Since 1989, we have been studying the second stable zone (zone II) which has a form of narrow gap as shown in Fig.V.1.4-1. In this diagram, a and q are the dc and

rf voltages applied to the quadrupole electrodes, respectively. The voltages required for a given ion for the zone II are about 13 and 4 times as large as those for the zone I.

Figure V.1.4-2 shows a comparison between the mass spectra obtained by applying the zone II and zone I to a QMS head[1.4-1]. When the zone II is used, the peak shape becomes sharp and the tail component arising from the adjacent peaks decreases considerably. This enables us to detect very small peaks which adjoin large ones.

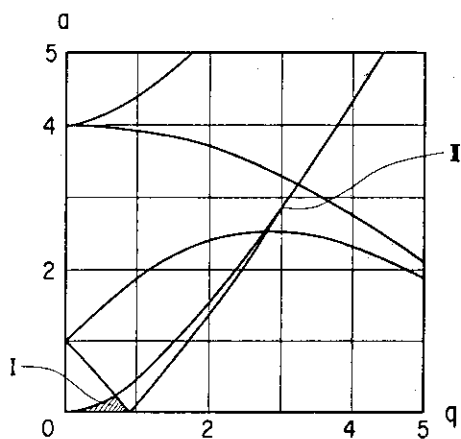


Fig.V.1.4-1 Mathieu's stability diagram involving the zones I and II. $a=(8eU)/mr_0^2\omega^2$ and $q=(4eV)/mr_0^2\omega^2$, where U: dc voltage, V: rf voltage, m: mass of ion, e: charge of ion, r_0 : distance from center axis to quadrupole, ω : angular frequency.

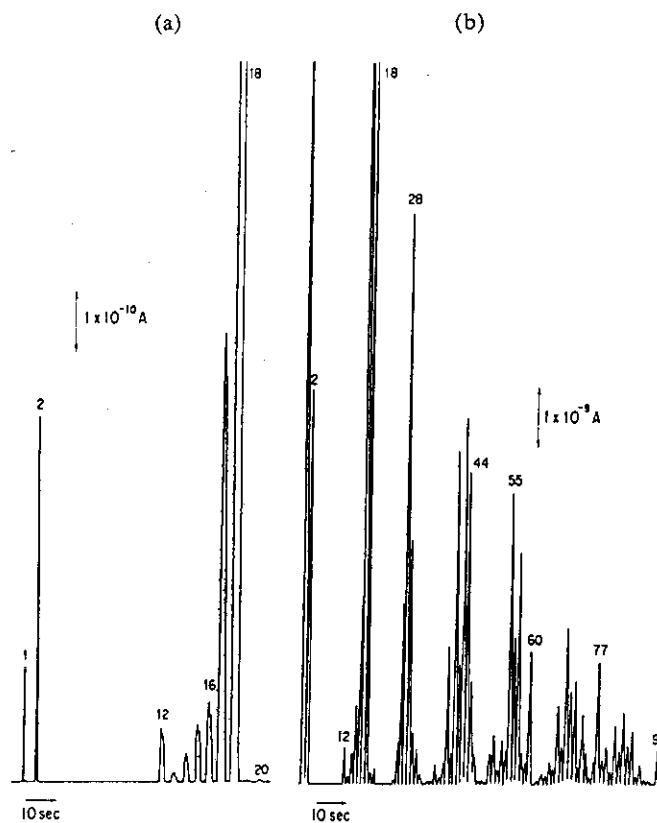


Fig.V.1.4-2 Typical examples of mass spectra obtained by applying (a) the zone II and (b) the zone I. The rod shape is hyperbolic and r_0 is 4 mm. The rf frequency used is 2.5 MHz.

References

[1.4-1] S. Hiroki, T. Abe and Y. Murakami, to be published in Rev. Sci. Instrm. 62 (1991).

1.5 Coating techniques for ITER/FER in-vessel components

The in-vessel components in ITER and FER will be placed in severe operation conditions such as high temperatures and large electromagnetic forces induced by plasma disruptions. To reduce the disruption-induced effects on the components, it is useful to coat the surface of the

components with ceramic materials with adequate electrical conductivity and anti-abrasion property.

Al_2O_3 and Cr_3C_2 have been selected as the insulation and conduction coating materials for the stainless steel components because the both materials show a little nuclear transmutation effect on the electrical properties and good anti-abrasion property. In our trial production, the plasma spray method has been employed for the both coatings. A Ni/Cr layer is inserted in between stainless steel and Al_2O_3 to increase the bonding strength as well as to release the thermal stress in the coatings.

Table V.1.5-1 shows some test results of the coated samples. The test items have been chosen by considering the operation conditions of ITER and FER. In the Al_2O_3 -Ni/Cr-stainless steel system, the adhesion property of the coatings does not change up to a thickness of 600 μm . Therefore, the thickness of the coatings can be selected from the breakdown voltage required.

Table V.1.5-1 Mechanical and electrical properties of two ceramic coatings deposited on stainless steel by plasma spraying.

Coating material	Al_2O_3	Cr_3C_2
Coating method	Plasma spraying	Plasma spraying (JET-KOTE)
Resistivity ($\Omega \text{ cm}$)	3.5×10^8	7.2×10^{-5}
Thermal conductivity ($\text{J cm}^{-1} \text{ }^\circ\text{C}^{-1} \text{ sec}^{-1}$)	0.0465	0.1422
Tensile strength (kgf mm^{-2})	0.9 (590 μm) 1.4 (590 μm) 1.2 (620 μm)	1.9 (125 μm) 2.2 (125 μm)
Thermal shock resistance (RT \leftrightarrow 77 K, 10 cycles)	Good (200 μm) Good (660 μm)	Good (125 μm)
Breakdown voltage* (V)	2,500 (210 μm) > 5,000 (580 μm)	< 200 (125 μm)

* sample size: 30mm x 30mm x 3mm, test condition: < 1 mA for 60 sec

1.6 Development of ceramic-insulated wires

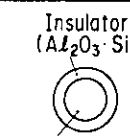
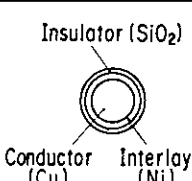
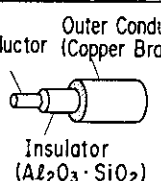
In many vacuum devices, electric wires are used for transmitting powers and signals or as various windings. Insulation of such wires is usually made by coating of polyimide resin or by covering with Teflon sleeves since these organic materials have relatively low outgassing rates at moderate temperatures. Even these materials, however, can not be used at the baking temperatures higher than 300 $^\circ\text{C}$ because they decompose and contaminate vacuum devices at the elevated temperatures. Ultra-high and clean vacuum techniques naturally demand to develop electric wires insulated with heat-resistant inorganic materials.

Different types of ceramic-insulated wires have been developed by a joint work between JAERI and Sumitomo Electric Industries, Ltd. The major specifications of the wires are listed in Table V.1.6-1. The core metal is aluminum or copper. Al_2O_3 or SiO_2 is coated on the aluminum wire, and SiO_2 is used on the copper wire inserting a nickel layer in between the two materials.

The nickel layer works to prevent inter-diffusion and improve adhesion between copper and SiO_2 . The aluminum-type wire excels the copper-type wire in flexibility, whereas the copper-type wire excels the aluminum-type wire in surface smoothness. The coaxial ceramic-insulated wire has an outer conductor which is braided with copper thin thread. All the wires have the following features:

- 1 The insulating layers never peel off at elevated temperatures up to 500 °C.
- 2 Both gas absorption and desorption are negligibly small.
- 3 The wires are flexible and smooth enough to wind coils for practical applications.

Table V.1.6-1 Major specifications of the ceramic-insulated wires.

	Solid Type		Coaxial Type	
Structure	 Insulator ($\text{Al}_2\text{O}_3 \cdot \text{SiO}_2$) Conductor (Al)	 Insulator (SiO_2) Conductor (Cu) Interlayer (Ni)	 Inner Conductor (Al) Outer Conductor (Copper Braiding) Insulator ($\text{Al}_2\text{O}_3 \cdot \text{SiO}_2$)	
Diameter (mm)	1.0	1.0	Inner 0.5 Outer 1.0	
Thickness of Insulator (μm)	20	10	20	
Tensile Strength (kg/mm^2)	10	30	10	
Limit Radius of Curvature (mm)	5	10	5	
Breakdown Voltage (V)	250	200	250	

2. Superconducting Magnet Technology

2.1 Introduction

The superconducting magnet development work is being carried out for the purpose of engineering establishment on the magnet system in fusion reactors such as the Fusion Experimental Reactor (FER) and the International Thermonuclear Experimental Reactor (ITER). The goal is to demonstrate that the following three kinds of coils and refrigerator system can be designed and fabricated with reliability.

- (1) Toroidal Coil : DC Coil Max. Field 12 T Height 12 m
- (2) Outer Poloidal Coil : Pulsed Coil Max. Field 7 T Diameter 5-20 m
- (3) Central Solenoid Coil : Pulsed Coil Max. Field 13 T Diameter 3-4 m
- (4) Refrigerator System : Refrigeration Power 30 x 4 kW at 4 K

The highlights in FY1990 are as follows:

- 1) Fabrication of a pancake coil using a 30 kA-12 T, Nb₃Sn hollow conductor and its verification test,
- 2) Achievement of a ramp rate of 10 T/s to 5.7 T on the US-DPC and demonstration of no critical current degradation in Nb₃Sn using a Incoloy 908 conduit,
- 3) 18.4 T generation at 4.2 K with 32 mm bore coil in the world record,
- 4) Achievement of 500 A/mm² critical current density at 12 T with Nb₃Al/Cu wire,
- 5) Design of cryogenic system with a flow rate of 100 g/s for the test stand of poloidal model coils of ITER-R&D.

2.2 Proto coil project

The hollow cooling monolithic conductor is one of candidate conductors for the non-circular shaped toroidal coils for fusion reactors because of small degradation of critical current, small mechanical disturbance, and much experience of manufacturing. However, the monolithic conductor has to be improved for its large AC loss and low stability margin. The following verification tests were carried out. The model pancake coil is being manufactured to develop the manufacturing techniques and to inspect the performance of full size conductor at the pancake configuration.

2.2.1 Verification tests

(1) Critical current: The critical currents of a full scale sample and strands during optimization of bronze ratio were measured at 12 T and 4.2 K. The maximum of the critical current density is 404 A/mm² at 12 T, which could not be demanded for the model pancake coil because a strand was cracked in a drawing process of mass production line. The strand of the model pancake coil was used by the sample with the critical current of 315 A/mm² at 12 T. The critical current measurement of the real size conductor was carried out at 13 T and 4.2 K in the summer of 1990. There was no degradation of the critical current of a full size conductor compared with the straight sample before cabling.

(2) AC loss: The AC loss of full size conductor were measured in parallel and perpendicular fields. The time constant of a copper housing is 30 ms and the one of large loop with the copper housings and strands is 400 ms. The measured time constant of parallel direction is 4 ms. The results of the time constant measurements is larger than calculated value in each direction.

(3) Stability margin: The stability margin for the reduced size (1/23) conductor was measured in order to estimate the stability of the hollow cooling monolithic conductor. However, the critical current and the copper ratio of this sample is different from that of the full sized conductor from manufacturing reasons. The input energy to conductor of less than 45 mJ/cc-metal

during 50 ms is cooled by the coolant in case of 2.0 kA-8 T. The conductor will get quench at the nominal point, whose joule heating is larger than one at 8 T, 2.0 kA, as soon as current shearing occurs. The stability margin of the full size conductor will be 40 mJ/cc-metal at nominal point assuming long length disturbance, which is estimated by experimental results of the reduced size conductor and the thermal analysis.

(4) Internal joint resistance: An internal joint resistance of a real scale test sample was measured at 6 T and 4.2 K. The joint resistance value is a 7 n Ω at 6 T measured with the potential taps of 1.72 m width. A heat generation is estimated to be 6.3 W at the internal joint. This heat generation is smaller than the heat generation by the nuclear heating which is about 30 W per a cooling flow pass at the environment of the ITER TF coils. It is confirmed that this internal joint method is applicable to the ITER TF coils.

2.2.2 The model pancake coil

A 30 kA-12 T full sized conductor of 90 m length was completed in April 1991 after the trial manufacturing of the TMC-FF conductor and the verification tests. The model pancake coil is presently being manufactured. The performance tests of the pancake coil will be started in the DPC test facility from early 1992.

(1) Conductor: The different point between the original conductor and the mass production conductor, as shown in Fig.V.2.2-1, for the model pancake coil is only the shape of conduit. The hot roll process is required to make square angle at conduit corner. In the model pancake, the bending formation from stainless steel slip tape developed in the manufacturing method at the DPC-EX is adopted for this model pancake coil. The outer dimensions of the conductor are 38.0 mm x 16.8 mm without insulation. The conduit is 2.0 mm-thick and is made with stainless steel JCS-JN1 which is high-strength stainless steel. The Tungsten Inert Gas welding is applied to close the conduit of the JCS-JN1.

(2) The Model Pancake Coil: The cross-sectional view of the test pancake is shown in Fig.V.2.2-2. The dimensions of the test coil are listed in Table V.2.2-1. It is simple work that the pancake coil is set in the DPC test stand. Because this coil has current leads made by the Nb-Ti conductor. And the few turns of the coil near the current leads are made by the Nb-Ti conductor.

A semi-cured tape and a bismaleimide triazine (BT) resin are chosen by the electric insulation. The BT resin can keep the mechanical property under the nuclear radiation. The manufacturing process of the coil insulation can be easier by the semi-cured tape than that of vacuum impregnation.

Table V.2.2-1 Major parameters of the model pancake coil.

Inner diameter		1000 mm
Outer diameter	Winding	1500 mm
	Total	2060 mm
Thickness	Winding	99 mm
	Total	225 mm
Turn number of turns		22
Coil configuration		One double pancake
Cable length	(NbTi) ₃ Sn	30 mm
	Nb-Ti	30 m x 2
Cooling length		90 m

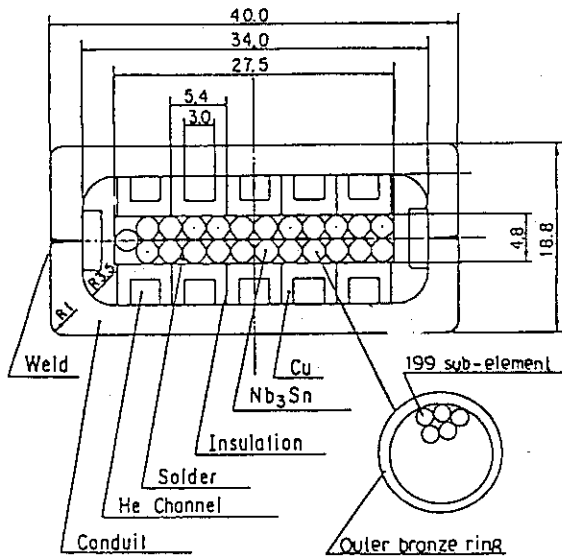


Fig.V.2.2-1 Cross-sectional view of the monolithic conductor.

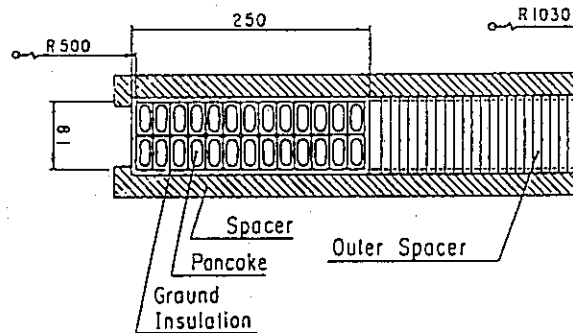


Fig.V.2.2-2 Cross-sectional view of the model pancake coil.

2.3 The Demo Poloidal Coil project

2.3.1 Project status

To develop superconducting poloidal coils required in a fusion experimental reactor, the Demo Poloidal Coil (DPC) program has been initiated at JAERI in 1985. The goals of the DPC project are to obtain experimental data, to demonstrate reliable operation of large pulsed superconducting coils, and to prove design principles and fabrication techniques for poloidal coils. In the DPC project two 30-kA Nb-Ti pulsed coils (DPC-U1 and U2) and one 10-kA Nb₃Sn pulsed coil (DPC-EX) have already been fabricated and tested. In addition to these coils, a 30-kA Nb₃Sn coil (US-DPC) was fabricated by MIT/DOE in the framework of the international collaboration between Japan and the U.S. All of the coils have circular shape and the same winding inner diameter of 1 m, and are cooled by forced-flow helium. In 1989, experiments on the DPC-EX was performed and it achieved the designed pulsed field of 7 T/s, demonstrating the applicability of Nb₃Sn superconductor to a poloidal coil [2.3-1]. In this reported period, experiments on the US-DPC took place successfully in the test facility of JAERI. The 8 MJ, 1.8-m outer diameter coil was charged to the design current of 30 kA in DC tests without showing any instabilities. It also performed well in pulsed charging tests, achieving approximately 70 % of its ambitious design goal of 10 T/s. Emphasized is that ample of achievements were produced through this tight international collaboration in the area of superconducting magnet.

2.3.2 Experimental results of the US-DPC

The US-DPC arrived at JAERI in August of 1990, and the installation work immediately started as shown in Fig.V.2.3-1. The coil was set between the DPC-U1 and -U2 and tightened together in a co-axial configuration by stainless steel rods. It took 150 hours to cool the coils to the cryogenic temperature without causing an excessive thermal stress. The coil was then subjected to a variety of testings [2.3-2].

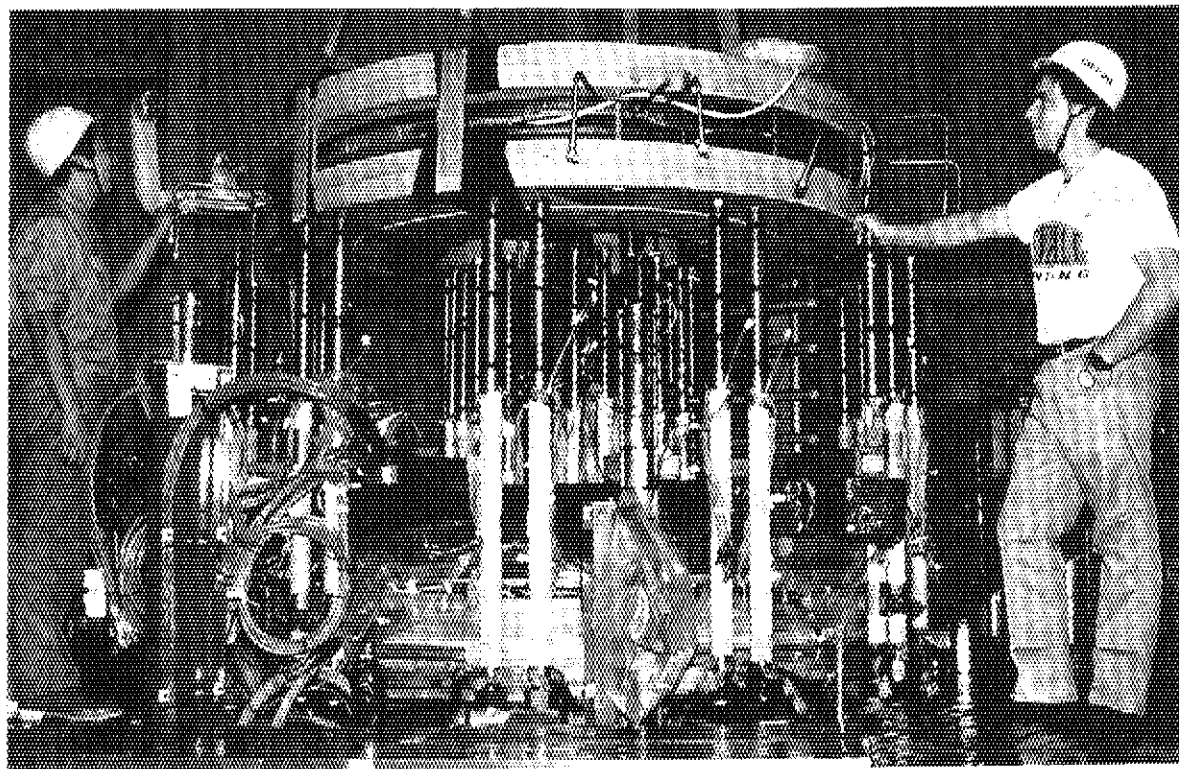


Fig.V.2.3-1 The US-DPC being installed in JAERI's test facility under the collaboration of Japan and MIT/DOE.

2.3.2.1 Coil design of US-DPC

The US-DPC conductor has low-loss, titanium-alloyed, internal-tin, modified-jelly-roll Nb_3Sn wires. Two Incoloy 908 conduits are selected to enclose 225 stranded wires to minimize compressive axial strain in Nb_3Sn superconductor (Fig.V.2.3-2). The coil consists of three double-pancakes, and its winding inner diameter, outer diameter, and height are 510 mm, 910 mm, and 154 mm, respectively. Its current density is 50 A/mm^2 , rather high in comparison with the other large-scale magnets fabricated so far.

2.3.2.2 Major achievements of US-DPC

In single coil charging, the US-DPC reached its design current of 30 kA without showing any instabilities and produced the peak field of 5.7 T. In series charging with the DPC-U1 and

DPC-U2, the US-DPC attained 8 T at 25.9 kA, but further charging failed due to the limitation of the backup coils. In the pulsed operation of the US-DPC alone, a ramp rate of 10 T/s to 5.7 T was thought to be achievable, but an unexpected barrier of either field or current versus ramp rate was encountered. In linear pulses to 30 kA the highest charging was obtained at 0.71 T/s and higher ramping rate caused a coil quench. However, the ramps with superimposed sinusoidal ripple, ramps with rounded edges, and some other wave forms could achieve higher ramping rates without a coil quench. Such a phenomenon was revealed for the first time by the US-DPC, and became important issue to be clarified. AC loss characteristics were also investigated during pulsed operations. Figure V.2.3-3 shows the measured AC losses of the middle pancakes against the reciprocal of ramp time with flattop current as a parameter. As an example, with 0.3-s ramp time and 20-kA flattop, the losses of the coil was 1650 J, which corresponds to only 0.05 % of the 3.3 MJ stored energy of the double-pancake. This proved the low-loss characteristics in this design. In the DC operation, both the critical current measurements and current-sharing temperature measurements were performed. These results indicated the coil showed no damage on the performance of Nb₃Sn superconductor compared with a single wire, probably owing to a wind-and-react technique and Incoloy 908 employed for the conductor conduit.

References

- [2.3-1] T. Ando, et al., IEEE Trans. Magn., Vol.27 No.2 (1991) 2060.
 [2.3-2] M. M. Steeves, et al., Proc. of Cryo. Engin. Conf. (CEC), Huntsville, USA (1991).

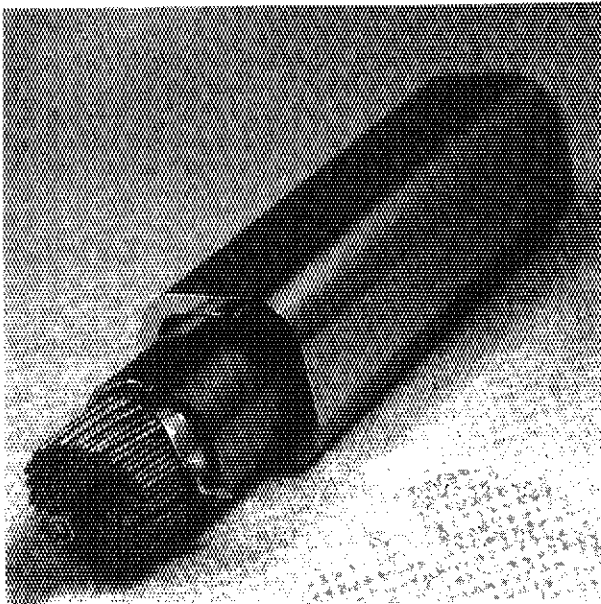


Fig.V.2.3-2 Nb₃Sn 30-kA conductor for US-DPC.

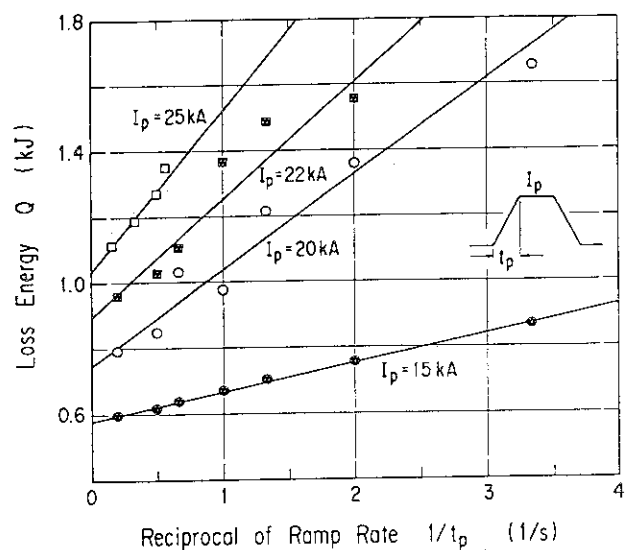


Fig.V.2.3-3 Measure AC losses of the middle double-pancake of the US-DPC.

2.4 High field coil development

Two high-performance superconducting coils were developed and the study of the Nb₃Al superconductor for practical use much advanced in this period.

A 32-mm-bore coil, which was wound with multifilamentary (NbTi)₃Sn superconductors, was developed (Fig.V.2.4-1). This coil was tested in the 140-mm-diameter bore of a 13-T superconducting coil installed in a 4.2-K bath and the maximum magnetic flux density of 18.4 T was obtained, which was the world record achieved by the superconducting coil at 4.2 K [2.4-1]. The total energy stored in this coil system was only 1.48 MJ and the charging time from 0 T to 18 T was only 12 minutes, which indicate that this coil system is a compact and high-performance one as the 18 T-30 mm bore class superconducting coil system.

A 240-mm-bore high-field superconducting coil was developed and the designed magnetic flux density of 13.0 T was obtained stably in its center at 4.2 K. The average current density was 101 A/mm², the maximum magnetic flux density on the coil was 13.9 T, the stored energy was 4.8 MJ, and the charging time was 18.5 minutes. These parameters shows that this coil is a compact high-performance coil [2.4-2].

High-capacity advanced superconductors are investigated using these two coils mentioned above as background field coils.

The Nb₃Al superconductor has higher latent capacity and much better characteristics for strain than the (NbTi)₃Sn superconductor. In this period, the critical current density per non-copper area of the copper-stabilized multifilamentary Nb₃Al superconductor improved to be more than 500 A/mm² at 12 T, which is the same level as those of (NbTi)₃Sn commercial wires [2.4-3]. With 324 Nb₃Al strands, a large cable-in-conduit forced-cooled-type conductor, whose designed capacity was 10 kA-12 T and critical current was 20 kA-12 T, was fabricated and waits for being tested [2.4-4].

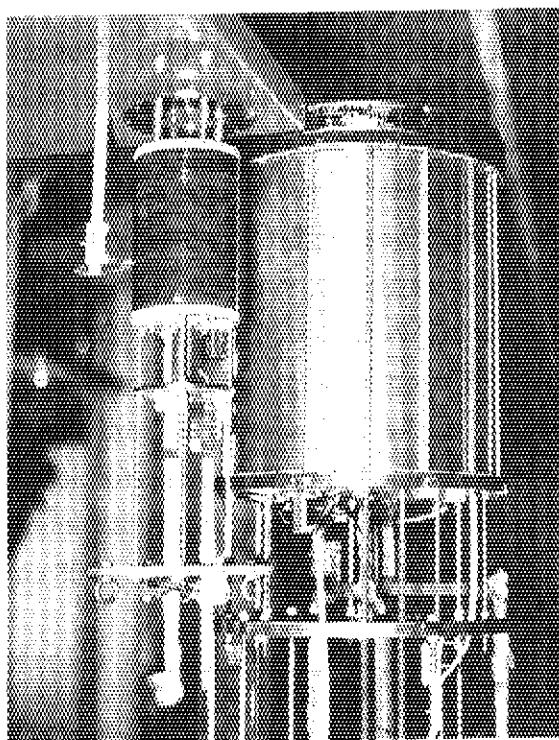


Fig.V.2.4-1 A developed 32-mm-bore high-field superconducting coil and its 13-T background-field coil. With this coil system, the magnetic flux density of 18.4 T was obtained at 4.2 K, which was the world record achieved with the superconducting coil operated at 4.2 K.

References

- [2.4-1] M. Nishi, T. Isono, Y. Takahashi, et al., IEEE Trans. on Magnetics, Vol. 27, pp.2280-2283, 1991.
 [2.4-2] M. Nishi, T. Ando, T. Isono, et al., to be presented at 12th International Conf. on Magnet Technology, Leningrad (USSR), 1991
 [2.4-3] T. Ando, Y. Takahashi, M. Nishi, et al., to be presented at Cryogenic Engineering Conf./International Cryogenic Material Conf., Huntsville (USA), 1991
 [2.4-4] T. Ando, Y. Takahashi, M. Nishi, et al., IEEE Trans. on Magnetics, Vol. 27, pp.1775-1778, 1991

2.5 Cryogenic system development

In this period, there were following activities in the field of the cryogenic system development; (1) A basic specification of the cryogenic system for the C.S. Scalable Model Coils was determined and (2) A large helium turbo-expander with variable capacity was developed.

2.5.1 Cryogenic system for the C.S. scalable model coils

Cooling requirements of the C.S. scalable model coils are as follows:

- | | |
|--|--------------------|
| (1) Supercritical helium supply mass flow rate | Total 1000 g/s |
| (2) Supercritical helium supply temperature | Minimum 3.8 K |
| (3) Supercritical helium supply pressure | 0.5-1.0 MPa |
| (4) Allowable coil pressure drop | Less than 0.2 MPa |
| (5) Current lead capacity | 40-50 kA x 3 pairs |

The capacity of the cryogenic system which satisfies these requirements is determined to have the refrigeration capacity of 8 kW at 4.5 K or the liquefaction capacity of 1,200 l/h. A cryogenic pump system will be adopted as the system which supplies the supercritical helium to the coil system. The basic block diagram is shown in Fig.V.2.5-1. This cryogenic system will be the biggest helium cryogenic system in Japan.

2.5.2 Development of a large helium turbo-expander with variable capacity

A large helium turbo-expander with variable-flow-capacity mechanism has been developed, which will perform the effective refrigeration power control. A type of variable nozzle vane heights is selected as the mechanism. The performance test was carried out and the turbine efficiency was measured in the large range of the blade-jet speed ratio (U/Co) from around 0.2 to 0.85. In the results, the smooth operation of variable flow capacity and the effective turbine power control were verified. The design specification and the structure of the developed turbine are shown in Fig.V.2.5-2.

2.6 Development of cryogenic structural materials

The Japanese Cryogenic Steels (JCS) were successfully developed in collaboration with four steel companies. Evaluation of tensile, Charpy, and fracture properties of JCS was completed and fatigue tests were started to generate design data base for ITER superconducting magnets. Fatigue crack growth rates (FCGR) of several JCS were measured using computerized

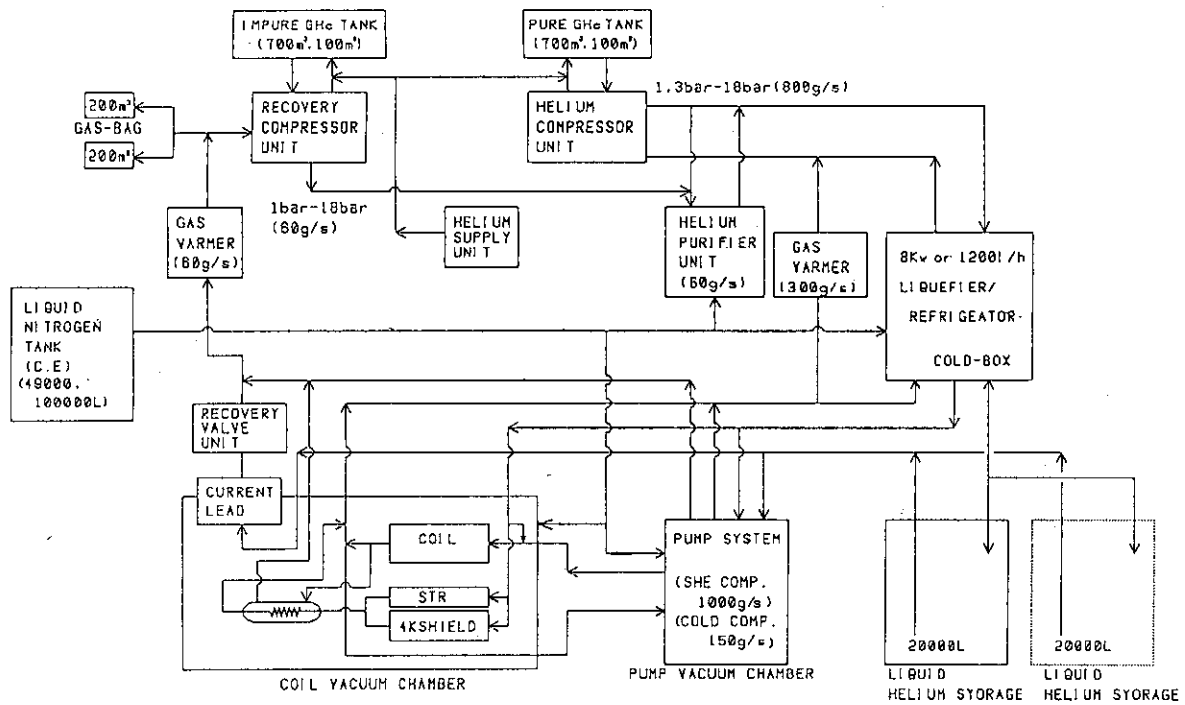
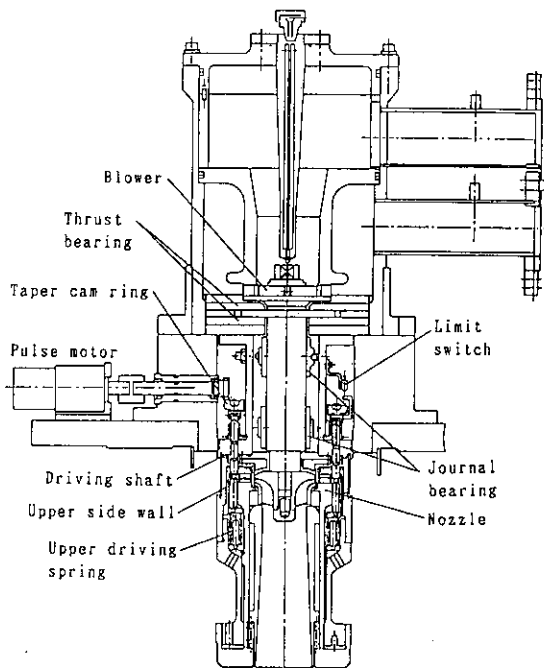


Fig.V.2.5-1 C.S. scalable model coil cryogenic system block diagram.



		Design
Type		Radial inward flow
Bearing	Journal	Tilting pad type gas bearing
	Thrust	Spiral grooved type gas bearing
Nozzle opening (%)		0 ~ 130
100% Nozzle opening		
Flow rate (kg/s)		0.356
Inlet temp. (K)		18
Inlet pressure (MPa)		0.63
Pressure ratio		5.8
Rotating speed (rps)		1121

Fig.V.2.5-2 Design specification and structure of the turbo-expander with variable-flow-capacity mechanism.

compliance technique at 4 K. FCGR tests were performed under the condition; constant load of 3500 and 4800 kg, frequency of 10 Hz, and stress ratio of 0.1. The representative result of CSUS-JN1 is shown in Fig.V.2.6-1. A linear relation between FCGR and stress intensity factor range is obtained. The relation in accordance with Paris's law is expressed the following equation.

$$da/dN = 2.1 \times 10^{-12} (\Delta K)^{3.7}$$

where, da/dN and ΔK are in mm/cycle and in $\text{kg}/\text{mm}^{1.5}$, respectively.

Serious problems when stainless steels are used as a conduit material of a Nb_3Sn conductor are (1) degradation of superconducting properties due to thermal strain and (2) degradation of ductility of a conduit material after aging for Nb_3Sn reaction. Thermal contraction of titanium is similar to that of Nb_3Sn . Therefore, titanium is one of candidates for a conduit material. Tensile and Charpy tests were conducted at 4 K to examine mechanical properties of titanium after aging. Since the elongation and Charpy absorbed energy increased after aging it was verified that titanium was useful as a conduit material of a Nb_3Sn conductor.

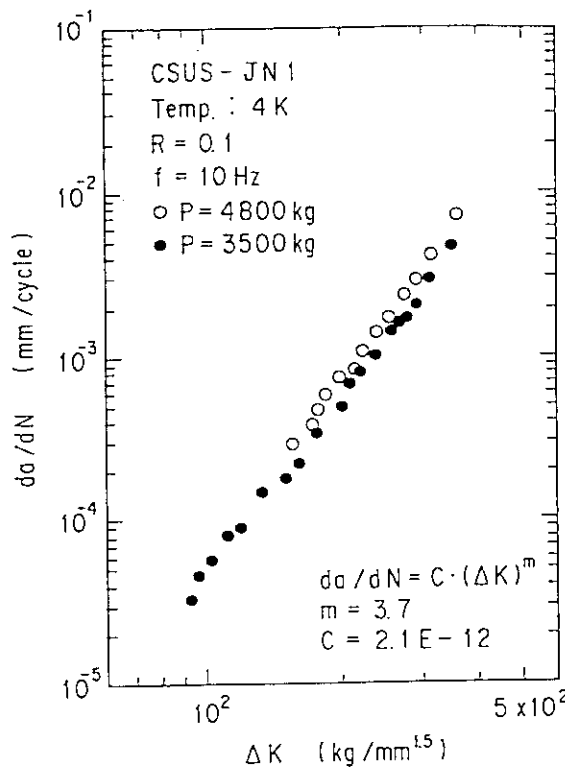


Fig.V.2.6-1 FCGR of CSUS-JN1 at 4 K.

3. Beam Technology

3.1 Introduction

Beam technology oriented to neutral beam (NB) injector has been advanced mainly in a negative ion source R&D. After succeeding in 10 A negative hydrogen ion beam production, the efforts are concentrated on long pulse operation and high energy acceleration of the negative ion beams. In parallel, design works on a negative-ion-based NB system has been progressed to figure out a more reasonable current drive and heating system for the next generation fusion devices. Positive ion beam technology R&D has also been continued for applications toward a long life ion source and a plasma neutralizer.

3.2 Negative ion beam technology

For the next generation fusion devices such as ITER, development of negative ion source is a key to realize the negative-ion-based NB system. The required performance is to produce high current (> 10 A), high energy (500 keV \sim 1.3 MeV) negative ion beams for long durations (10 s \sim 2 weeks). To satisfy these specifications, much effort[3.2-1] has been devoted in these years. The R&D's were progressed in the following directions.

3.2.1 Improvement of high current source[3.2-2]

Further R&D's on high current negative ion source has been desired to improve the negative ion production efficiency over a wide operational condition. Especially, operation at lower pressure is of importance not only to reduce stripping loss of the ions in the accelerator but also to minimize gas evacuation instruments of the NB system.

A semi-cylindrical plasma generator combined with an extractor was tested. The plasma generator has large volume (34 cm dia., 104 cm long) and strong cusp magnets, resulting in good confinement of the source plasma. The negative ion was extracted from center region of the plasma generator through 133 apertures (9 mm dia.). Figure V.3.2-1 shows a result, negative ion current as a function of gas filling pressure, obtained with and without seeding cesium into the source. Before seeding cesium (without Cs), the current decreased rapidly as reducing the gas pressure. The optimum pressure was 1.2 Pa in the pure volume

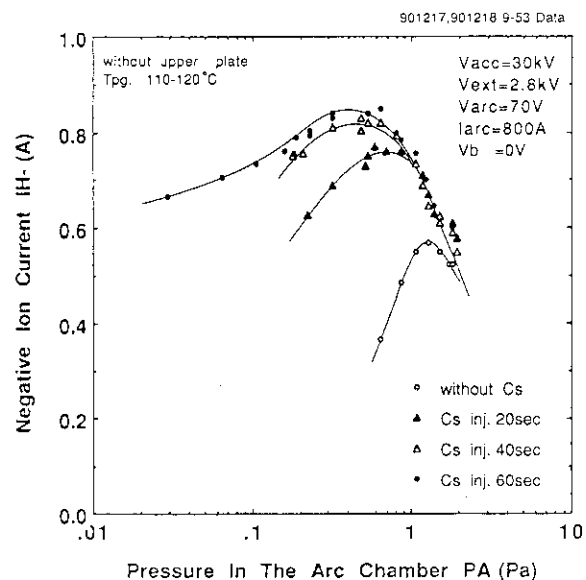


Fig. V.3.2-1 Negative ion current as a functions of gas filling pressure in the large plasma generator.

operation. By seeding cesium, the current at the lower pressure increased drastically. After 60 s injection of cesium, the current attained a considerable value of 0.67 A (8 mA/cm^2) even at very low pressure of 0.03 Pa.

This operational pressure is one order of magnitude lower than that of former sources. These results are utilized for the larger negative ion source experiment in cooperative activities concerning an energy recovery system using a negative ion beam, between JAERI and EC (CEA - Cadarache).

3.2.2 Long pulse operation

In a long pulse operation of negative ion beam, the crucial points are the cesium consumption and the durability of the source. For these tests, a source was manufactured adopting a heatproof structures; e.g. material choice, arrangement of water cooling pipes, stress absorbing structures in the accelerator grids, and so on.

After seeding a small amount of cesium (approximately less than 200 mg), the source was operated for 2000 shots of 0.2 s pulse, then the pulse length was expanded to 1 s for 1000 shots. During the test, no evidence of cesium shortage was observed in the source; i.e. the current was kept high value of cesium seeded condition. High voltage holding in the accelerator was functional without influence of the cesium leakage. As a result, it was demonstrated that the cesium consumption rate is very low in the case of volume production type negative ion source.

The source was served to a source durability test. In the cesium seeded condition, operation of 1000 s pulse was succeeded with the H^- current density of 13 mA/cm^2 . Infrared camera and thermocouple monitors showed that the source was cooled effectively by the heatproof structure. As shown in Fig. V.3.2-2, the source was operated stably producing a well converged H^- beam, showing that the H^- beam property, such as the beam current of the cesium seeded volume production type source, does not change during the pulse.

3.2.3 High energy acceleration and the beam optics

A new test stand with the capability of 350 keV, 200 mA was constructed, and has been served to a high energy acceleration experiment. As the first

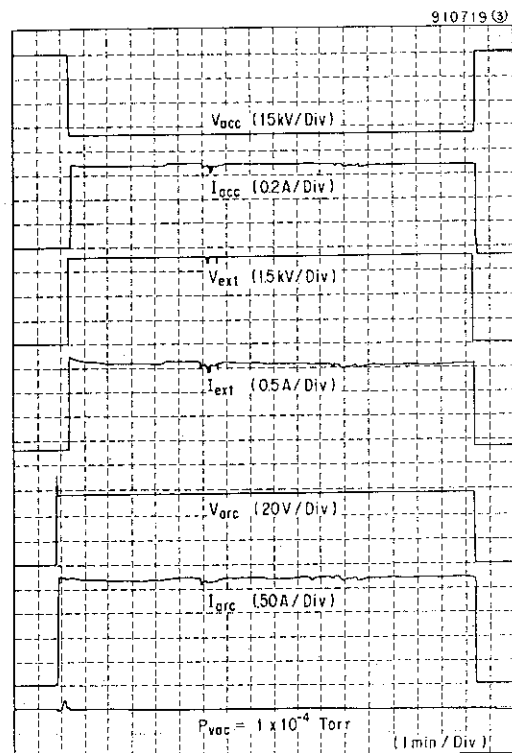


Fig. V.3.2-2 History of source parameters for 1000 s pulse operation. Monotonous signal shows stable discharge and beam acceleration.

step of the experiment, '250 keV negative ion source[3.2-3]' was installed to the test stand. A unique feature of the source was the long gap for single stage electrostatic acceleration. The accelerator column was made of FRP sustaining a DC voltage of 250 keV. Figure V.3.2-3 shows an example of the beam formed by the source. The beam divergence was reduced to 1.5 mrad at the optimum operation of 70.2 keV, 3 mA. The beam emittance was estimated to be a remarkably small value of less than $\epsilon_n(1/e) = 0.008 \pi \text{ cm mrad}$. The beam energy was increased up to 240 keV, and any trouble on neither voltage holding nor beam optics were observed.

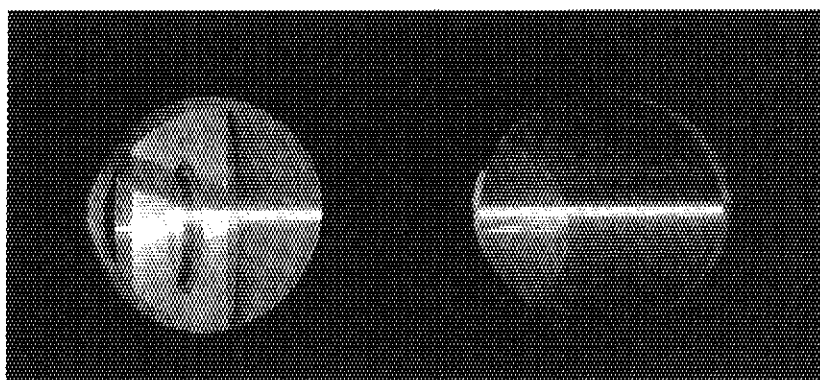


Fig.V.3.2-3 Finely converged negative ion beam propagating in a vacuum.

For the next step, a new source called '350 keV source' was fabricated as shown in Fig. V.3.2-4. The source has a two-stage, multi-aperture accelerator system to demonstrate the integrated performance of 350 keV, 0.1 A and 5 minutes negative ion beam production.

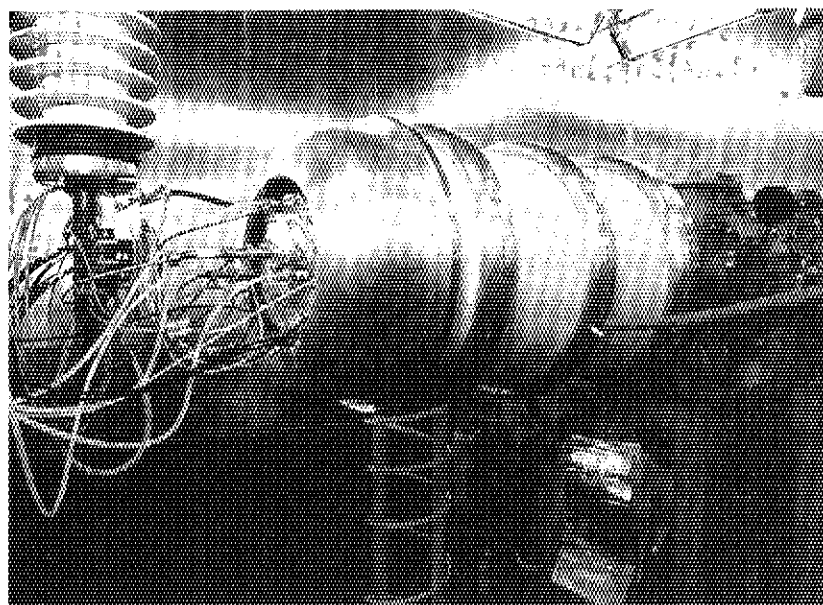


Fig.V.3.2-4 '350 keV source' installed to negative ion acceleration test stand.

References

[3.2-1]Y. Ohara et al., JAERI-M 90-154.

[3.2-2]Y. Okumura et al., Proc. 5th European Workshop on the Production and Application of Light Negative ions, Belfast (1991), 35

[3.2-3]T. Inoue et al., Proc. 14th Symp. on ISAT'91, Tokyo (1991), 137

3.3 Design work of negative-ion-based NB system

As the final year of ITER CDA phase, the Japanese contribution on ITER NB system design was reviewed and summarized[3.3-1]. Fig. V.3.3-1 shows a plane view of the ITER NB system. In FY1990, following two issues were investigated. i)Maintenance[3.3-2]: System concept was defined by developing the assemble/disassemble scheme on a basis of checking parts and components. The maintenance scenario was considered as to be fully remote-handled. ii)Neutronics[3.3-3]: Neutronics environment in the NB system was made clear by a two dimensional computation. It was found that beamline components were exposed to a considerable high flux of high energy neutrons. The flux of high energy (>0.1 MeV) neutrons were evaluated to be orders of $10^9 \sim 10^{11}$ n/cm²s at the ion source position. However, induced radioactivity in NB room wall could be reduced to a permissible level by adopting a SS neutron shield around the NB module.

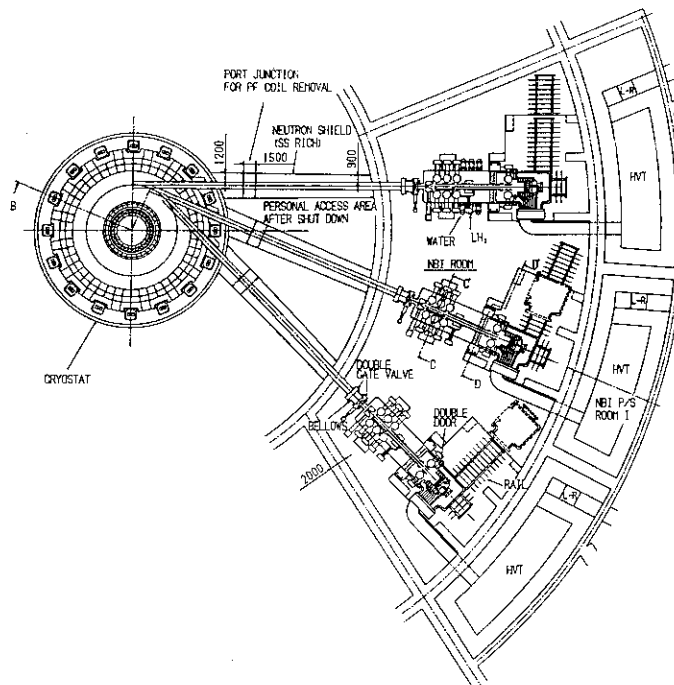


Fig.V.3.3-1 A plan view of ITER NB system.

References

[3.3-1]Y. Ohara et al., JAERI-M 91-052.

[3.3-2]S. Tanaka et al., to be appeared in Fusion Eng. Design.

[3.3-3]T. Inoue et al., to be appeared in Fusion Eng. Design.

3.4 Positive ion beam technology

3.4.1 ECR/RF plasma generator[3.4-1]

For R&D on plasma neutralizer and long life ion source, fundamental research on ECR/RF plasma generator was progressed. One of challenges was made by injecting 2.45 GHz microwave into a cylindrical multicusp plasma generator. Fig. V.3.4-1 shows a variation of ion saturation current obtained by a Langmuir probe measurements. After mode changes of discharge, a hydrogen plasma of 1.6×10^{11} n/cm³ was produced above a threshold power of 1.3 kW. The plasma density was more than twice higher than the cutoff density of 2.45 GHz microwave. Spatial uniformity of the plasma was confirmed over an area of 12 cm in diameter.

This results are available not only in beam technology for fusion but also in a wide range of industrial applications.

3.4.2 Large scale cryo-sorption pump

In fusion reactor, it is required to evacuate not only hydrogen isotopes but also helium gas. By applying know-how accumulated in R&D's of JT-60 NB injector cryopump, we have developed a large scale cryo-sorption pump using SF₆ condensed layer. Basic data of the pump have been obtained up to 800 m³/s class pumps.

Reference

[3.4-1]H. Tanaka et al., Proc. 14th Symp. on ISIAT'91, Tokyo (1991), 35.

4. RF Technology

4.1 Introduction

In FY 1990, an emphasis has been placed on the construction of a gyrotron test facility which will be used to develop the high power long pulse gyrotron and the ECH components, for JT-60U and ITER/FER. We also have demonstrated that a high-power 120 GHz whispering-gallery-mode gyrotron with a built-in quasi-optical mode converter generates the maximum power of 548 kw, 1 msec with an efficiency of 30.4%.

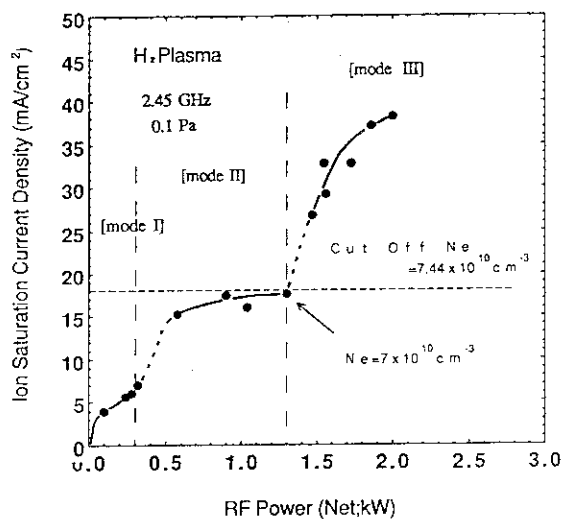


Fig. V.3.4-1 Ion saturation current dependence on ECR power in a multicusp plasma generator.

4.2 Construction of gyrotron test facility and development of the LHRF launcher

To investigate mm-wavelength components at a frequency of 110-140 GHz for JT-60 and ITER technology R & D; launcher, polarizer, vacuum window, mode converter etc., at the power level of 0.5-1 MW, the klystron test facility at JAERI, Naka, originally intended for developing a 1 MW, 2 GHz klystron and relating high power microwave components for JT-60 has been modified for testing of the high power gyrotron at -90 kV with a load current of 30-35 A dc. The load duty cycle is 1/15 for 10 seconds duration of up to -90 kV. Fabrication and installation of the gyrotron test facility is completed in March, FY1991 and its final testing is to be ended by April, FY1991. Figure V.4.2-1 shows the photograph of the gyrotron test facility.

Design, fabrication and low power test of a new type of the multi-junction grill has been made. It consists of six element multi-junction with a tapered waveguide from the standard sized guide to the oversized guide in 2 GHz range. This concept will be applied to the next LHCD launcher manufactured for JT-60U in FY1991-92.

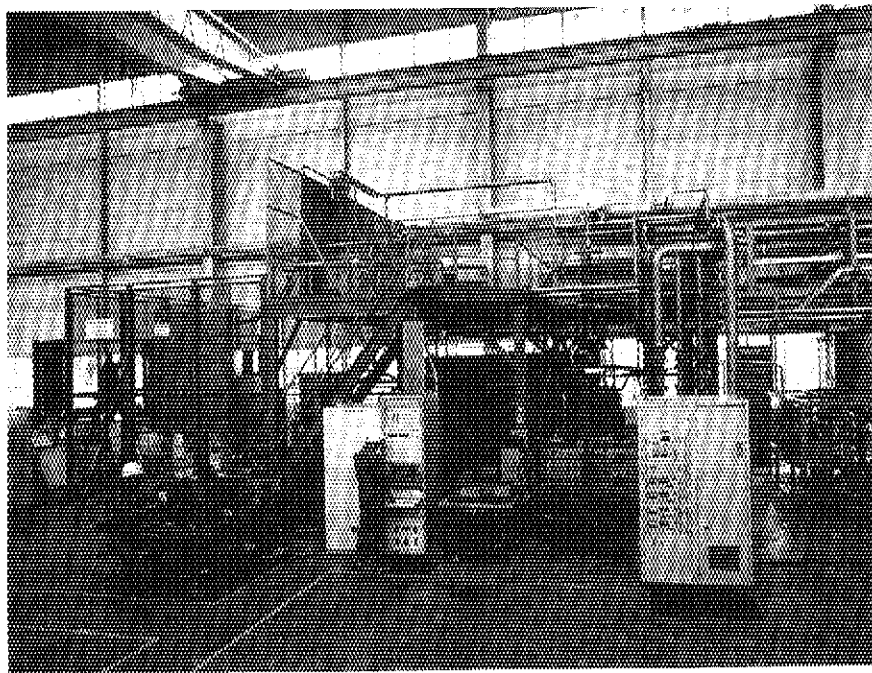


Fig.V.4.2-1 JAERI test facility of gyrotron and millimeter wavelength components.

4.3 Investigation of high power gyrotron and ECH components

4.3.1 Developments of 120 GHz gyrotron

Research and development of a 120 GHz gyrotron have been carried out at JAERI for the application to an electron cyclotron resonance heating (ECH) in a fusion reactor. In the work of FY1989, the power generation of more than 500 kW at 120 GHz was succeeded by using a

whispering gallery mode. In FY1990, the development of the gyrotron built in a quasi-optical mode converter is carried out [4.3-1,4.3-2].

The configuration of gyrotron is illustrated in Fig.V.4.3-1. The millimeter wave power generated in a cavity with the whispering gallery mode is radiated by the α -cut Vlasov type radiator and parallel beam is formed by using the flat and curved reflectors. The output power is lead out as the Gaussian beam through the ceramic window attached on the side of the gyrotron. The heat load density of the collector by the electron beam is one of the major problem of the high power long pulse gyrotron. The collector diameter can be extended by separating the path of millimeter wave and the electron beam after passing cavity, as a result, the heat load density of the collector by the electron beam is decreased significantly. The field patterns of the output beam are shown in Fig.V.4.3-2. Figs.V.4.3-2(a), (b) are the calculated results and the experimental result at low power, respectively. The clear Gaussian power distribution is obtained in both cases.

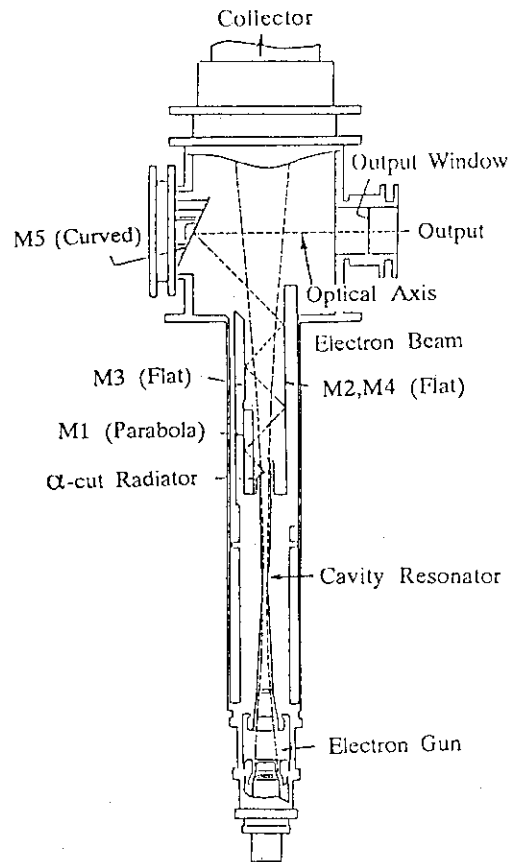


Fig.V.4.3-1 Configuration of the gyrotron.

The maximum output power is 548 kW at a pulse duration of 1 msec. The pulse duration is restricted by the capacity of the power supply. The efficiency of 30.4% is obtained at a beam voltage of 76.7 kV and a beam current of 24 A. . The dependence of the output power and the efficiency on the beam current are shown in Fig.V.4.3-3. The research and development of an 120 GHz gyrotron will be continued in FY1991, and testing of the long pulse gyrotron will be carried out using the JAERI gyrotron test facility in FY1991.

4.3.2 Component of high power millimeter wave transmission system

The improvement of the conversion efficiency from the whispering gallery mode, which is a most typical operation mode of the high power gyrotron, to the Gaussian beam is important for the improvement of the transmission efficiency of the ECH system. Also, it is crucial problem for a built-in converter gyrotron itself (described in Fig.V.4.3.1) because the escaped power is absorbed inside the gyrotron, which may cause the arcing or welding of the inside wall. The

research of the quasi-optical mode converter is carried out aiming the improvement of the conversion efficiency.

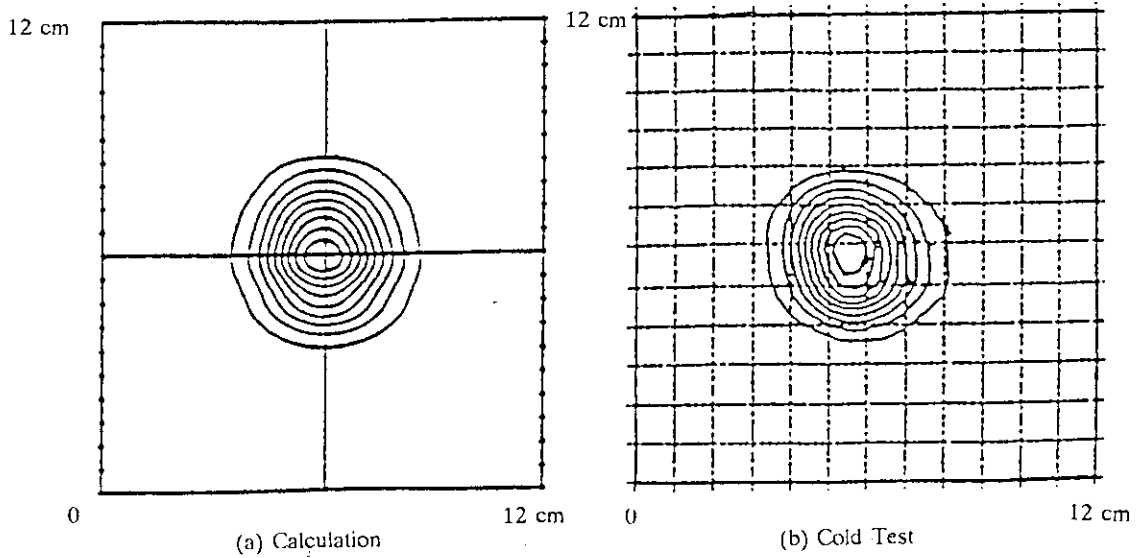


Fig.V.4.3-2 Cross section profile of wave at 389 mm from final reflector of the gyrotron.

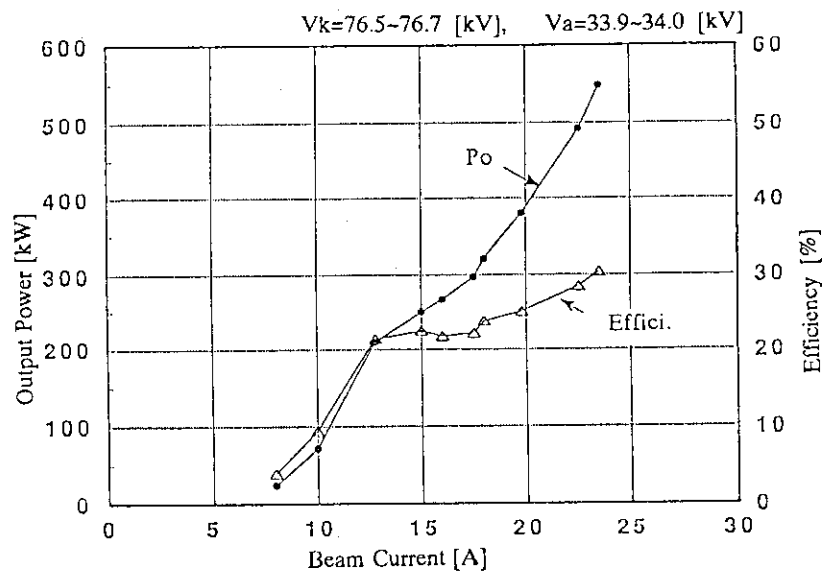


Fig.V.4.3-3 Output power and efficiency v.s. beam current of the gyrotron.

The newly proposed converter by JAERI generates the Gaussian beam directly from the whispering gallery mode using the two 3 dimensional reflection mirrors. The radiated rays by

the radiator is reformed into the the center peaked power distribution using the first mirror, and these rays are reformed into the parallel beam sequentially using the second mirror. As the result, the diffraction loss decreases and the efficiency increases. In FY1990, the design of the converter and the fabrication are carried out for the quasi-optical transmission system on MTX, which is going on under the US-Japan international collaboration.

The path of rays are illustrated in Fig.V.4.3-4. The density of rays corresponds to the power density of the beam. It is found that the ray of Gaussian power distribution with the parallel beam can be formed. The fabrication was done using the 3-axes milling machine. In FY1991, the low power test using the whispering gallery mode generator at 140 GHz and this converter system will be applied to the MTX on LLNL.

References

- [4.3-1] T.Nagashima, K.Sakamoto, S. Maebara et al., in Proc. of Inter. Workshop on Strong Microwaves in Plasmas, Suzdal, USSR, Sep. 1990.
- [4.3-2] Y.Mitsunaka, T. Kariya, A. Yano et al., in the Conf. Digest of 15th Inter Conf. on infrared and Millimeter waves, Orlando, U.S.A. Dec. 1990.

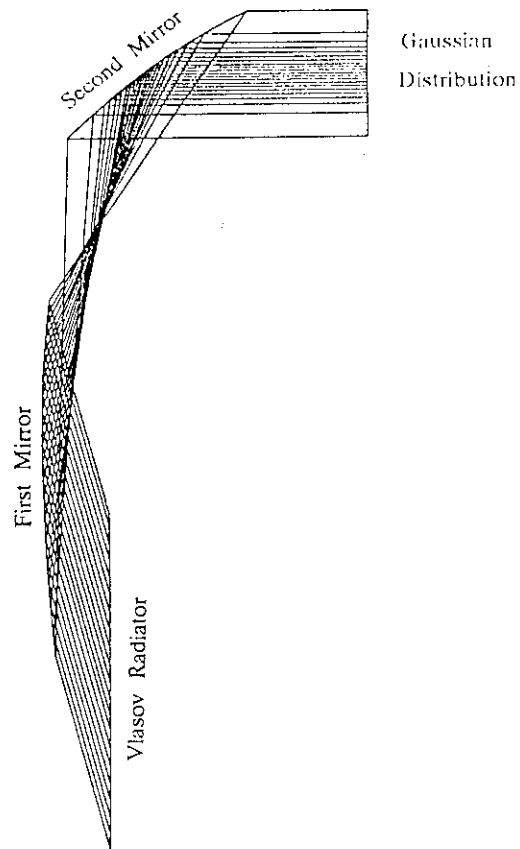


Fig.V.4.3-4 Ray path of Vlasov Converter.

4.4 FEL research

Millimeter wave Free Electron Laser (FEL) has been experimentally investigated using 1 MeV, 3 kA induction linac [4.4-1].

In the experiment, a focusing type wiggler has been used; the surface of each magnet is sinusoidally curved which suppress the electron beam divergence when passing through the wiggler. The wiggler pitch is 5 cm and the total pitch number is 30 (Fig.V.4.4-1).

From 30 GHz to 60 GHz, super radiation due to FEL mechanism was observed (Fig.V.4.4-2); the growth rate was about 0.4 dB/cm which means original noise radiation at the entrance of the wiggler is amplified by about million times at the exit of the wiggler (Fig.V.4.4-3).

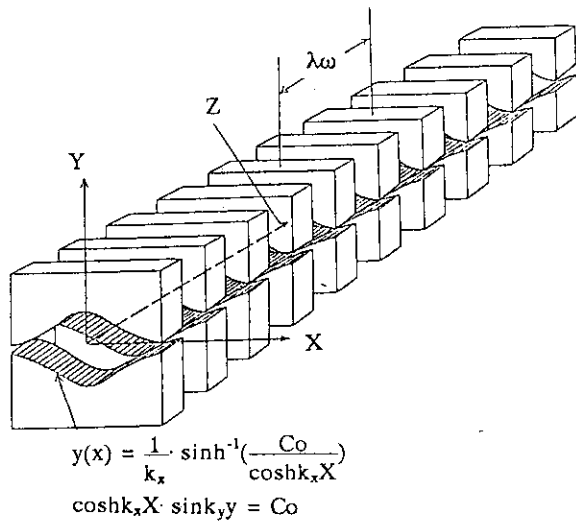


Fig.V.4.4-1 Focusing Wiggler and coordinate system.

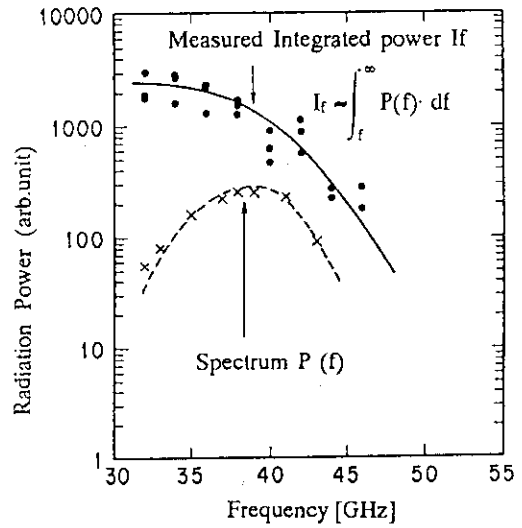


Fig.V.4.4-2 Spectrum of super radiation.

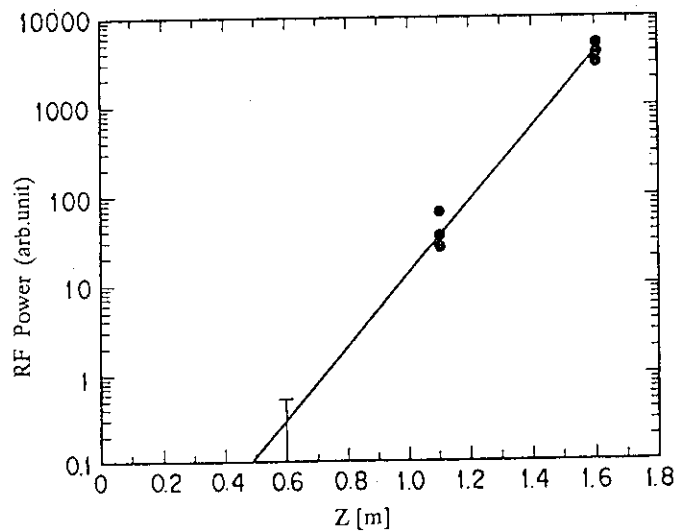


Fig.V.4.4-3 Relation between radiation power and integration length.

References

[4.4-1] K.Sakamoto, S.Maebara, A.Watanabe et al., JAERI-M 91-036.

4.5 Design study of RF heating and current drive system for FER and ITER

Conceptual design has been completed on the LHRF, ECRF and ICRF heating systems for FER and ITER [4.5-1,4.5-2,4.5-3]. As for FER, 30 MW, 5 GHz LHRF system is selected for current ramp-up assist and current drive in the outer region of the plasma, together with 50 MW, 0.5-1 MeV NB as central current drive and heating system. In order to supplement a central

heating capability, either 20 MW, 50-85 MHz ICRF system or 20 MW, 140 GHz EC system is added. Table V.4.5-1 summarizes the design parameters of the rf heating and current drive systems for FER and ITER. Numbers in the parenthesis are for ITER.

Table V.4.5-1 Design parameters of the LHRF, ECRF and ICRF heating and current drive system for FER and ITER (Numbers in the parenthesis are for ITER).

	LHRF	ECRF	ICRF
Injection power [MW]	25 (45)	25 (20)	25 (115)
Frequency	5 GHz	140 (120) GHz	120~160 (15~80)MHz
Pulse length	1000 sec (2 Weeks)	ibid.	ibid.
No. of ports	1 (2)	1	1 (5;40 antennas)
RF source:			
number	78 (104)	28	24 (40)
type	klystron	gyrotron	tetrode
unit power [MW]	0.7	1	1.5 (3)
Launcher:			
type	multi-junction array	multi-mirror	loop array
power density [kw/cm ²]	3.3 (4)	2.3	0.75 (0.43)
Total efficiency	0.44 (0.43-0.50)	0.36 (0.28)	0.53 (0.67)

References

- [4.5-1] K. Uehara, T.Nagashima, Y.Ikeda et al., to be published in JAERI-M (1991).
 [4.5-2] Y. Yamamoto, K.Sakamoto, M.Tsuneoka et al., to be published in JAERI-M (1991).
 [4.5-3] H.Kimura, M.Saigusa, Y.Saitoh et al., JAERI-M 91-094.

5. Tritium Technology

5.1 Introduction

Research and development for tritium technology have been performed for the purpose of engineering establishment of the tritium processing, blanket technology, tritium safe handling, and related technologies for fusion reactors. For the tritium processing and related technology, experimental studies of fuel cleanup, hydrogen isotope separation, and tritium analysis and measurements were accomplished by using ~1.5 g of tritium. Joint operation of Tritium Systems Test Assembly (TSTA) at Los Alamos National Laboratory under Annex IV has been continued in the fourth year of the collaboration. As a major activity in F.Y. 1990, experiments and operational tests were carried out for major components of the JAERI Fuel Cleanup System, which is a full-scale plasma exhaust processing device developed and designed by JAERI. The tritium systems including the solid and liquid waste treatment systems as well as the tritium recovery system for the driver blanket have been designed for Fusion Experimental Reactor (FER) and ITER. The

safety systems of Tritium Process Laboratory were fully in tritium service for the above-mentioned experimental apparatus, and were successfully operated without off-normal tritium release.

5.2 Development of tritium processing technology in TPL

5.2.1 Fuel cleanup

The experiment of the fuel cleanup system (FCU) was continued to improve the operation stability and performance in processing simulated plasma exhaust. Continuous feed of the DT flow to the system inlet at around 2 liter/min was successfully maintained in a 3 days run. Nitrogen and methane were tested as impurities. Electrolysis cell showed better performance with oxygen-free carrier for the regeneration of the cold traps. Poor trapping of tritiated water vapor at the cold traps was observed when the traps were switched. More improvement is needed on the transient characteristics of the traps. To date, more than 3 million Curies of tritium was processed in the FCU. The major objective of the FCU experiment to establish the technology to process plasma exhaust and to demonstrate the ability to handle large amount of tritium in a closed loop were almost achieved. Future experiments will emphasize the better understanding of the performance of the components and possible modification on the configuration of the process.

5.2.2 Hydrogen isotope separation

Distillation experiments of single columns and a two-column cascade were carried out with H-D-T system (1.5 g of tritium) for both the steady-state and dynamic separation characteristics. The columns used were different inner diameters (1 cm and 2 cm) and the sizes of the packings (3 mm Dixon ring for the larger column and 1.5 mm Dixon ring for the small column). In the two-column cascade operation, the larger column was used as that of the lead, and a bottom flow was supplied to the second column as a feed. The experimental observations for composition distributions at the steady-state were in close agreement with calculated results for all the components regardless of the column dimensions and operation modes. The HETP values measured were in the range from 3 to 6 cm. In the single column experiments, the steady-state compositions distributions were formed within 2 hr. For the two-column cascade operation, the system needed about 6 hr to reach the steady-state. The dynamic variation of the composition in the bottom product stream experimentally observed was well predicted by computer-aided simulation. On the other hand, for the top product stream, the variation was significantly slow in comparison with that of the calculated result using the assumption that the liquid holdup in the condenser was negligible. Figure V.5.2-1 shows an example of dynamic variation of composition distribution in the top product stream of the lead column under the two-column cascade operation. Experimental and calculated conditions are listed in Table V.5.2-1. Considering the above-mentioned results, it can be expected that the columns have the appreciable liquid holdups at the condensers.

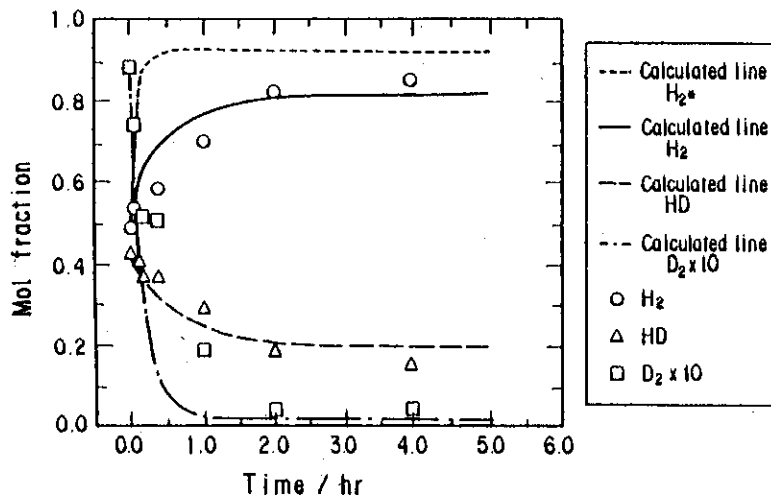


Fig. V.5.2-1 Dynamic variation of composition in the top product stream of the column. (* The dynamic variation is calculated on the assumption that the liquid holdup at the condenser is negligible.)

Table V.5.2-1 Experimental and calculated conditions.

	lead column	second column
Liquid holdup (mol)		
reboiler	1.58	4.92
Packed section	0.86	0.22
condenser	2.1	0.8
Top flow rate (mol/h)	5.6	2.2
Bottom flow rate (mol/h)	3.9	1.7
Number of total theoretical stages	10	10
Feed stage number	5	7
Pressure (Torr)	576	534
Vapor velocity (cm/s)	5.6	8.0
Reflux ratio	7.1	5.3

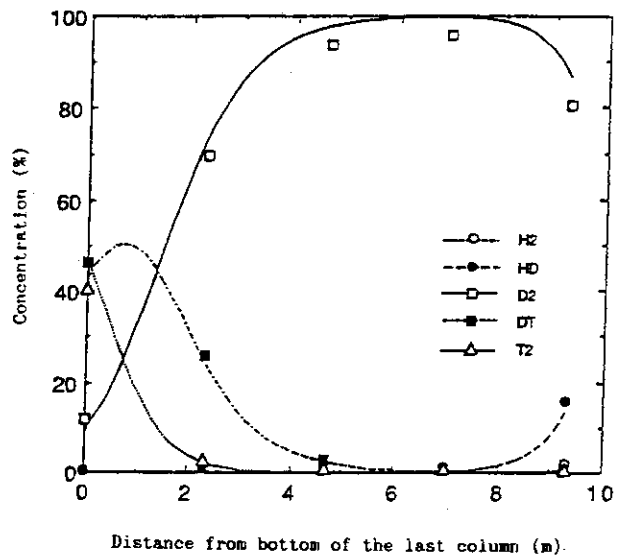


Fig. V.5.2-2 Composition distribution within the four columns.

The hydrogen isotope separation experiments by the thermal diffusion have been performed with H-T, D-T, and H-D systems. The apparatus is composed of four thermal diffusion columns, and is designed to recover tritium diluted by operation and experiments at TPL (Tritium Process Laboratory). Each column is 29.4 mm in inner diameter and 2.5 m long, whose outer wall is cooled with chilled water (~283 K). The hot wire temperature can be raised up to 1,273 K. First series of experiments was carried out by using a single column with H-T, D-T, and H-D systems to examine optimum operating condition (especially for column pressure). Next series of experiments was carried out by inter linking the four columns at a total reflux mode with

H-T (0.7 g of tritium) system under the optimum operating conditions determined for the single column experiments. In Figure V.5.2-2, the composition distribution experimentally observed is presented with the calculated result for the column whose height is four times as large as that of the single column. The experimental observation is in close agreement with the calculated result. It was thus verified that the thermal diffusion system could be divided into several columns without loss of separation performance.

It has recently been pointed out by theoretical works that the thermal diffusion column whose wall is refrigerated to cryogenic temperature (liquid nitrogen temperature) has a possibility of remarkable enhancement factor compared with an ordinary-cold wall using water. We have designed and constructed an experimental apparatus of the above-mentioned cryogenic-wall thermal diffusion column, and have initiated separation experiments with H-D system.

5.2.3 Tritium analysis and measurement

To establish system control and tritium inventory accounting in fusion fuel processing systems, analytical method for processing gases should be developed. From this viewpoint we have continued development of a real time and in-situ process gas analyzer using laser Raman spectroscopy. To accumulate basic data for analysis of various gases expected in plasma exhaust, Raman spectra of hydrogen isotopes except tritium and various deuterided methanes had already measured during the last fiscal year.

In this fiscal year, our attention was focused on measurement of tritium gas spectrum. In Figure V.5.2-3 is shown an apparatus for measurement of tritium gas spectrum. The apparatus is installed into a hood in which 10 Ci (3.7×10^{11} Bq) tritium gas can be handled. Raman scattering spectra of tritium gas were measured successfully using the apparatus shown in Figure V.5.2-3. Figure V.5.2-4 shows the Stokes rotational lines of the Raman spectrum for $H_2+D_2+T_2$ gas mixture ($H_2:D_2:T_2=1:1:1$). As can be seen from the figure, it is possible to identify the six hydrogen isotopes by selecting appropriated Stokes lines. The Stokes lines of 200, 245, 415, 395, 267, and 587 cm^{-1} were selected as those for analysis of T_2 , DT, D_2 , HT, HD, and H_2 , respectively. Quantitativeness of those Stokes lines were also studied. The intensity of the Stokes lines of 587 cm^{-1} for H_2 and 415 cm^{-1} for D_2 were measured as a function of their partial

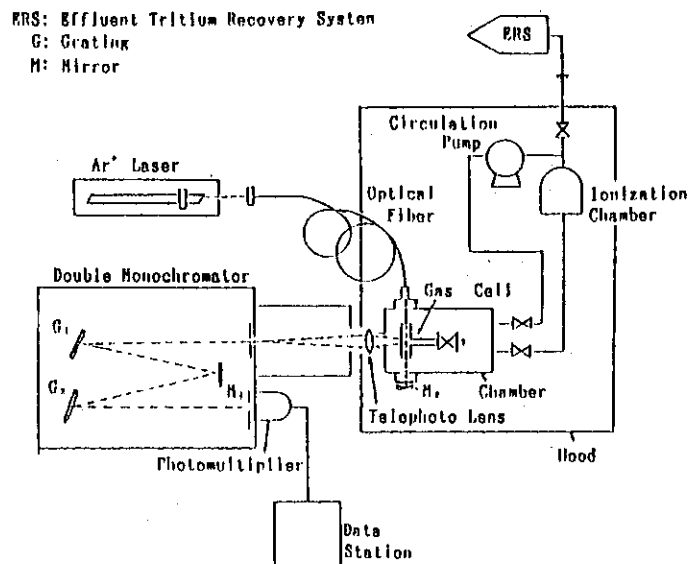


Fig. V.5.2-3 Laser Raman spectroscopic analyzer for tritium gas measurement and treatment.

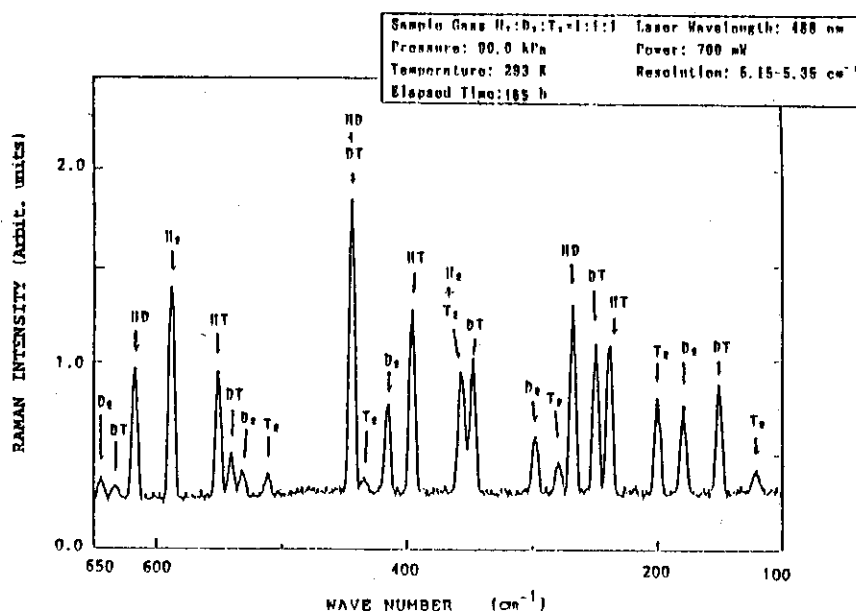


Fig. V.5.2-4 Stokes rotational Raman spectrum of H₂, D₂ and T₂ (1:1:1) complex gas.

pressure in the cell. The experimental result is shown in Figure V.5.2-5. A good linearity was shown between the Stokes line intensities and the partial pressure from 0.05 to 100 kPa. This fact means that the Stokes lines are useful for a quantitative analysis for the hydrogen isotopes. Detection limits of partial pressure were estimated to be about 0.05 kPa for H₂ and 0.1 kPa for D₂, assuming S/N=2. The detection limits of 0.05 and 0.1 kPa are equivalent to 500 and 1,000 ppm at normal atmospheric pressure gas, respectively. The detection limits obtained in the present study are not always sufficient for the process gas analyzers of the fusion fuel processing systems. It, however, can be possible to increase the detection limits more than two order magnitudes using multiple pass technique and a higher power laser. From the experimental results described above, Raman spectroscopy is expected to be applicable to a real time and the in-situ gas analyzer for the fusion fuel processing systems.

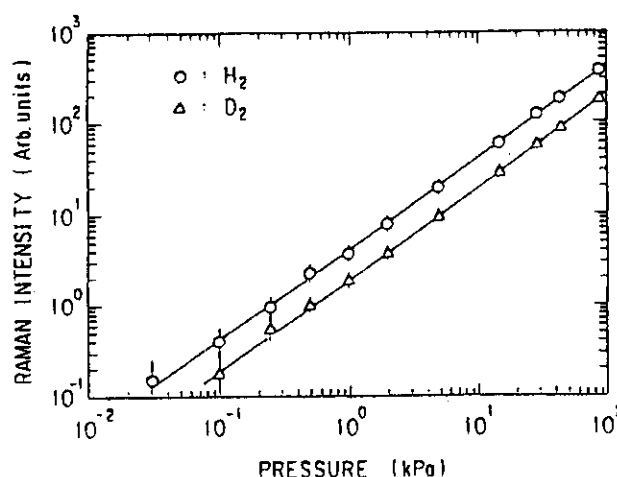


Fig. V.5.2-5 Relationship between partial pressure of H₂ and D₂ and Raman intensity. Laser wavelength, 488 nm; power, 700 mW; spectrum resolution, 5 cm⁻¹.

5.2.4 Tritium-material interaction

Ion implantation-driven permeation of tritium into first wall coolants could be a serious problem from a viewpoint of

tritium safety in D-T fusion reactors. To estimate tritium permeation fluxes through candidates of constructional materials of first walls, we have accumulated experimental data using an apparatus which produces hydrogen isotope ion beams in the energy range from 100 to 2,000 eV. In this fiscal year, we paid our attention to investigation of permeation behavior of deuterium implanted into iron, aluminum and molybdenum. We studied dependencies of incident ion energy, incident ion fluxes and temperatures on the permeation fluxes of deuterium implanted into those metals.

5.3 Development of fuel processing technology under JAERI-LANL(DOE)

The research program under the "Annex IV to the Implementing Arrangement between JAERI and United States Department of Energy on Cooperation in Fusion Research and Development for the DOE-JAERI Collaborative Program" (hereinafter referred as the Annex IV) entered in the fourth year of the collaboration. The Joint operation of TSTA at Los Alamos National Laboratory (LANL) resulted the operations of the integrated loop including the Fuel Cleanup and Isotope Separation.

Major efforts were focused on the JAERI Fuel Cleanup System (JFCU), a full-scale plasma exhaust processing device developed and designed by JAERI and installed in the TSTA in early 1990. A number of cold testing and modifications were performed on the JFCU. Components such as the palladium diffuser, cold traps, catalytic reactor, scroll pump and electrolysis cell were tested independently as well as in the integrated process tests.

The permeability of hydrogen isotopes were measured with the palladium diffuser-scroll pump loop. Baking of the membrane at 450°C in oxygen followed by hydrogen reduction improved the poor initial permeability suspected to be affected by a surface contamination. Figure V.5.3-1 summarizes the permeation flux of hydrogen through the diffuser as the function of differential partial pressure across the membrane. Effect of the baking is indicated. Satisfactory processing rate with tritium can be expected, according to the isotopic ratio of permeability obtained in the previous studies.

A Normetex scroll pump that evacuates the permeated side of the palladium diffuser, and compresses

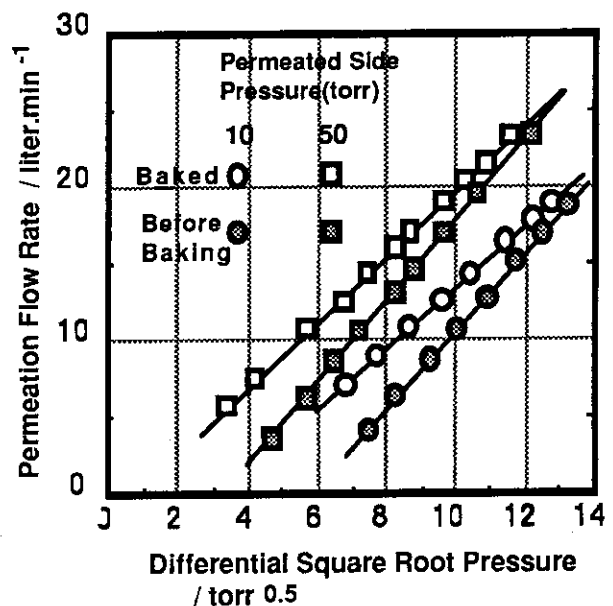


Fig.V.5.3-1 Permeabilities of pure hydrogen isotopes through the palladium diffuser before and after activation. Permeation flow rate is plotted against differential square root of pressure across the diffuser.

purified hydrogen isotopes for supply to the ISS was tested with He, H₂ and D₂. Poor compression of light gas by the pump, probably due to the mechanical property of the gas was observe as shown in the Fig. V.5.3-2. It was revealed that the scroll pump that was expected to compress hydrogen isotopes from 5 torr to 800 torr at the throughput of 6 liter/min will not meet the requirement. A metal bellows pump MB-601 was installed at the discharge side of the scroll pump to improve the compression. Both compression ratio and ultimate pressure of the system were improved and designed throughput was met with either deuterium or hydrogen.

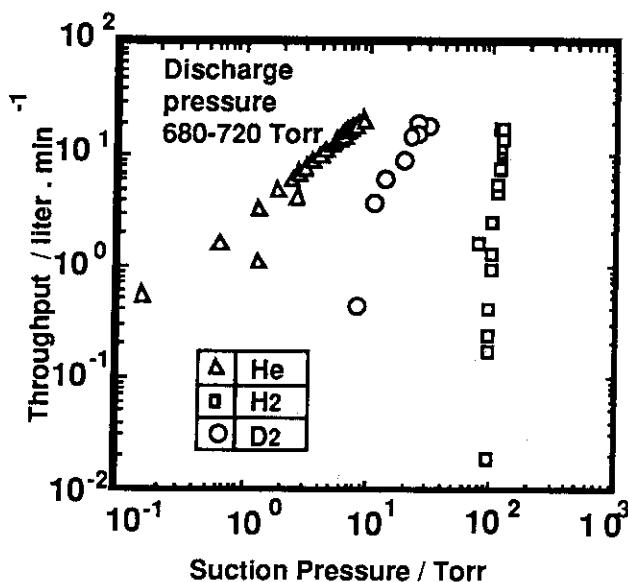


Fig.V.5.3-2 Comparison of pumping characteristics for hydrogen, deuterium and helium in the Scroll pump.

Conversion of CH₄ and NH₃ at the catalytic reactor was tested as the function of temperature. Both species were completely oxidized at the temperature above 450°C. Gas chromatograph system was used for the measurement and some difficulty in operation was experienced.

The total performance tests of the JFCU was conducted with deuterium-impurity mixtures. Purification of deuterium, oxidation of impurities(CH₄ and NH₃), trapping and decomposition of water, and gas analysis by the GC system, and supply and recovery of deuterium with the large Zirconium-Cobalt Bed were successfully tested in a interlinked process. A problem was uncovered on the cold traps and some modifications were attempted. During the integrated test, humidity spikes at the outlet of the trap. Addition of baffle or filter in the traps, control of pressure and flow rate across the traps, or change of valve sequence did not improve trapping

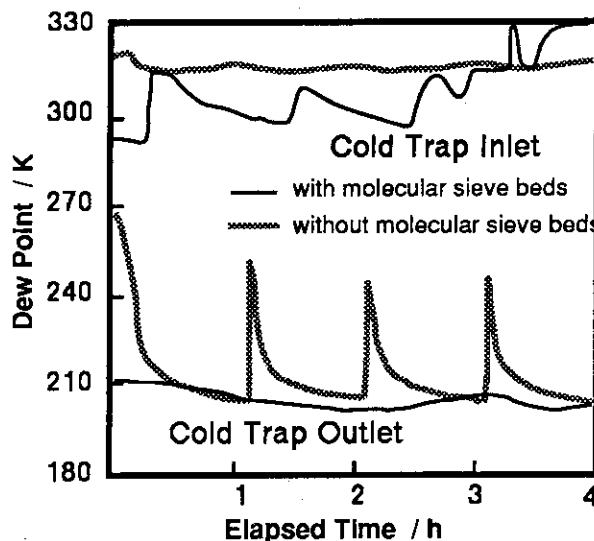


Fig. V.5.3-3. Moisture trapping by the cold traps of the JFCU. Effect of the small molecular sieve beds at the outlet of each traps are shown.

efficiency. Small molecular sieve beds installed at the outlet of the traps removed the humidity spikes completely. Figure V.5.3-3 shows the humidity at the outlet of the cold traps with and without the molecular sieve beds.

Preparation for the tritium experiment of the JFCU required intensive efforts. Hardware modifications performed on the JFCU besides the metal bellows pump and cold traps are; replacement of the Ceramic Electrolysis Cell, Modification of oxygen control system, minor change of plumbing, and addition of tritium monitor at the outlet of the system. Process connections between TSTA loop and JFCU and their secondary containments were completed in February by the intensive effort of mechanical technicians. Process vacuum and glovebox control service are provided by existing TSTA system. Secondary containment for the scroll pump was installed and tested in March, 1991. Some minor safety problems were found on electric system and corrected. Communication software between JFCU and the TSTA computer was completed and tested. Emergency shutdown command from the TSTA computer to JFCU was also installed. A number of documents were prepared for the Safety analysis and Operation Readiness Review of the JFCU in order to obtain an approval for tritium operation.

Isotope separation experiment with 3-column cryogenic distillation was an major accomplishment. Very stable operation and low tritium concentration in the TD exhaust stream were successfully achieved. Column profile was measured with gas chromatographs and the result agreed well with the numerical simulation obtained with the code developed by JAERI. Advanced analysis system with laser Raman spectroscopy was interfaced.

Experimental apparatus for the Raman spectroscopy installed in the last year started to operate with tritium. Radiochemical reaction with tritium and other gases were being studied with this system. This system is also used for the analysis of the gas sampled from the Isotope Separation System.

5.4 Development of tritium safe handling technology

5.4.1 Separation of tritium using polyimide membrane

Polyimide membrane has a selective permeability for hydrogen gas and water vapor contained in air. A gas separation module containing hollow filament membranes made of polyimide has been developed to reduce volume of air contaminated with tritium. Figure V.5.4-1 shows a conceptual flow diagram of the polyimide separation module. This module separates air contaminated with tritium into

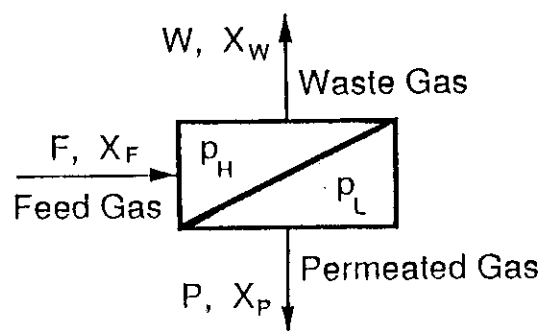


Fig. V.5.4-1 Conceptual flow diagram of the polyimide separation module

two streams: air essentially free from tritium and small amount of gas in which tritium is concentrated. Factors affecting separation characteristics of the module, (Recovery ratio ; $R = (P \times X_P / F \times X_F) \times 100$), are the ratio of flow rate of permeated gas (P) to feed gas (F), (Cut ; $\theta = P / F$), the ratio of feed gas side pressure (p_H) to permeated side (p_L), (Pressure ratio ; $\gamma = p_L / p_H$), and operation temperature. Preliminary tests have been performed with nitrogen containing small amount hydrogen gas, where permeated side of membrane was evacuated. Relation between cut and recovery ratio of hydrogen gas is shown in Figure V.5.4-2. As an example, in the case where the pressure is 1,500 Torr for the feed gas and 10 Torr for the permeated side of the membrane (Pressure ratio = 7.0×10^{-3}), cut is 0.17 and recovery ratio is 96 %. This indicates that the permeation flow rate was 1/6 of that of feed, and concentration of hydrogen in the feed stream was reduced to 1/20.

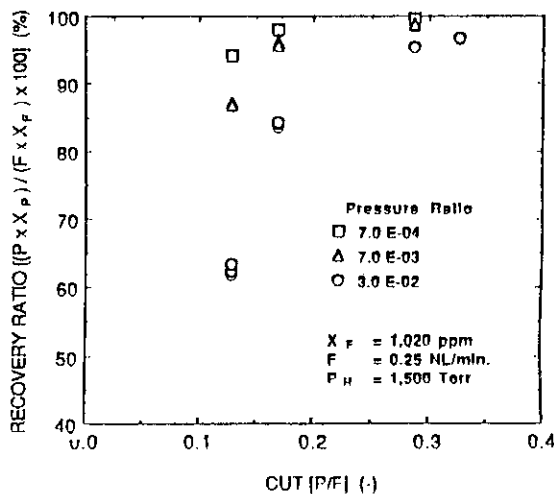


Fig .V.5.4-2 Relation between cut and recovery ratio of hydrogen gas

5.4.2 Operation of tritium safety systems

The safety systems which composed of Glovebox, Glovebox gas Purification System (GPS), Effluent tritium Removal System (ERS), Air Cleanup System (ACS), Dryer Regeneration System (DRS) etc., were fully in tritium service without off-normal tritium release. Effluent from the experiments processed was about 1,900 m³ in total and 550 Ci of tritium was recovered. Figure V.5.4-3 shows monthly release of tritium from TPL stack. Total tritium release to environment was less than 0.2 Ci in this period.

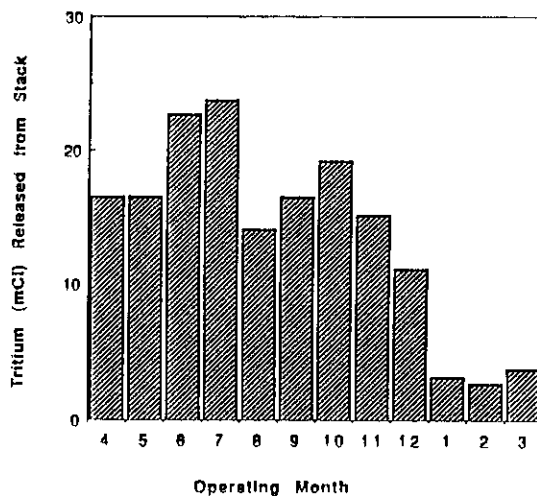


Fig. V.5.4-3 Monthly release of tritium from TPL stack (FY1990)

5.5 Development of blanket technology

5.5.1 Design works

Conceptual design works were carried out on Blanket Out-of-pile Testing facility which is intended to be constructed in Naka site for the development of breeding blankets of International Thermonuclear Experimental Reactor (ITER). The Blanket Out-of-pile Testing Facility is designed for the basic blanket elements tests and the integrated functional tests of scalable blanket test units.

Also, the incorporating effort was continued to the design works on Blanket In-pile Testing Facility which was being carried out by the Department of Japan Material Testing Reactor Project. The design of Blanket In-pile Testing Facility was proposed to be the common facility for the blanket in-pile test.

5.5.2 Experimental works

As part of the short term R & D of ITER Conceptual Design Activity (CDA), experimental works for the development of the blanket technology were carried out on the following items.

i) Industrial production technology development

Kilogram order of small sphere breeders and multiplier (1mm diameter of Li_2O , Li_2ZrO_3 , Li_4SiO_4 and Be, respectively) were produced to demonstrate the technology.

ii) Thermo-mechanical evaluation tests of multiplier

Thermal fatigue tests (200 °C ~ 700 °C, 1,000 cycles) and thermal stress tests (200 °C ~ 700 °C, 0 ~ 5 kg/cm², 10,000 cycles) were initiated with produced Be sphere (1mm diameter).

iii) Thermo-chemical evaluation tests

Mass transfer experiments of breeders were carried out in humidified He gas (10,000 ppm, H_2O). Also, material compatibility tests were performed with breeders, multiplier and structure materials (SUS 316, SUS 316L and PCA) to certify the acceptable temperature limit, corrosion rate and so on. Figure V.5.5-1 shows one of obtained results by Be/SUS316 compatibility test. Corrosion thickness was certified to have the linear relationship with the square root of time.

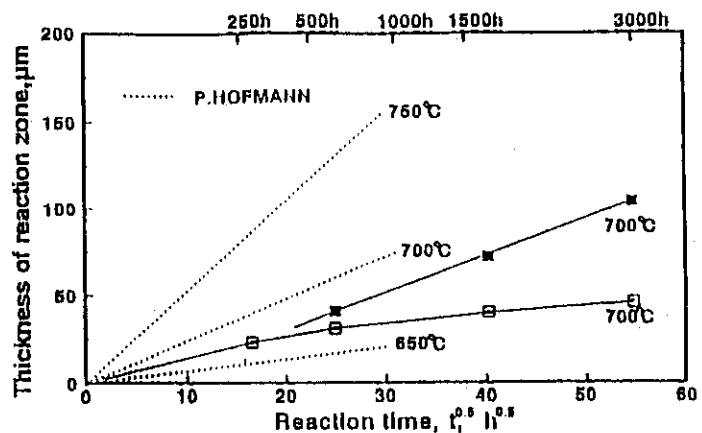


Fig. V.5.5-1 Extent of chemical interaction of Be with stainless steel as a function of the square root of time

Oxidation experiments of the multiplier was performed in humidified He gas (10,000 ppm H_2O) under various temperature conditions. It was demonstrated that Be is oxidized slowly to reach the acceleration step of oxidation and that the time duration is dependent on the temperature.

iv) Thermal conductivity tests of packed beds of breeders

Effective thermal conductivity was measured with beds packed with 5 mm and 1 mm diameter of Al_2O_3 and 5mm diameter of Li_2O . v) Thermo-hydrodynamics tests of LiPb. As an alternative blanket to lithium ceramic blanket, liquid LiPb is an attractive material because it can be used as the self-cooled blanket. On this view point, the basic operation characteristics were tested

with the LiPb Test Loop by using liquid $\text{Li}_{17}\text{Pb}_{83}$. The test result contains the characteristic curve of electro-magnetic pump, the pressure drop of the loop and so on. Figure V.5.5-2 shows the pressure drop in the loop. It was demonstrated that the pressure drop of the liquid LiPb flow can be estimated with the conventional equation referred in Chemical Engineer's Handbook.

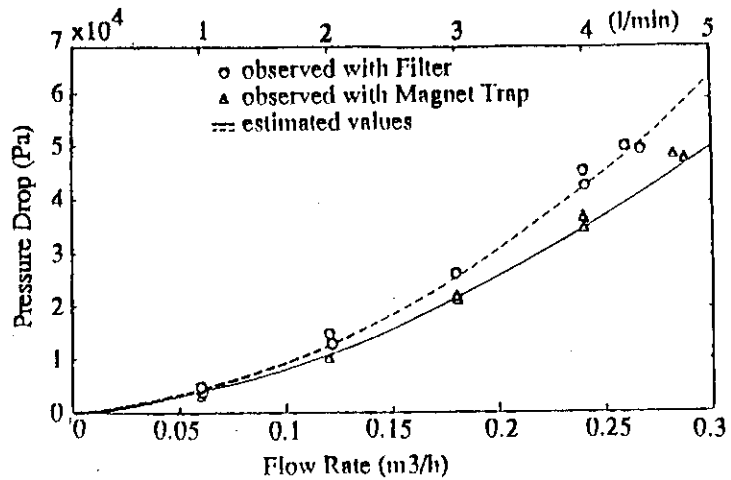


Fig. V.5.5-2 Observed pressure drop in LiPb Test Loop at TPL, JAERI

5.6 System analysis

5.6.1 Design works of tritium systems

Incorporated in the Fusion Experimental Reactor Design Team, conceptual design works of tritium systems for Fusion Experimental Reactor (FER) and ITER were continued and the results were presented as Japanese proposal to ITER in the specialists meeting of ITER in Germany. The tritium systems of ITER consists of the fuel circulation system, primary coolant water detritiation system, blanket tritium recovery system and safety system.

The fuel circulation system was designed by using concepts of the components that are under development by JAERI (the pellet injector, the large scale (25,000 l/s) magnetic bearing type turbo molecular pump, the palladium alloy permeator, the cryogenic distillation system and catalytic reduction recombiner). Also, the applicability of thermal diffusion column to the isotope separation system was discussed in the design work.

The primary coolant water is designed to be supplied to the divertor, the first wall and the blanket. As the first step of the design work, the evaluation of the tritium permeation from each system to the coolant water was performed to give the design condition of the detritiation system.

The safety system was designed to be operated under the normal operation, the maintenance mode and maximum accident mode. Also, the preliminary consideration for the accidental loss of coolant water out of the vessel (out of vessel LOCA) was performed and gave the primary information that the pressure and the temperature in the reactor hall can increase explosively and immediately after the initiation of the out of vessel LOCA.

The blanket system was designed to use the palladium alloy permeator, electrolysis cell and the recombiners for the recovery of tritium from the breeder layer and the multiplier layer.

The design work of the blanket proceeded to confirm the feasibility of Japanese proposal (Li_2O and Be sphere packed beds of layered structure). The further effort on the thermo-dynamics

and the neutronics design should be needed to optimize the structure and the thickness of each layer.

In addition to the design works of the tritium systems, the solid waste storage facility was designed to store the replaced divertors and the first wall armour. Also it was certified that further R & D is necessary to design the tritium recovery system from graphite used as the divertor and the first wall.

5.6.2 Development of components for the FER

Preliminary R & D was initiated for the waste treatment technology for graphite of the first wall armour material under the collaboration with the Department of Fuels and Materials Research, the Department of Chemistry and the Department of Fusion Facility.

6 High Heat Flux Technology

6.1 Introduction

Since it is essential for the next step large devices, such as ITER/FER, to develop the plasma facing components (PFC), JAERI has carried out the experimental and analytical studies on PFCs. Our major effort has been concentrated to develop the divertor plate and first wall of the ITER and FER. Major issue of the divertor plate is to develop bonding structures which will be able to endure a heat flux of 15 MW/m^2 . For the first wall, to develop connecting structures between armour tiles and substrates is the key issue. In order to develop PFCs, two test facilities have been utilized at JAERI. One is a hydrogen ion beam irradiation test stand, called the Particle Beam Engineering Facility (PBEF), and the other is an electron beam irradiation test stand, called the JAERI Electron Beam Irradiation Stand (JEBIS).

One of the significant features of the JEBIS is that it can produce intense electron beams which can simulate a heat load onto the surface of PFCs during plasma disruption. Many carbon based materials and metals have been tested to evaluate erosion loss during the plasma disruption in the JEBIS. Japan-European Community collaborative experiments has also been performed in the JEBIS.

6.2 Activities on divertor plate development

In a design parameter of the ITER PFC, divertor plates will be exposed to a heat flux of more than 15 MW/m^2 . The divertor plate is covered with armour tiles which are brazed on an actively cooled metal structures. Carbon based materials are primary candidate as armors in the physics phase of ITER, and metal materials are proposed in the technology phase. One of the key technology of manufacturing the divertor plate is the bonding technique of the armour tiles to the metal structure. We manufactured divertor modules with armor tiles made of carbon based

materials. Carbon fiber reinforced carbon composite(CFC) and graphite are selected as the armor tile. As the cooling tube, a straight tube is utilized for a short pulse experiment and a swirl tube, in which a twisted tape is inserted to enhance the heat transfer, is adopted for experiments with a steady state heat load.

6.2.1 Thermal cycling experiments on divertor modules without a swirl tube at PBEF

The thermal cycling experiments on divertor plates with the straight tube have been performed in PBEF. Heating conditions are 16MW/m^2 for 1.5 s and for 2.0 s, which are equivalent heat load of 10MW/m^2 and 12.5MW/m^2 at the bonding interface, respectively. The divertor module consists of ten CFC/OFHC Cu and C/OFHC Cu bonded blocks. The results are summarized in Table V.6.2-1. The CFC-Cu bonding structures can endure 1000 thermal cycles at the equivalent heat flux of 10MW/m^2 , although the C-Cu bonding structures show cracks at the bonding interface. For the equivalent heat flux of 12.5MW/m^2 , no bonding structures can not survive.

Table V.6.2-1 Summary of Thermal Cycling Tests of Divertor Modules in PBEF

Armor Material	Braze	Interlayer	Heat flux (MW/m^2)	
			10	12.5
<u>CFC</u>				
CX2002U	Ag-Cu-Ti	none	Good	Separation
	Ti-Cu	Mo	Good	
	Ag-Cu-Ti	TZM		Cracks
PCC-2S	Ag-Cu-Ti	none	Good	Cracks
AO5	Ti-Cu	none		Separation
JCC	Ti-Cu	none		Separation
<u>Graphite</u>				
IG430U	Ti	none	Cracks	Cracks
PD330S	Ag-Cu-Ti	none		Cracks

6.2.2 Thermal cycling experiments on divertor modules with a swirl tape in JEBIS

The thermal cycling experiments on the divertor modules with the swirl tube has been performed in JEBIS. The heat transfer coefficient of the swirl tube is about two times larger than that of the straight tube and the critical heat flux is 35MW/m^2 with a flow velocity of 10 m/s at an inlet pressure of 1 MPa. Heating conditions are 10MW/m^2 for 20 to 50 s, which is longer

enough than the thermal constant of the divertor modules. After 1000 thermal cycles, no cracks and damages are found in the CFC-Cu bonding structures, while cracks and separation of the armour tiles are occurred in the C-Cu bonding structures.

6.3 Development of a first wall

Most of the first wall is exposed to a heat flux of 0.2 MW/m^2 . In front of the toroidal coils a heat flux of 0.6 MW/m^2 is locally deposited on the first wall because of ripple losses. The CFC armour tiles of the first wall are mechanically attached on the cooled substrate, which is made of stainless steel. Two kinds of the first wall structures are proposed; a conductively cooled first wall for lower heat fluxes, and a radiatively cooled first wall for higher heat fluxes, which can re-radiate a part of incident heat flux to the conductively cooled armour. A major issue of the conductively cooled first wall concept is to obtain good thermal contact between the armour tile and substrate during heating. On the other hand, a critical issue of the radiatively cooled first wall concept is whether the tile can be sufficiently thermally insulated from the substrate, and whether the tile attachment mechanism has enough durability.

The conductively first wall mock-ups have been manufactured by JAERI and were tested in the JEBIS. The CFC armour is fixed on the substrate by the stainless steel bolts and nuts. A carbon compliant layer of 0.2 - 0.6 mm in thickness is inserted between the armour and substrate to obtain high thermal conductivity. The conductively cooled first wall is tested at a heat flux of 0.2 MW/m^2 for 20 - 60 minutes. The surface temperature remains at $350 \text{ }^\circ\text{C}$ for a compliant layer thickness of 0.6 mm. The maximum surface temperature of $700 \text{ }^\circ\text{C}$ occurs at a cover cap of the attachment nut. No temperature degradation is found for 60 thermal cycles.

Radiatively cooled first wall elements have also been fabricated and tested. The carbon armour is fixed on the substrate by a couple of ceramic bolts and nuts. The ceramic nut is brazed in a Ti cover which is screwed into a TZM pedestal brazed on the substrate. The surface of the substrate is coated with Cr_2O_3 to enhance radiation heat transfer between the armour and the substrate. The heating conditions are 0.6 MW/m^2 for 20 to 50 minutes. The surface temperature reaches over $1000 \text{ }^\circ\text{C}$. After 50 thermal cycles, no damage was found on the armour tile and substrate. The Ti cover of the ceramic nut, however, is melted. It means that the thermal insulation by the ceramic bolt and nut results in high temperature at the Ti cover.

6.4 Disruption simulation experiments

The JEBIS can produce a heat flux of 2000 MW/m^2 for 1 ms and more within an area of 0.8 cm^2 . This means that the JEBIS can simulate a real heat load during the disruption. An evaluation of the erosion loss during the disruption has been performed in the JEBIS. Several CFC materials are tested with a heat flux of 300 MW/m^2 to 1800 MW/m^2 for 3 ms to 10 ms and the results are compared with numerical predictions. It is found that the erosion depth is 2 to 5 times

larger than the predictions because of particle emissions from the surface. The Japan-EC collaborative experiments on disruptive erosion are also performed in the JEBIS. Carbon based materials and metals specimen were brought from EC and tested a heat flux of 300 MW/m² to 1800 MW/m². The analysis of the results are under way.

VI. NEXT STEP FOR JAERI TOKAMAK PROGRAM

1. International Thermonuclear Experimental Reactor (ITER)

1.1 Introduction

International Thermonuclear Experimental Reactor (ITER) was initiated at summit meetings of governmental leaders so as to develop an experimental fusion reactor through the united efforts. The major objectives of ITER are to demonstrate controlled ignition and extended burn of DT-plasma, with steady state operation as an ultimate goal and to demonstrate the integrated reactor technology essential to a fusion power reactor.

In response to the summit initiatives, joint design work on ITER Conceptual Design Activities (CDA) under the auspice of the IAEA by four Parties, Japan, the United States, the Soviet Union and the European Community was conducted from April 1988 to December 1990. The conceptual design prior to the engineering design was to assess the total system feasibility and identify critical technical issues. As a result, the feasible design concepts, the widest possible technical basis and the future R&D program were successfully developed.

As a whole, the conceptual design including the missions and objectives of ITER and the future plan were reviewed several times by experts involved in the fusion research and development in Japan. The overall conclusion is that no substantial motivation has been observed to modify the present ITER objectives and the conceptual design, although some small modifications are needed for design consistency, which will be implemented in the early phase of the coming Engineering Design Activities (EDA).

1.2 ITER conceptual design

The design concept of ITER was based on a reasonable technological basis taking into account future progress of plasma physics and engineering technology development. Also, an operational and experimental flexibility, which is a key design feature for achieving the ITER objectives, was adopted as much as possible within this achievable technical scope.

The overall layout and maintenance scheme of the ITER basic devices and its key parameters are given in Fig.VI.1.2-1 and Table VI.1.2-1, respectively. The nominal fusion power generated in the reactor is approximately one gigawatt and the rated plasma current is 22 MA. A non-circular cross-section plasma with an elongation of approximately two is employed. Helium ash exhaust and impurity control are accomplished through the use of a double-null divertor configuration.

Table VI.1.2-1 ITER major parameters.

Plasma major radius	6 m
Plasma minor radius	2.14 m
Elongation, 95% flux surface	2.0
Toroidal field on axis	4.85 T
Nominal plasma current	22 MA
Nominal fusion power	1 GW
Pulse length	200 s to continuous
Energy multiplication	5 to infinity

The goal of achieving extended burn (ultimately steady-state) dictates the use of

superconducting coil systems. The poloidal field (PF) coils are located outside of the toroidal field (TF) coils in order to facilitate assembly and maintenance. The maximum field of TF coil is specified to be 11.2 T to provide toroidal field of 4.85 T on the plasma axis with a radius of 6 m. The center solenoid coil, which is located in the machine center inside of the TF coil inner leg, is designed to be capable of providing magnetic flux of about 325 V-seconds and sustaining 22 MA-plasma for at least 200 seconds inductively. The maximum field of the center solenoid coil is specified to be 13.5 T.

The vacuum vessel is a key containment structure to provide the first barrier of tritium. In addition, the vacuum vessel has to provide one-turn toroidal resistance and nuclear shielding functions. In CDA, two different concepts, which are thick vessel partially insulated by resistive elements and thin vessel with toroidally uniform resistance, were developed.

Breeding blankets, located inside the vacuum vessel, are composed of the first wall, breeding and shielding structures: this supplies most of the required tritium fuel and provides the nuclear shielding for superconducting magnets and personal access. A breeding

blanket can be maintained/replaced independently from others by using the remote handling system located on the upper access port, as shown in Fig.VI.1.2-1. Divertor plates, located top and bottom region inside the vacuum vessel, are operated under high heat flux and frequently maintained. A rail-mounted vehicle system as shown in Fig.VI.1.2-1 is selected for the divertor maintenance and the feasibility has been demonstrated in a 1/5-scaled-model test.

Heating of the plasma and non-inductive current drive of the plasma current are achieved with a multi-function heating and current drive system. The first option for this system is based on 1.3 MeV negative-ion neutral beams working in conjunction with lower hybrid and electron

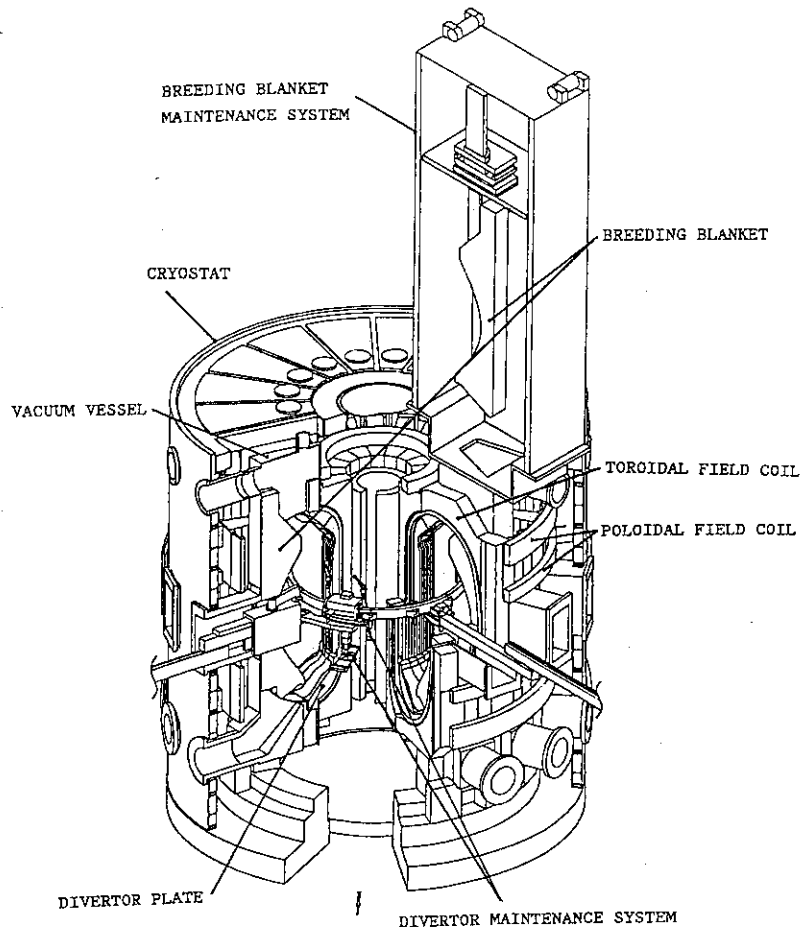


Fig.VI.1.2-1 ITER overall layout and maintenance scheme of major components.

cyclotron sources.

1.3 CDA R&D

1.3.1 Physics R&D

During the ITER CDA, extensive physics R&D for ITER design has been done in JT-60, JFT-2M and Theory/Analysis group, as well as WT-3 in Kyoto University and the linear divertor simulator NAGDIS in Nagoya University. Number of each contributions are 19(JT-60), 16(JFT-2M), 3(Analysis), 4(WT-3), 2(NAGDIS). In the course of ITER design, physics group identified necessary data base for the design. According to this identification, all of these contributions focused on the specific data base for the use of ITER design rather than generic data base, which actually impacted ITER design directly or indirectly. Several examples of the important contributions are as follows. In JT-60, high current drive efficiency by Lower Hybrid waves are achieved, which are already comparable to ITER design basis. Volt-second saving during current ramp-up by LH waves is also demonstrated, which supports quantitatively the usage of this scheme in ITER. Fairly high bootstrap current fraction is demonstrated, which triggered the reference use of this current to prolong the burn time and mitigate the engineering requirement for steady state operation. L-mode confinement data with different parameter regimes from other large devices clarifies the unknown parametric factors included in the ITER L-mode scaling and serves to minimize the uncertainty in the predictions of ITER performance. Simulation experiments for center born helium ash by He beam injection provides confirmation of ash exhaust capability and moderate helium de-enrichment in ITER. JFT-2M provides affluent data base for H-mode confinement, which serves establish ITER H-mode scaling law. Various kinds of active plasma control schemes are examined, e.g., Ergodic Magnetic Layer (EML), divertor biasing. EML provides the prospect for realizing controlled steady H-mode in addition to the possible enlargement of power scrape-off width, as well as for the possibility of controlling disruption in ITER. WT-3 demonstrates that plasma breakdown and current initiation can be achieved even by virtually zero loop voltage with combined EC and LH waves, which support low loop voltage breakdown in ITER.

1.3.2 Technology R&D

A wide range of the technology R&D is inevitably required to bridge from the present technology to the realization of ITER construction. The R&D involves key technology development, such as reactor structure, remote maintenance, superconducting magnet, plasma facing components, heating and current drive, fuel cycle, breeding blanket, diagnostics and plant systems. The key component technologies are being developed accumulating activities of hardware developing laboratories in JAERI under a good collaboration with industries. The major R&D activities and results contributed to the CDA of ITER are described below.

- (1) In a DEMO. Poloidal Coil (DPC) Program, two NbTi pulsed coils (DPC-U1 and DPC-U2) and Nb₃Sn pulsed coil (DPC-EX) each of which has an inner diameter of 1 m have been developed. DPC-EX was successfully charged under the background field of DPC-U1 and U2 up to the coil current of 17 kA and 7 T in one second, generating 20 MJ by the three coils.
- (2) Thermal cycling tests were performed in a Particle Beam Engineering Facility (PBEF) on divertor samples composed of carbon-copper bonded materials. A 1000-cycle test has proved the durability of the samples in a steady-state heat flux of 10 MW/m².
- (3) A 10 A at 50 keV negative hydrogen ion beam has been produced successfully using a cesium-seeded plasma volume type ion source.
- (4) A high power tetrode developed in the United States for an ICRF system was tested in JAERI under the U.S.-Japan collaboration program. The output power of 1.7 MW for 5.4 s has been obtained at 13 MHz.
- (5) A 1/5-scale model of the rail-mounted vehicle in-vessel maintenance system has been fabricated and the feasibility of the concept has been demonstrated.
- (6) A test rotor of turbomolecular pump (TMP) with electromagnetic bearings, which corresponds to that of TMP with pumping capacity of 25 m³/s, has been fabricated and the feasibility of the large capacity TMP with electromagnetic bearings was confirmed.

1.4 Long-term R&D program

1.4.1 Physics R&D

The long-term physics R&D program for the years 1991-1995 has been established which covers all R&D needs to provide support to the optimization of the ITER design and eventually to complete the data base necessary for taking the decision to start ITER construction. It was based on a detailed description of the R&D needs for ITER and the associated time schedules. Suggestions received from many members of the fusion community were also taken into account. The program covers the following five areas and subdivided in 22 tasks, supplemented by subtasks, more specific questions for ITER: 1) power and particle exhaust physics, 2) disruption control and operational limits, 3) enhanced confinement, 4) optimization of operational scenario and long-pulse operation, and 5) physics of a burning plasma.

The most crucial problems, to validate the ITER design concept and complete the physics data base required for starting ITER construction, in practical terms, are: 1) The demonstration, in experiments prototypical for ITER, that operation with a cold divertor plasma ($T_e \leq 30$ eV) is possible, that the peak heat flux onto the divertor plate can be kept below about 10 MW/m², and that helium exhaust conditions corresponding to a fractional burnup larger than 3% can be ensured; 2) A characterization of disruptions which allows to specify their consequences for the plasma-facing components, and evidence that the number of disruptions to be expected allows an acceptable lifetime of these components; 3) The demonstration that steady-state operation in a

regime with enhanced confinement (in particular in the H-mode) and satisfactory plasma purity is possible, and provision of the scaling of energy confinement for this mode which allows predicting the performance of ITER with satisfactory accuracy; 4) Ensurance that the presence of an appreciable population of fast ions does not jeopardize plasma performance in ITER.

A lot of contributions to the program have been proposed from the ITER partners. The coverage of the program is generally good. However, further efforts on the edge plasma in ITER-relevant divertor configurations and operating conditions need to be enhanced.

1.4.2 Technology R&D

A plan of long-term technology R&D for the period 1991 through 1995 has been discussed and established during the conceptual design phase. The plan is focused on the R&D necessary to support a decision to be taken by the end of 1995 to start ITER construction. International collaboration is expected to be maximized to best use the required resources and to minimize unnecessary duplication of effort.

The plan includes R&D for nine major systems of ITER; Magnets, Containment Structures, Assembly and Maintenance, Current Drive and Heating, Plasma Facing Components, Blanket, Fuel Cycle, Structural Materials and Diagnostics. For each system, the R&D objectives, the tasks, the schedule and costs, and the needed facilities have been clarified.

It appears possible that all major testing programs can be conducted in existing, but modified, facilities. A few new facilities may be required and this determination must be made as part of the implementation of the plan. Major facilities needed to support the proposed R&D program include center solenoid and TF magnet test facilities, containment structure/assembly & maintenance test facility, neutral beam model test facility, fuel cycle test stands and blanket in-pile and out-of-pile test facilities.

The preliminary estimates of the costs for all nine areas of the technology R&D plan are made. The cost estimates indicate a total cost over the five years of about 800M\$ in US dollars (1990). The costs per area over the five years vary from about 35M\$ to about 185M\$.

Task sharing by the four parties is an essential ingredient to the successful implementation of the plan. This plan does not specifically indicate which party or parties will perform which tasks or what degree of parallel effort is needed or expected. Separate efforts have been in process to develop the task sharing consideration.

2. Fusion Experimental Reactor (FER)

2.1 Introduction

The Fusion Council of Japan recommended in the National Research and Development Program that the next step fusion device should have a mission of achieving a long ignited and controlled DT burn. In 1987, the design study of FER (Fusion Experimental Reactor) with the

above mission was conducted. Because the joint work of the ITER has begun in May, 1988, a new organization (Fusion Experimental Reactor Team) was established to support the ITER activities and also to design FER.

2.2 FER design

The FER which is more compact than the ITER, had been defined as the engineering-oriented machine for demonstrating the engineering feasibility of a fusion reactor. The design guideline of the FER has been established during 1988. The next step tokamaks that will provide sufficient physics informations and technology experiences to proceed to the DEMO fusion reactor which will demonstrate electric power generation by the fusion reactions,

- 1) the FER is to be the minimum-sized domestic machine which includes the highest technical reliability in its construction, and
- 2) the ITER is to be the maximum-sized international tokamak machine with the maximum jump in the technology from the present level of achievements.

The FER major parameters listed in Table VI.2.2-1 enable us to obtain the following plasma performances. Firstly the fusion multiplication factor $Q=5-10$ is a basic plasma performance with the enhancement factor of 1.5-2.0 for both Shimomura-Odajima(SO) and Goldston(G) L-mode energy confinement scaling laws. The burn time more than 1000 sec is to be achieved by introducing a hybrid operation mode in which some fraction of the plasma current is driven inductively with significant assistance of non-inductive and bootstrap current. Demonstration of a steady state operation is one of the key issues for DEMO reactor. A 0.5-1.0 MeV negative-ion-based injection system is used for both heating and current drive.

Table VI.2.2-1 FER major plasma parameters.

Plasma current	(MA)	15	-	20
Major radius	(m)	4.5	-	4.7
Minor radius	(m)	1.6	-	1.8
Elongation		1.6	-	2.0
Plasma volume	(m ³)	400	-	600
Field on axis	(T)	5.2	-	5.4
OH coil flux	(Vs)	160	-	170
Fusion power	(MW)	200	-	500
Burn time	(s)	100	-	1000
Heating/CD power	(MW)	80		

The conceptual design study has been continued until March, 1991. During the conceptual design activities, the configuration development studies were aimed at deriving a reactor concept that integrated the results of several concurrent efforts. The major design features of FER were identified as follows:

- (1) The basic machine is the semi-permanent part of the reactor and it is designed for the lifetime of the plant. It consists of the supporting system which allows the separate assembly of the major components, the cryostat, the TF and PF coils system and the vacuum vessel/shield structure.
- (2) The in-vessel components, which include the plasma facing components, are renewable. They are substituted because of the end of life, or accident, or for experimental purposes. They are segmented and mechanically attached and guided inside the vessel, from which they can be removed for substitution.

(3) The rail-mounted vehicle type has been chosen for the in-vessel maintenance systems (inspection and substitution). Four of 12 horizontal ports are used for the rail deploying, the rail supporting and the substitution of the divertor plate and the first wall.

(4) Preliminary design study of the plant system has been carried out. Especially, this is the first time that, as shown in Fig.VI.2.2-1, the building for solid radio-waste treatment and storage has been studied. The detritiation process from the solid radio-waste is possible in that building.

As a result of the conceptual design study, a concept with a consistent set of technical characteristics was well developed and the basic feasibility was preliminary evaluated by the design analysis. In addition, technical issues, whose feasibility should be demonstrated by future engineering R&D and detail analysis, were pointed out and the engineering R&D plan was developed.

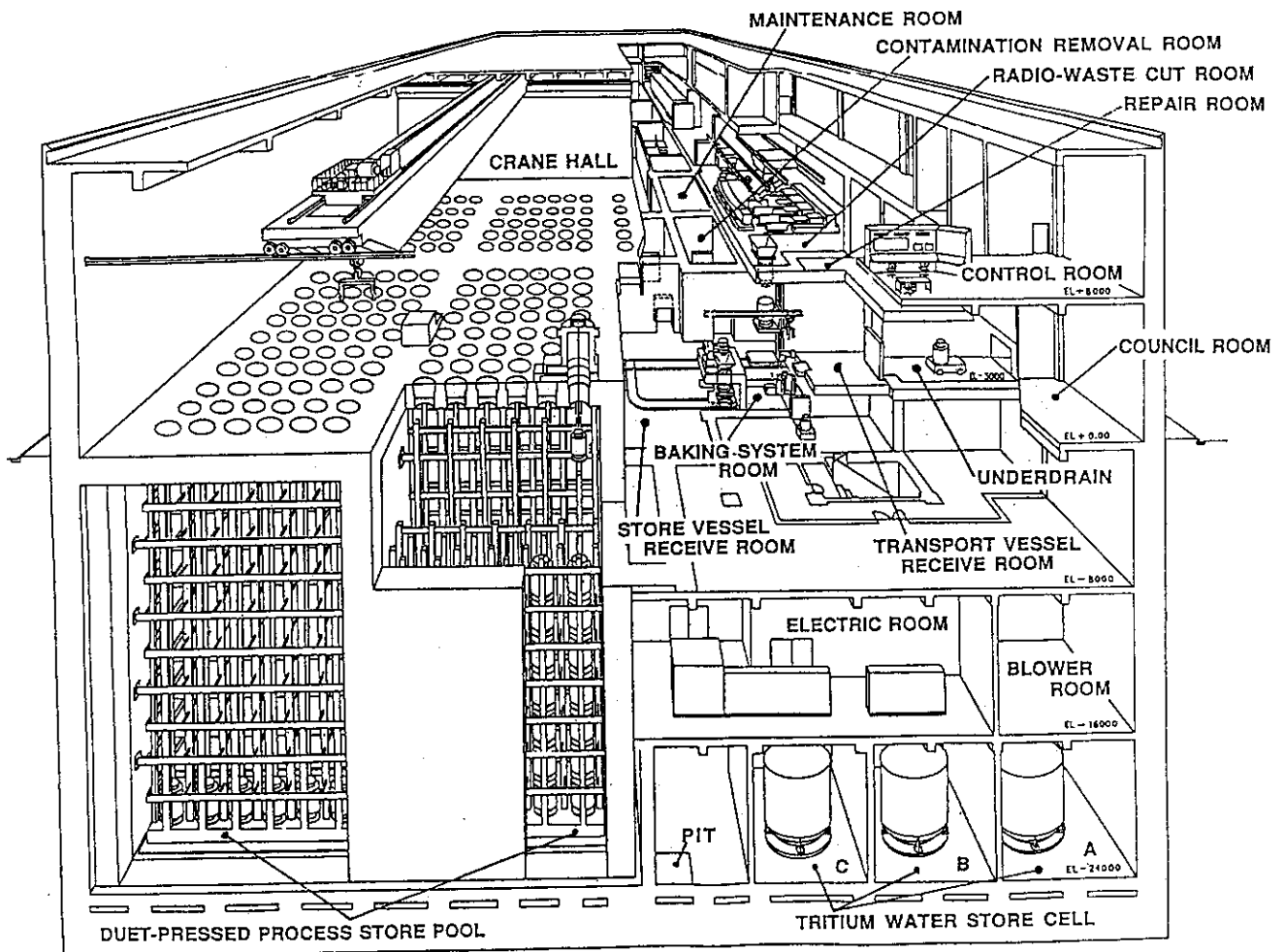


Fig.VI.2.2-1 Building for solid radio-waste treatment and storage in FER.

2.3 Technology R&D

Through the conceptual design study, the technology R&D plan was developed. As an initial stage of R&D activities, the elemental technology developments common to a tokamak reactor have been started. Among them, the locking mechanism for supporting in-vessel replaceable components, the technique for insulation/conduction coating and the rail-mounted vehicle system for in-vessel maintenance procedure (inspection and substitution) are in the height of the development.

For the locking mechanism, a caulking cotter driven by hydraulic pressure has been employed. Three kinds of driving mechanism have been manufactured by trial: a "piston jack" type, a "bellows" type and a "flexible tube" type. In the last type, the required stroke is obtained by changing the cross section of the flexible tube from a flat racetrack shape to a fat shape by hydraulic pressure. The superplastic material (Ti-6Al-4V) was selected for the flexible tube.

Al₂O₃ as the material and a plasma spray as the method have been selected for the insulation coating. Cr₃C₂ and JET-KOTE method have been selected for the conduction coating.

The half torus model of the rail-mounted vehicle system in one fifth scale was manufactured as shown in Fig.VI.2.3-1. Through the basic tests of the rail mounting and the divertor plate substitution, the system feasibility of this concept has been verified.

In addition, the two-sector plastic model of the basic machine and in-vessel components in one fifth scale has been fabricated in order to verify the design feasibility, mainly geometrical consistency. Then some design modification were found to be needed for some of the components based on the manufacturing experience.

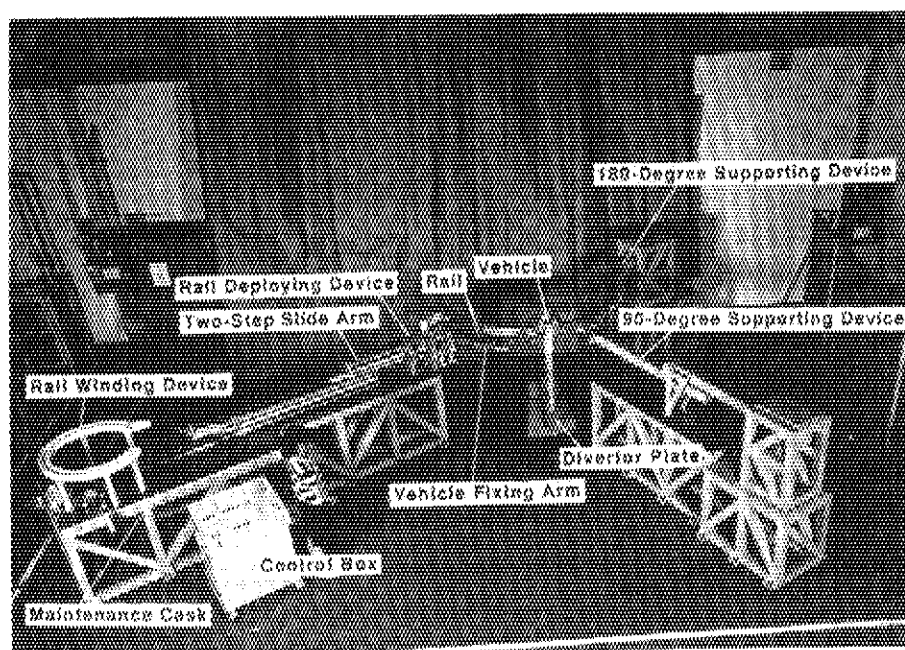


Fig.VI.2.3-1 One fifth scale model of the rail-mounted vehicle system for the in-vessel maintenance. (inspection and substitution)

3. Fusion Reactor Design

3.1 Introduction

Fusion reactor design and related research are conducted to identify attractive reactor concepts in terms of safety, environmental and economic aspects. This fiscal year, the concept study of the SSTR has been carried out in order to clarify a realistic concept of a fusion reactor.

3.2 Steady State Tokamak Reactor (SSTR) Design

The concept study of the SSTR has been carried out utilizing 1) the new experimental data obtained in the large tokamaks such as JT-60, 2) the progress in the fusion reactor technology, 3) recently developed design methodologies and database through the conceptual design studies for ITER and FER.

Specifically, the observation [3.2-1] of the bootstrap current driving about 80% of the plasma current in JT-60 lead us to a tokamak reactor concept with a small current drive power and hence, the possibility of overcoming a pulse mode operation to achieve a steady state operation. This observation gave the motivation for the proposal of the basic concept [3.2-2] of the SSTR.

A realistic power reactor concept has been attained based on the technological progress based on the recent achievements such as the substantial progress in the negative-ion-based NBI (NNBI) development in JAERI and the development of 16.5 T high field superconductor filaments in the industries.

From the ITER/FER conceptual designs, many useful ideas such as the "twin loop concept" to enhance the vertical stability of the plasma and the use of hydraulic pressure cotter for easy coupling and de-coupling of the blanket modules have been employed. That this study has been essentially completed in a remarkably short period of about a half year is owing to the utilization of the experience and the methodology developed in the conceptual designs of ITER/FER.

Main parameters of the SSTR are given in Table VI.3.2-1 and a bird's-eye-view is shown in Fig. VI.3.2-1. The major feature of the SSTR is focussed on the maximum utilization of the bootstrap current in order to reduce the power required for the steady-state operation. A significant fraction (75 %) of the total plasma current is sustained by the bootstrap current resulting in the Q-value of ~50. This requirement leads to the choice of low current, and high β_p for the device, which are achieved by selecting high aspect ratio and high toroidal magnetic field. The NNBI system is adopted for both heating and current drive. This NNBI system also enables to control current profile

Table VI.3.2-1 Main parameters of SSTR.

Plasma major radius	7.0 m
Plasma minor radius	1.75 m
Aspect ratio	4
Plasma current	12 MA
Plasma elongation	1.8
Magnetic field on axis	9 T
Maximum on coil	16.5 T
Plasma volume	760 m ³
NBCD	80 MW
Fusion power	3000 MW
Net electric power	1080 MW
Max. neutron wall load	5 MW/m ²
Q-value	~50
Tritium breeding ratio	>1.0
Divertor	Single null

and heating profile. Notable engineering features of SSTR are: the use of a uniform vacuum vessel and periodical replacements of the first wall and blanket layers and significant reduction of the electromagnetic force with the use of functionally gradient material. It is shown that a tokamak machine comparable to ITER in size can become a power reactor capable of generating about 1 GW of electricity with a plant efficiency of ~30%.

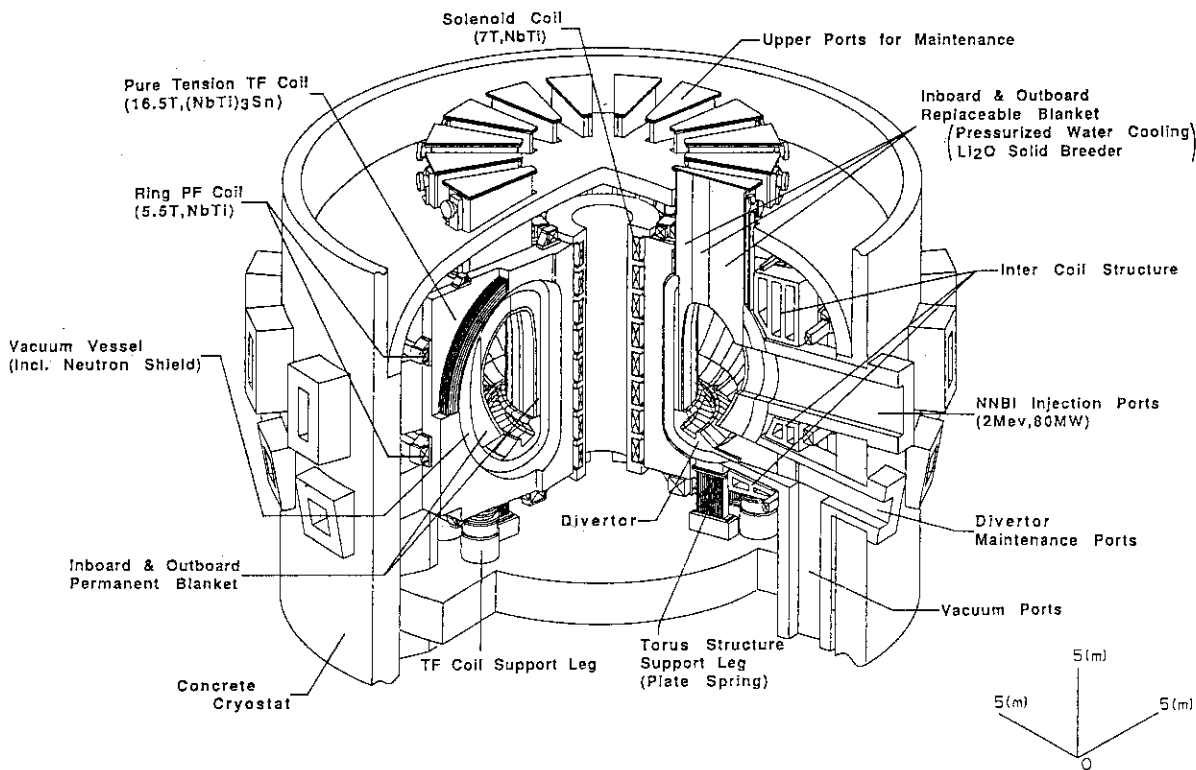


Fig.VI.3.2-1 Bird's eye view of SSTR.

The main objective of the SSTR concept design [3.2-3] is to establish a power reactor concept which can be built in the near future based on the above new informations. So that the concept is made to be as realistic as possible sometimes not optimized in terms of safety and economics. Now that we have established the basic concept of the realistic SSTR, we plan to improve the safety and economics of the reactor concept to make it more acceptable to the society.

References

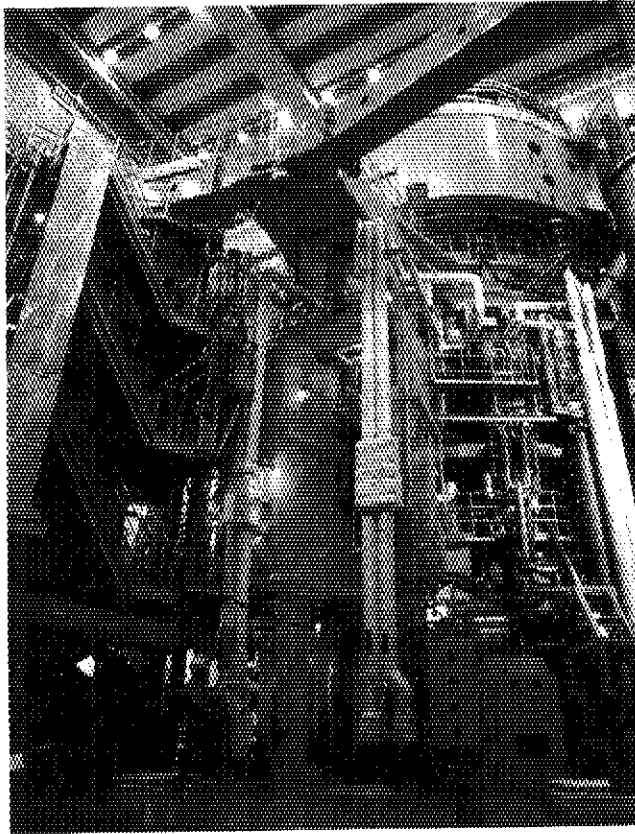
- [3.2-1] M. Kikuchi, et al., Nuclear Fusion 30 (1990) 343-355.
- [3.2-2] M. Kikuchi, Nuclear Fusion 30 (1990) 265-276.
- [3.2-3] Y. Seki et al., 13-th Int. Conf. Plasma Physics and Controlled Nuclear Fusion Research, IAEA-CN-53/G-1-2 (1990), to be published.

3.3 Safety analyses

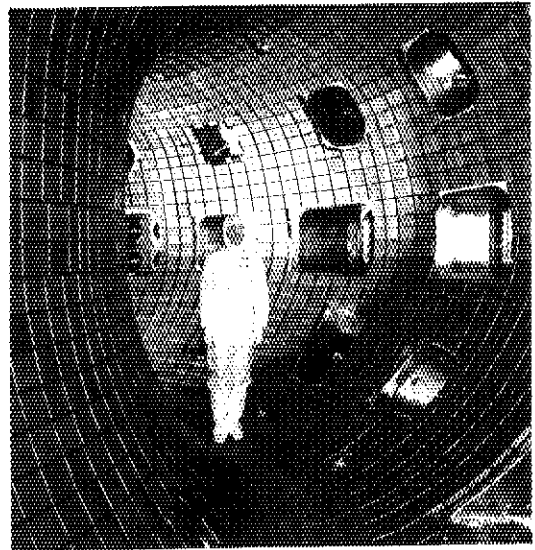
The development of a methodology for a comprehensive safety evaluation of a fusion reactor system has been continued. A calculational model for a fusion reactor system has been developed. Using the model, the radioactive inventory and the radioactive release pathway under normal operation and maintenance mode have been evaluated. An intermediate progress report has been produced.

The evaluation methodology for the radioactive release under accidental condition is yet to be developed. The final goal is in the evaluation of the public and worker risk as the product of equivalent dose and the probability.

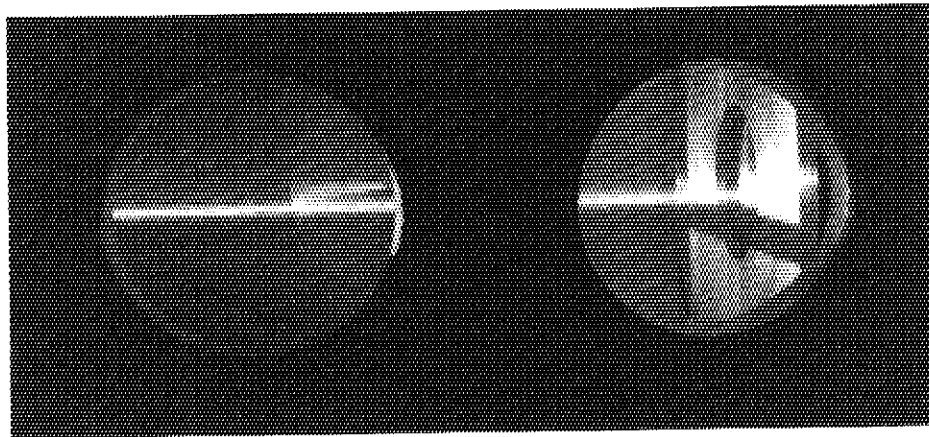
SOME PICTURES IN COLOR



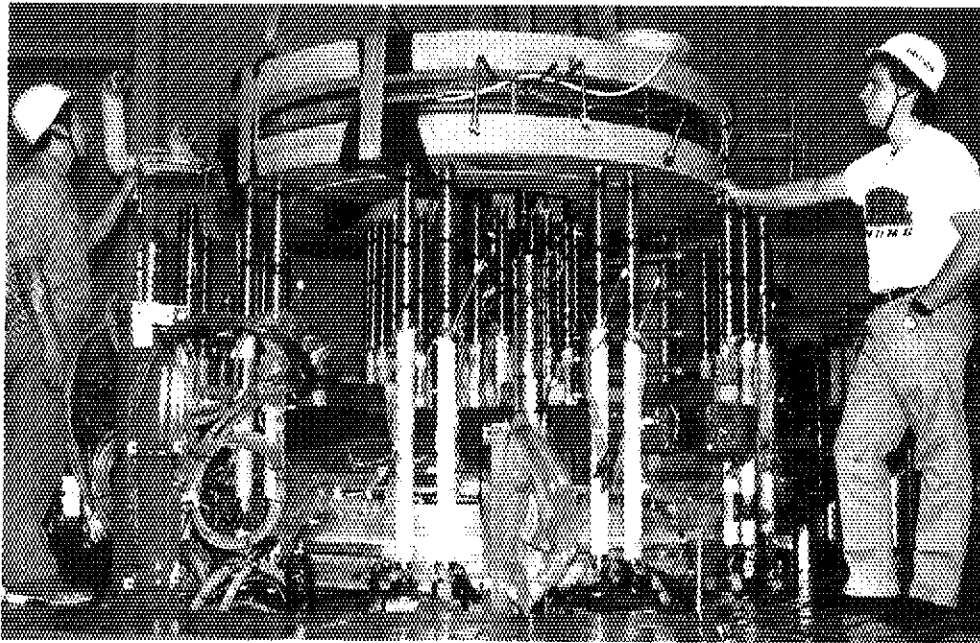
JT-60U device completed in March 1991.



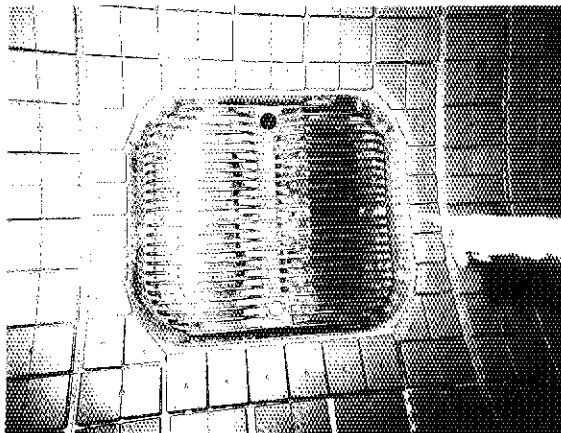
Inside view of JT-60U vacuum vessel.



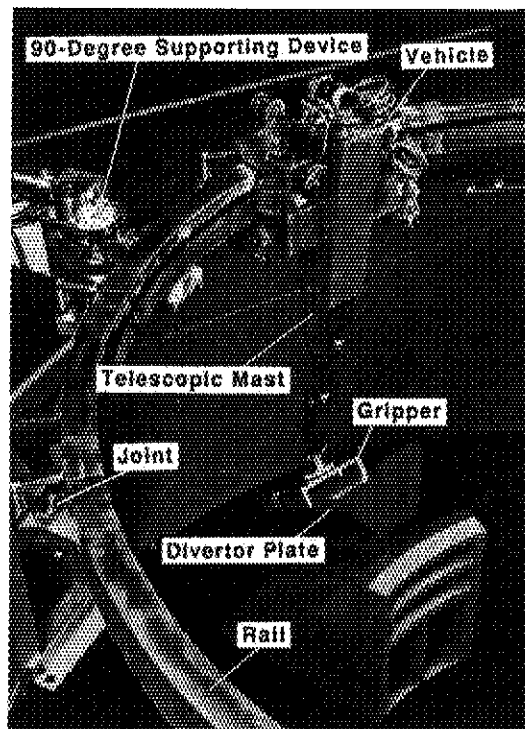
Finely converged negative ion beam propagating in a vacuum. (See Section 3.2.3 in Chapter V.)



The US-DPC being installed in JAERI's test facility under the collaboration of Japan and MIT/DOE.
(See Section 2.3.1 in Chapter V.)



ICRF antenna installed into the JT-60U tokamak.
(See Section 2.5.2 in Chapter IV.)



One fifth scale model of the rail-mounted vehicle system for the in-vessel maintenance.
(See Section 2.3 in Chapter VI.)

APPENDICES

A.1 Publication List (April 1990 - March 1991)

A.1.1 List of JAERI-M reports

- 1) Isei N., Ishida S., Sato M., et al., "ECE Calibration for Fourier Transform Spectrometer", JAERI-M 90-066 in Review of JT-60 Experimental Results from January to October 1989.
- 2) Kubo H., Sugie T., Nishino N., et al., "Current Profile Measurement Using Neutral He Beam in JT-60 Tokamak", *ibid.*
- 3) Konno M., Yoshida K., Isono T., et al., "Manufacturing of Superconducting Wiggler Coil", JAERI-M 90-077
- 4) Kamada Y., Hosogane N., Hirayama T., et al., "Density Limit in JT-60" JAERI-M 90-081.
- 5) Matsuoka M., Akino N., Horiike H., et al., "Modification of JT-60 NBI System from Quasi- Perpendicular to Tangential Injection", JAERI-M 90-086.
- 6) Odajima K., Ohasa K., Shiho M., et al., "MTX Microwave-Electric Field Diagnostics", JAERI-M 90-088.
- 7) Ogawa T., Ohasa K., Hoshino K., et al., "Neutron Diagnostic for MTX", JAERI-M 90-105.
- 8) Isaji N., Kurihara K. and Kimura T., "Quality Control of the Software in the JT-60 Computer Control System", JAERI-M 90-114.
- 9) Yamamoto M., Ando T., Takatsu H., et al., "Evaluation Tests on First Wall and Divertor Plate Materials for JT-60 Upgrade", JAERI-M 90-119.
- 10) Kamada Y., Ozeki T., Azumi M., et al., "Central MHD Activities and Role of the $q=1$ Surface for Pellet Fuelled JT-60 Plasmas," JAERI-M 90-123.
- 11) Maebara S., Miyake S., Tsuneoka M., "1.4 MW Power Test of 2 GHz Klystron", JAERI-M 90-132.
- 12) Ohara Y. et al., "Areview of JAERI R&D Activities on the Negative-Ion-Based Neutral Beam Injector System", JAERI-M 90-154.
- 13) Miura Y., Yoshida H., Sakuma T., et al., "Effect of Coated Window on Electron Temperature and Density Evaluation in JT-60 Thomson Scattering Diagnostic", JAERI-M 90-167.
- 14) Ozeki T. Azumi M., et al., "Effects of Pressure Profile and Plasma Shaping on $n=1$ Internal Kink Mode in JT-60/JT60U Pellet Fueled Plasmas", JAERI-M 90-170.
- 15) Aikawa H., "Comments on Dissipative Drift Wave Turburence and L-H Transition", JAERI-M 90-175.
- 16) Moriyama S., Kimura H., Fujii T., et al., "Analysis of Antenna Impedance Matching and Study of Automatic matching on JT-60 ICRF Heating System", JAERI-M 90-184.
- 17) Matsuda T., Miura Y., Suzuki N., et al., "The Assembly and Analysis of the ITER H-mode Database in JFT-2M", JAERI-M 90-200.
- 18) Matsuda T., Amagai A., "Development of the JFT-2M Data Analysis Software System on the Mainframe Computer", JAERI-M 90-201.
- 19) Kishimoto Y, Oda H, Shiho M, "Energy Conversion Efficiency in High Current Raman regime free electron laser II Multi-mode Analysis", Research Report of Japan Atomic Energy Research Institute JAERI-M 90-211.
- 20) Watanabe K., Araki M., Dairaku M., et al., "Production of a High Proton Yield Beam in a Semi- Cylindrical Plasma Generator", JAERI-M 90-212.
- 21) Watanabe K. et al., "Development of a Negative Ion Measurement Probe and Initial Results of Experiments", JAERI-M 90-219.
- 22) Arakawa K., et al., "Analysis of Operation and Maintenance in JT-60", JAERI-M 90-226.
- 23) Yoshida H., Enoeda M., Ohara A., et al., "Parameter Study on Japanese Proposal of ITER Hydrogen Isotope Separation System", JAERI-M 90-233.
- 24) Ogiwara N., "Studies on Development of Pressure Measurement Methods for a Large Fusion Experimental Device", JAERI-M 91-007.
- 25) Shimizu K., Yoshino R, Kamada Y., et al., "Simulation Analysis of JT-60 Pellet Injection Experiments", JAERI-M 91-016.
- 26) Maki K., Takatsu H., Kuroda T., et al., "Shielding Design of Reactor Core Region in Fusion Experimental Reactor", JAERI-M 91-017.
- 27) Shirai H., Hirayama T., Azumi M., "Ion Temperature Profile Analysis of JT-60 Plasma with Ion Temperature Gradient Mode", JAERI-M 91-018
- 28) Yagi M., "The Energy Confinement Scaling based on Microturbulence Transport and Neoclassical Conductivity in a Tokamak", JAERI-M 91-022.
- 29) Hirayama T., Kikuchi M., Shirai H. et al., "Local Transport Analysis of L-mode plasmas in JT-60 Tokamak", JAERI-M 91-026.
- 30) Koide Y., Ishida S., Sakasai A., "The Role of Integer Mode Rational Surface on Peaked Profile Formation in Toroidal Rotation Velocity and Ion Temperature", JAERI-M 91-041.
- 31) Maki K., Takatsu H., Kuroda T., et al., "Japanese Contributions to ITER Shielding Neutronics Design", JAERI-M 91-046.
- 32) Yoshino R., Nishio S., Shinya K., "Control of the Plasma Configuration in ITER," JAERI-M 91-049.
- 33) Nakamura H., "Plasma Surface Interaction", JAERI-M 91-050.
- 34) Ohara Y. et al., "ITER Neutral Beam Injection System -Japanese Proposal-", JAERI-M 91-052
- 35) Kawasaki H., Maki K., Seki Y., "Improvement of Apple for Neutron and Gamma-ray Flux, Spectrum and Reaction Rate Plotting Code, and Its Code Manual", JAERI-M 91-058.

- 36) Kuroda T., Yoshida H., Takatsu H., "Japanese Contributions to ITER Testing Program of Solid Breeder Blankets for DEMO", JAERI-M 91-063.

A.1.2 List of papers published in Journals

- 1) Zeritis D., Ando T., Takahashi Y., et al., "Transient Stress on the Critical Current of Jelly-roll Multifilamentary Nb₃Al Wires", *Appl. Phys. Lett.* **57** (1990) 506.
- 2) Diamond P.H., Drake J.F., Matsumoto H., et al., "Progress in Research on Plasma Edge Turbulence and Transport", *Comments Plasma Phys. Control. Fusion* **13** (1990)327.
- 3) Diamond P.H., Drake J.F., Matsumoto H., et al., "Progress in Research on Plasma Edge Turbulence and Transport", *ibid.* **13**(1990)327.
- 4) Ando T., Painter T., "Direct Measurement of the Time Constant of Coupling Current in a Multifilamentary Superconducting Wire", *Cryog. Eng.*, **25** (1990) 390.
- 5) Fujii T. and JT-60 Team, "Interaction between RF and Edge Plasma during ICRF Heating in JT-60", *Fusion Eng. Des.***12** (1990) 139.
- 6) Tamai H., Ogawa T., Odajima K., et al., "Edge Plasma Characteristics during ICRF Heating on JFT-2M Tokamak", *ibid.* **12** (1990) 25.
- 7) Kobayashi N., Kimura H., Saigusa M., et al., "Plunger Design and RF Leakage Measurement of Choke Stub for JT-60 ICRF Heating System", *ibid.* **12** (1990) 481.
- 8) Naruse Y., Matsuda Y., Tanama K., "Tritium Process Laboratory at the JAERI", *ibid.* **12** (1990) 293.
- 9) Imai T., Ikeda Y., Maehara S., et al., "Development of Super High Power Klystron-System for JT-60 LHRF Heating and Current Drive", *ibid.* **13** (1990) 177.
- 10) Ikeda Y., Imai T., Honda M., et al., "Technical Performance of Fast Frequency Shift of JT-60 LHRF System during a Plasma Shot", *ibid.* **13** (1990) 209.
- 11) Imai, T., Ikeda, Y., Maehara, S., et al., "Development of super high power klystrons-system for JT-60 LHRF heating and current drive", *ibid.* **13** (1990) 177.
- 12) Imai T., Ikeda Y., Maehara S., "Development of Super High Power Klystron system for JT-60 LHRF Heating and Current Drive", *ibid.* **13** (1990)177.
- 13) Araki M., Ohara Y., Okumura Y., "Design Study of a Beam Energy Recovery System for a Negative-Ion-Based Neutral Beam Injector", *Fusion Technol.* **17** (1990)555.
- 14) Tani K., Azumi M., Takizuka T., "Passive Burn Control in a Tokamak Plasma using Toroidal Field Ripple", *ibid.* **18** (1990) 625.
- 15) Tani K., Azumi M., Takizuka T., "Passive burn control in a tokamak plasma using toroidal field ripple", *ibid.* **18** (1990) 625.
- 16) Matsuoka M., Horiike H., Itoh T., et al., "Active Shielding System for Removal of Stray Tokamak Magnetic Fields in JT-60 Neutral Beam Injectors", *ibid.* **19** (1991) 113.
- 17) Matsuoka M., Horiike H., Itoh T., et al., "JT-60 Shielding System for Removal of Stray Tokamak Magnetic Fields in JT-60 Neutral Beam Injectors", *ibid.* **19** (1991).
- 18) Nishi M., Isono T., Takahashi Y., et al., "Development of a Compact 18-T MF-(NbTi)₃Sn Coil", 1990 Applied Superconductivity Conference, *IEEE Trans.* **27** (1991). 2280.
- 19) Ando T., Takahashi Y., Nishi M., et al., "Development of 10 kA Class Nb₃Al Superconducting Cable by Jelly-roll Process", *ibid.* 1775.
- 20) Zeritis D., Iwasa Y., Ando T., "The Transverse Stress Effect on the Critical Current of Jelly-roll Multifilamentary Nb₃Al Wires", *ibid.* 1829.
- 21) Ando T., Okuno K., Nakajima H., et al., "Experimental Results of the Nb₃Sn Demo poloidal coil (DPC-EX)", *ibid.* 2060
- 22) Isono T., Takahashi Y., Sugimoto M., et al., "Critical Current Measurement using 13-T Split Coils and 100-kA Superconducting Transformer", *ibid.* 1839.
- 23) Konishi S., Ohno H., Hayashi T., et al., "Investigation of Lithium Diffusion in Octalithium Plumbate by Conductivity & NMR Measurements", *J. Am. Ceram. Soc.* **73** (1990) 1710.
- 24) Kikuchi M., "High Efficiency Fusion Reactor Based on Bootstrap Current", *J. Atomic Energy Soc. Jpn.* **32** (1990) 950.
- 25) Kozawa Y. and Seki Y., "VII. Safety Assuring Procedure-Realization of Magnetic Confinement Fusion Reactor and Super-Technology Aided Development-", *ibid.* **33** (1991) 31.
- 26) Takeda T, Tokuda S, "Computation of MHD Equilibrium of Tokamak Plasma," *J. Comput. Phys.* **93** (1991) 1.
- 27) Ikeda Y., Imai T., Ushigusa K., et al., "Plasma-Launcher Interaction during Lower Hybrid Current Drive and Heating on JT-60", *J. Nucl. Mater.* **176 & 177** (1990) 306.
- 28) Shimada M., Ozaki A., Petersen P., et al., "Limiter Bias Experiments in DIII-D", *ibid.* **176&177**(1990)821.
- 29) JT-60 Team by Miya N., "Recent Results in JT-60 Advanced Experiment", *J. Nucl. Sci. Technol.* **27**(1990).
- 30) Naruse T., Okuno K., Yoshida H., et al., "Developments of Tritium Technology for Next-Step Fusion Devices under JAERI-DOE (LANL) Collaboration", *ibid.* **27** (1990) 1081.
- 31) Hoshino K., "Electron Cyclotron Heating (ECH) of Tokamak Plasmas", *ibid.* **27** (1990) 391.
- 32) Mori S., Seki Y., "Systematic Analysis of Decay Gamma-Ray Streaming through Narrow Gap in Fusion Experimental Reactor", *ibid.* **27**(1990)SO3.

- 33) Ozeki T., Azumi M., "Stability of the n=1 Internal kink Mode in Plasmas with Centrally Peaked Pressure", *J. Phys. Soc. Jpn.* **59** (1990) 4338.
- 34) Ogawa H., Kasai S., Tamai H., et al., "Impurity Behavior during the H-mode in JFT-2M", *ibid.* **59** (1990) 3962.
- 35) Kishimoto Y., Oda H., Shiho M., et al., "Effect of electrostatic field on energy conversion efficiency in high current Raman regime free electron laser," *ibid.* **59** (1990) 118 .
- 36) Kamitani A., Kaneko S., Tsunematsu T., et al., "Stability analysis of spheromak by ERATO-J against internal modes," *ibid.* **60** (1991) 512.
- 37) Ogiwara N. and Maeno M., "Outgassing Mechanism after the Current Decaying Phase in Disruptive and Normal Discharges in a Tokamak", *J. Vac. Sci. Technol.* **A8** (1990) 3855.
- 38) Hiroki S., Abe T., Murakami Y., "Development of a Movable Quadrupole Mass Spectrometer for Measuring Gas Density", *ibid.* **A9** (1990) 154.
- 39) Ogiwara N. and Maeno M., "Outgassing during a Plasma Disruption in the JT-60 Tokamak", *J. Vac. Soc. Jpn.* **33** (1990) 381 (in Japanese).
- 40) Obara K., Murakami Y., Naganuma M., et al., "Leak Testing of Modified Knife-edge-type Metal-seal Flanges(II)", *ibid.* **33** (1990) 326 (in Japanese).
- 41) Murakami Y., "My view on Outgassing Rate of Vacuum Materials", *ibid.* **33** (1990) 461 (in Japanese).
- 42) Obara K., Murakami Y., "Performance Tests of Metal Gaskets of Ag-bearing OFC, Zr-bearing OFC and Original OFC for Knife-edge-type Flanges", *ibid.* **33** (1990) 804 (in Japanese).
- 43) Shibanuma K., Akino N., Dairaku M., et al., "Helium Pumping by a Cryosorption Pump with Condensed SF₆ Gas Layer as a Sorbent in JT-60 NBI System", *ibid.* **33** (1990) 307 (in Japanese).
- 44) Shibanuma K., Akino N., Dairaku M., et al., "Helium Pumping by a Cryosorption Pump with Condensed SF₆ Gas Layer as a Sorbent in JT-60 NBI System", *ibid.* **33**(1990)219(in Japanese)
- 45) Sugawa M., Dodo T., Ide S., et al., "Electron cyclotron emission measured in lower hybrid current drive plasma on WT-3 tokamak," *Jpn. J. Appl. Phys.* **29** (1990) 1907.
- 46) Tamai H., Ogawa T., Matsumoto H., et al., "Ion Bernstein Wave Experiment on JFT-2M Tokamak", *ibid.* **29** (1990) L1911.
- 47) Yamauchi T., Dimock D., "Angular Dependence of Transmissivity in a High-pass Optical Fiber for Thomson Scattering Measurement", *ibid.* **29** (1990) 1345.
- 48) Kimura H., Fujii T., Saigusa M., et al., "ICRF Experiments", *Kaku Yugo Kenkyu* **65**/Supplement (1991) 133.
- 49) Imai T., Ushigusa K., Ikeda Y., et al., "LHRF Current Drive Experiments on JT-60", *ibid.* **65**/Supplement (1991) 99.
- 50) Imai T., Ushigusa K., Ikeda Y., et al., "LHRF Heating Experiments on JT-60", *ibid.* **65**/Supplement (1991) 119.
- 51) Ninomiya H., Hosogane N., Yoshino R., et al., "Physics Operations in JT-60", *ibid.* **65**/Supplement (1991) 13.
- 52) Kikuchi M., Naito O., Yoshida H., et al., "Energy Confinement Characteristics of JT-60 L-mode", *ibid.* **65**/Supplement (1991) 51.
- 53) Yoshino R., Kamada Y., Shimizu K., et al., "Pellet Injection Experiments on JT-60", *ibid.* **65**/Supplement (1991) 163.
- 54) Shimada M., Suzuki N., Nakamura H., et al., "H-mode Experiments", *ibid.* **65**/Supplement (1991) 185.
- 55) Kikuchi M. and Azumi M., "Bootstrap Current in the JT-60 Tokamak", *ibid.* **65**/Supplement (1991) 225
- 56) Tsuji S., Nakamura H., Yoshida H., et al., "Improved Divertor Confinement and Divertor Characteristics", *ibid.* **65**/Supplement (1991) 243.
- 57) Nakamura H., Tsuji S., Shimizu K., et al., "Particle Confinement Characteristics and Helium ash Exhaust Experiments in JT-60 Tokamak", *ibid.* **65**/Supplement (1991) 261.
- 58) Hosogane N., Yonekawa I., Itami K., et al., "Energy Loss during Disruptions and Statistical Analysis on Disruptions", *ibid.* **65**/Supplement (1991) 323.
- 59) Shimada M., "Present status of Impurity Transport study", *ibid.* **64** (1990) 144.
- 60) Hosogane N. and Yoshino R., "Major Results from JT-60 Experiments", *ibid.* **63** (1990) 311.
- 61) Tsuji S., "Measurements of Particle Confinement in Tokamaks", *ibid.* **63** (1990) 460.
- 62) Matsuda S., Shibanuma K., "Main R&D Needs for Fusion Experimental Reactors and the perspectives", *ibid.* **64** (1991)184.
- 63) Kimura H., Fujii T., Saigusa M., et al., "ICRF Experiments", (Special Issue of JT-60 Experiments), *ibid.* **65** /Supplement, March 1991.
- 64) Fusion Experiment Reactor Team, "ITER : Engineering Design", *ibid.* **65** (1991).
- 65) Matsuda S., "Fusion Research and ITER Programme", *ibid.* **65**(1991)25.
- 66) Tomabechi K., "Report on International Conceptual Design Activities", *ibid.* **65**(1991)32.
- 67) Fujisawa N., "Long-Term Physics R&D Programme", *ibid.* **65**(1991)39.
- 68) Shimamoto S., " Long-Term Technology R&D Plan", *ibid.* **65**(1991)43.
- 69) Sugihara M., Tsunematsu T., " Physics Design of ITER (International Thermonuclear Experimental Reactor)", *ibid.* **65**(1991)143.
- 70) Tada E., Takata H., Shimomura Y., "Conceptual Design of the ITER Basic Devices", *ibid.* **65**(1991)167.
- 71) Iida H., Seki Y., Takatsu H., et al., "Engineering Design (Safety Aspect and Plant Design)", *ibid.* **65**(1991)312.
- 72) Takatsu H., Kuroda T., Yoshida H., "ITER:Engineering Design (Nuclear Engineering)", *ibid.* **65**(1991)323.
- 73) Shimomura Y., Mizoguchi T., "Impact of Engineering Constraints on Fusion Reactor", *ibid.* **65**(1991)115.

- 74) Takizuka T, "Divertor plasma in tokamak," *ibid.* **64** (1990) 255.
- 75) Niikura S., Nagami M., "Improvement of Fusion Reactivity and Fusion Power Multiplication Factor in the Presence of Fast Ions", *Nucl. Eng. Design* (1990).
- 76) Ozeki T., Chu M.S., Lao L.L., et al., "Plasma Shaping, Edge Ballooning Stability and ELM Behaviour in DIII-D", *Nucl. Fusion* **30** (1990) 1425.
- 77) Ozeki T., Chu M.S., Lao L.L., et al., "Plasma Shaping, Edge Ballooning Stability and ELM Behaviour in D-III", *ibid.*
- 78) Nagashima K., Fukuda T., Kikuchi M., et al., "Investigation of Particle Transport in JT-60 Using a Perturbation Method", *ibid.* **30** (1990) 2367.
- 79) Yoshino R., Ushigusa K., Imai T., et al., "Numerical Simulation of Current Profile Flattening during Lower Hybrid Current Drive in JT-60," *ibid.* **30** (1990) 711.
- 80) Naito O., Ushigusa K., Ikeda Y., et al., "Volt-sec Saving by Lower Hybrid Current Drive in JT-60", *ibid.* **30** (1990) 1137.
- 81) Nakamura H., Tsuji S., Nagami M., et al., "H-mode Experiments with outer and Lower Divertors in JT-60", *ibid.* **30** (1990) 235.
- 82) Naito O., Hosogane N., Tsuji S., et al., "Global Energy Confinement in JT-60 Neutral Beam Heated L-mode Discharges", *ibid.* **30** (1990) 195.
- 83) Kikuchi M. and Azumi M., "Model of Heat Pinch Transport in the JT-60 Tokamak", *ibid.* **30** (1990) 2211.
- 84) Ozeki T., Chu M.S., Kinoshita S., et al., "Plasma Shaping, Edge Ballooning Stability and ELM Behaviour in DIII-D", *ibid.* **30**(1990)1425.
- 85) Uesugi Y., Yamamoto T., Kawashima H., et al., "Coupling of Fast Waves Launched into the JFT-2M Tokamak by a Phased Four-Loop Antenna Array", *ibid.* **30** (1990) 297.
- 86) Ogawa T., Tamai H., Matsumoto H., et al., "Characteristics of ICRF Loading during the H-Mode in the JFT-2M Tokamak", *ibid.* **30** (1990) 499.
- 87) Uesugi Y., Yamamoto T., Kawashima H., et al., "Absorption of Fast Waves Excited by a Phased Four-loop Antenna Array in the JFT-2M Tokamak", *ibid.* **30** (1990) 831.
- 88) Yushmanov N, Takizuka T, et al., "Scaling for tokamak energy confinement," *ibid.* **30** (1990) 1999.
- 89) Shatarov G., Iida H., et al., " Nuclear Technology", *ibid.* **30** (1990).
- 90) Ozeki T., Azumi M., Kamada Y., et al., "Ideal MHD Stability of Pellet Fueled Plasma in JT-60 ", *ibid.* **31** (1991) 51.
- 91) Kimura H. and JT-60 Team, "Experimental Study on Beam Acceleration with Combined NBI Heating and Second-Harmonic ICRF Heating in JT-60", *ibid.* **31** (1991) 83.
- 92) Fujii T. and JT-60 Team, "Heating and Confinement Characteristics of Second Harmonic Heating in the Ion Cyclotron Range of Frequencies on the JT-60 Tokamak", *ibid.* **31** (1991) 137.
- 93) Kamada Y., Yoshino R., Nagami M., et al., "Effect of $q=1$ Surface and Sawtooth Activity in Pellet Fuelled JT-60 Limiter Plasmas", *ibid.* **31** (1991) 23.
- 94) Fujita T., Saito K., Matsui J., et al., "Anomalous Ion Heating in REPUTE-1 ultra Low q and Reversed Field Pinch Plasmas", *ibid.* **31** (1991) 3.
- 95) Nagata H., Kihara N., Yamashita T., et al., "Module-type Flat-field Grazing-incidence Spectrographs for Large Tokamak (JT-60) Plasma Diagnosis", *Nucl. Instrum. Methods Phys. Res.* **A294** (1990) 292-298.
- 96) Burrell K.H., Carlstrom T.N., Matsumoto H., et al., "Physics of the L to H Transition in the DIII- D Tokamak", *Phys. Fluids* **B2**(1990)1405
- 97) Wooton A.J., Carreras B.A., Matsumoto H., et al., "Fluctuations and Anomalous Transport in Tokamaks", *ibid.* **B2**(1990)2879.
- 98) Burrell K.H., Carlstrom T.N., Matsumoto H., et al., "Physics of the L to H Transition in the DIII-D Tokamak", *ibid.* **B2**(1990)1405.
- 99) Kishimoto Y., Oda H., Shiho M., "Parasitic Wave Excitation in High Current Raman Regime", *Phys. Rev. Lett.* **65** (1990) 851.
- 100) Kishimoto Y, Oda H, Shiho M, "Parasitic wave Excitation by Multi-mode Coupling in Raman Regime Free Electron Laser", *ibid.* **65** (1990) 851.
- 101) Ninomiya H., Ando T., Horie T., "JT-60 Upgrade Device for Confinement and Steady State Studies", *Plasma Devices & Operations* **1** (1991) 43.
- 102) Ninomiya H., Ando T., Horie T., et al., "JT-60 upgrade Device for Confinement and Steady State Studies", *ibid.* **1** (1990) 43.
- 103) Tobita K., Itoh T., Sakasai A., et al., "Measurements of Neutral Beam Stopping for Hydrogen and Helium in the JT-60 Plasma", *Plasma Phys. Control. Fusion* **32** (1990) 428.
- 104) Ushigusa K. and JT-60 Team, "Recent Results of LH Experiments on JT-60 Tokamak," *ibid.* **32** (1990) 869.
- 105) Watanabe K., Araki M., Dairaku M., et al., "Effect of Primary Electron Distribution on Ion Species Yield on Ion Source", *Rev. Sci. Instrum.* **61**(1990) 1694.
- 106) Matsuoka M., Akiba M., Arimoto K., et al., "Beam Energy Control during a Beam Pulse in a Neutral Beam Injection System", *ibid.* **61** (1990) 2614.
- 107) Matsuoka M., Akiba M., Arimoto K., et al., "Beam-Energy Control during a Beam Pulse in a Neutral Beam Injection System", *ibid.* **61** (1990) 2614.
- 108) Nishitani T., Nagashima K., Kondoh T., et al., "Pellet Ablation Profile Measurements on the JT-60 Tokamak", *ibid.* **61** (1990) 3090-3092.
- 109) Kusama Y., Tobita K., Itoh T., Nemoto M., Tsukahara Y., Kimura H., Takeuchi H., "Confined Alpha Particle Diagnostics in JT-60U", *ibid.* p.3220-3222.

- 110) Kusama Y., Nemoto M., Tobita K., et al., " Compact and Wide-range Charge Exchange Neutral Particle Analyzer with an Acceleration Tube", *ibid.* p.3107-3109.
- 111) Ishida S., Nagashima A., Sato M., Isei N., Matoba T., " Twenty-channel Grating Polychromator Diagnostic System for Electron Cycrotron Emission Measurement in JT-60", *ibid.* p.2834-2836.
- 112) Fukuda T., Nagashima A., Matoba T., et al., "Broadband Reflectometry for the Density Profile and Fluctuation Measurements in the JT-60 Tokamak", *ibid.* 61 (1990)
- 113) Oda T., Odajima K., Mizuno K., et al., "Stark-effect Measurement of High Free-electron Laser Electric Fields in MTX by Laser-aided Particle-probe Spectroscopy", *ibid.* 61 (1990) 1.
- 114) Ogawa T., Ohasa K., Hoshino K., et al., "Neutron Diagnostic for MTX", *ibid.* 61 (1990) 3181.
- 115) Casper T., Allen S., Foote J., et al., "MTX Diagnostic and Timing System for Free Electron Laser Heating", *ibid.* 61 (1990) 3274.
- 116) Miura Y., Okano F., "Low-energy Neutral Particle Analysis by a Time-of-flight Method on JFT-2M", *ibid.* 11 (1990) 3851.
- 117) Nishi M., Shimamoto S., "Transient heat transfer in superconducting devices", *Trans. Jpn. Soc. Mech. Eng.* 93 (1990) 38 (in Japanese)
- 118) Abe T., Murakami Y., Hikida K., et al., "Development of Ceramic Turbomolecular Pumps for fusion Devices", *Vacuum* 41 (1990) 1992.

A.1.3 List of papers published in conference proceedings

- 1) Hasan M.Z., Kunugi T., Yokokawa M. et al., "Response of the ARIES-I Divertor Plate to Plasma Disruption", *Proc. 9th ANS Topical Meeting on Tech. Fusion Energy, Oak Brook, 1990.*
- 2) Kunugi T., Tillack M.S., Abdou M.A., "Analysis of Liquid Metal MHD Fluid Flow and Heat Transfer Using the KAT Code", *ibid.*
- 3) Hasan M. Z., Kunugi T., "Entry-Length Effects on the Thermal-Hydraulic Design of Plasma-Facing Components of Fusion Reactors, Part-II: Electrically Conducting Coolant in Circular Tube", *ibid.*
- 4) Kunugi T., Hasan M.Z., "Entry-Length Effect on the Thermal-Hydraulic Design of Plasma-Facing Components of Fusion Reactors, Part-I: Electrically Non-Conducting Coolant in Circular Tube", *ibid.*
- 5) Wong C., Kunugi T., and the ARIES Team, "ARIES-I SiC Composite Low Activation Blanket Design", *ibid.*
- 6) Sharafat S., Grotz S.P., Hasan M.Z., et al., "Divertor Engineering for the ARIES-I Reactor", *ibid.*
- 7) Kunugi T., Hasan M.Z., "Heat Transfer with Nonuniform Surface Heat Flux and Thermal-Hydraulic Design of the Plasma-Facing Components of Fusion Reactors", *ibid.*
- 8) Seki Y., Noguchi H., Maki K., et al., "Activation Products Effluents Evaluation for ITER", *ibid.*
- 9) Doggett J., Honda T., "ITER Maintenance", *ibid.*
- 10) Seki Y., Noguchi H., Maki K. et al., "Activation Products Inventory Evaluation for ITER", *ibid.*
- 11) Iida H., "ITER Systems Studies", *ibid.*
- 12) Honda T., Doggett J., "ITER Maintenance", *ibid.*
- 13) Iida H., Piet S., "ITER system Studies", *ibid.*
- 14) Seki Y., Noguchi H., Maki K., "Activation Products Effluents Evaluation for ITER", *ibid.*
- 15) Piet S., Iida H., Seki Y., et al., "ITER System Study - Safety Aspects", *ibid.*
- 16) Kamada Y., Snider R., "Sawtooth Frequency Studies in DIII-D", *Proc. 32th APS Conf., 1990.*
- 17) Kamada Y., Snider R., et al., "Sawtooth Frequency Studies in DIII-D", *ibid.*
- 18) Yamagiwa M., Kimura H., Takizuka T, et al., "D-He³ Fusion Yield in Higher Harmonic ICRF Heated Plasma," *Proc. 17th EPS Conf. on Control. Fusion & Plasma Heating, Amsterdam, 1990*
- 19) Luxon J., Fukuda T., Kamada Y., et al., "Recent Results From DIII-D and Their Implications For Next Generation Tokamaks," *ibid.*
- 20) Matsumoto N., Burrell K.H., Carlstrom T.N., et al., "Physics of the L to H Transition in DIII-D", *ibid.*
- 21) Hamamatsu K., Kimura H., Fujii T., et al., "Theoretical Analysis of Higher Harmonic ICRF Heating in JT-60", *ibid.*
- 22) Hamamatsu K., Fukuyama A., Itoh S-I., et al., "Possibility Ion Current Drive by RF Helicity Injection", *ibid.*
- 23) Matsumoto H., Burrell K.H., Carlstrom T.N., et al., "Physics of the L to H Transition in DIII-D", *ibid.*
- 24) Luxon J., Fukuda T., Matsumoto H., et al., "Recent Results From DIII-D and Their Implications for Next Generation Tokamaks", *ibid.*
- 25) Shoji T., Fujita T., Mori M., et al., "Ergodized Edge Experiments in JFT-2M", *ibid.*
- 26) Mizuno K., Foote J., Oda T., et al., "Design of Microwave Electric Field Diagnostics (LAPPS)", *Proc. 17th IEEE Int. Conf. on Plasma Sci., Oakland, 1990*
- 27) Stambough R., Fukuda T., Kamada Y., et al., "DIII-D Research Program Progress", *Proc. 13th Int. Conf. on Plasma Phys. & Control. Nucl. Fusion Research, Washington, D.C., 1990.*
- 28) Matsuoka M., Okumura Y., Akiba M. et al., "Research and Development Work for Negative-Ion Based Neutral Beam Injector at JAERI", *ibid.*
- 29) Burrell K., Matsumoto H., et al., "Transport in Auxiliary-Heated, Hot-Ion H-Mode and L-Mode Discharges in the DIII-D Tokamak", *ibid.*
- 30) Taylor T., Kamada Y., et al., "Profile Optimization and High Beta Discharges and Stability of High Elongation Plasmas in the DIII-D Tokamak", *ibid.*
- 31) Peebles W., Matsumoto H., et al., "Internal Microturbulence Studies on DIII-D, TEXT and TFTR", *ibid.*

- 32) Luce T., Okazaki T., Saigusa M., et al., "Electron Cyclotron Heating and Current Drive Results from the DIII-D Tokamak", *ibid.*
- 33) JT-60 Team by Nagami M., "Recent Experiments in JT-60", *ibid.*
- 34) Seki Y., Kikuchi M., Ando T., et al., "The Steady State Tokamak Reactor (SSTR)", *ibid.*
- 35) Tokuda S., Kurita G., Azumi M., et al., "MHD Stability Limits of Tokamak Plasmas Obeying Neoclassical Ohm's Law and Radiative Thermal Instabilities in Tokamak," *ibid.*
- 36) Uckan N., Yushmanov N., Takizuka T., et al., "Energy and Particle Confinement in ITER," *ibid.*
- 37) Tsunematsu T., Borrass K., et al., "Operational Limits and Disruption in ITER," *ibid.*
- 38) Borrass K., Fujisawa N., Tuda T., et al., "Plasma Operation Control in ITER," *ibid.*
- 39) Fukuyama A., Itoh S-I., Hamamatsu K., et al., "Non Resonant Current Driven by RF Helicity Injection", *ibid.*
- 40) Matsuoka M., Okumura Y., Araki M., et al., "Negative Ion Source and Accelerator Systems for Neutral Beam Injection in Large Tokamaks; Part B: Research and Development Work for Negative-Ion-Based Neutral Beam Injector at JAERI", *ibid.*
- 41) Sugie T., Itami K., Nakamura H., et al., "Impurity Control and Helium Exhaust Experiment in JT-60", *ibid.*
- 42) Ishida S., Kikuchi M., Hirayama T., et al., "High-Poloidal-Beta Experiment with Hot-ion Enhanced Confinement Regime in the JT-60 Tokamak", *ibid.*
- 43) Kamada Y., Yoshino R., Nagami M., et al., "Pellet Injection with Improved Confinement in JT-60," *ibid.*
- 44) Imai T., Kimura H., Kusama Y., et al., "Lower Hybrid Current Drive and Higher Harmonic ICRF Heating Experiments on JT-60," *ibid.*
- 45) Tsuji S., Ide S., Seki M., et al., "The limiter H-mode with Lower Hybrid Current drive", *ibid.*
- 46) Nagami M. and JT-60 Team, "Recent Experiments in JT-60", *ibid.*
- 47) Stambaugh R.D. and DIII-D Team, "DIII-D Research Program Progress", *ibid.*
- 48) Taylor T.S., Lazarus E.A., Chu M.S., et al., "Profile Optimization and High Beta Discharges and Stability of High Elongation Plasmas in the DIII-D Tokamak," *ibid.*
- 49) Terumichi Y., Tanaka S., Maekawa T., et al., "Electron Cyclotron, Lower Hybrid Current Drive and Heating on the WT-3 Tokamak," *ibid.*
- 50) Vieider G., Akiba M., Cardella A., et al., "Plasma Facing Components in ITER", *ibid.*
- 51) Stambaugh R., Kamada Y., Matsumoto H., et al., "DIII-D Research Program Progress", *ibid.*
- 52) Burrell K., Matsumoto H., et al., "Transport in Auxiliary-Heated, Hot-Ion H-Mode and L-Mode Discharges in the DIII-D Tokamak", *ibid.*
- 53) Taylor T., Kamada Y., et al., "Profile Optimization and High Beta Discharges and Stability of High Elongation Plasmas in the DIII-D Tokamak", *ibid.*
- 54) Peebles W., Matsumoto H., et al., "Internal Microturbulence Studies on DIII-D, TEXT and TFTR", *ibid.*
- 55) Luce T., Okazaki T., Saigusa M., et al., "Electron Cyclotron Heating and Current Drive Results from the DIII-D Tokamak", *ibid.*
- 56) Miura Y., Aikawa H., Hoshino K., et al., "Studies of Improved Confinement on JFT-2M", *ibid.*
- 57) Matsuda S., Tsuji H., Akutsu Y., et al "Conceptual Design Study of the Fusion Experimental Reactor(FER)", *ibid.*
- 58) Tomabechi K., "ITER Conceptual Design", *ibid.*
- 59) Shimomura Y., "ITER Operational Scenario", *ibid.*
- 60) Iida H., "ITER : Safety Aspects", *ibid.*
- 61) Uckan N.A., Takizuka T., Tsunematsu and ITER Team, "Energy and Particle Confinement in ITER", *ibid.*
- 62) Tsunematsu T., Mizoguchi T., Yoshino R. and ITER Team, "Operational Limits and Disruptions in ITER", *ibid.*
- 63) Cohen S.A., Mizoguchi T., Shimada M. and ITER Team, "Power and Particle Control for ITER", *ibid.*
- 64) Nevins W.M., Fujisawa N., Kimura H. and ITER Team, "ITER Current Drive and Heating Physics", *ibid.*
- 65) Lindquist W., Fujisawa N., Kimura H. and ITER Team, "ITER Current drive and Heating Systems", *ibid.*
- 66) Borrass K., Fujisawa N., Fukuyama A. and ITER Team, "Plasma Operation Control in ITER", *ibid.*
- 67) Miller J.R., Koizumi K., Tada E. and ITER Team, "ITER Superconducting Magnets Systems", *ibid.*
- 68) Honda T. and ITER Team, "ITER Remote Maintenance", *ibid.*
- 69) Bottura L., Nishio S. and ITER Team, "Transient Electromagnetics in ITER", *ibid.*
- 70) Smith D., Kuroda T., Mori S. and ITER Team, "Tritium Breeding Blanket", *ibid.*
- 71) Vieider G., Akiba M., Takatsu H. et al., "Plasma Facing Components in ITER", *ibid.*
- 72) Perkins J., Iida H., Mizoguchi T. et al., "ITER Systems Studies and Design Space Analysis", *ibid.*
- 73) Wesley J., Kurihara K., Shimomura Y., et al., "The ITER Poloidal Field System", *ibid.*
- 74) Mukhovatov V., Yamamoto S., Ishida S. and ITER Team, "ITER Operation and Diagnostics", *ibid.*
- 75) Engelman F., Fujisawa N., Sugihara M. and ITER Team, "Physics R and D Programme", *ibid.*
- 76) Cordey J.G., Miura Y., Suzuki N., et al., "A Preliminary Analysis of the ITER Energy Confinement H-Mode Data Base", *ibid.*
- 77) Ogiwara N. and Maeno M., "Large Amounts of Gas Release just after Disruptive Discharges in the Fusion Device JT-60", Proc. 9th Int. Conf. on Plasma-Surface Interaction in Control. Fusion Devices, Bournemouth, 1990.
- 78) Shimada M., Ozaki A., Petersen P., et al., "Limiter Bias Experiments in DIII-D", *ibid.*
- 79) Shimada M., Kubo H., Itami K., et al., "Remote Radiative Cooling in JT-60," *ibid.*
- 80) Sengoku S. and the JFT-2M Team, "H-mode and Recycling Control in JFT-2M", *ibid.*
- 81) Matsuzaki Y., Omori K., et al. "Development in High-power and High-switching-Frequency Inverters of IGBT Devices for Plasma Control in Tokamak", Proc. Int. Power Electron. Conf., Tokyo 1990.
- 82) Shimamoto S., Okuno K., Ando T., et al., "Development of Superconducting Pulsed Poloidal Coil in JAERI", Proc. 13th Int. Cryog. Eng. Conf., 1990.

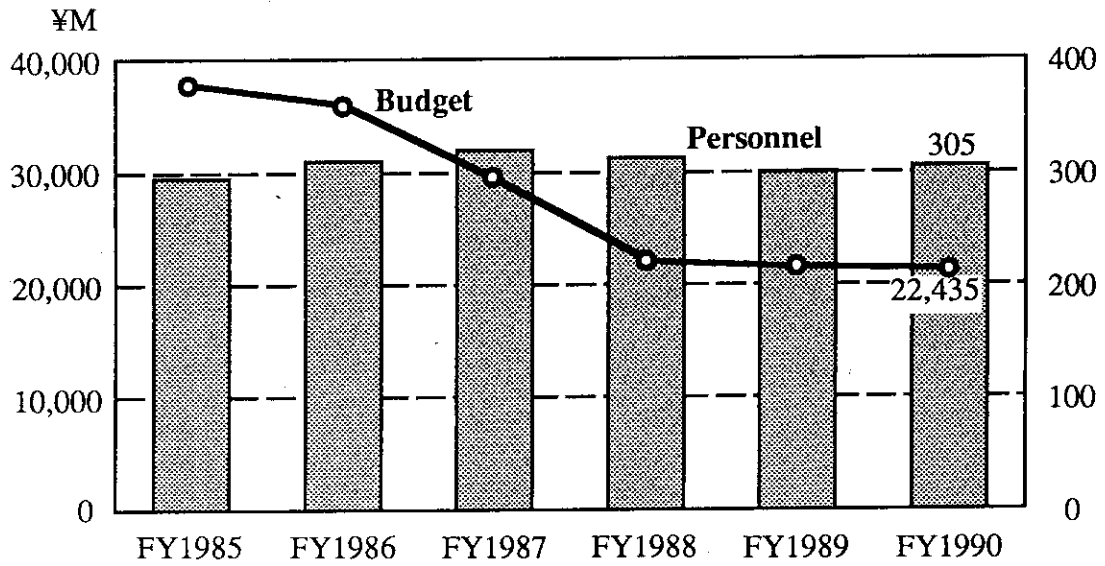
- 83) Takahashi Y., Yoshida K., Ando T., et al., "Experimental Results of the Nb₃Sn Demo Poloidal Coil (DPC-EX)", Proc. Int. Symp. on Supercond. Stability, Yokohama, 1990.
- 84) Ando T., Takatsu H., Yamamoto M., et al., "Material Characteristics of Graphite First Wall and C/C Composite Divertor Plate for JT-60U", Proc. Symp. on Carbon New Processing & New Applications, Tsukuba, 1990.
- 85) Eto M., Fukaya K., Oku T., et al., "Evaluation of Graphite and C/C Composite Materials Used as the Plasma First Wall Component of JT-60", *ibid.*
- 86) Seki M. and Ando T., "Carbon as a Plasma Facing Material", *ibid.*
- 87) Seki M., Ando T., "Carbon as a Plasma Facing Material", *ibid.*
- 88) Bolt H., Linke J., Akiba M., "Behavior of Carbon and Boron-carbon Materials under Disruption Heat Loads in Tokamaks --- Electron Beam Simulation Experiments", *ibid.*
- 89) Araki M., Akiba M., Ise H., "High Heat Flux Experiments of CFC and Graphite Materials for Fusion Applications", *ibid.*
- 90) Kishimoto Y., "Parasitic Wave Excitation in Raman FEL," Proc. Int. Symp. on Free Electron Laser, Tokyo, 1990.
- 91) Oda T., Mizuno K., Hooper E.B., et al., "Electric Field Measurements in Fusion Plasmas", Proc. 4th Int. Symp. on Laser-aided Plasma Diagnostics, Fukuoka, 1990.
- 92) Shiho M., Sakamoto K., Maehara S. et al., "JAERI Millimeter FEL Experiment by using Focusing Wiggler", Proc. 12th Int. Free Electron Laser Conf., Paris, 1990.
- 93) Kishimoto Y., Shiho M., Oda H., et al., "Parasitic Wave Excitation by Multi-mode Coupling in Raman Regime Free Electron laser," *ibid.*
- 94) Kishimoto Y., Shiho M., Oda H., "Parasitic Wave Excitation in High Current Raman Regime", *ibid.*
- 95) Yagi M., "Numerical Study of Ion Temperature Gradient Modes", Proc. 2nd Int. Toki Conf. on Nonlinear Phenomena in Fusion Plasmas, Toki, 1990.
- 96) Tuda T., Yagi M., Azumi M., "Fluctuation Spectrum of Ion Temperature Gradient Driven Modes in Sheared Magnetic Fields," *ibid.*
- 97) Matsuzaki Y., Aoyagi T., Terakado T., et al., "New Digital Control Systems of Poloidal Field Power Supplies for JT-60 Upgrade". Proc. 16th Symp. on Fusion Tech., London, 1990.
- 98) Kushima T., Ando T., Koizumi K., et al., "Toroidal Field Coil Reinforcement for Upgrade of JT-60", *ibid.*
- 99) Shizuoka Y., Numata I., Watanabe T., et al., "Manufacture of Poloidal Field Coil for JT-60U", *ibid.*
- 100) Takatsu H., Eto M., Ando T., et al., "Material Behavior of Graphite and C/C Composite Divertor Plates in JT-60", *ibid.*
- 101) Seki M., Ikeda Y., Konishi K., et al., "Construction and Testing of the New Multijunction LHRF Launcher for JT-60 Upgrade", *ibid.*
- 102) Fujii T., Kobayashi N., Moriyama S., et al., "Upgrade of JT-60 ICRF Heating System", *ibid.*
- 103) Remsen D. B., Loring C. M., McNees S. G., et al., "Results of Test of the X-2274 High Power Tetrode in a JT-60 110 to 130 MHz ICRH Amplifier", *ibid.*
- 104) Araki M., Akiba M., Seki M., et al., "Recent results of Developmental Study on Plasma Facing Components at JAERI", *ibid.*
- 105) Yamazaki S., Mohri K., Akiba M., et al., "Development of First Wall with Radiative Cooled Graphite armor tile", *ibid.*
- 106) Gotoh Y., Okamura H., Seki M., et al., "Felt-type Carbon-carbon Composite/Copper Brazed Structures for Active Cooling Plasma Facing Components", *ibid.*
- 107) Okumura Y., et al., "A 10 Ampere Negative Ion Source for High Energy Neutral Beam Injector", *ibid.*
- 108) Ando T., Hiyama T., Tsuji H., et al., "Fabrication and Test of the Nb₃Sn Demo Poloidal Coil (DPC-EX)", *ibid.*
- 109) Sugimoto M., Yoshida K., Hasegawa M., et al., "Mechanical Test of Superconducting Magnet System for Fusion Experimental Reactor", *ibid.*
- 110) Kato T., Tada E., Hiyama T., et al., "Cryogenic System Design and its Component Development for Fusion Experimental Reactor (FER)", *ibid.*
- 111) Ando T., Hiyama T., Tsuji H., et al., "Fabrication and Test of the Nb₃Sn Demo Poloidal Coil (DPC-EX)", *ibid.*
- 112) Sugimoto M., Yoshida K., Hasegawa M., et al., "Mechanical Test of Superconducting Magnet System for Fusion Experimental reactor", *ibid.*
- 113) Kato T., Tada E., Hiyama T., et al., "Cryogenic System Design and its Component Development for Fusion Experimental Reactor (FER)", *ibid.*
- 114) Tada E., Nishio S., Sato K., et al., "Containment Structure Design and Component Development for Fusion Experimental Reactor", *ibid.*
- 115) Shibanuma K., Honda T., Sato K. et al., "Remote Maintenance System Design and Component Development for Fusion Experimental Reactor," *ibid.*
- 116) Kojima H., et al., "A Large Multicusp Source Producing a 10 A, 50 keV, 0.1 s H⁻ Ion Beam", Proc. 13th Symp. on Ion Sources & Ion-assisted Tech., Tokyo, 1990.
- 117) Okumura Y. et al., "Effect of Cesium Vapor Injection in a Large Volume H⁻ Ion Source", *ibid.*
- 118) Watanabe K., et al., "Beam optics of a Multi-Ampere Negative Ion Source", *ibid.*
- 119) Miura Y., Okano F., "Low Energy Neutral Particle Analysis by a Time-of-flight Method on JFT-2M", Proc. 8th Topical Conf. on High Temp. Plasma Diagn., Massachusetts, 1990.
- 120) Oda T., Odajima K., Mizuno K., et al., "Stark-effect Measurement of High FEL Electric Field in MTX by Laser-aided Particle Probe", *ibid.*
- 121) Ogawa T., Ohasa K., Hoshino K., et al., "Neutron Diagnostic for MTX," *ibid.*

A.1.4 List of other reports

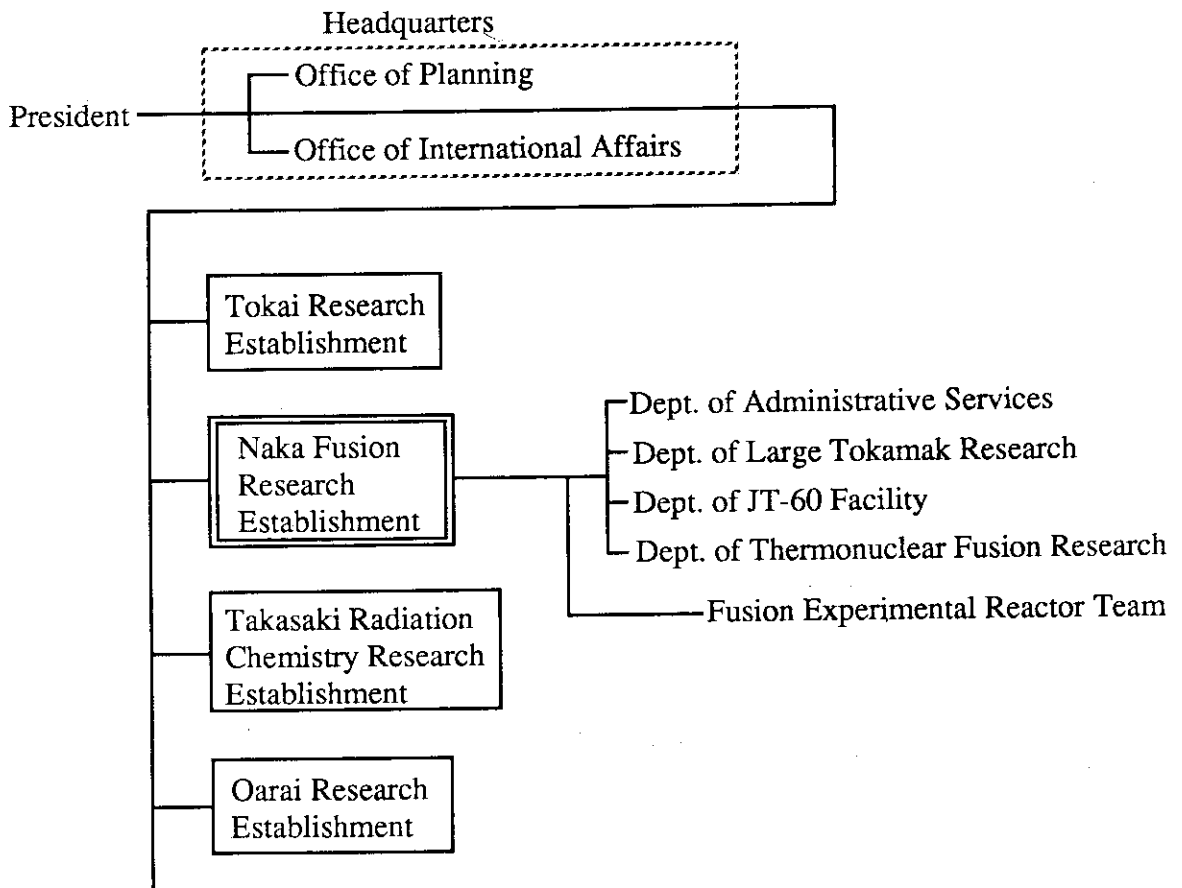
- 1) Burrell K.H., Groebner R.J., Matsumoto H., et al., "Comparison of Thermal and Angular Momentum Transport in Neutral Beam-Heated Hot-Ion H- and L-Mode Discharges in DIII-D", GA-A20058(Jun. 1990).
- 2) Matsumoto H., Burrell K.H., Carlstrom T.N., et al., "Physics of the L to H Transition in DIII-D", GA-A20081(Jun. 1990).
- 3) Doyle E.J., Groebner R.J., Matsumoto H., et al., "Modifications in Turbulence and Edge Electric Fields at the L-H Transition in DIII-D", GA-A20366(Jan. 1991).
- 4) Matsumoto H., Burrell K.H., et al., "Suppression of the Edge Turbulence at the L to H Transition in DIII-D", GA-A20383(Feb. 1991).
- 5) Shimada M., Ozaki A., Petersen P., et al., "Limiter Bias Experiments in DIII-D", GA-A20120 (1990).
- 6) Simomura Y. and ITER Team, "ITER Conceptual Design Report", IAEA/ITER /Documentation Series(DS)/18.
- 7) Fujisawa F. and ITER Team, "Physics and Technology R&D for ITER Physics and Technology Conceptual Design", IAEA/ITER /DS/19
- 8) Alikeev V., Fujisawa N., Honda T., et al., "Research and Development Needs for ITER Engineering Design", IAEA/ITER /DS/20.
- 9) Post D.E., Fujisawa, N., Sugihara M., et al., "ITER Physics", IAEA/ITER /DS/21.
- 10) Perkins L.J., Iida H., Mizoguchi T., et al., "ITER Parametric Analysis and Operational Performance", IAEA/ITER /DS/22.
- 11) Pacher G.W., Shimomura Y., Fujisawa N., et al., "ITER Operation and Research Programme", IAEA/ITER /DS/23.
- 12) Abdou M., Kuroda T., Mori S., et al., "ITER Test Programme", IAEA/ITER /DS/24.
- 13) Doggett J., Akiba M., Hasegawa M., et al., "ITER Tokamak Device", IAEA/ITER/DS/25.
- 14) Bottura L., Hasegawa M., Koizumi K., et al., "ITER Magnet", IAEA/ITER /DS/26.
- 15) Shimomura Y., Matsuoka F., Sugihara M., et al., "ITER Poloidal Field System", IAEA/ITER /DS/27.
- 16) Sadakov S., Tada E., Hasegawa M., et al., "ITER Containment Structures", IAEA/ITER/DS/28.
- 17) Smith D., Kuroda T., Maki K., et al., "ITER Blanket, Shield and Material Data Base", IAEA/ITER /DS/29.
- 18) Kuroda T., Akiba M., Araki M., et al., "ITER Plasma Facing Components", IAEA/ITER /DS/30.
- 19) Leger D., Yoshida H., Asahara M., et al., "ITER Fuel Cycle", IAEA/ITER /DS/31.
- 20) Parail V., Fujisawa N., Kimura H., et al., "ITER Current Drive and Heating System", IAEA/ITER /DS/32.
- 21) Mukhovatov V., Yamamoto S., Iguchi T., et al., "ITER Diagnostics", IAEA/ITER /DS/33.
- 22) Honda T., Tada E., Kondoh M., et al., "ITER Assembly and Maintenance", IAEA/ITER /DS/34.
- 23) Kolbasov B., Hosobuchi H., Iida H., et al., "ITER Plant Systems", IAEA/ITER /DS/35
- 24) Raeder J., Iida H., Seki Y., et al., "ITER Safety", IAEA/ITER /DS/36.
- 25) ITER Team, "ITER Physics Design Guidelines: 1989", IAEA/ITER/ DS/10.
- 26) ITER Team, "ITER Conceptual Design: Interim Report", IAEA/ITER/DS/7.
- 27) Mukhovatov V., Hopmann H., Yamamoto S., et al., "ITER Diagnostics Conceptual Design", ITER Documentation Series, (1990).
- 28) Hamamatsu K., Fukuyama A., Itoh S-I, et al., " RF Helicity Injection and Current Drive", NIFS-34(1990)
- 29) Itoh K., Sanuki H., Itoh S-I, et al., " Effect of Radial Electric Field on a-particle Loss in Tokamak", NIFS-66.

A.2 Personnel and Financial Data

A.2.1 Change in number of personnel and annual budget (FY1985-1990)



A.2.2 Organization chart (March 31, 1991)



A.2.3 Scientific staffs in the Naka Fusion Research Establishment (March 31, 1991)

Naka Fusion Research Establishment

IJIMA Tsutomu (Director General)

SEKIGUCHI Tadashi (Scientific Advisor)

TANAKA Masatoshi (Scientific Adviser)

TOMABECHI Ken (Scientific Advisor)

Department of Administrative Services

IJIMA Tsutomu (Director)

MOROZUMI Minoru (Deputy Director)

Department of Large Tokamak Research

TAMURA Sanae (Director)

KISHIMOTO Hiroshi (Deputy Director)

HINO Shuhji (Administrative Manager)

Large Tokamak Program Division

KISHIMOTO Hiroshi (Head)

KONOSHIMA Shigeru

NAGAMI Masayuki

TOYOSHIMA Noboru

MATSUMOTO Hiroshi

NAKAJIMA Shinji (*28)

MIYA Naoyuki

OIKAWA Akira

Diagnostic Division

FUNAHASHI Akimasa (Head)

AOYAGI Tetsuo

FUKUDA Takeshi

ISHIDA Shinichi

KANEKO Takashi

KONDOH Takashi

MIURA Yoshikazu

NAKAJIMA Toshiyuki (*78)

NISHITANI Takeo

SAITO Naoyuki

SATO Masayasu

TAKAHASHI Toranosuke

TSUKAHARA Yoshimitsu

YAMASHITA Osamu

MATOBA Tohru (Duputy Head)

ARAGUCHI Kazumi

GUNJI Hideo

ITAMI Kiyoshi

KAWANO Yasunori

KUBO Hiroataka

NAGASHIMA Akira

NEMOTO Masahiro

NUMAZAWA Susumu

SAKASAI Akira

SHITOMI Morimasa

TAKEUCHI Hiroshi

TSUGITA Tomonori

YOSHIDA Hidetoshi

CHIBA Shinichi

ISEI Noriaki

KAKIZAKI Sadayuki

KOIDE Yoshihiko

KUSAMA Yoshinori

NAGASHIMA Keisuke

NEYATANI Yuzuru

OHSHIMA Takayuki

SAKUMA Takeshi

SUGIE Tatsuo

TOBITA Kenji

URAMOTO Yasuyuki

Large Tokamak Experimental Division I

SHIMOMURA Yasuo (Head)

HOSOGANE Nobuyuki

KAMADA Yutaka

NAKAMURA Hiroo

TSUJI Shunji

IDE Shunsuke

KIKUCHI Mitsuru

NINOMIYA Hiromasa

USHIGUSA Kenkichi

IMAI Tsuyoshi

NAITO Osamu

SHIMADA Michiya

YOSHINO Ryuji

Large Tokamak Experimental Division II

AZUMI Masafumi (Head)

HAMAMATU Kiyotaka

SHIMIZU Katsuhiro

YAGI Masahiro

HIRAYAMA Toshiro

SHIRAI Hiroshi

OZEKI Takahisa

TANI Kenji

Fusion Reactor System Laboratory

FUJISAWA Noboru (Head)

SEKI Yasushi

Department of JT-60 Facility

TANAKA Yuji (Director)

SHIRAKATA Hirobumi (Deputy Director)

JT-60 Administration Division

HINO Shuhji (General Manager)

JT-60 Facility Division I

SHIMIZU Masatsugu (Head)
 AKASAKA Hiromi
 FURUKAWA Hiroshi(*30)
 ICHIGE Hisashi
 ISAKA Masayoshi
 KURIHARA Kenichi
 MUTOH Mitugu
 OMORI Kenichiro
 SAKATA Shinya
 TAKAHASHI Minoru
 TERAKADO Tsunehisa
 YAMAGISHI Koujirou

AKIBA kenichi(*79)
 HONDA Mitsuteru(*38)
 KEDA Yukiharu
 KAWAMATA Youichi
 MATSUKAWA Makoto
 NAGAYA Susumu
 OMORI Shunzo
 SEIMIYA Munetaka
 TAKESHITA Akira (*15)
 TOTSUKA Toshiyuki
 YASUDA Taizou(*28)

ARAKAWA Kiyotsugu
 HUMPHREYS David(*6)
 ISAJI Nobuaki(*39)
 KIMURA Toyooki
 MATSUZAKI Yoshimi
 NOBUSAKA Hiromichi (*28)
 OMORI Yoshikazu
 SEKIGUCHI Shunichi(*30)
 TANI Takashi
 YAGYUU Jyunichi
 YONEKAWA Izuru

JT-60 Facility Division II

KONDO Ikuo(Head)
 ANDO Toshiro
 HONDA Masao
 JIMBOU Ryutaro
 KOIKE Tsuneyuki
 MIYACHI Kengo
 NAGAYAMA Kiyoshi
 SASAJIMA Tadashi
 TANAKA Takejiro
 YOSHIOKA Yuji

ARAI Takashi
 HORIIKE Hiroshi
 KAMINAGA Atsushi
 KUSHIMA Takanori
 MIYAKE Kazuyuki
 NAKAFUJI Takashi
 SUNAOSHI Hidenori
 TSURUMI Satoshi

HIRATSUKA Hajime
 HOSHI Shizuo
 KODAMA Kozo
 MAENO Masaki
 MIYO Yasuhiko
 OGIWARA Norio
 TAKASAKI Manabu
 YAMAMOTO Masahiro

JT-60 Facility Division III

OHTA Mitsuru (Head)
 ANNOH Katsuto
 KUSAKA Makoto(*28)
 KOBAYASHI Teruyuki(*27)
 SATOH Minoyo
 SHINOZOKI Shinichi
 TAKAHASHI Shunji
 UEHARA Kazuya

FUJII Tsuneyuki
 KITAI Tatsuya(*28)
 KOGURE Shigeyuki(*73)
 SAWAHATA Masayuki
 SUGANUMA Kazuaki
 TAKASA Akira
 YOKOKURA Kenji

IKEDA Yoshitaka
 KIYONO Kimihiro
 MORIYAMA Shinichi
 SEKI Masami
 SUZUKI Norio
 TERAKADO Masayuki

JT-60 Facility Division IV

KUNIEDA Shunsuke (Head)
 AKINO Noboru
 KAWAI Mikito
 KITAMURA Shigeru
 MATSUOKA Mamoru
 NEMOTO Hironori (*28)
 OHUCHI Shouji (*32)
 SUGAWARA Tadayoshi (*2)
 USAMI Hiroji (*2)

HIRUTA Kazuharu (Deputy Head)
 EBISAWA Noboru
 KASHIMURA Takanori (*30)
 KOMATA Masao
 MIZUNO Makoto
 NOMOTO Hiroki (*31)
 OHUCHI Yutaka
 SUZUKI Yasuo (*4)
 USUI Katsutomi

ITOH Takao
 KIKUCHI Katsumi (*30)
 KURIYAMA Masaaki
 MOGAKI Kazuhiko
 OHGA Tokumichi
 OOHARA Hiroshi
 SHIMIZU Kazuhiko(*30)

Department of Thermonuclear Fusion Research

SHIMAMOTO Susumu (Director)

KOMAKI Akira (Administrative Manager)

Facility Operational and Engineering Division

SUZUKI Norio (Head)
 HAMANO Takashi (*30)
 KASHIWA Yoshitoshi
 OKANO Fuminori
 SUZUKI Sadaaki

HASEGAWA Koichi
 KAZAWA Minoru
 SHIBATA Takatoshi
 TOKUTAKE Toshikuni

HONDA Atsushi
 KIKUCHI Kazuo
 SHIINA Tomio
 UNO Sadanori

Plasma Theory Laboratory

TAKEDA Tatsuoki(Head)
 KISHIMOTO Yasuaki
 NAKAMURA Yukiharu
 TSUNEMATSU Toshihide

KURITA Gen-Ichi
 TAKIZUKA Tomonori
 TUDA Takashi

NAKAMURA Masatoshi(*68)
 TOKUDA Shinji
 YAMAGIWA Mitsuru

Experimental Plasma Physics Laboratory

MAEDA Hikosuke (Head)		
AIKAWA Hiroshi	HOSHINO Katsumichi	KASAI Satoshi
KAWAKAMI Tomohide	KAWASHIMA Hisato	MATSUDA Toshiaki
MORI Masahiro	MIURA Yukitoshi	ODAJIMA Kazuo
OGAWA Hiroaki	OGAWA Toshihide	OHOASA Kazumi
SENGOKU Seio	SHOJI Teruaki	TAMAI Hiroshi
YAMAMOTO Takumi	YAMAUCHI Toshihiko	

Plasma Engineering Laboratory

MURAKAMI Yoshio(Head)		
ABE Tetsuya	HAMAZAKI Masanori(*30)	HIROKI Seiji
OBARA Kenjiro		

Superconducting Magnet Laboratory

TSUJI Hiroshi (Head)		
ANDO Toshinari	HANAWA Hiromi (*30)	HIYAMA Tadao
HIUE Hisaaki	ISHIDA Hideaki	ISONO Takaaki
KAMIYAUCHI Youichi(*18)	KATO Takashi	KAWANO Katsumi
KOISUMI Norikiyo	NAKAJIMA Hideo	NISHI Masataka
OHUCHI Hideyoshi (*30)	OKUNO Kiyoshi	ONO Michitaka
SUGIMOTO Makoto	TADA Eisuke	TAKAHASHI Yoshikazu
YOSHIDA Kiyoshi	YOSHIDA Jun(*2)	

Plasma Heating Laboratory I

SEKI Masahiro (Head)	AKIBA Masato	ARAKI Masanori
DAIRAKU Masayuki	IIDA Kazuhiro	INOUE Takashi
ISE Hideo(*16)	NAKA Masanobu (*2)	OHARA Yoshihiro
OKUMURA Yoshikazu	SUZUKI SatoshiTA	TANAKA Hideki
TANAKA Shigeru	WATANABE Kazuhiro	YOKOYAMA Kenji

Plasma Heating Laboratory II

NAGASHIMA Takashi (Head)		
FUJITA Hideo (*25)	MAEBARA Sunao	SAIGUSA Mikio
SAKAMOTO Keishi	SEKI Norikazu (*25)	SHIHO Makoto
TSUNEOKA Masaki	WATANABE Akihiko(*40)	

Tritium Engineering Laboratory

NARUSE Yuji (Head)		
AMANO Junzo (*23)	ENOEDA Mikio	HAYASHI Takumi
HIRATA Kazuhiro	HONMA Takashi	INOUE Masahiko (*23)
ITO Hideki (*16)	KONISHI Satoshi	KURASAWA Toshimasa
MATSUDA Yuji	NAKAMURA Hirobumi	NAKAMURA Takuya (*29)
OHARA Atsushi (*4)	O'HIRA Shigeru	OKUNO Kenji
SUZUKI Takumi	WATANABE Tetsurou (*16)	YAMADA Masayuki
YAMANAKA Keiichi (*16)	YAMANISHI Toshihiko	YOSHIDA Hiroshi

Fusion Experimental Reactor Team

MATSUDA Shinzaburo (Head)		
HASEGAWA Mitsuru(*15)	HONDA Tsutomu(*4)	HOSOBUCHI Hideo(*17)
IIDA Hiromasa	KANAMORI Naokazu(*2)	KIMURA Haruyuki
KOIZUMI Koichi	KURODA Toshimasa(*16)	MAKI Koichi(*2)
MATSUOKA Fusiki(*23)	MIZOGUCHI Tadanori(*2)	NAKAZATO Toshiko(*4)
NISHIO Satoshi	OHKAWA Yoshinao	SATO Keisuke
SATO Koichi(*16)	SEKI Shogo(*83)	SHIBANUMA Kiyoshi
SUGIHARA Masayoshi	TAKATSU Hideyuki	TERAKADO Takuya(*31)
YAMAMOTO Shin		

- *1 General Atomics, USA
- *2 Hitachi Ltd.
- *3 Lawrence Livermore National Laboratory, USA
- *4 Toshiba Corp.
- *5 Max-Planck Institut für Plasmaphysik, FRG
- *6 Massachusetts Institute of Technology, USA
- *7 Mitsubishi Atomic Power Industry Inc.
- *8 The University of Tokyo
- *9 Nagoya University
- *10 Okayama University
- *11 Kyoto University
- *12 Hiroshima University
- *13 Institut für Reaktorbauelements, KfK, FRG
- *14 Ishikawajima-Harima Heavy Industries
- *15 Mitsubishi Electric Co., Ltd.
- *16 Kawasaki Heavy Industries, Ltd.
- *17 Hazama-gumi Ltd.
- *18 Kobe Steel Ltd.
- *19 Oak Ridge National Laboratory, USA
- *20 Century Research Center Corp.
- *21 Northwestern Laboratory
- *22 Institute of Plasma Physics, Nagoya University
- *23 Mitsubishi Heavy Industry Ltd.
- *24 NAIG Nuclear Research Laboratory
- *25 Japan Atomic Industrial Forum
- *26 Central Research Institute for Electric Power
- *27 Nippon Electric Co., Ltd.
- *28 Kaihatsu Denki Co.
- *29 Sumitomo Heavy Industry Co.
- *30 Nuclear Engineering Co., Ltd.
- *31 Tomoe Shokai
- *32 Ibaraki Kohsan
- *33 Tokyo Nuclear Service Co., Ltd.
- *34 ULVAC Co.
- *35 Kyushu University
- *36 Contract Researcher
- *37 Princeton Plasma Physics Laboratory, USA
- *38 LITEC Co., Ltd.
- *39 Japan Expert Clone Corp.
- *40 Nissei Sangyo Co., Ltd.
- *41 JET Joint Undertaking, UK
- *42 Hodaka Seiki Ltd.
- *43 Sumitomo Electric Industry Co.
- *44 Nikon Corp.
- *45 National Laboratory for High Energy Physics
- *46 Tsukuba University
- *47 Los Alamos National Laboratory, USA
- *48 Japan Radiation Engineering Co.
- *49 MEITEC Co., Ltd.
- *50 Osaka University
- *51 Imperial College, UK
- *52 Institute of Research Hydro-Quebec, Varenns, Canada
- *53 KFA-IPP, FRG
- *54 Ewic Engineering Co., Ltd.
- *55 ORC Manufacturing Co., Ltd.
- *56 Koike Sanso Kogyo Co., Ltd.
- *57 Hitachi Oxygen Co., Ltd.
- *58 Fuji Electric Co., Ltd.
- *59 Nissin Electric Co., Ltd.
- *60 Sandia National Laboratories, USA
- *61 JGC Corp.
- *62 Tokyo Institute of Technology
- *63 Nuclear Research Center Karlsruhe, FRG
- *64 Argonne National Laboratory, USA
- *65 ITER Team
- *66 Yokohama National University
- *67 Nihon Software Kaihatsu, Inc.
- *68 Kanazawa Computer Service Corp.
- *69 University of California at Los Angeles, USA
- *70 University of Texas, USA
- *71 Varian Company Co.Ltd.
- *72 Nagaoka University of Technology
- *73 Denki Kogyo Co. Ltd.
- *74 The NET Team
- *75 National Institute for Fusion Science
- *76 I.V. Kurchatov Institute of Atomic Energy
- *77 Keio University
- *78 Mitsubishi Cable Industries, Ltd.
- *79 Nippon Advanced Technology Co., Ltd.
- *80 Hamatsu Photonics KK
- *81 University of California at San Diego, USA
- *82 University of Maryland
- *83 Atomic Data Service Corp.